Author:
Sparks, Joanna F

Title:
Utilising inorganic protocells in hydrogel-based prototissues

Utilising inorganic protocells in hydrogel-based prototissues

By

JOANNA FLORENCE SPARKS

Department of Chemistry
UNIVERSITY OF BRISTOL

A dissertation submitted to the University of Bristol in accordance with the requirements of the degree of DOCTOR OF PHILOSOPHY in the Faculty of Science.

JULY 2020

Word count: 58,167

Abstract

A new challenge in bottom-up synthetic biology is the construction of multi-protocellular communities capable of exhibiting emergent behaviours. The aim of this thesis is to produce rudimentary synthetic prototissues by embedding colloidosome-based protocells within polysaccharide hydrogels, which mimic the natural extracellular matrix.

Colloidosome protocells are chosen due to their previously demonstrated stability and the ability to encapsulate a range of molecules. Investigations into their structure and function are presented in Chapter 3. Instead of simple aqueous-filled capsules, the colloidosomes have an internal silica network which varies with the formation conditions. As a consequence, colloidosomes sequester above equilibrium concentrations of certain molecules from solution. Retention of proteins within the colloidosomes, which is essential to their function as protocells, is shown to be strongly facilitated by interaction with the entrapped silica rather than by physical encapsulation within the membrane.

Chapter 4 outlines the design and characterisation of prototissues formed by embedding colloidosomes in agarose hydrogels. A modular system is used to pattern colloidosomes within the hydrogel and when a substrate is homogeneously applied, chemical communication between protocell populations results in patterned enzymatic reactions. The patterning is extended to shapes in 3-dimensions and due to its transient nature forms in situ, pre-programmed chemical gradients thus opening up the possibility of creating directional gradients between protocell populations in a way which is not possible for protocells in suspension.

Chapter 5 describes a prototissue designed to exhibit chemo-mechanical transduction upon addition of chemical fuels, through the collective behaviour of the component parts. Binary colloidosome populations capable of producing pH changes due to enzymatic turnover of chemical fuels are embedded in a novel, pH responsive, photocrosslinked hydrogel bilayer. Due to the use of antagonistic enzyme-containing colloidosomes the synthetic prototissue exhibits pre-programable motion which is a promising step towards the controlled fabrication of out-of-equilibrium soft materials.

Dedication and acknowledgements

I have learnt an incredible amount during my PhD and have had some wonderful experiences. None of this would have been possible without my supervisor Professor Stephen Mann, and I am incredibly grateful for the opportunity and for his guidance and teaching.

I would like to thank Dr Mei Li and Dr Avinash Patil for their help and advice. My thanks also go to all of the Mann group for stimulating scientific discussions and support over the years. I am particularly grateful to my fellow PhD students in the group, who have provided great comradery. I am so happy to have met you all and I look forward to hearing about the wonderful things you all do in the future.

Huge thanks to Dr Nicolas Martin and Dr Pierangelo Gobbo, whose mentorship and encouragement was crucial in the last couple of years of my PhD. I have no doubt you are both are at the start of fantastic, exciting careers, and that there will be many PhD students in the future who will be lucky to have your support!

I was fortunate to have the opportunity to work with two great BSc students during my PhD: Gift Wejchapan and Imogen Millington. I would like to thank them both for their hard work, and for helping me become a better teacher and supervisor.

I would like to extend my gratitude to those across the University of Bristol who have helped me with various aspects of this work, including Dr Jean-Charles Eloi and Dr Sean Davis from the Chemical Imaging Facility, Alan Leard, Dr Stephen Cross and the rest of the team from the Wolfson Bioimaging Facility, Rafael Moreno Tortolero who has helped me extensively with both SEM and Rheology and Mary Jenkinson-Finch for help with NMR and organic chemistry. A huge thank you to Mary Jenkinson-Finch, Dr Pierangelo Gobbo, Dr Nicolas Martin, Dr Nichola Clarke and Aidan Cassidy for proof reading this thesis.

I am overwhelmingly grateful to my wonderful family, especially my mum, dad and fantastic sister Nell for their support and unfaltering belief in me, and my chosen sisters Carrie and Selam, and their beautiful families, for bringing so much love and joy into our lives. Thank you to all my lovely friends, who have stuck with me, even though my workaholic tendencies have made me rather unreliable! Our chats, adventures, afternoons, festivals, cups of tea, glitter, silliness and dancing have kept me sane: you guys are the best. I would like to thank Lauren, who has been a wonderful friend and fantastic support to me over the years, despite us being so far apart.

A huge thank you must go to my partner and my best friend, Aidan. For holding my hand through the tough bits, making me laugh, believing in me so completely and for being such an

inspiration.

This thesis is dedicated to my beautiful grandma Heather, who was so kind, funny and intelligent, my biggest cheerleader and my dear friend.

AUTHOR'S DECLARATION

I declare that the work in this dissertation was carried out in accordance with the requirements of the University's Regulations and Code of Practice for Research Degree Programmes and that it has not been submitted for any other academic award. Except where indicated by specific reference in the text, the work is the candidate's own work. Work done in collaboration with, or with the assistance of, others, is indicated as such. Any views expressed in the dissertation are those of the author.

SIGNED: .....  ..... DATE: 1.7.20

Table of Contents

List of Tables

List of Figures

CHAPTER 1

INTRODUCTION

One of the current challenges in the field of bottom-up synthetic biology is the creation of interacting protocell populations. Mimicking the multicellular nature of many organisms, examples have begun to emerge of protocells being organised into synthetic multicellularities or prototissues. The aim of this research was to use an inorganic protocell model (colloidosomes) with hydrogels to create new prototissues capable of novel and biomimetic behaviours. Since this thesis brings together two distinct fields of research, protolife and hydrogels, this introductory chapter provides background in both, outlining the key concepts to provide context for the work in the following chapters.

1.1 Protolife

1.1.1 Protocells

Although life on earth is wonderfully diverse, closer inspection reveals that the underlying mechanisms in living organisms are surprisingly similar [1]. The basic unit of life is a cell, an autonomous system of chemical reactions and processes of extraordinary complexity [1, 2]. Cells are delineated by a phospholipid bilayer, a semi-permeable membrane that provides control over the passage of material in and out of the cell, and allows the cell to function as a discrete, coordinated chemical system. Key to life is the ability to self-replicate and pass on hereditary information. Processes within the cell are guided by the polymeric molecule deoxyribonucleic acid (DNA),and when cells divide, DNA is replicated via templated polymerisation and the information is passed on to the next generation. DNA codes for the formation of proteins, which carry out chemical reactions within the cell (metabolism). Proteins also perform many other functions within the cell, such as structure, membrane transport, signalling and sensing. Interaction with

the external environment is essential to the autonomy of the cell. Furthermore, cells exist under non-equilibrium conditions and thus must gain energy from the environment to sustain this and carry out all the cellular processes [1, 2].

Since the cell is in fact a chemical system, the question arises as to how the inanimate matter present on an early earth, transitioned into the complexity that is living matter [2]. Furthermore, we may ask whether life is something that we could replicate in vitro [2]. Although the first question is something that may remain a mystery, attempts to replicate life-like systems in a laboratory may provide some insight. Within synthetic biology two different but complimentary fields have emerged in the formation of artificial cells models or protocells (Figure 1.1) [2, 3]. Top-down approaches focus on the simplification of modern cells, for example by removing genetic material, in an attempt to create a minimal cell. The bottom-up approach aims to build cell-like compartments from abiogenic material. In building such synthetic cells the aim is to replicate some of the features that are essential to living cells as discussed above (compartmentalization, replication/ hereditary information, energisation, sensing, metabolism, evolution) [2]. An alternative approach for the bottom up construction of protocells is to encapsulate biological molecules, such as proteins or DNA, in compartments that can then carry out primitive biochemical reactions and thus exhibit some of the cell like behaviours [3, 4]. This type of artificial cell is less relevant for origin of life work (since it doesn‘t seem that such molecules were present under pre-biotic conditions) [3]. However, such systems are forms soft matter capable of complex functions or smart/ intelligent behaviour and are therefore of interest for a wide range of fields such as drug delivery or microbioreactors [4].

Compartmentalisation is a key feature of all protocell models and, within the field of bottom-up synthetic biology, several different strategies have emerged. Since modern cells are surrounded by a self-assembled membrane of amphiphilic lipid molecules, the most common approach is to mimic this. Many examples of protocells based on synthetic lipid or fatty acid vesicles capable of complex behaviours have been published but limitations arise due to the permeability of phospholipid vesicles and the low stability of fatty acid vesicles [4]. As well as protocells formed from lipid vesicles, a plethora of studies have reported non-lipid based synthetic cell-like structures. The nature of these structures means they are further removed from both modern cells and most likely, primitive cells (except in the case of coacervates, as it has been suggested they may have some relevance to the development of early cells). Nonetheless, alternative protocells can be engineered to show a wide range of properties and functions and therefore show promise in the advancement of technological applications of protocells [4]. Protocells have been reported with membranes formed from inorganic nanoparticles (colloidosomes) [5], protein-polymer nanoconjugates (proteinosomes) [6] or polymer amphiphiles (polymersomes) [7]. A more detailed discussion of the properties of colloidosomes is provided in Section 1.1.1.2. Membrane-free compartments in the form of coacervates (aqueous phase separation) [8] have also shown great potential as protocell models, as have hybrid systems [9, 10].

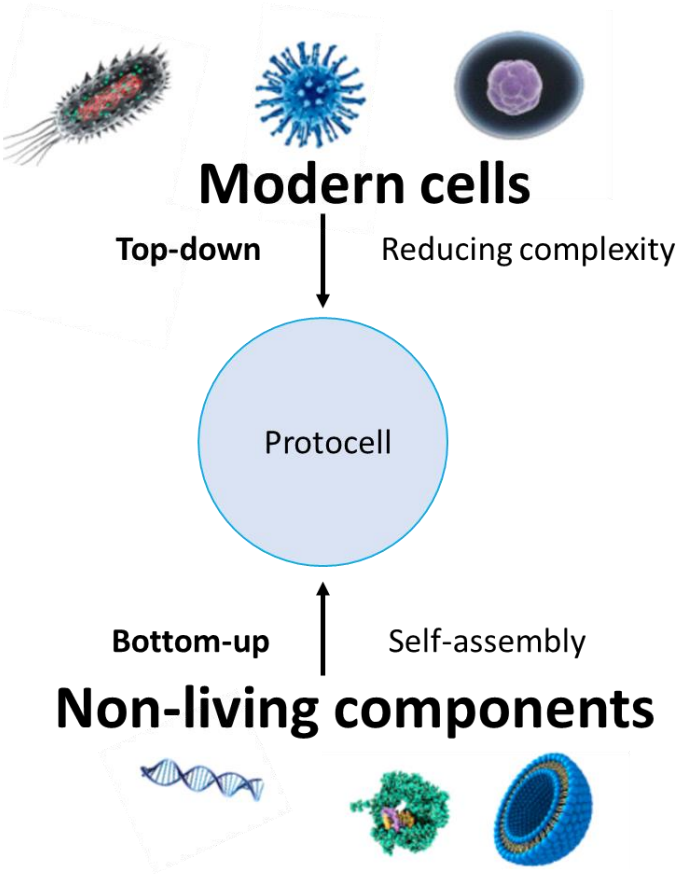

FIGURE 1.1. A schematic showing the two different approaches to forming protocells. Top-down synthetic biology involves simplifying living organisms by removing components such as unnecessary genes. Bottom-up synthetic biology aims to produce compartments that mimic cell like behaviours by assembling non-living components [2–4].

Non-lipid protocells have been used for a range of biomimetic behaviours. Guest molecules can be sequestered by some compartments [8] or encapsulated in others due to the selective membrane permeability [6]. As a result, non-lipid protocells have been used to house gene directed protein synthesis [6], enzymatic reactions and cascades [11, 12], and nanoparticle based catalytic activity [8]. Systems have also been designed that can show a range of other behaviours such as catalytically active membranes [11], stimuli responsive changes in permeability [6, 7] and light harvesting [7].

1.1.1.1 Colloidosomes

An emulsion is a dispersion of droplets of a liquid in a bulk phase of a second liquid with which it is immiscible. There is an energy cost to the formation of an interface between two immiscible liquids. The interfacial tension (γ) is the work that must be done per unit area to increase the interface, and therefore characterises the tendency of the interface to contract. Emulsions can be stabilised via the adsorption of surfactant molecules at the oil-water interface. Surfactants molecules are amphiphilic and sit at the interface in a particular orientation (Figure 1.2). Adsorption of surfactants at the oil-water interface lowers the interfacial tension, thus stabilising the system [13].

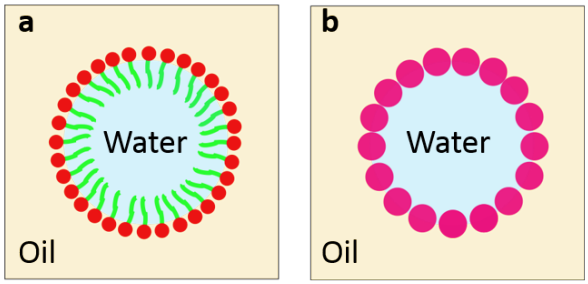

FIGURE 1.2. A cartoon showing water-in-oil emulsions stabilised by (a) surfactant molecules or (b) solid particles. Adapted from a figure in work by Chevalier et al [14].

Under the right conditions solid particles, such as silica nanoparticles, can also stabilise emulsions via spontaneous adsorption at the oil-water interface (Figure 1.2). To form the emulsion the particles are suspended in one of the immiscible liquids, the two phases are mixed, and a force is applied to break the dispersed phase into droplets at the interface of which the particles will adsorb. Such emulsions are called Pickering emulsions, and the mechanism of adsorption at the interface and droplet stabilisation is different from that in classical emulsions [14, 15]. Particles that adsorb at the interface do not have to be amphiphilic (janus) particles but must have the correct surface chemistry to allow partial wetting by both the oil and water phases [14, 15]. This can be quantified using the contact angle, which is defined in Figure 1.3. The contact angle in water (θ_w) is related to that in oil (θ_o) by Equation 1.1 and depends on the interfacial tensions of the oil-water γ_{ow}, water-solid (γ_{ws}) and oil-solid (γ_{os}) interfaces as described by Equation 1.2

(Young's law) [14, 15].

(1.1) $$\theta_o = \pi - \theta_w$$

(1.2) $$cos\theta_w = \frac{\gamma_{os} - \gamma_{ws}}{\gamma_{ow}}$$

A solid particle adsorbing at the oil-water interface does not reduce γ_{ow} like a surfactant does, but instead decreases the area of the oil-water interface [15]. The energy required to remove a particle of radius r from an oil-water interface (E) is described by Equation 1.3. For a particle being moved into the water phase the sign inside the bracket is negative, and if it is being moved into the oil phase it is positive [15].

(1.3) $$E = \pi r^2 \gamma_{ow}(1 \pm cos\theta_w)^2$$

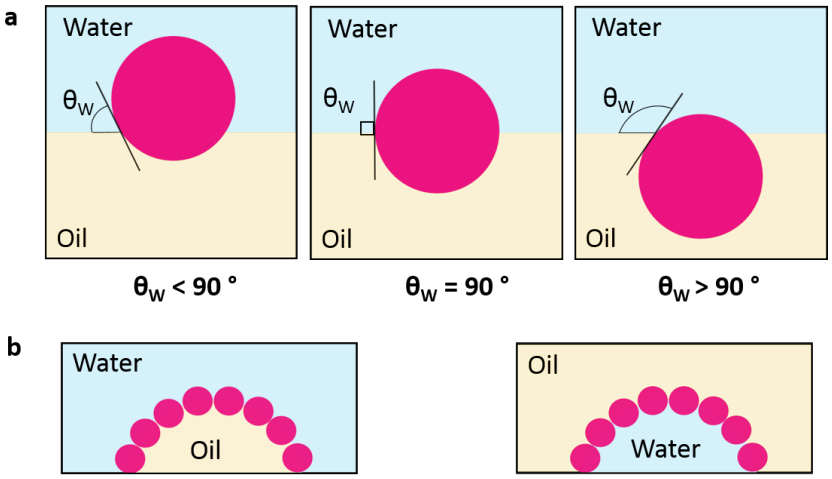

FIGURE 1.3. (a) The position of a solid particle at the oil-water interface as it would vary with the contact angle with water (θ_w). The contact angle is marked on the images. (b) The curvature of the oil-water interface when $\theta_w < 90°$ (image on the left) or $\theta_w > 90°$ (image on the right) with oil-in water or water-in-oil emulsions be favoured respectively. Figure adapted from work by B.P.Binks [15].

When θ = 90°, E is at is maximum value and the particle is most strongly adsorbed at the interface. If the particle is too hydrophobic or hydrophilic (θ_w varies greatly from 90°) the adsorption energy becomes comparable to thermal energy k_BT (where k_B is the Boltzmann constant and T is the temperature) and thus the particle is completely wetted by one of the

phases [14, 15]. The surfaces of particles can be modified to alter the contact angle and allow Pickering emulsion formation. This is often the case for silica particles, since they are too hydrophilic when unmodified [14]. Strong adsorption of particles at the oil-water interface means Pickering emulsions can be very stable. The mechanical barrier provided by the solid particles inhibits coalescence.

When particles are adsorbed at the oil-water interface, they will tend to sit further into the phase with which they have the lowest contact angle, forming emulsions where this is the dispersing phase (Figure 1.3) [14, 15]. However, because adsorption at the interface favours the use of particles with intermediate values of hydrophobicity/ hydrophilicity (θ_w close to 90°), the type of emulsion formed may also be affected by the ratio of the two liquids and the phase in which the particles are initially dispersed [14, 15].

For particles adsorbing at the interface in a closely packed monolayer, the total interfacial area of the emulsion is determined by the amount of solid particles per volume [14]. A lower particle concentration results in larger droplets since this gives a lower surface area. However, it has been shown that emulsions can be stable with incomplete coverage of the surface, or with particles aggregated at the interface [14]. Furthermore, the emulsification process also plays a role in determining the size. When a high concentration of particles is used but low shearing force is applied to form the emulsion, large droplets will form leaving the remaining solid in suspension [14].

When the particles stabilising the Pickering emulsion are crosslinked or fused the resulting microcapsule is called a colloidosome, in analogy to a liposome. Colloidosomes have been formed from a range of materials such as latex particles [16] and silica nanoparticles [17].

1.1.1.2 Colloidosome protocells

In the past decade several papers have been published demonstrating the use of colloidosomes as synthetic cell models. Colloidosome protocells have been formed with membranes of clay or magnetite particles [18, 19], but most of the examples thus far are based on silica. To form the colloidosome protocells, silica nanoparticles were surface modified to give hydrophobic/ hydrophilic character by replacing some of the surface silanol (-O_3SiOH) groups with dimethylsilane groups (-O_2Si(CH_3)$_2$). The particles were used to stabilise water-in-oil Pickering emulsions and within the aqueous phase both enzyme reactions and gene directed synthesis of the fluorescent protein eGFP were demonstrated [5].

The colloidosomes can be crosslinked via the addition of an alkoxysilane such as tetramethyl orthosilicate (TMOS) (see Section 3.2.1) [5]. During the crosslinking process methanol is produced as a by-product and moves into the emulsion aqueous phase. Li at al utilised this to produce populations capable of a rudimentary form of self-replication and division [20]. Adding large volumes of TMOS to the silica stabilised emulsion caused an influx of methanol to the aqueous phase which increased its volume to the point that it ruptured. This rupture caused the

colloidosomes to bud drops of liquid. Addition of supplementary hydrophobic silica nanoparticles to the oil phase of the emulsion stabilised these droplets and, under the right conditions, allowed the formation of a distinct population of second generation colloidosomes.

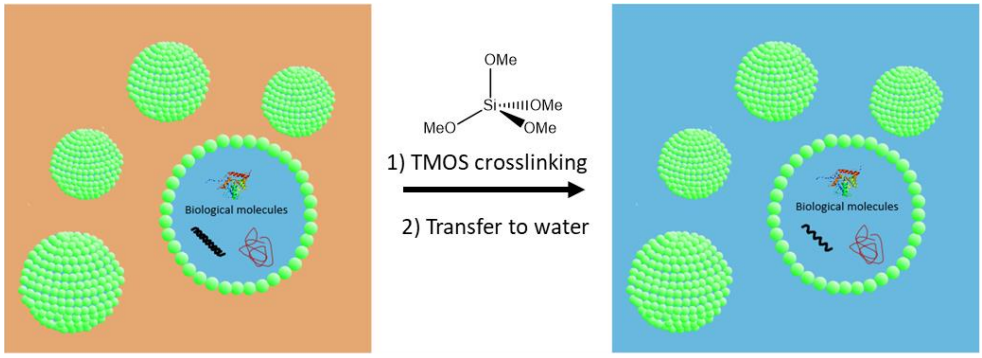

FIGURE 1.4. A schematic depicting the formation procedure for colloidosome protocells. Hydrophobic silica nanoparticles (shown in green) are used to stabilise a water-in-oil Pickering emulsion. Biological material, such as proteins, is included in the emulsion aqueous phase. The Pickering emulsion is crosslinked using TMOS and transfered to water, resulting in an aqueous suspension of the colloidosome protocells.

The addition of lower amounts of TMOS crosslinks the membrane without causing rupture or division, and thus allows colloidosomes to be transferred into the bulk aqueous phase [21]. This results in a capsule with a porous membrane, and thus large molecules are retained within the colloidosomes after transfer to water whereas smaller molecules are released [21]. Enzymes housed in colloidosomes show enzymatic activity after transfer to water, allowing the colloidosomes to show cell like behaviour [19, 21, 22] . Thus far there has been little investigation into the internal and membrane structure of the colloidosome after transfer to water, or the actual size cut off for molecules to be retained within the capsule. However, further work by Li et al demonstrated that grafting a pH responsive polymer allowed electrostatic control and gating of molecules moving across the membrane [21]. The changes in permeability could be used to control the rates of enzyme reactions within the colloidosome lumen.

1.1.2 Collective interactions between protocell populations

Many papers have been published developing new protocell models or adding increasing complexity or functionality to existing ones. However, when working within the field of biomimicry it is important to look back to nature, and therefore to consider that living cells do not exist in isolation. Mimicking this via the creation of interacting protocells could be of use in the creation of synergistic sensing systems or complex networks of microreactors [23]. Recently papers have emerged focusing on collective behaviour within protocell communities or ecosystems, for example through mimicking predator/prey [23] relationships, phagocytosis [18] and chemical communication [24].

In nature, intracellular communication is ubiquitous and usually occurs via diffusible factors such as small molecules or proteins [25, 26]. Primitive forms of communication between protocell populations can be achieved by encapsulating the different components of an enzymatic cascade reaction in the different populations. The intermediate in the reaction must diffuse from one population from another to initiate the second step in the cascade. This has been shown using the glucose oxidase (GOx)/ Horseradish peroxidase (HRP) enzyme cascade in both proteinosomes [11] and co-polymer stabilised coacervates [10]. GOx converts glucose to gluconic acid and in the process produces hydrogen peroxide, which HRP can use in the oxidation of colorimetric or fluorescent substrates. Taking this further and utilising the ability of protocells to house cell-free gene expression, Tang et al demonstrated gene-directed chemical communication between liposomes and proteinosomes [24].

Communication between cells means that the behaviour of certain individuals can be modified by others and this can also be mimicked in protocells [25]. For example, chemical communication between two colloidosome populations can cause new properties in one of the populations [19]. As before, silica colloidosomes containing GOx release H_2O_2 upon addition of glucose. The H_2O_2 diffuses to the second population of colloidosomes, which due to their catalytically active clay membrane, then polymerise N-isopropylacrylamide (NIPAAm), resulting in a polymer coated membrane. This membrane then exhibits altered permeability and stimuli responsive properties. Since biological cells also utilise chemical communication, this can allow direct communication between protocells and living cells. For example, Lentini et al created artificial cells that released a chemical signal, which induced gene expression in a population of bacteria, modifying their behaviour without altering them directly [27].

1.1.3 Prototissues

Looking at nature again, we see that even unicellular microbial organisms often live in colonies where the interaction and communication between neighbours provides an advantage [28]. In multicellular organisms, cells are organised into tissues: groups of similar cells that work together for specific functions [1]. Tissues exhibit emergent properties, meaning they can perform functions that individual cells cannot [1]. This collective behaviour within a tissue relies on communication,

which allows the behaviour of cells to be influenced by each other and the environment [1, 29]. To come together and form a tissue, cells form direct cell-to-cell adhesions or are held within an extracellular matrix (ECM) [1]. Based on the organisation of cells into tissues, the idea of interacting protocells can be taken further, with protocells being assembled into 3-dimensional (3D) constructs referred to as *prototissues* or *synthetic tissues*. Mimicking living tissues via the creation of prototissues is a challenge synthetic biology is just beginning to address. Within a prototissue, communication and cooperation between the constituent protocells should lead to emergent properties [29, 30]. Furthermore, communication both between protocells and with the external environment (sensing) could be used to regulate function [30]. As well as being of interest in synthetic biology, these properties mean that prototissues represent an interesting class of materials that could be used for tissue engineering, cell-protocell interactions for purposes such as drug delivery, sensors and microbio-reactor technology [29, 31].

Although the construction of prototissues is a relatively novel concept, several key examples have been published. Carrara et al assembled negatively charged giant unilamellar vesicles (GUVs) into colonies via the addition of positively charged polypeptides such as poly-L-arginine [28]. Although referred to as colonies rather than tissues, these assemblies exhibit characteristics essential to a prototissue: colonies showed emergent properties upon formation. GUVs within the colonies showed increased permeability towards certain molecules and were able to show solute exchange between neighbours, a property not seen in isolated vesicles. Furthermore, GUVs within colonies were less physically stable than GUVs in isolation, and fused more easily.

The Bayley lab have produced a series of papers demonstrating synthetic tissues built from lipid coated aqueous droplets in oil [31, 32]. Thousands of picolitre droplets are printed into a bulk oil phase and when the lipid coated aqueous droplets meet, the formation of a stable lipid bilayer between them sticks them together. In this way macroscopic, self-supporting materials have been formed. Communication between neighbouring droplets can be achieved by including membrane pores [32]. This allows not only conduction of small molecules, but, via movement of ions, electrical signals, both phenomena seen in living tissues. Patterns can be created within the material by printing multiple droplet types [32] or including a light activated DNA promoter along with the required transcription and translation machinery [31, 33] and irradiating the desired sections. Macroscopic shape changes of the tissues could be achieved by patterning droplets with different salt concentrations and thus creating osmolarity gradients within the material. Water moves across the bilayer membrane between droplets of differing osmolarity, causing shrinking or swelling of droplets thus the change of shape of the prototissue [32]. This shape change is another interesting example of an emergent, biomimetic property in a tissue-like material.

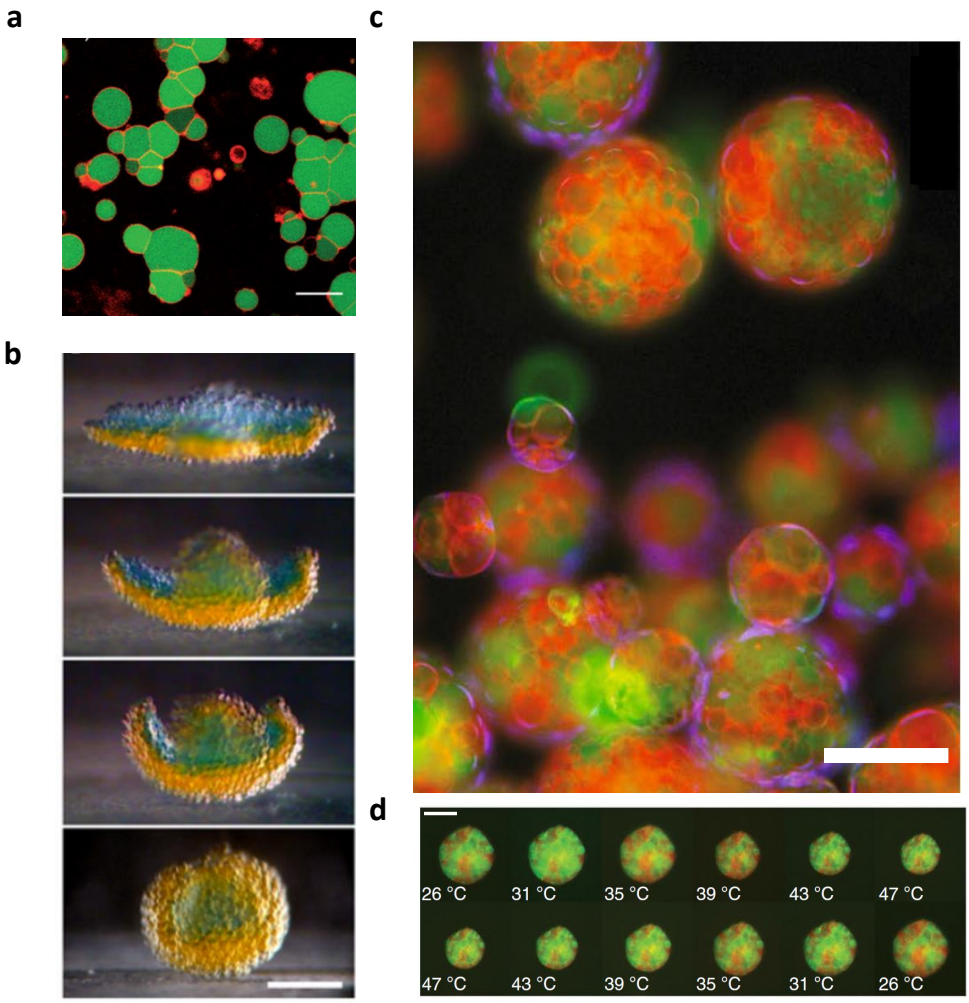

FIGURE 1.5. (a) A fluorescence microscopy image of GUV colonies. Reproduced from reference [28]. Scale bar 30 μm. (b) Photographs of a flower shaped synthetic tissue formed from a network of lipid coated aqueous droplets in oil. The blue and orange droplets were printed with different osmolarities and over time the synthetic tissue folds. Reproduced from reference [34]. Scale bar 200 μm. (c) Prototissue spheroids formed from bio-orthogonally ligated crosslinked proteinosomes and (d) fluorescence microscopy images of prototissue spheroids upon application of temperature changes. (c) and (d) are reproduced from reference [29]. Scale bars (c) 100 μm and (d) 50 μm.

An elegant example of a prototissue formed from a non-lipid-based protocells comes from Gobbo et al [29]. Two populations of bio-orthogonally active proteinosomes were prepared by attaching either an azide or strained alkyne moiety to the protein-polymer nanoconjugate which is used to stabilise the Pickering emulsion. By mixing the two populations and using them in the formation of a water-in-oil-in-water Pickering emulsion, they are brought into close contact.

Crosslinking and removing the oil then induces an interfacial strain-promoted alkyne-azide cycloaddition reaction between the two populations, resulting in self-supporting prototissue spheroids, which could demonstrate a range of collective behaviours. Proteinosomes have been previously demonstrated to show temperature dependant contractile behaviour due to the use of the thermoresponsive polymer poly(N-isopropylacrylamide) PNIPAAm in their membrane. The prototissue spheroids showed a volume contraction far greater than that seen for isolated proteinosomes. This contraction could be halted by the enzyme mediated formation of a hydrogel within the prototissue spheroid. Furthermore, as an example of mechanochemical transduction the researchers showed that contraction of prototissue spheroids could be used to modulate the rate of enzyme reactions housed within the proteinosomes. The authors suggested that in the future these prototissues could be developed with a wide range of functions using the techniques previously employed to create proteinosomes capable of behaviours such as gene-directed protein synthesis and hierarchical storage and release behaviour.

1.2 Hydrogels

A hydrogel is a hydrophilic 3D network of fibres or polymers that contains large quantities of water. Tangling or crosslinking within the network mean that it is insoluble despite the high-water content [35–37]. Hydrogels are viscoelastic materials [38], and exhibit both solid like and liquid like properties [35, 39]. A simple method for demonstrating the formation of a hydrogel is the vial inversion method. The gelation steps are carried out in the base of a vial or tube, before the vial is inverted. A liquid will flow as the vial turns but if a gel has been formed it will remain in the original shape. Rheology is a more quantitative approach for looking at the mechanical properties that are characteristic of hydrogels and this is discussed in Chapter 2.

The mechanical, swelling or stimuli responsive properties of hydrogels vary with the composition and method of formation of the hydrogel and the details of this are discussed in the rest of this chapter [40]. The unique characteristics of hydrogels, as well as the diversity that is possible, have led to their use for biomedical applications such as drug delivery, contact lenses, tissue engineering and wound dressings, and for other applications such as diapers and water retention agents in soil [41].

1.2.1 Polymer hydrogels

Two major classes of hydrogel are polymer hydrogels and molecular hydrogels (supramolecular hydrogels) [35]. Molecular gels are formed via the assembly of low molecular weight gelators (LMWGs) due to non-covalent interactions such as Van der Waals, hydrogen bonding, dipole interactions or π-π stacking. LMWGs assemble into fibres, which then tangle to form a network, causing the solution to become a hydrogel [35].

The hydrogels utilised in this thesis are polymer gels, and thus most of the discussion presented here focuses on these. Polymer hydrogels consist of chemically or physically crosslinked hydrophilic polymer chains [36, 39, 41]. The polymers in question can be synthetic or natural, and the chemistry of the polymer and the way it is crosslinked affects the properties of the resulting hydrogel.

1.2.1.1 Biopolymer hydrogels

Naturally occurring macromolecules (biopolymers) can be crosslinked to form hydrogels [41]. For biomedical applications these often show an advantage over synthetic hydrogels since they are biomimetic and tend to show high biocompatibility [41, 42]. Biopolymers include polysaccharides, polypeptides and polynucleotides [41]. In nature polynucleotides (nucleic acids) such as DNA are used for information storage, but they are also a useful building block for the assembly of materials [43]. Polynucleotides are formed from nucleotides, made up of a nuclear base, a sugar and a phosphate ester, linked via phosphodiester bonds [44]. Hydrogels can be formed via various methods, some of which lack precise control and some of which take advantage of the specific binding possible with polypeptides to form hydrogels with control over the molecular structure [43].

Polypeptides, which in nature are referred to as proteins, are polymers of amino acids linked via amide bonds [44]. Common natural polypeptides used in hydrogel formation are the structural proteins fibrin and collagen [42]. Pre-designed polypeptides can also be synthesised in the laboratory and used for hydrogel formation.

Polysaccharides are polymers formed from sugars linked via acetal (or glyosidic) bonds. Sugars are cyclic hemiacetals in which all the carbons of the ring are attached to an OH or C=O group [44]. One example of a polysaccharide that is often used to synthesise hydrogels is cellulose. Cellulose is a polymer of 1,4 linked glucose rings and is the most abundant polymer in nature [45]. Importantly the glucose rings are linked via an β linkage (equatorial) meaning that the cellulose molecule is linear and extra hydrogen bonds form between the OH groups of carbon 3 of the rings making the molecule rigid. Cellulose is insoluble in water but can be dissolved in solvent systems, such as sodium hydroxide/ urea mixtures, to allow hydrogel formation [46]. Water soluble derivatives of cellulose are also used in hydrogel synthesis [47, 48]

Other polysaccharides commonly used in hydrogels include agarose, alginate, dextran and chitosan [42, 49–52]. Chitosan is a derivative of chitin, a polysaccharide formed from amino sugars (N-acetyl-D-glucosamine) (sugars that have nitrogen functional groups). Chitin has a structure like cellulose and is insoluble [45]. Chitin is (partially) deacetylated to form chitosan which, when enough deacetylation has occurred, is soluble in aqueous acidic solution due to the presence of amine groups [45]. Chitosan or derivatives of chitosan are regularly used to form cationic hydrogels and depending on the functionalisation can be crosslinked via a variety of methods [50, 53].

1.2.1.2 Physically crosslinked hydrogels

Physically crosslinked polymer hydrogels form as a result of non-covalent interactions between polymer chains. Physical crosslinks include hydrogen bonds, complexation, hydrophobic association, dipole interactions, helices and regions of crystallisation [36, 37, 54]. The interactions may occur at specific points (point crosslinks) or over regions (junction zones) [36]. Due to the nature of these interactions, the formation of the network is reversible and the hydrogel can be converted back to a solution, often by an increase in temperature (thermoreversible) [36, 37].

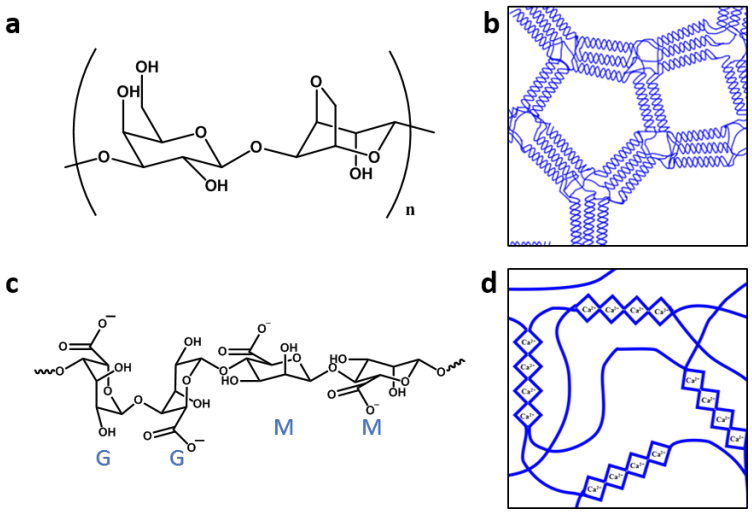

FIGURE 1.6. (a) The chemical structure of agarose, which is formed from repeating units of the diasacharide agarbiose (1, 3-linked α-D-galactopyranose and 1,4-linked 3,6-anhydro-R-L-galactopyranose). (b) a cartoon representation of the structure of an agarose hydrogel. Individual polymer chains interact to form double helices, which then aggregate. (c) A representation of the chemical structure of alginate, labelled G and M indicating guluronic acid and mannuronic acid respectively. In reality some regions of the polymer may containg only G or only M and some regions may be mixed. (d) a cartoon of the structure of an alginate hydrogel. G containing regions chelate Ca^{2+} ions causing crosslinking of the polymer chains.

A well-known example of a thermoreversible hydrogel is that formed by the biopolymer agarose. Agarose is made up of repeat units of 1,3-linked α-D-galactopyranose and 1,4-linked 3,6-anhydro-R-L-galactopyranose (Figure 1.6a) [55]. As the temperature of a hot agarose solution is cooled polymer chains associate via hydrogen bonds and form double helices, which aggregate together to form a hydrogel upon further cooling (Figure 1.6b). The aggregation of the junction zones results in large water-containing pores in the network, which affords the diffusion of a

range of molecules [55]. Agarose hydrogels are often weakly ionic due to the presence of impurities [49].

Some polyelectrolytes can be crosslinked via the addition of multivalent ions, resulting in the formation of ionotropic hydrogels. One commonly used example of such a gel is the crosslinking of alginate by calcium ions (Figure 1.6c-d). Alginate is a polysaccharide of β-d-mannuronic acid (M) units and α-l-guluronic acid (G) units. It is a block copolymer, since some regions of the polymer contain only M or G units and some regions are formed of alternating M and G units. Addition of Ca^{2+} ions forms a hydrogel because guluronic acid chelates the multivalent cation [42].

1.2.1.3 Chemically crosslinked hydrogels

Chemically crosslinked polymer hydrogels consist of polymers covalently linked to form an infinite network and such hydrogels are usually irreversible [36]. The hydrogels can be formed by crosslinking of existing polymers or in situ formation of a crosslinked network through polymerisation of an aqueous solution of monomers (Figure 1.7) [41, 56].

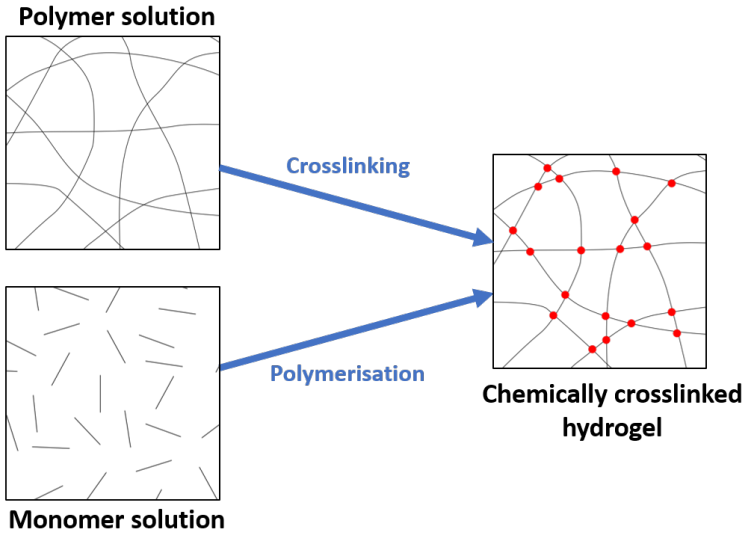

FIGURE 1.7. A scheme showing the formation of chemically crosslinked hydrogels via covalent crosslinking of pre-existing polymers or polymerisation of monomer solutions.

1.2.1.4 Bifunctional chemical crosslinkers

Polymers can be crosslinked via the addition of a bifunctional (or higher levels of functionality) crosslinking agent that can react with functional groups present on the polymer chain [41]. This method of crosslinking is particularly common for biopolymers. Thoroughly mixing chemical crosslinkers with their substrates is needed if a homogeneous hydrogel is to be achieved, and this

can be difficult if the reaction occurs rapidly when the two are combined. Relying on diffusion of the crosslinker can result in heterogeneous crosslink density [54]. Common chemical crosslinkers include glutaraldehyde or epichlorohydrin for crosslinking hydroxides or amines on polymers such as polyvinyl acetate (PVA) [54], chitosan [57], [58] or cellulose [46, 59]. Many other systems have also been developed, such as the use of click chemistry based crosslinkers. Click chemistry reactions are very specific and occur rapidly under mild conditions which makes hydrogels using this chemistry of particular interest for in situ hydrogel formation in biological applications. One example is the hydrogel reported by Truong et al, in which azide functionalised chitosan is crosslinked by a three-armed peg crosslinker containing an activated ester alkyne [60].

1.2.1.5 Free radical polymerisation

Free radical polymerisation is a method commonly used to form polymers from vinyl monomers, converting the unsaturated bond to an alkane. The polymerisation occurs via three steps: initiation (Equation 1.4), chain propagation (equations 1.5 to 1.7) and termination (equations 1.8 to 1.9). In the initiation step, ultraviolet (UV) or visible light, temperature or redox is used to homolytically dissociate an initiator molecule to form radicals. Homolysis under relatively mild conditions requires the presence of a weak bond within the initiator molecule and so common examples of initiators include peroxides and azo compounds. The radicals formed by the cleavage of the initiator react with the double bonds in the vinyl monomers, forming a new radical (Equation 1.5). These radicals react with more monomers, and this step repeats over and over in the propagation stage, growing the polymer chain (Figure 1.8). Coupling of two radicals or disproportionation via the reaction of two radicals terminates the chain growth, halting the polymerisation [61]. Radical polymerisation reactions are often carried out in oxygen free environments because oxygen inhibits the reaction. When a radical reacts with molecular oxygen the species formed is much less reactive and thus the chain propagation is slowed.

(1.4) $$I \rightarrow 2R^{\bullet}$$

(1.5) $$R^{\bullet} + M \rightarrow RM^{\bullet}$$

(1.6) $$RM^{\bullet} + M \rightarrow RMM^{\bullet}$$

(1.7) $$RM_n^{\bullet} + M \rightarrow RM_{n+1}^{\bullet}$$

(1.8) $$RM_n^{\bullet} + RM_m^{\bullet} \rightarrow RM_{n+m}$$

(1.9) $$RM_n^{\bullet} + RM_m^{\bullet} \rightarrow RM_n + RM_m$$

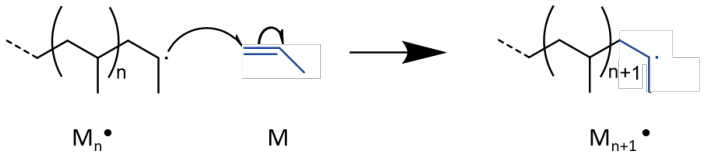

FIGURE 1.8. Mechanism for chain propagation during free radical polymerisation.The radical on the growing chain ($M_n^\bullet$) attacks the double bond on the vinyl monomer (M), resulting in a longer polymer chain $M_{n+1}^\bullet$). The reaction corresponds to Equation 1.7. The blue colour identifies the vinyl monomer before and after radical attack.

Polymerisation of hydrophilic monomers in the presence of a bifunctional crosslinker such as ethylene glycol dimethacrylate or methylene bisacrylamide can be used to form a hydrogel [41]. Co-monomers can be introduced to change the properties of the resulting hydrogel, although polymerisation of monomers with different reactivity can be problematic [41, 61]. When biological materials such as cells or proteins are present during the gelation, it is important to consider the conditions used. For example, radical initiators such as the ammonium persulphate (APS)/ tetramethylethylenediamine (TEMED) pair can damage proteins, as can UV light [40].

Functionalisation with groups that can undergo radical polymerisation means that free radical polymerisation can also be used to crosslink pre-existing polymers into a hydrogel [41]. Commonly used polymerizable moieties include methacrylate, acrylate and styrene. Numerous examples of hydrogels formed via functionalisation of polymers such as dextran [62, 63], hyaluronic acid [64], carboxymethyl cellulose [47], glycol chitosan [53], PVA [54] and PEG [65] have been reported. The approach for addition of polymerizable groups to the polymer varies according to its inherent functionality [47, 53, 62–64]. As with polymerisation of monomers, the stimuli that induces hydrogelation (such as light or heat) depends on the initiator used.

1.2.1.6 Photogelation

A common method for forming hydrogels using light (photogelation or photocrosslinking) is the use of a photoinitiator with one of the species described in Section 1.2.1.4, but some molecules have functionality that allows crosslinking upon irradiation via a different mechanism. For example, Yin et al functionalised carboxymethyl chitosan with azidobenzaldehyde [66]. Upon UV irradiation the azide group loses N_2 and forms a nitrene, which can undergo a number a of different reactions to crosslink the polymers. The most likely is reaction with the amine groups of the chitosan [67].

Photogelation (both using radical initiators or direct functionality) is an attractive method for hydrogel formation because it is rapid, can be readily applied to a range of polymers and to form a range of hydrogel shapes and can be carried out at physiological temperatures [53, 63]. Furthermore, if the light responsive moieties are distributed evenly in solution or on the polymer,

then problems of uneven crosslinking resulting from diffusion of chemical species, which occur in chemical crosslinking are avoided [54]. Photogelation also allows facile patterning of the hydrogel (see Section 1.2.5) [65, 68].

The crosslinking in hydrogels formed by light is affected by the extent of functionalisation with crosslinkable groups, depth of the sample, the power of the light source and the irradiation time and hence these factors can influence the mechanical and swelling properties of the hydrogel [53, 66]. Since light is absorbed as it passes through the hydrogel, the photo crosslinking is reduced in lower parts of the gel. This imparts a limit on the size of the hydrogel that can be crosslinked using this method, unless layer by layer manufacture or more sophisticated methods using focused lasers are applied [53, 69].

1.2.1.7 Other routes to chemically crosslinked hydrogels

The design of new hydrogels with different methods of formation or properties is a huge field of research, and thus it is unsurprising that there are routes to forming chemically crosslinked hydrogel which have not yet been touched upon in this discussion. Examples include enzymatic crosslinking and high energy radiation. Many enzyme crosslinked hydrogels rely on the enzyme HRP which can crosslink phenolic hydroxide groups in the presence of H_2O_2. The polymer desired for the hydrogel backbone can be functionalised with phenol containing functional groups to allow HRP mediated crosslinking. The concentration of enzyme controls the gelation kinetics whereas the concentration of H_2O_2 and functionalisation on the polymer control the extent of crosslinking and thus the mechanical properties [70].

High energy radiation (gamma or electron beams) can be used to crosslink polymers to form hydrogels since the radiation causes homolytic cleavage of C-H bonds, resulting in radicals, which recombine to form covalent crosslinks. Examples of polymers which can be crosslinked in this way include PVA and polyacrylic acid (PAAc) [40].

1.2.1.8 Mechanical properties of hydrogels

Polymer hydrogels often have poor mechanical properties: they are relatively weak, soft and brittle and have low tensile strength (break upon large deformation) [40, 71]. This is put down to the high-water content but also the inhomogeneity of the network due to defects such as loops or dangling chains [40, 71]. The mechanical properties are also affected by the overall polymer concentration, crosslink density, conditions of formation and nature of the polymer [40] [39]. Increasing the density of crosslinking improves the mechanical properties, although above a certain optimum value hydrogels go from ductile to brittle [37]. Increasing the hydrophobicity of the polymers used for the hydrogel formation or reducing the porosity of the hydrogel can also improve the mechanical properties [37].

Often the rubber/ elastic behaviour of materials is characterised using tensile testing to find the elastic modulus, but for hydrogels with poor deformability this can be difficult. The elastic

modulus is a measure of a materials resistance to elastic (reversible) deformation by an applied stress. Other techniques such as fracture strength tests and compressive testing can also give information on the mechanical properties of hydrogels [72, 73]. A commonly used test for looking at the viscoelastic properties of hydrogels is oscillatory rheology and the details of rheological testing are outlined in Chapter 2 [40].

1.2.1.9 Composite hydrogels

Interpenetrated network (IPN) hydrogels are formed by the gelation of two separate networks in one hydrogel. The two networks are entangled and interact physically but are not covalently bonded to each other [74]. IPN hydrogels can show enhanced mechanical properties, and increased magnitude and kinetics of swelling [74]. Semi-IPN hydrogels, where one polymer in the network exists as linear polymer rather than being crosslinked, can also show altered properties due to interactions between the polymer and the hydrogel or changes in the structure of the hydrogel network [52, 74]. Double network (DN) hydrogels are specific kind of IPN hydrogel, in which a loosely crosslinked non-ionic hydrogel is formed within the network of a dense ionic hydrogel, and they exhibit very high mechanical strength and toughness [75].

Hydrogels containing nanometre sized objects, such as metal or silica nanoparticles, clays or carbon nanotubes, are referred to as nanocomposite hydrogels. The nanostructures can be absorbed into the gel after formation, present in the mixture during the gelation process or in some cases are used as the crosslinker [71, 76]. Including different nanostructures within a hydrogel can affect the mechanical properties or swelling. It can also provide additional functionalities or stimuli responsive behaviours to hydrogels, for example by using nanoparticles functionalised with cell adhesion peptides [71, 76]. There are various possibilities as to why the inclusion of nanoparticles within hydrogels can significantly improve the mechanical properties. In some cases, it has been shown to be due to interactions between the particles and the polymer, which effectively induces physical crosslinking in addition to the crosslinking already present [77–79]. For example, silica nanoparticles form hydrogen bonds with polymers such as polyacrylamide (PAAm) and have thus been shown to increase the elastic modulus of the hydrogel above levels that can be achieved with increased chemical crosslinking alone [80].

1.2.2 Hydrogel swelling

The hydrophilic nature of the polymers used within hydrogels means that water moves into the polymer matrix causing it to swell, however due to the crosslinking of the polymer an elastic retraction force resists the expansion. This is described by considering the total change in Gibbs free energy (ΔG_{total}):

$$\Delta G_{total} = \Delta G_m + \Delta G_{el} \tag{1.10}$$

Here ΔG_m is the Gibbs free energy change of mixing and ΔG_{el} is the Gibbs free energy change due to the elastic retractive forces. When ΔG_{total} is zero, the osmotic and elastic forces are balanced, and the hydrogel has reached its equilibrium swelling [40, 41]. Like the mechanical properties, the extent of swelling of a hydrogel is affected by the crosslinking and the overall polymer concentration: the higher the crosslink density or the polymer concentration, the lower the swelling capacity [37, 71]. The nature of the polymer also affects the equilibrium swelling. For ionic (polyelectrolyte) hydrogels, macroscopic electroneutrality demands that all the counterions of the ionic groups are contained within the hydrogel volume [81]. Unequal distribution of mobile ions between the hydrogel and the surrounding solution increases the osmotic pressure, and thus the ionic contribution to the Gibbs free energy (ΔG_{ion}) must also be considered [37, 39]. The higher the charge density of the polymer network, the greater the swelling, because more counterions move into the hydrogel, which causes a greater osmotic pressure [37, 39].

Various methods have been reported to quantify the swelling of hydrogels. Most commonly a gravimetric method is used [40, 58, 66, 82–84]. A hydrogel is first completely dried in order to find the dry mass (M_d), and is then allowed to reach equilibrium in the desired swelling medium. Excess solution is removed and the swollen weight (M_s) of the hydrogel measured. The normalised swelling ratio (S_r) can be calculated as:

$$S_r = \frac{M_s - M_d}{M_d} \tag{1.11}$$

In some cases, the gravimetric method is applied by comparing the weight of the swollen hydrogel to the weight of the as formed gel, rather than the dry gel [50]. Other methods have also been reported, such as calculating a volume ratio using the volume of the as formed gel and the swollen gel [85, 86], or simply monitoring the diameter of a gel piece or bead [68, 87].

As well as looking at the extent of swelling of a hydrogel, the rate of swelling is also important for many applications. The swelling of hydrogels is complex, involving both the diffusion of water into the network and the relaxation of the polymer chains [88]. The reliance on slow diffusion of water in or out of the network limits the swelling or deswelling kinetics [39, 40]. Decreasing the size of the hydrogel can increase the rate of swelling or deswelling (the rate is inversely proportional to the square of the gel size) [39]. Increased hydrophilicity of the polymers used in the hydrogel and increased porosity also increase the rate of swelling. Water can move through the interconnected pores of microporous hydrogels via convection, and since this is faster than diffusion it they demonstrate increased rates of swelling [39].

1.2.3 Diffusion and partitioning in hydrogels

A solute added to the bulk aqueous solution around a hydrogel will partition between the aqueous and hydrogel phases and the partitioning is affected by steric, electrostatic interactions and specific chemical interactions [49]. Large molecules that cannot pass between the polymer chains may be totally excluded from the hydrogel. In the absence of interactions between the polymer

chains and the solute, the concentration of solute in the bulk aqueous phase would be equal to that in the aqueous phase of the hydrogel, although the overall concentration within the hydrogel is also dependant on the volume fraction of water within the gel. Repulsive electrostatic interactions between the solute and polymer can cause the solute to be excluded from the hydrogel, thus resulting in a lower concentration of solute in the hydrogel than the bulk [49]. Attractive interactions (specific or non-specific) lead to concentration of the solute within the hydrogel [49]. Changes in pH and ionic strength can affect the electrostatic interactions and thus the partitioning [49].

Mass transport within a liquid occurs via diffusion or convection [13]. Diffusion occurs when a concentration gradient is present, in accordance with the second law of thermodynamics [13]. Individual particles move in a random walk due to collisions with surrounding molecules, but overall the solute moves from a region of high concentration to low concentration. Fick‘s law relates the solute flux to the concentration gradient via a constant known as the diffusion coefficient [13]:

$$J = -D\frac{dc}{dx} \tag{1.12}$$

where J is the flux of a particle, D is the diffusion coefficient and $\frac{dc}{dx}$ is the change in concentration in space. The diffusion coefficient can be described as [13, 89]:

$$D = \frac{(k_B T)}{f} \tag{1.13}$$

where $k_B T$ is Boltzmann constant, T is the temperature and f is the frictional force, that relies on the size and shape of the particle and the viscosity of the solution [13].

Solute molecules diffuse through the water filled spaces and pores of a hydrogel and the diffusion coefficients are reduced compared to that in bulk aqueous solution [49, 90]. The reduction in diffusion coefficient occurs due to solute interactions with the polymer chains, the hydrogel obstructing the passage of a solute or an increase the hydrodynamic drag on the solute (increasing f) [49, 89]. Decreased pore size, free space or water content of a hydrogel cause lower values of D, and so the polymer concentration and crosslinking density of the hydrogel are important [89, 90]. The size of the solute will affect its ability to pass through the spaces in the gel and thus its diffusion [89]. Changes in pH or ionic strength that effect the electrostatic interactions between the polymer and solute, also lead to changes in D [49]. In some cases, changes in pH or ionic strength (or other stimuli) may affect the swelling of the hydrogel (see Section 1.2.7) and this can affect diffusion.

1.2.4 Enzyme immobilisation in hydrogels

Hydrogels loaded with enzymes have been developed for the creation of biomaterials, biocatalysts and biosensors [91, 92]. Immobilisation of enzymes within hydrogels can improve their

recyclability and stability [87, 92] but it can be problematic since the porous nature of hydrogels means that proteins can often diffuse through the structure, leading to leakage into bulk solution [49, 92, 93]. To try and physically trap enzyme in the gel the crosslinking of the hydrogel can be increased [94]. Various other strategies for immobilising enzymes have been reported, such as covalent attachment onto the hydrogel [87, 95], electrostatic interactions with the hydrogel [94], attaching the enzyme onto nanoparticles used in the formation of a nanocomposite [78] and trapping within polymersome microcapsules in the hydrogel [93].

1.2.5 Creating patterns and gradients in hydrogels

For many applications of hydrogels, it is desirable to be able to create patterns, structures or gradients within the gel. This is important in achieving a non-uniform response to stimuli required for actuators and soft robotics (see Chapter 5) and for mimicking the heterogeneity of living tissues when using hydrogels for tissue engineering. Gradients or patterns can be created in the hydrogel matrix itself, relating to a variety of properties such as overall polymer concentration, porosity, crosslink density, mechanical properties and nature and functionality of the polymer [96]. Gradient hydrogels can be created by first creating a gradient of prepolymer solutions and then crosslinking, but other methods include gradient UV exposure for photocrosslinking [96–98]. Gradients or patterns of functional molecules can also be attached to the hydrogel network after crosslinking. For example, Vega et al created a hydrogel uniformly functionalised with norbornene moieties to which they could attach thiolated peptides using a photoclick reaction [99]. By applying graded UV light they could create multiple concentration gradients of different peptides on the hydrogel scaffold. Using light to crosslink hydrogels or functionalise them post-synthesis also allows more complex 2D or 3D patterning via methods such as photomasking [65, 95], two photon polymerisation [69] and laser writing [95, 100].

Another method which is increasingly being used in the fabrication of hydrogels is 3D printing. 3D printing is an additive manufacturing technique in which hydrogel inks are deposited onto a surface via extrusion or as droplets, to gradually build up structures [101]. This technique can be used to build up complex hydrogel geometries, and by using multiple inks can also be used to create heterogeneity within the hydrogel, for example by patterning microparticles within the matrix [102]. Other methods for patterning nano or micro particles (including cells) within hydrogels usually first create the pattern in the pre-gel solution and then gelate to trap the particles in the desired arrangement. Methods which have been used for patterning include acoustic trapping [103] and electropatterning [65, 104].

Heterogeneity in hydrogel structure can also be introduced by joining together hydrogel pieces with different functionalities or concentrations of soluble molecules. Hydrogel pieces can be joined by physical or covalent bonds. Chiang et al created heterogeneous hydrogels by using electric manipulations to pattern prepolymer droplets and microgels into larger patterns [104]. Adding dyes to certain pieces allowed the creation of soluble chemical gradients upon crosslinking.

Gradients of soluble molecules are of particular interest in tissue engineering. Such gradients can be set up in hydrogels by localised delivery of a molecule, for example using flow based systems such as microfluidic devices [105]. Choi et al created hydrogels with built in microfluidic channels that could be used for controlled delivery and creation of chemical gradients [106]. Hydrogels can also be fabricated with soluble molecules localised in specific areas so that they diffuse outwards over time [107]. Patterns or gradients of functional molecules attached to the hydrogel network can also be released to create soluble gradients if a cleavable crosslinker is included [95]. Another approach is to load micro or nanoparticles with the biomolecules of interest and pattern them within the hydrogel so that they release it over time or on application of a stimulus [102].

1.2.6 Smart hydrogels

A smart or intelligent material is one which has some property that changes in response to an external stimulus. Hydrogels can be designed to respond to a range of physical or chemical stimuli by incorporating different chemistries into their structures. The response is often a change in the swelling or reversal of the sol-gel process (Figure 1.9) [40]. Some smart hydrogels respond to stimuli in other ways such as a change in optical properties or colour [108] or bond cleavage resulting in release of a functional molecule [95]. Stimuli to which hydrogels can be programmed to respond can be divided into chemical stimuli (pH, ionic strength, recognition of specific molecules, redox) and physical stimuli (temperature, electric current, magnetism, light) [40]. Smart hydrogels are of interest for a wide range of applications, including drug delivery, valves in microfluidics, actuators (see Chapter 5) and sensors [68, 109].

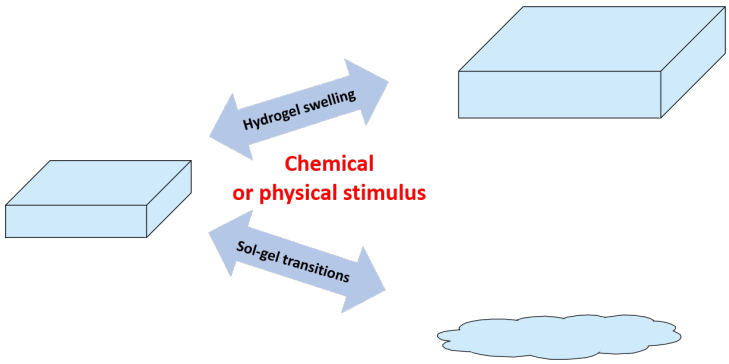

FIGURE 1.9. Cartoon depiction of the swelling or sol-gel response of a hydrogel upon application of a chemical or physical stimulus.

1.2.7 Stimuli responsive hydrogel swelling

1.2.7.1 pH responsive hydrogel swelling

Hydrogels containing pendant acidic (anionic) or basic (cationic) groups exhibit pH responsive swelling behaviour due to the variation in degree of ionisation with pH [40]. As with all hydrogels the swelling degree is a balance between the osmotic driving force and the elasticity of the hydrogel network [46, 58]. All the counterions of the ionic groups are within the hydrogel [81]. So, as pH change causes an increase in ionisation, it also causes an increase in counterions within the hydrogel and thus an increase in the swelling. The change in swelling occurs around the pK_a or pK_b of the ionic group [40]. As a result, basic hydrogels show maximum swelling at low pH when they are protonated (and positively charged) whereas acdic hydrogels show maximum swelling at high pH when they are deprotonated (negatively charged) [37]. The electrostatic repulsion between charged groups also plays a role in the swelling or deswelling [81, 88].

As previously discussed (Section 1.2.2), the extent of crosslinking, overall concentration, nature of the polymers and porosity can affect the swelling. In the case of polyelectrolyte hydrogels some additional factors must be considered. The number of pH responsive functional groups within the hydrogel affects swelling. More pH responsive groups means the charge density and number of counterions is greater and therefore so is the swelling. The nature of the swelling media is also important. Swelling of polyelectrolyte hydrogels is reduced by higher ionic strength of solution as this reduces the difference in concentration of counterions between the inside and outside and increases charge screening between ionic groups within the hydrogel [37, 39, 46]. Increased valency of the counterions can also reduce polyelectrolyte hydrogel swelling as can specific ion effects (at constant valency and concentration), relating to the Hofmeister series [110]. The pH responsive swelling of bulk hydrogels is usually tested by equilibrating the hydrogel in buffers or HCl/ NaOH solutions at varied pHs and measuring the swelling using a gravimetric or volume-based method [58, 66, 83, 87, 111]. Often the ionic strength of the solutions is controlled by calculating ionic strength and adjusting all solutions to the same value, for example by adding sodium chloride [46, 88].

Cationic biopolymer hydrogels are often formed using the amine containing polymer chitosan and its derivatives [57, 58, 66, 88, 111], but there are other methods, including the use of quaternised cellulose [46]. Anionic hydrogels can be formed from a range of carboxylic acid containing biopolymers such as carboxymethyl cellulose [46, 112]. Synthetic hydrogels can be designed to show pH dependant swelling by utilising monomers with responsive functional groups, such as N-(2-(dimethylamino) ethyl)-methacrylamide (DMAEMA) (cationic) [83], or acrylic acid (anionic) [68]. Ampholytic hydrogels can be formed by combining polymers with cationic and anionic functional groups, or by using polymers that contain both [46, 66]. In this case, the swelling varies not just with pH but with the ratio of the two functional groups [46]. When the positive and negative charges are equally abundant, strong electrostatic attractions between the positive and negative charges leads to a dense, deswollen structure. Changes in the ratio of

functional groups or in the pH lead to changes in the electrostatic interactions and the osmotic pressure and thus changes in the swelling [46, 66].

Often the swelling response of a bulk hydrogel to a change in pH is slow, on the timescale of hours [58, 111, 112]. Factors which could increase swelling kinetics were discussed in Section 1.2.2. One important factor is the size of the hydrogel. For example, by creating hydrogel pieces just hundreds of micrometres in size, Beebe et al showed that the best cases the gels had a response time of less than 10 seconds after a change in pH [68].

1.2.7.2 Swelling in response to other chemical stimuli

Hydrogels can be designed to swell or deswell in response to specific molecules such as glucose, antibodies or DNA [40]. One example is the formation of hydrogels with phenylboronic acid side chains. When glucose is added it binds the phenylboronic acid, shifting the equilibrium between the neutral and anionic forms and thus changing increasing the osmotic pressure and swelling of the hydrogel [86]. Such systems are of great interest for the detection or treatment of diabetes.

Incorporating redox active moieties into a hydrogel allows the formation of gels that exhibit changes in swelling in response to oxidising or reducing conditions, and the mechanism of the volume change depends on the details of the system used. The redox process can change interactions between sections of the polymer. For example, Greene et al reported a system in which reduction of viologen containing sections of the polymer backbone resulted in radical cations that interacted and stacked, causing collapse of the polymer chain and shrinking of the gel via a fully reversible process [85]. Another method for conferring redox sensitivity to a hydrogel is the use of a redox sensitive crosslinker such as the supramolecular complexation of β-cyclodextrin polymer and ferrocene. Combining this with covalent (non-redox sensitive) crosslinking creates a hydrogel in which the swelling can be altered by redox reactions without reversal of the sol-gel transition [113].

1.2.7.3 Thermoreponsive hydrogels

Hydrogels that swell or deswell in response to changes in temperature are called thermoresponsive hydrogels. The behaviour arises from the thermoresponsive properties of the polymers used to form the hydrogel, which relates to changes in miscibility of the polymer and solvent at different temperatures. Some polymers exhibit direct thermoresponsive behaviour, where the polymer and solvent are immiscible below the upper critical solution temperature (UCST) and miscible above it. Other polymers show inverse thermoresponsive behaviour, with the polymer and solvent instead being fully miscible below a lower critical solution temperature (LCST) [40]. Thermoresponsive behaviour is due to changes in the Gibbs free energy of mixing (ΔG_m). For UCST the behaviour is governed by the magnitude of the enthalpic contribution, whereas in the case of polymers that have a LCST, the behaviour is controlled by an entropic effect [36].

Hydrophobic interactions and hydrogen bonds are key for this behaviour and thus thermoresponsive hydrogels tend to be those with hydrophobic side groups, or groups that are susceptible to aggregation [40]. PNIPAAm is common because the LCST is close to body temperature [40, 83]. Co-polymerising with other monomers can change the LCST and thermoresponsive behaviour [40, 83].

1.2.7.4 Swelling in response to other physical stimuli

Other physical stimuli that hydrogels can be engineered to respond to include magnetism, electricity and light [40]. Electric current responsive hydrogels are formed from polyelectrolytes, like those that respond to changes in pH [84]. Redox sensitive hydrogels can often also be controlled via electrochemical processes as well as chemical oxidation [114].

The advantage of using physical stimuli to alter hydrogel swelling is that they can be remotely controlled [40]. Light has an additional advantage in that it is easy to control spatially as well, and the changes caused are often reversible [115]. Photoresponsive hydrogels are formed by incorporating a photoreactive molecule into the polymeric network. Upon irradiation at the correct wavelength the photoresponsive moiety undergoes some change (typically isomerisation, cleavage or dimerization) that alters the properties of the hydrogel [115]. Photoresponsive moieties can be added as pendant groups on the polymers and, when irradiated, alter the hydrophilicity of the network. Alternatively, photoresponsive supramolecular complexes can be utilised as crosslinkers within the hydrogel. Thermoresponsive hydrogels can be converted into photoresponsive hydrogels via the inclusion of particles (such as gold nanoparticles) which convert light (near infrared) into heat, and thus cause swelling/ deswelling of the hydrogel [115].

Hydrogels can also be designed to exhibit response to more than one stimulus by combining some of the properties discussed so far. For example, a hydrogel formed by co-polymerising NIPAAm with DMAEMA showed both temperature and pH dependant swelling, as did an IPN hydrogel of Poly(2-ethyl-2-oxazoline) with crosslinked chitosan [83, 111].

1.2.7.5 Reversible hydrogels as smart materials

Polymer hydrogels can also be designed so that in response to a chemical or physical stimulus, the sol-gel transition is reversed [40]. For example, using light [115] or redox [116] responsive supramolecular complexes as the crosslinking mechanism for hydrogels means that it can be disassembled upon irradiation or application of chemical or electrochemical redox processes. These gels also show promise for creating self-healing hydrogels [116]. Many physically crosslinked hydrogels like agarose show thermoreversibility due to the nature of their bonding.

Molecular hydrogels are thermoreversible, but there are also many examples of molecular hydrogels that are designed to assemble or disassemble in response to other stimuli such as light, pH, redox or the presence of particular ions or molecules [35, 109, 115] .The stimulus interrupts interactions or causes some change in structure of the LMWG that allows or prevents

the interactions that lead to fibril and network formation (such as hydrogen bonding or π-π stacking) through a change in chemistry or sterics [115].

1.2.7.6 Smart hydrogels using enzymes

In nature, many processes are controlled by enzymes, and there is a growing trend for materials that mimic this by exhibiting changes in response to enzymatic stimuli [117]. Truly enzyme responsive hydrogels are those in which the enzyme acts directly on the hydrogel matrix causing some change in its properties [117], but this discussion also considers systems designed to exhibit an indirect response to an enzyme by, for example, responding to the presence of a product of the enzymatic reaction.

The use of enzyme sensitive crosslinkers, polymers or LMWGs can allow hydrogels to swell or exhibit sol-gel or gel-sol transitions in the presence of particular enzymes [22, 117]. For the formation of smart biomaterials, hydrogels can be designed to respond to enzymes already present in the body such as proteases [117]. Designing an enzyme-hydrogel system such that the hydrogel responds to a stimulus released by the enzymatic reaction essentially expands the number of chemical stimuli to which the hydrogel can respond [109]. As previously discussed many hydrogel systems have been designed to respond to changes in pH and these systems can be paired with enzymes such as glucose oxidase (GOx) or urease (URS), which bring about changes in pH upon reaction with their substrates. As mentioned in Section 1.1.2, GOx breaks down glucose to gluconolactone. Gluconolactone is hydrolysed to gluconic acid, and thus the enzymatic reaction causes a pH decrease. Using GOx in pH responsive hydrogels therefore allows them to respond to the presence of glucose. Numerous examples of such GOx containing systems have been reported including hydrogels that shrink or swell in response to the addition of glucose, dye containing hydrogels that show a fluorescence emission change in response to glucose and the assembly or disassembly of LMWGs upon addition of glucose [108, 118]. Urease breaks down urea into ammonia and carbon dioxide, resulting in a pH increase. Like GOx, it has been incorporated into hydrogels to allow changes in swelling or sol-gel transitions [119, 120].

Hydrogels can also be coupled to other enzyme induced stimuli. Ikeda et al created a self-assembled peptide hydrogel that disassembled in the presence of H_2O_2 and another which disassembled in the presence of NADH (nicotinamide adenine dinucleotide) and the enzyme nitroreductase [109]. Encapsulating enzymes such as oxidases or redox enzymes, which upon turnover of their substrates produce H_2O_2 or NADH respectively, meant that the hydrogels could exhibit sol to gel transitions in response to a wide range of biomolecules such as choline or glucose. Combinations of different enzymes and hydrogels allowed the authors to create hydrogels which exhibited OR and AND logic gate responses.

1.2.7.7 Increasing complexity

A variety of smart hydrogel systems have been built that exhibit increased complexity in their responses. These complex responses include autonomous behaviour, spatio-temporal patterning and oscillations. Such materials represent an important step towards intelligent, lifelike, hydrogel-based materials [121]. In classical stimuli responsive hydrogels perturbation of some environmental condition shifts an equilibrium, and the system changes to reach that state which is now most thermodynamically favourable [122]. External triggers determine when the change occurs and in order to reverse the change a different or opposite stimulus must be applied. Autonomous behaviour implies that the material exhibits some degree of self-regulation. In hydrogels such behaviours are often pre-programmed developments and changes over time [122, 123] and to achieve this some kinetic control is required, often using catalytically controlled processes [122].

Jaggers et al presented an example of self-regulated behaviour in a material by creating hydrogels in which different parts of the hydrogel respond to a uniformly applied stimuli at different times [120]. The system utilised the urease/ urea system to cause a pH increase. The hydrogel was formed by crosslinking alginate with Ca^{2+} and contained oil droplets in which there was pH indicator. A pH change caused a change in colour of the hydrogel, or in the presence of ethylenediaminetetraacetic acid (EDTA), which at high pH chelates Ca^{2+}, disassembly of the hydrogel and release of the oil droplets into solution. Hydrogels were initially in acidic solution, and at this pH urease shows low activity. The increase in pH upon addition of urea is autocatalytic because as the pH is increased urease become more active. Utilising this positive feedback mechanism, the researchers were able to programme the dormancy period between application of stimuli and degradation of the hydrogel by varying the enzyme concentration. Spatio-temporal patterning was achieved by heterogeneously distributing the enzyme within the hydrogel such that when urea was uniformly applied, regions with higher enzyme concentration responded quicker than those with low concentrations. Utilising the same system, the researchers were also able to create distinct hydrogel objects which were programmed to degrade or change colour at different times in response to the same stimuli. As an example of chemical communication between the objects the authors showed that interactions between the objects altered the time period over which the change occurred [123].

One well investigated mechanism for creating autonomous oscillatory behaviour in hydrogels is to couple them to the Belousov Zhabotinsky (BZ) reaction. The BZ reaction is an oscillatory chemical reaction and is a classic example of non-equilibrium system. The exact composition and conditions can vary but, in general, an organic substance is oxidised by bromate in the presence of a metal catalyst and under acidic conditions. The oscillatory behaviour occurs due to positive feedback and delayed negative feedback within the catalytic cycle and, because of it, in an unstirred system chemical waves arise [121]. Hydrogels can be formed from a co-polymer of NIPAAm and $Ru(bpy)_3$. $Ru(bpy)_3$ acts as a catalyst for the BZ reaction and the varying oxidation

state of the $Ru(bpy)_3$ moiety during the reaction cycle changes the hydrophilicity of the polymer. These changes cause the hydrogel to swell or shrink and change colour. Microgels exhibit overall size oscillations, whereas bulk hydrogels show the characteristic chemical waves of the BZ reaction propagating across the gel as swollen and shrunken regions [124].

Few examples of truly self-oscillating reactions in closed systems exist because they are incredibly complex to engineer. Oscillations are easier to engineer in open systems in which reagents can be continuously supplied and waste constantly removed, but such systems are not as interesting for the creation of self-regulating materials. The Walter lab have developed an alternative approach to creating self-regulating, autonomous behaviour that can be coupled to hydrogels [122, 125, 126]. The method revolves around the creation of programmable, transient pH states using *internal feedback systems* (IFS). It is important to note that this behaviour is inherently different to that seen in self-oscillating systems. The basic principle relies on two pH changing species, one *fast promotor* which rapidly changes the pH, activating the system, and one *dormant deactivator*, which gradually returns the pH to its original state. The difference in kinetics of the two processes is key, since addition of two species which both act rapidly in opposite directions will result in no change over time. The fast promotor is provided in the form of a shot of buffer of the desired pH state which instantly changes the system [122]. The dormant deactivator must be a slower process and can be generated by a slowly decaying species [126] or a catalytic (enzymatic [122]) process, such as the breakdown of urea by urease. The amplitude of the pH jump and development over time depends on the concentration of species used and the buffering capacity of any buffers. Furthermore, when the dormant deactivator is produced enzymatically, both the enzyme and substrate concentration can be used to program the autonomous behaviour and additional complexity is added to the system because the rate of an enzymatic reaction is also dependant on the pH. Building on this principle Heinen et al, developed a system in which both the activator and deactivator are dormant and generated by enzymatic reactions upon addition of a substrate [125]. Urease, which generates a pH increase, and esterase, which generates a pH decrease, were used as the antagonistic pair of enzymes. In order to achieve a transient pH state the rate of production of the activator was tuned to be higher than that of the deactivator by taking advantage of the inherent difference in activity of the enzymes used and using an excess of the enzyme responsible for the activation. In this case the time before activation occurred (lag time) as well as the lifetime of the transient state could be controlled by altering buffer concentration, overall enzyme concentration or the ratio of the different enzymes [125]. To couple this dynamic behaviour to hydrogels, they combined the systems with molecular hydrogels, formed from peptides or modified DNA, which showed pH dependant sol-gel transitions. When combined with the fast promoter/ dormant deactivator or dormant activator/dormant deactivator systems the hydrogels exhibited transient sol-gel cycles with the pH changes [122]. Utilising the system for the creation of transient pH states developed by the Walter lab, Che et al reported the formation of microgels that exhibited self-regulated, time-controlled changes in size [87]. The

hydrogel was based on the pH responsive polymer poly(N,N-diethylaminoethyl methacrylate) (PDEAEMA) and contained covalently linked urease. Addition of a mixture of acidic buffer and urea instantly dropped the pH and caused the microgels to swell. The urease then broke down urea and thus gradually increased the pH, causing shrinking of the microgels. The process could be repeated several times.

The use of antagonistic enzymes to create a transient pH state demonstrated by Heinen et al is an example of a biocatalytic reaction network. Such systems utilise enzymes and take advantage of positive and/or negative feedback. One advantage of these systems over inorganic systems such as the BZ reaction, is that they function under mild conditions [121]. Other examples of the use of biocatalytic reaction networks to bring autonomous behaviour to hydrogel systems include the temporal control of gel-sol-gel transitions by enzymes acting directly on the hydrogel network [127].

1.2.8 Thesis aims and overview

The aim of this thesis is to produce and characterise rudimentary synthetic prototissues by embedding colloidosome-based protocells within polysaccharide hydrogels, and to demonstrate that these prototissues are capable of interesting, programable behaviours, including communication, non-uniform response to stimuli, and chemo-mechanical transduction. As a simple mimic of the properties of living tissues, the goal is that such behaviours should be due to the collective behaviour of the components of the prototissue (and therefore be emergent properties).

The discussion in this introductory chapter outlined some of the key concepts which act as background to the work presented in the rest of this thesis. Building on these concepts, the following chapters present investigations into the structure of colloidosome protocells, and the formation of two novel, hydrogel-based prototissues.

CHAPTER 2

EXPERIMENTAL SECTION

2.1 Chapter outline

This chapter provides an outline of the materials and experimental methods and techniques used throughout this thesis. General information which applies throughout is presented at the start of the chapter and then detailed experimental methods are provided for each of the later chapters.

2.2 Materials

5-(4,6-Dichlorotriazinyl) Aminofluorescein (DTAF), DyLight^{TM} 650 NHS Ester (DL650) and DyLight^{TM} 405 NHS Ester (DL405) were purchased from ThermoFischerScientific. Universal indicator solution (pH 3 to 10) was purchased from Honeywell Fluka. All other materials used in this thesis were purchased from Sigma-Aldrich. All materials were used without further purification unless otherwise stated.

2.3 General techniques

2.3.1 Data analysis

Numerical data was analysed in Microsoft Excel and plotted in Origin graphing software. Images were analysed or processed in Fiji Image J or Volocity.

2.3.2 Microscopy

2.3.2.1 Optical microscopy

Samples to be imaged using optical microscopy were placed onto microscope slides or glass coverslips. Bright field optical microscopy images were captured on an Olympus BSX53 optical microscope.

For solutions/ suspensions to be imaged using fluorescence or confocal microscopy, channel slides were formed (Figure 2.1) and samples injected into the channels for imaging. Fluorescence microscopy images were captured on a Leica DMI 3000 inverted optical microscope with variable wavelength ultra-violet (UV) lamp attached. Widefield fluorescence microscopy images were captured on a Leica DMI6000 inverted epifluorescence microscope (Wolfson Bioimaging Facility), which was fitted with a motorised stage. In both cases the filter used varied with the nature of the fluorescent species being imaged. To image large areas widefield fluorescence microscopy was used with a tile scanning feature, in which the software captures multiple images across a sample and stitches them together. Images from all optical microscopy techniques were processed and analysed using Fiji Image J.

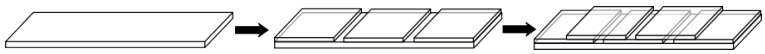

FIGURE 2.1. A scheme showing how channel slides are formed from glass slides and cover slips. Cover slips were stuck in place using UV cured glue.

2.3.2.2 Confocal microscopy

Confocal microscopy uses a pinhole to block out-of-focus light. This provides control of depth of field which is not possible using other optical microscopy, because fluorescence from areas other than that at the focal plane, is not detected. Confocal microscopy allows optical sections to be imaged and collecting multiple sections throughout the height of a sample (referred to as a Z stack) allows a 3-dimensional (3D) images to be compiled.

Confocal microscopy was carried out on Leica SP5II, Leica SP5 and Leica SPE microscopes (multi-laser CLSM, Wolfson Bioimaging facility) using a variety of dry lenses (x5, x10, x20 magnification). The settings were varied according to the fluorophore being imaged.

2.3.2.3 Scanning electron microscopy

Scanning electron microscopy (SEM) is a technique in which a beam of electrons is used to produce an image of a sample. As the electron beam is scanned over the surface, it interacts with the sample producing secondary electrons, backscattered electrons and x-rays. The imaging in this thesis uses the secondary electrons, which are electrons which are knocked out of the atoms near the surface of the sample due to inelastic collisions. Secondary electrons are detected and

used to compile the image. Variation in the angle of incidence of the electron bean on the surface affects how many secondary electrons are emitted and changes the brightness, and so the 3D nature of the surface is captured. To prepare sample for SEM imaging they were first dried using air drying or lyophilisation. Dry material was placed onto a carbon sticky pad on an aluminium SEM stub, and sputter coated with approximately 15 to 25 nm silver to prevent surface charging. Samples were imaged using a SEM IT300 microscope.

2.3.3 Photography and colour quantification

Colour can be represented numerically using several different systems. Often colour is reported as an RGB value, which refers to the combination of red, green and blue light needed to produce that particular colour. The RGB system reports a colour as three numbers between 0 and 255, referring to the intensity of the red, green and blue. The representation of colour using a cylindrical coordinates is more useful for some applications [128] and there are several different approaches to this. The work in this thesis utilises a HSL cylindrical coordinate system. In this system colour is represented by three values: hue, saturation and lightness. These are depicted by the schematic in 2.2. Hue is the angle around the central axis of the cylindrical coordinate system (what is essentially a colour wheel), with red at 0°, green at 120° and blue at 240°. Saturation is the intensity and lightness is how bright or dark a colour is. To fully describe a colour all three values are needed, but for some purposes hue can be used as a numerical representation of colour [123].

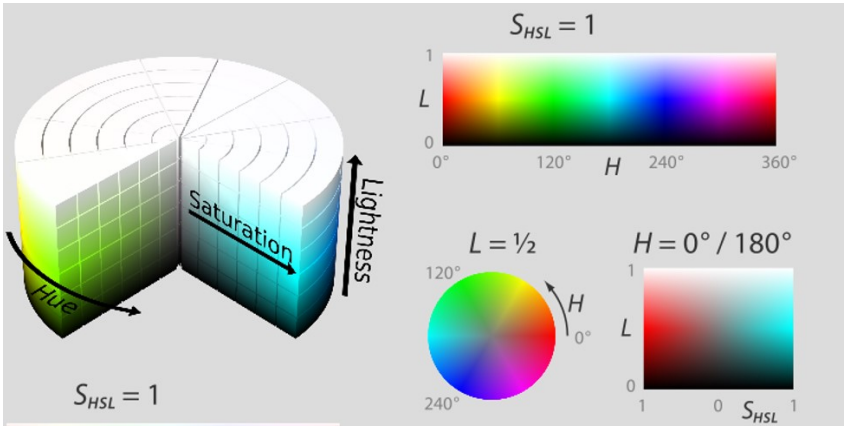

FIGURE 2.2. Depiction of the HSL coordinate space reproduced from reference [129]. On the right three cross sections are shown.

To convert an RGB measurement to hue angle the following method was used. Each of the R, G and B values is first converted to a value between 0 and 1 by dividing by 255:

$$\frac{R}{255} = r \tag{2.1}$$

$$\frac{G}{255} = g \tag{2.2}$$

$$\frac{B}{255} = b \tag{2.3}$$

Depending on which of these values is largest, a different formula is used for the hue angle calculation:
If r is the maximum:

$$hue = \frac{g-b}{max-min} \tag{2.4}$$

If g is the maximum:

$$hue = 2 + \frac{b-r}{max-min} \tag{2.5}$$

If b is the maximum:

$$hue = 4 + \frac{r-g}{max-min} \tag{2.6}$$

Where *max* is the maximum of the rgb values and *min* is the minimum. To convert hue to an angle it is multiplied by 60. If the value is above 360°, 360 is subtracted.

To calculate a value for the saturation first a value for L is needed:

$$L = \frac{max+min}{2} \tag{2.7}$$

$$S = \frac{max-min}{1-\sqrt{(2L-1)^2}} \tag{2.8}$$

A Canon EOS 500D SLR camera was used to capture photographs of hydrogels. Photographs were taken on a white background with a light above (referred to as top lit) or, when the image was to be used for colour measurements, on top of a lamp/ LED board (referred to as backlit). Backlighting in this way prevented issues with uneven illumination and glare which would affect the RGB values. Camera settings vary depending on the project and are specified where necessary. To measure average RGB values within a region the RGB measure plugin for Fiji Image J was used [130]. RGB value profiles along a line were collected using the RGB profile plugin [131]. RGB values were converted to hue angle (and in some cases saturation) using the calculations described above.

2.3.4 Spectroscopy

2.3.4.1 Ultraviolet-visible spectroscopy

Ultraviolet-visible spectroscopy (UV/Vis) experiments were carried out on Perkin-Elmer Lambda 25 or Lambda 35 UV/Vis Spectrometers in 1 cm wide quartz cuvettes. A background spectrum was taken using deionised water before measurements were taken.

2.3.4.2 Fourier transform infrared spectroscopy

FT-IR (Fourier transform infrared spectroscopy) experiments were undertaken on dry sample using a Perkin Elmer-Spectrum One FT-IR Spectrometer.

2.3.4.3 Nuclear magnetic resonance spectroscopy

Nuclear magnetic resonance spectra were collected using a a Varian 500a NMR spectrometer. All samples were dissolved in deuterated water (D_2O).

2.3.4.4 Fluorescence spectroscopy

Fluorescence spectroscopy experiments were carried out using a CLARIOstar plate reader (BMG LabTech). Access to this equipment was provided by BrisSynBio.

2.3.5 Measurement and adjustment of solution pH

An Inlab micro pH electrode attached to a Metler Toledo pH meter was used to measure solution pH at room temperature. Prior to use the system was calibrated using standard solutions. Adjustment of sample pH was carried out using HCl or NaOH. For experiments measuring pH over time a pH meter was connected to a computer for use with LabX software and the pH was automatically measured every 30 s.

2.3.6 Rheological characterisation of hydrogels

Rheology studies how matter deforms when a force is applied (Figure 2.3).

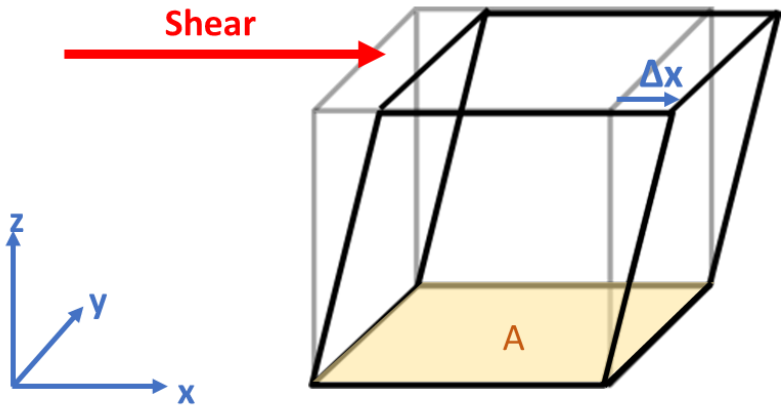

FIGURE 2.3. Application of a shear force over an area A results in deformation of the material (Δx).

Stress (σ) is defined as a force (F) per unit area, which in the context of Figure 2.3 is

$$\sigma = \frac{F}{A} \tag{2.9}$$

For the purposes of rheology, we consider shear stress, which is applied across a surface. When a stress is applied to an object, it deforms, and we define the strain (γ) as the deformation per unit length:

$$\gamma = \frac{\Delta x}{y} \tag{2.10}$$

Considering the behaviour of solids, when a force is applied to an elastic solid and it deforms and the energy is stored (as elastic potential energy). After removal of the force the energy is lost as the solid returns to the original shape [38, 77]. For a Hookean solid at low stresses and strains, stress is proportional to strain:

$$\sigma = G\gamma \tag{2.11}$$

Where G is the shear modulus. Fluids are often described as materials that flow; they deform when a force is applied and do not recover their original shape when the force is removed [38]. If a constant shear stress is applied to the surface of a liquid, it will move at constant velocity (u) until the force is removed [77]. Between the upper surface where the force is applied, and the bottom surface of the liquid, u will decrease. The rate of strain (also called the shear rate) (γÃá) is definde as [77]:

$$\frac{d\gamma}{dt} = \dot{\gamma} = \frac{du}{dz} \tag{2.12}$$

For a simple, newtonian fluid, shear stress is proportional to shear rate:

$$\sigma = \eta\dot{\gamma} \tag{2.13}$$

Where η is the viscosity [77]. As a force is applied to deform a liquid, viscous forces resist the movement, and the energy is rapidly dissipated as heat. Once the force is removed there is no energy remaining and hence no further deformation (or return to the original shape) occurs [38]. Liquids relax rapidly after application of a force. The time dependence of the stress strain relationship is a characteristic of viscous liquid behaviour, since for a solid the relationship between stress and strain is independent of time [38].

Hydrogels are viscoelastic materials which means that they exhibit properties which are a combination of solid like (energy storage) and liquid like (energy dissipation) behaviour [38]. This means that the relationship between shear stress and strain will show contributions from both elastic and viscous components [77].

A common rheological method for testing the mechanical properties of hydrogels is small-amplitude oscillatory shear (SAOS) experiments, where periodic torsional oscillations are applied to a sample z [38, 72, 77]. The sample is placed between a plate, which oscillates applying a given strain, and a cone. As periodic strain oscillations are applied an oscillating stress response will occur in the cone.

The lag period between the strain and stress response is referred to as the phase difference, δ (in radians). If the strain oscillations are applied to an elastic solid, the stress response is immediate (and in proportion to the strain) resulting in a $\delta = 0$. On the other hand, if a viscous fluid is tested the stress is instead proportional to the rate of strain and $\delta = \frac{\pi}{2}$. For testing a viscoelastic material the stored component will be in phase but the loss component will be out of phase with some value of $0 < \delta < \frac{\pi}{2}$. For a given angular frequency of oscillation (ω) the ratio of the maximum stress (σ_0) and maximum strain (γ_0) is constant, and is referred to as the complex modulus (G^*):

$$\left|G^*(\omega)\right| = \frac{\sigma_0}{\gamma} \tag{2.14}$$

Where σ_0 and γ_0 and the maximum stress and maximum strain respectively. The complex modulus can be described by two components, the storage/elastic modulus (G‘) and the loss/viscous modulus (G“) as follows [77]:

$$G^* = G^{'} + iG^{''} \tag{2.15}$$

G‘ represents the energy stored during the shear process (the solid like response) and G“ represents the energy dissipated (the liquid like response), so when G‘>G“ the material acts more like a solid and when G‘<G“ the material acts more like a liquid. SAOS experiments measure, δ, G‘ and G“ as a function of the strain (at fixed frequency) or frequency (at fixed strain). Usually a strain sweep is run to determine the linear viscoelastic region (where the absolute value of G^* is constant and independent of strain) and frequency tests are run within this region [72, 73].

Rheological testing of hydrogels was carried out using a Malvern Kinexus pro rheometer. Hydrogel samples were placed between a base plate and a parallel plate geometry (20 mm) and the system set to a temperature of 25 ° C for all experiments.

2.4 General experimental methods

2.4.1 Preparation of silica colloidosomes

Colloidosomes were formed using a method based on that developed by Li et al [5, 20, 21] and specific details of the colloidosomes used in each chapter of this thesis are described below (Sections 2.5.1, 2.6.1.1 and 2.7.1). In general silica nanoparticles with ca. 50% silanol and 50% dimethyl silane groups (supplied with this functionalisation, not prepared as part of this work), were added to 2 mL dodecane and sonicated for 5 minutes to disperse evenly. The desired aqueous phase (containing any large molecules to be encapsulated) was added (100 μL, ϕ_w = 0.2) and a Pickering emulsion was formed by shaking hard for 1 minute. To crosslink the colloidosomes, tetramethyl orthosilicate (TMOS) was added to the oil phase and samples were placed on a rotator for 24 to 48 hours. Colloidosomes were transferred into a continuous aqueous phase using solutions of increasing polarity. A 70% solution of ethanol in water (5 mL) was added to the colloidosomes in oil and the sample rotated to facilitate transfer from the oil to the aqueous phase. The sample was then centrifuged (3 krpm, 1 minute) and the oil and aqueous phases removed, leaving the colloidosome pellet. Colloidosomes were gently dispersed in 10 mL 70% ethanol and centrifuged again (2 krpm, 1 minute) to allow removal of the aqueous solution. This process was repeated in 50% ethanol and then deionised water. After transfer to water colloidosomes were dispersed in the desired aqueous phase (Deionised water (from now on referred to as DI water) or buffer).

2.4.2 Fluorescent labelling of proteins

Protein (20 mg) was dissolved in 8 mL sodium carbonate buffer (100 mM pH 8.5) and 200 μL dye solution (fluorescein isothiocyanate (FITC), Rhodamine B isothiocyanate (RITC), DyLight^{TM} 650 NHS ester or DyLight^{TM} 405 NHS ester), all 1 mg/mL in DMSO) was added dropwise. The solution was stirred at room temperature for 5 hours before purification. Unreacted dye was removed by dialysis using 12 kDa dialysis tubing. When working with enzymes such as GOx or HRP solutions were first dialysed against a weak buffer solution overnight (roughly 10 mM Tris with a pH 6 to 8) to reduce protein aggregation and precipitation. Dialysis against water for roughly 6 hours then removed the buffer salts and remaining dye. Hardier proteins such as BSA could be immediately dialysed against DI water without significant precipitation. Precipitate was removed via centrifugation at 5 krpm and the solution then lyophilised.

In order to tag Urease (Chapter 5) this method was adjusted slightly. Urease is supplied in a powder which contains a large amount of buffer and therefore the weighed mass cannot be used

as an approximation of the amount of protein. Urease (200 mg) was dissolved in 8 mL 100 mM pH 8.5 sodium carbonate buffer solution and 200 μL dye solution in DMSO added.

2.5 Methods for Chapter 3

2.5.1 Preparation of silica colloidosomes under varied conditions

To investigate the structure of silica colloidosomes some conditions of their formation were varied whilst the general method was kept the same. The aqueous phase was added (100 μL, ϕ_w= 0.2) and shearing force was applied via shaking hard for 1 minute. The aqueous phase typically consisted of 100 mM buffer with pH ranging from 3 to 8. Where stated, the aqueous phase also contained 3 mg/mL bovine serum albumin (BSA) or FITC labelled bovine serum albumin (FITC-BSA). TMOS (10 μL) was added to the oil phase of the Pickering emulsion and samples left to crosslink under rotation for 24 to 48 hours. Transfer of the crosslinked colloidosomes to water was carried out using the method described in Section 2.4.1.

2.5.2 Colloidosome characterisation

2.5.2.1 Preparation of fluorescent silica nanoparticles and colloidosomes

The method for fluorescently labelling silica nanoparticles was based on that previously reported [20, 22]. Surface modified silica nanoparticles were dispersed in ethanol (100 mg in 8 mL). Ethanolic solutions of 3-aminopropyltriethoxysilane (40 μL of 10 mg/mL) and triethylamine (40 μL of 5 mg/mL) were added and the reaction was stirred at room temperature for 24 hours. FITC in DMSO (100 μL of 1 mg/mL) was added dropwise and stirring continued for 5 hours. The mixture was centrifuged at 5 krpm for 5 minutes to collect the nanoparticles and washed with ethanol three times to remove unreacted dye. To transfer the labelled nanoparticles to dodecane they were first dispersed in a 50:50 mixture of ethanol and dodecane before being centrifuged and dispersed in dodecane via sonication and stirring. Colloidosomes were formed using unlabelled silica doped with 25% FITC-silica particles.

2.5.2.2 Dye adsorption experiments

The uptake of the small molecule dyes Rhodamine B and fluorescein was studied by incubating colloidosomes (20 μL) with aqueous dye solutions (80 μL of 0.02 mg/mL) and imaging after 1 hour using confocal microscopy. To study the pH dependence of the uptake of fluorescein the dye solution was adjusted to pH 3.5 and the experiment repeated.

To stain silica with Rhodamine B, colloidosomes (20 μL) were incubated with Rhodamine B in water (80 μL of 0.2 mg/mL) for 1 hour. Samples were then washed three times by dispensing in 1 mL of water and centrifuging at 2 krpm for 30 s. Samples were imaged using confocal microscopy.

2.5.2.3 Permeability experiments using FITC-dextran

Colloidosomes (20 μL) were mixed with FITC labelled dextran (FITC-dextran, 80 μL, 2 mg/mL) of various molecular weights and incubated at room temperature. Aliquots of the sample were taken and imaged at 1.5 and 24 hours using confocal microscopy and to allow direct comparison imaging conditions such as laser power and magnification were kept constant. During imaging the approimate midpoint in the height of individual colloidosomes was identified to allow accurate determination of the internal polymer content. In order to assess the polymer uptake, line profiles were drawn over each colloidosome and the ratio of the internal and external fluorescence calculated. The experiment was carried out on three different colloidosome samples for each molecular weight tested and multiple colloidosomes were imaged in each sample. The average values of the fluorescence intensity ratio and the standard deviation were calculated and are shown in the plotted graphs. Curves were fitted to the data using Origin. To find a value for the molecular weight cut off (MWCO) the uptake of 4 kDa FITC-dextran was assumed to be 100% and the uptake at 250 kDa was 0%. The data was replotted according to this and the MWCO calculated as the point of 10% uptake on the graph.

2.5.2.4 Protein adsorption by silica colloidosomes

To assess the passage of globular proteins across the colloidosome membrane colloidosomes (20 μL) were incubated with aqueous solutions of fluorescently labelled proteins (FITC-BSA, FITC-HRP or FITC-GOx) for 1.5 hours before being imaged using confocal microscopy. Samples were imaged again after 24 hours to assess the time dependence of the protein uptake. To assess retention of protein the samples were then washed with DI water and imaged again.

2.5.2.5 SEM of colloidosomes

Colloidosomes were prepared as previously described (Section 2.5.1), with aqueous phases containing 3 mg/mL BSA at pHs from 4 to 8. After crosslinking and transfer to water colloidosomes were dried for SEM imaging via lyophilisation. Roughly 50 μL of colloidosomes suspension was added to a carbon pad on top of an aluminium SEM stub. The SEM stub was submerged in a shallow pool of liquid nitrogen to induce rapid freezing (the liquid nitrogen level was below the rim of the stub). The stubs containing the frozen samples were removed and rapidly placed into samples containers and lyophilised for several days in an in house constructed system to maintain constant pressure (the trap was in dry ice to encourage water removal). Prior to imaging samples were sputtered with silver.

2.5.3 Enzyme containing colloidosomes

2.5.3.1 Formation of enzyme containing colloidosomes

Colloidosomes were formed using the method previously described (Section 2.5.1). Prior to emulsion formation, HRP was added to the aqueous phase at concentration 740 U/mL. The pH of the aqueous phase was refined to find the optimum in terms of activity and structure, following which all samples were formed using pH 7 Tris buffer for HRP. The Pickering emulsion was formed via hand shaking for one minute and after the addition of TMOS (10 μL) samples were left to crosslink for 48 hours. The first 5 hours of crosslinking was carried out on a rotator at room temperature, after which samples were placed into the fridge (2 - 8 °C) for the remainder of the time. After transfer to a continuous aqueous, phase samples were kept in a refrigerator in Tris buffer (pH 7, 100 mM).

2.5.3.2 Enzymatic activity of colloidosomes

The activity of HRP colloidosomes was investigated using the HRP mediated oxidation of *o*-phenylenediamine (*o*PD) to the fluorescent molecule 2,3-diaminophenazine (DAP), in the presence of hydrogen peroxide (H_2O_2). Fluorescence spectroscopy (CLARIOstar plate reader (BMG LabTech)) was used to monitor the fluorescence indicative of DAP production (λ_{ex} = 405 - 415 nm, λ_{em} = 520 - 550 nm). Colloidosomes in pH 7 Tris buffer (final concentration 50 mM) were allowed to settle to the bottom of the sample well in a 96 well plate, before automated addition of *o*PD and H_2O_2 (total sample volume 300 μL). The wells were gently shaken to mix. To minimise light scattering the top optic was used and the focal length was set above the top of the colloidosomes within the liquid (focal height 7.0 mm). Experiments were repeated in triplicate and average values and standard deviations calculated.

To look at the effect of the number of colloidosomes present, constant substrate concentrations of 500 μM *o*PD and 450 μM H_2O_2 were used. The amount of colloidosomes added to the well was varied between 10 μL and 500 μL. For colloidosome volumes of greater than 50 μL, a colloidosome suspension was centrifuged to form a pellet and buffer removed to reduce the total volume to 50 μL. To investigate the light scattering or product adsorption by increased colloidosome volumes the final read out from reactions which had been allowed to run for 1 hour (to reach a plateau) was plotted. In order to calculate the DAP concentration ([DAP]) from the fluorescence intensity, the final value of experiments carried out using 50 μL colloidosomes was averaged and this value taken as the fluorescence intensity of 225 μM DAP (equivalent to full conversion of 450 μM H_2O_2 with excess *o*PD). This value was then used to convert all fluorescence intensities into concentrations. Controls were carried out with no colloidosomes present. For determination of K_M and v_{max} the final H_2O_2 concentration was varied from 0 μM to 150 μM at a constant *o*PD concentration of 500 μM (so that there was always an excess of *o*PD). The Michaelis-Menten

equation is

$$\frac{d[P]}{dt} = v = \frac{v_{max}[S]}{K_M + [S]} \tag{2.16}$$

Where [P] is the concentration of product, K_M is the Michaelis-Menten constant and v_{max} is the maximum rate for the catalysed reaction. The data was plotted as a Lineweaver-Burke plot ($\frac{1}{[S]}$ against $\frac{1}{v}$) resulting in a straight line with y intercept $\frac{1}{v_{max}}$ and a slope of $\frac{K_M}{v_{max}}$ which was used to calculate K_M and v_{max}.

2.6 Methods for Chapter 4

2.6.1 Formation and characterisation of silica colloidosomes

2.6.1.1 Preparation of silica colloidosomes

Colloidosomes were formed using the method developed in Chapter 3. All samples were made using 20 mg silica nanoparticles in 2 mL dodecane. Aqueous phase (100 μL) was added, and the emulsion formed by manual shaking for one minute. Aqueous phase composition was varied according to the nature of the sample being prepared, as was the amount of TMOS added for crosslinking. Typical aqueous phase composition and TMOS volumes are shown in Table 1.1.

Table 2.1: Colloidosome formation parameters

Sample	Aqueous phase	Aqueous phase pH	TMOS volume /μL
BSA or FITC-BSA	3 mg/ mL BSA or FITC-BSA	4	10
HRP	5 mg/ mL (740 U/mL) HRP	7	15
HRP with DL650-BSA	5 mg/ mL (740 U/mL) HRP + 1 mg/mL DL650-BSA	7	15
DL650-HRP	2.5 mg/ mL HRP + 2.5 mg/mL DL650-HRP	7	15
GOx	10 - 20 mg/ mL (2270 U/mL) GOx	4	15 - 20
GOx with RITC-BSA	10 - 20 mg/ mL (2270 U/mL) GOx + 1 mg/mL RITC-BSA	4	15 - 20
DL650-GOx	5 mg/ mL GOx +5 mg/ mL DL650-GOx	4	15 - 20
FITC-GOx	7.5 mg/ mL GOx + 1 mg/ mL FITC-GOx	4	15 - 20

2.6.1.2 Colloidosome size analysis in aqueous suspension

Colloidosome samples were diluted by a factor of 25 in water and 100 μL placed on placed on a glass slide for imaging using bright field optical microscopy. Multiple images were taken across three different preparations of colloidosomes. Colloidosome diameter was measured on Fiji Image J and the average value and standard deviation calculated.

2.6.2 Hydrogel and prototissue formation

2.6.2.1 Basic method for hydrogel formation

Agarose solutions were made by combining agarose powder with water and heating to 90 °C until dissolved. The hot agarose solution was cooled to 55 °C in a heater (Grant Dry Block Thermostat) before addition of colloidosomes. Colloidosome suspensions were combined with warm agarose and the mixture immediately transferred to a mould and placed into the fridge (2 - 8 °C) for 10 minutes to induce gelation. Hydrogel shapes were formed using PMMA (Poly(methyl methacrylate), or acrylic) moulds of different dimensions clipped to a glass base. After injection of the pre-gel solution to the mould a second piece of glass was clipped on top. Figure 2.4 shows a schematic and photos of the moulding system used. For hydrogel wires, the agarose suspension was injected into a glass capillary tube and the hydrogel pushed out under air pressure after 10 minutes in the fridge. Hydrogels were stored in sealed petri dishes in the fridge (2 - 8 °C) until use.

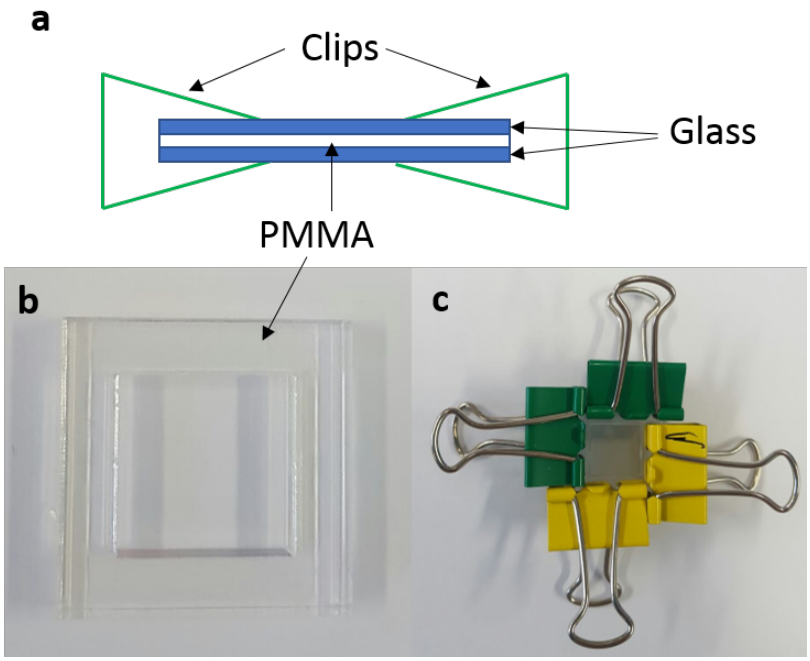

FIGURE 2.4. (a) A schematic showing the setup for creating moulded hydrogels, where the PMMA mould shown in (b) is clipped to a piece of glass as seen in (c).

2.6.2.2 Composite prototissue formation

Striped capillary hydrogels were formed using agarose hydrogel by injecting a small volume of pre-gel solution into a glass capillary and leaving at room temperature for three minutes. A second volume was then added, and the steps repeated until all desired layers had been completed

the hydrogel was then placed in the fridge (2 - 8 °C) for 10 minutes and ejected using air pressure.

To create more complex patterned hydrogels an interpenetrating network hydrogel system was created. Alginate is a polysaccharide which gels in the presence of Ca^{2+} ions. Alginate was included in the pre-gel mixture alongside agarose. Equal volumes of warm 2% w/v agarose and 2% w/v sodium alginate were added to an eppendorf (final concentration 0.5% w/v each) and thoroughly mixed prior to addition or buffer and/ or colloidosomes. The agarose was gelled in the fridge (2 - 8 °C) for 10 minutes as normal. Hydrogel pieces were then pressed together for 30 minutes before 50 mM $CaCl_2$ was added to gelate the alginate and join neighbouring pieces together.

In some cases, one hydrogel piece was embedded within another by placing an agarose hydrogel (containing uncrosslinked alginate) into a mould and surrounding with a second pre-gel solution. After embedding, these composites were assembled with other hydrogel pieces and then crosslinked using $CaCl_2$.

2.6.3 Characterisation of colloidosome hydrogels

2.6.3.1 Microscope characterisation of colloidosome hydrogels

Hydrogels were prepared with FITC-BSA colloidosomes to allow imaging using fluorescence microscopy. The number of colloidosomes within the hydrogel matrix was altered by varying the volume of colloidosomes added to the pre-gel solution. To assess distribution across a hydrogel (or image the patterned colloidosome populations described in Section 2.6.2.2), whole hydrogels were imaged using the tile scan feature on a widefield fluorescence microscope. For more accurate investigation of colloidosome structure within the hydrogels, images were taken using confocal microscopy. Z stacks were reconfigured to 3D plots to allow imaging of the overall shape of colloidosomes within the hydrogel. Cross sections were cut from the bulk and tile scan and Z stack images collected in order to assess the distribution of colloidosomes throughout the height of the hydrogels (Figure 2.5). This avoided the problem caused by the scattering of light when trying to look directly through the height of a hydrogel.

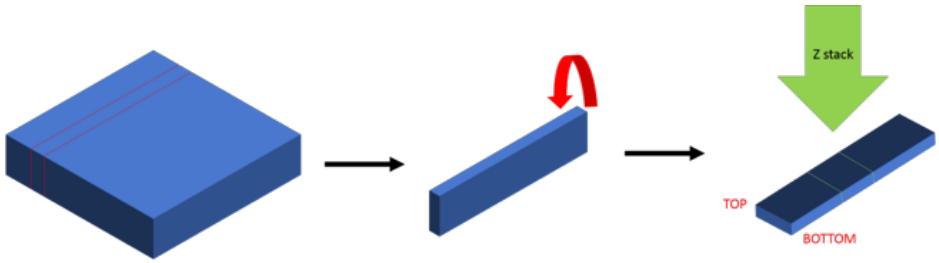

FIGURE 2.5. A cartoon depicting the procedure for taking a cross section of a colloidosome hydrogel, turning it on its side and then taking tile scan and Z stack images to assess distribution and size.

Size analysis was carried out on cross-section Z stacks in Fiji Image J. The midpoint of a colloidosome (point of greatest diameter) was found and the distance from the bottom of the hydrogel measured. For each agarose concentration studied (1% w/v agarose or 2.5% w/v agarose) a minimum of three of the Z stack images from different samples were analysed.

The Pearson correlation coefficient (r) measures the linear correlation between two variables. To calculate the correlation between colloidosome diameter and height in the hydrogel, the two data sets $(x_1, \ldots x_n)$ and $(y_1, \ldots y_n)$ are entered into the calculation:

$$r_{xy} = \frac{\sum_{i=1}^{n}(x_i - \bar{x})(y_i - \bar{y})}{\sqrt{\sum_{i=1}^{n}(x_i - \bar{x})^2}\sqrt{\sum_{i=1}^{n}(y_i - \bar{y})^2}} \tag{2.17}$$

Where n is the number of values within the data set, $\bar{x}$ is the sample mean calculated by:

$$\bar{x} = \frac{1}{n}\sum_{i=1}^{n} x_i \tag{2.18}$$

Similarly $\bar{y}$ is the sample mean for data set y. A Pearson correlation coefficient of -1 indicates strong negative correlation, 0 indicates no correlation and +1 indicates a strong positive correlation.

2.6.3.2 Polymer permeation studies

To label agarose with 5-DTAF (5-(4,6-Dichlorotriazinyl) Aminofluorescein) (DTAF) a method was adapted from that reported by Russ et al [52]. Agarose was added to 50 mL DI water in a round bottom flask and the solution placed into an oil bath and heated to 90°C for 1 hour, resulting in a clear viscous solution. A rubber stopper was placed loosely in to minimise evaporation. The oil bath temperature was reduced to 60°C and a little extra water added due to evaporation. After the temperature reached 60 °C 8 mg 5-DTAF in 15 mL 1% w/v Na_2SO_4 was added dropwise forming a turbid yellow solution. Sodium hydroxide (3 drops 10% w/v) was added to initiate the coupling reaction and the solution became clear. The solution was tested using pH paper every 30 minutes to ensure it remained around pH 10. The solution was stirred for two hours at 60°C, after which the flask was removed from the oil bath and 150 mL cold ethanol was added to precipitate. The flask was placed into the freezer for 15 minutes before the suspension was centrifuged for 10 minutes at 5 krpm. The supernatant was removed and replaced with cold ethanol. The washing was repeated 4 times to removed unreacted dye. The solid was dried under vacuum overnight giving a yellow powder.

The method for fluorescently labelling alginate with 2-(4-Amidinophenyl)-6-indolecarbamidine dihydrochloride (DAPI) was adapted from the procedure reported by Lee et al [132]. Alginate (500 mg) was dissolved in DI water to give a final concentration of 1% w/v. A solution of EDC (1-ethyl-3-(3dimethylaminopropyl)carbodiimide) and DAPI (1 mL of 11.4 mg/mL EDC and 11.4 mg/mL DAPI) was added and the reaction stirred overnight. The product was dialysed

using 12 kDa dialysis tubing against water for 24 hours to remove unreacted dye, before being lyophilised.

Hydrogels were formed using the fluorescently labelled polymers to assess permeation across the colloidosome membrane. BSA colloidosomes (no fluorescent label) were embedded in a 1% w/v agarose hydrogel (containing 0.5% w/v DTAF-agarose) or within an agarose-alginate IPN hydrogel made using 0.5% w/v unlabelled agarose and 0.5% w/v DAPI-alginate. Hydrogels were imaged using confocal microscopy. To gain extra information BSA colloidosomes were also incubated with a 0.1% w/v solution of DTAF agarose for one hour and imaged using confocal microscopy.

2.6.3.3 SEM of agarose hydrogels

Agarose hydrogels (with or without colloidosomes) were formed in PMMA moulds and sections cut off for SEM analysis. The hydrogels were placed into solutions of increasing ethanol concentration until the solvent had been completely exchanged for ethanol. Hydrogels were then critical point dried by exchanging the solvent for liquid CO_2 before evaporating the solvent totally. The dry hydrogels were carefully cut open to allow imaging of the internal structure rather than the smooth surface which forms during drying, and then placed on a carbon pad attached to an aluminium stub and silver coated for imaging.

2.6.3.4 Rheology of agarose hydrogels

To provide some evidence of the gel like character of the colloidosome containing hydrogels, basic rheological tests were carried out. Agarose hydrogels (1% w/v) with or without colloidosomes were prepared and stored overnight in a humid environment prior to testing. Hydrogels were placed onto the rheometer baseplate for testing, and the parallel plate geometry set at a height of 1 mm to allow direct contact with the hydrogel. After a 5 minute relaxation period SAOS strain amplitude sweeps were carried out from 0.1 to 100%. A constant frequency of 1 Hz was used based on characterisation of agarose gels in the literature [73]. Each hydrogel was used for one experiment and all experiments were carried out in triplicate.

2.6.4 Enzymatic activity of colloidosomes in agarose hydrogels

To measure the activity of HRP colloidosomes within agarose hydrogels, the method outlined in Section 2.5.3.2 was adjusted. The HRP mediated oxidation of *o*PD to the fluorescent molecule DAP was monitored using fluorescence spectroscopy (CLARIOstar plate reader (λ_{ex} = 405 - 415 nm, λ_{em} = 520 - 550 nm). Colloidosomes in pH 7 Tris buffer were mixed with warm agarose to form the pre-gel solution, which was then added to the sample well of a 96 well plate (100 μL hydrogel per well). The well plate was placed in the fridge (2 - 8 °C) to induce gelation. Tris buffer solution was then added on top of the hydrogel (final Tris concentration 50 mM and pH 7) and the samples left to equilibrate with the buffer and warm to room temperature. The reaction was initiated via

automated addition of *o*PD and H_2O_2 resulting in a total sample volume of 300 μL and the wells were gently shaken to mix. The focal height of the instrument was set to 7.0 mm. All experiments were repeated in triplicate and standard deviations calculated.

The final fluorescence value for experiments run with 500 μM OPD, 450 μM H_2O_2 and 50 μL colloidosomes was again used to calibrate the fluorescence data and convert to [DAP]. Initial reaction rates were calculated using the period between 100 to 400 s, as this excluded the initial lag period from the calculation. To investigate the effect of colloidosome concentration, the amount of colloidosomes (within the 100 μL hydrogel) was varied between 10 to 500 μL (for high colloidosome volumes samples were again centrifuged to concentrate before use) and substrate concentrations of 500 μM OPD and 450 μM H_2O_2 were used. The determination of K_M and v_{max} was again carried out by varying H_2O_2 concentration between 0 μM and 150 μM whilst the amount of colloidosomes and concentration of *o*PD were held constant. The method for these calculations was the same as described in Section 2.5.3.2.

The communication between colloidosome populations was studied using the cascade reaction in which glucose oxidase GOx converts glucose into gluconic acid and releases H_2O_2, which can then be used by HRP to oxidise *o*PD. Separate colloidosome populations containing GOx or HRP were added to the pre-gel mixture (25 μL of each in 100 μL hydrogel). The activity of the cascade was again monitored using the fluorescence spectroscopy method. Glucose (1 mM) and *o*PD (450 μM) were added by the well plate reader and the production of DAP monitored. The calibration to produce DAP concentrations was carried out in the same way as previously described.

2.6.5 Programmed reaction patterning

2.6.5.1 Programmed reaction patterning using ABTS

ABTS (2,2′-azino-bis(3-ethylbenzothiazoline-6-sulphonic acid)) can be used as an alternative substrate for HRP, producing a colorimetric signal instead of the fluorescent signal seen with *o*PD. Colloidosomes formed using the method described in Section 2.6.2.1 were used to create composite hydrogel prototissues using the method developed in Section 2.6.2.2. Pieces with GOx colloidosomes, HRP colloidosomes, mixed colloidosome populations or no colloidosomes were created and assembled in different combinations and shapes. For colloidosome containing pieces a total of 100 μL colloidosome sample was used per 200 μL hydrogel unless otherwise stated. When HRP and GOx colloidosomes were co-localised within a hydrogel piece, they were usually used in a 1:1 volume ratio. A control hydrogel where enzyme was free in solution within the hydrogel was formed by replacing colloidosome suspension with the same volume of HRP (74 U/mL) or GOx (113.5 U/mL) solution, with the overal amount of each enzyme within the hydrogel being kept approximately the same. After $CaCl_2$ crosslinking, all hydrogels were equilibrated with 50 mM Tris buffer for 30 minutes and then were submerged in a solution of ABTS (1 mM in 50 mM Tris pH7) overnight.

Source hydrogels containing glucose (final concentration 0.5 to 1 mM) were formed by adding buffer and glucose solution to warm agarose (final concentration 1% w/v). The solution was placed into a PMMA mould to give a hydrogel of equal dimension to the final composite hydrogel.

Pseudo 2D hydrogels were created in various shapes with a height of 1 mm. Before experiments were run hydrogels were placed into petri dishes and excess water removed from the surface by wicking with filter paper. To initiate the reaction the composite colloidosome hydrogel was placed on top of the source hydrogel. Alternative experiments were run where instead of combining with a source hydrogel the composite colloidosome hydrogel was placed into a solution of glucose in Tris buffer. The assembly was imaged from above (using automatic camera settings) and an LED lamp was placed underneath the hydrogels during imaging to give uniform illumination (Figure 2.6). The imaging was repeated over a period of 24 hours (every 15 minutes for 3 hours, then every 30 minutes until 7 hours, then at 24 hours). Hydrogels were removed from the light source between images and stored in the dark in petri dishes with pieces of filter paper saturated with DI water to reduce water loss from the hydrogels.

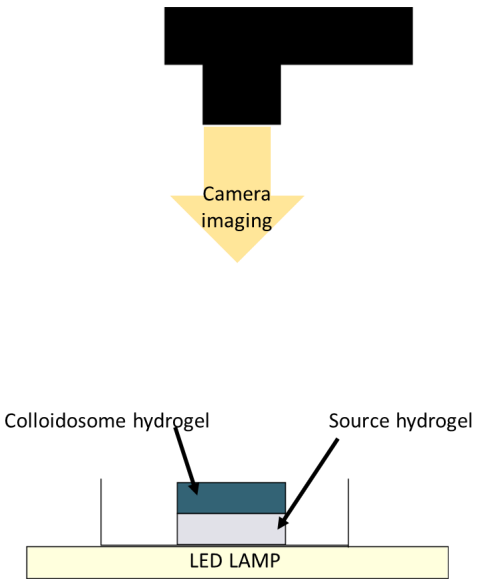

FIGURE 2.6. A cartoon depicting the procedure for imaging pseudo-2D patterning in colloidosome prototissues. Hydrogels were placed onto source hydrogels containing glucose to initiate the reaction, and imaged from above. An LED lamp illuminated the hydrogels from below during the imaging process.

Photographs of hydrogels were processed using Fiji Image J. The RGB Profiler plugin was used to measure RGB values across the hydrogel in each image [131]. Unadjusted images were used for all data analysis. RGB values were then converted to give hue angle and saturation

values (Section 2.3.3) which were plotted as contour maps. Since the hydrogels were not imaged continuously the software fills in the intervening regions of the data when the contour plot is created.

To study the evolution of the reaction within the hydrogels in 3D, more complex composite hydrogels were created. The method for creation of such hydrogels was the same as for the simpler pseudo 2D hydrogels described above, but this time layers were also combined vertically to create more complex structures. Before assembling the 3D structure, the hydrogel pieces were imaged using widefield fluorescence microscopy. Again, pieces were pressed together prior to crosslinking. For these larger hydrogels the $CaCl_2$ crosslinking time was extended to between 1 hour and 24 hours, as were the Tris and ABTS equilibration steps. As an example of an intricate hydrogel shape, a silicone mould in the shape of a chess piece, was used to create a HRP and GOx containing hydrogel. Once gelled the piece was placed into a larger mould for embedding within a second hydrogel matrix. This hydrogel piece was then embedded in a plain hydrogel and crosslinked as before. To image the reaction progression in 3D hydrogels were submerged in 5 mM glucose solution in tanks created from microscope slides. The reaction progression was monitored using two cameras set up as shown in Figure 2.7.

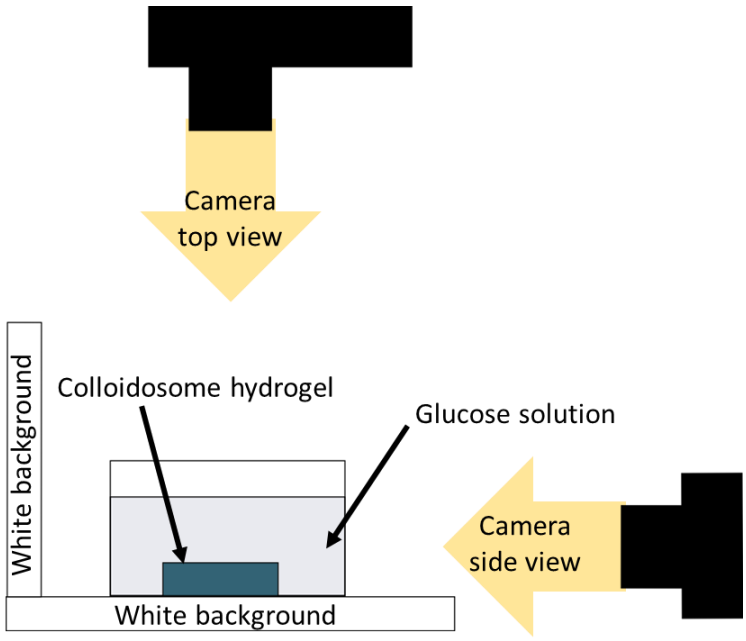

FIGURE 2.7. A cartoon of the procedure for imaging 3D patterning in colloidosome prototissues. A hydrogel prototissue was placed in glucose solution in a glass tank to initiate the reaction, and the system imaged over time. Cameras were placed at two different positions to allow the 3D nature of the patterning to be captured.

2.6.5.2 Programmed reaction patterning using *o*PD

Colloidosomes were formed as described in Section 2.6.5.1. The method for formation of composite hydrogel prototissues was adapted from that described in Section 2.6.5.1. The substrate *o*PD (final concentration within the gel 0.1 to 1 mM) was added to the pre-gel solution along with the colloidosomes to ensure homogeneous distribution (this cannot be done for the ABTS system since the crosslinking with $CaCl_2$ must be done in the absence of ABTS or precipitation occurs). The assembly and crosslinking steps for *o*PD containing hydrogels were carried out in the fridge (2 - 8 °C) and in the dark to reduce *o*PD oxidation within the hydrogel. $CaCl_2$ solution used for crosslinking contained *o*PD of equal concentration to the pre-gel solution. After crosslinking hydrogels were equilibrated with a solution of Tris buffer (50 mM, pH 7, containing *o*PD at concentration equal to that of the pre-gel solution). Samples were brought up to room temperature in the dark prior to running. Source hydrogels containing glucose (2.5 mM) were formed in 2.5 x 0.5 x 0.1 mm PMMA moulds to match the dimensions of the composite hydrogels.

To track the production of the fluorescent product DAP within the hydrogel, widefield fluorescence microscopy was used. Composite hydrogels were placed onto large coverslips along with strips of filter paper saturated with water. During imaging the system was covered with the base of a petri dish to reduce evaporation and drying of the hydrogel. To initiate the reaction the source hydrogel was placed on top of the composite hydrogel. The whole hydrogel was imaged every two minutes using the tile scan function. The reaction was run for one hour and the images merged on the Leica software to create a time-lapse of the whole hydrogel. Although each image within a tile scan is taken at a different time, the conditions of the experiment were refined so that the time difference between the first and last image of one scan were taken within a reasonable amount of time (the whole image takes roughly 30 s to collect) and from then on the whole tile scan image was treated as being taken at the time the scan was started.

To analyse the pattern within the hydrogel a rectangular region of interest was selected over the width of the hydrogel and the fluorescence intensity profile plotted across the length of the whole piece. This profile represented the average fluorescence across the width of the section. This data was collected for each image and contour plots created in Origin.

2.7 Methods for Chapter 5

Some of the initial work in this project, on the synthesis, characterisation and photogelation of N-methacrylated glycol chitosan was presented in the BSc thesis of Imogen Millington. Development of some of the methods in Sections 2.7.3.1, 2.7.4.1, 2.7.4.2, 2.7.4.3, and 2.7.5.1 was carried out by Imogen Millington, under the supervision of Joanna Sparks.

2.7.1 Formation of colloidosomes for pH changes

Colloidosomes were formed using the method described in Section 2.4.1. Silica nanoparticles (20 mg) were added to dodecane (2 mL) and sonicated for 5 minutes to disperse. Material to be encapsulated was dissolved in 100 mM buffer (various pHs were tested to find the optimum for each system) and 100 μL added to the oil phase before the mixture was shaken hard for one minute to form the emulsion. Glucose oxidase (GOx) and urease (URS) were used at various concentrations. TMOS (15 to 20 μL depending on the pH and sample) was added and the system rotated at room temperature. Samples were either left to rotate for 48 hours (URS) or removed from the rotator after 5 hours and the rest of the crosslinking carried out in the fridge at 2 - 8 °C (GOx). Colloidosomes were transferred using steps of decreasing ethanol concentration and centrifugation. After transfer to water colloidosome samples were dispersed in 10 mL DI water and left to settle. The aqueous phase was removed, and the sample resuspended to 500 μL total in DI water. Colloidosomes were imaged using bright field microscopy. After the initial tests to refine the conditions the colloidosomes were made using 2270 U/mL GOx in pH 4 acetate buffer or 2270 U/mL URS in pH 4.5 acetate buffer, crosslinked with 15 - 20 μL.

To assess the encapsulation of the enzymes, colloidosomes were made using fluorescently labelled protein. FITC-GOx colloidosomes were made using an aqueous phase of 7.5 mg/mL GOx and 1 mg/mL FITC-GOx in 100 mM pH 4 acetate buffer. DL650-URS colloidosomes were formed using a solution of 25 mg/mL URS with 1 mg/mL DL650-URS in 100 mM pH 4.5 acetate buffer. Crosslinking and transfer to water were carried out as normal. Colloidosomes were imaged in bulk water phase using fluorescence microscopy.

2.7.2 Monitoring pH changes in solution

URS colloidosomes and GOx colloidosomes were formed using the method described in Section 2.7.1 and transferred to water. Colloidosomes were suspended in 1 mM acetate buffer (of the desired starting pH) and the solution pH adjusted. The pH of this system was monitored for a period to ensure it was constant. Experiments using GOx colloidosomes were started at pH 8.5 and those using URS colloidosomes were started at pH 4. A solution of substrate (urea or glucose, varied concentration) was formed in 1 mM acetate and adjusted to the same pH as the colloidosome suspension. The substrate solution was added to the colloidosomes and the solution mixed gently by pumping with a pipette, to ensure that all colloidosomes mixed completely with

the substrate solution. The pH was recorded automatically every 30 s using an Inlab micro pH electrode and the LabX pH measurement software.

For transient pH change experiments, GOx colloidosomes and URS colloidosomes were mixed in a one-to-one volume ratio and suspended in 1 mM pH 4 acetate buffer. The solution pH checked and adjusted to pH 4 if necessary. A solution of urea and glucose was formed in 1 mM acetate and adjusted to pH 4. The substrate solution was added to the colloidosomes and the solution mixed gently by pumping with a pipette. The pH was recorded automatically every 30 s. The initial urea concentration upon addition to the colloidosomes was varied (1 mM, 2.5 mM or 5 mM) and the glucose concentration was 100 mM each time.

2.7.3 Polymer methacrylation

2.7.3.1 Synthesis N-methacrylated glycol chitosan

The synthesis of N-methacrylated glycol chitosan (GC-M) was adapted from previously reported procedures in the literature [53]. Glycol chitosan (GC) (2.5 g) was dissolved in water at a concentration of 1.9% w/v. The pH of the solution was found to be roughly 9 and hence no adjustment was needed. Glycidyl methacrylate (160 mg, 0.00113 mol) was added and the reaction proceeded at room temperature for 48 hours before being precipitated in acetone to remove impurities. The product was collected by first settling and then decanting the bulk of the acetone, before centrifuging at 5 krpm for 5 minutes. The polymer was dissolved in water and dialysed for 24 hours using a 12 kDa MWCO dialysis tubing. The solution was adjusted to pH 7 and lyophilised for at least 48 hours. To form polymers with varied degrees of substitution of methacrylate onto the polymer backbone, the ratio of GC to glycidyl methacrylate was varied.

2.7.3.2 Synthesis of methacrylated carboxymethyl cellulose

The method for methacrylation of carboxymethyl cellulose (CMC) was adapted from that reported by Reeves et al [47]. Carboxymethyl cellulose (90 kDa, 2.5 g, 0.012 mol monomer) was dissolved in water to give a final concentration of 0.5% w/v. EDC (2.875 g, 0.015 mol, 1.23 eq.) was added and the solution again adjusted to pH 6.5. A solution of aminoethyl methacrylate (AEM, 50 mL of 50 mg/mL, 0.015 mol, 1.23 eq.) was adjusted to a pH of 6.5 before being added dropwise to the polymer solution, with rapid stirring. After two hours the pH was readjusted to 6.5 and further aliquot of EDC (2.875 g, 0.015 mol, 1.23 eq.) was added. After a further two hours the pH was adjusted to 8.5 and the reaction left the run for a total of 24 hours. The solution was precipitated in acetone and the product collected by first settling and decanting the bulk of the acetone, and then centrifugation at 5 krpm for 5 minutes. The polymer was dissolved in DI water and dialysed for 24 hours using 12 kDa MWCO dialysis tubing. After centrifugation to remove remaining precipitate (5 krpm, 5 minutes) the solution was adjusted to pH 7 and lyophilised. To achieve varied degrees of substitution the molar ratio of the monomer to the AEM and EDC was

varied, and the same method was followed. For comparison the synthesis was also repeated using carboxymethyl cellulose of average molecular weight 250 kDa.

2.7.4 Polymer characterisation

2.7.4.1 NMR analysis of polymers

^{1}H NMR analysis was carried out on a Varian 500a NMR spectrometer. To prepare samples, polymer was dissolved in D_2O at a concentration of 20 mg/mL. For NMR of glycol chitosan and derivatives the sample was adjusted above pH 10 using 5 M NaOH, as described by the literature procedure [53]. The temperature was held at 90 °C for all experiments and samples were equilibrated for 5 minutes before shimming. The use of high temperature allowed better resolution of peaks on the polymer chain. NMR spectra were processed in Mestranova, and were manually phase adjusted, bassline corrected and smoothed (Savitsky golay normal).

Calculation of the degree of substitution (DOS) (the percentage of monomers which have a methacrylate group attached) of the polymers was calculated using the ^{1}H NMRs based on previously reported methods [47, 53]. During the functionalisation of GC, the degree of deacetylation should not change and hence this can be used as an internal check of any integration carried out. The percentage of monomers with remaining amide groups can be calculated as follows:

$$Deacetylation = 1 - \left(\frac{\frac{I_{2.64}}{3}}{I_{5.03} + I_{5.20}} \right) \times 100\% \tag{2.19}$$

Where I_x represents the integration value of the peak at the chemical shift indicated relating to the amide ($I_{2.64}$) and the acetylated ($I_{5.03}$) and deacetylated ($I_{5.20}$) forms of the sugar ring. The degree of substitution of methacrylate groups onto glycol chitosan (DOS) can be calculated as follows:

$$DOS_{GC-M} = \frac{(I_{5.86} + I_{6.20})/2}{I_{5.03} + I_{5.20}} \times 100\% \tag{2.20}$$

Where I_x represents the integration value of the peak at the chemical shift indicated relating to the vinyl protons ($I_{5.86}$+$I_{6.20}$) and the acetylated ($I_{5.03}$) and deacetylated ($I_{5.20}$) forms of the sugar ring. Based on a previously published method the degree of substitution of methacrylate onto CMC was calculated as follows:

$$DOS_{CMC-M} = \frac{(I_{6.3} + I_{6.7})/2}{I_{5.1}} \times 100\% \tag{2.21}$$

Where I_x represents the integration value of the peak at the chemical shift indicated relating to the vinyl protons ($I_{6.3}$+$I_{6.7}$) and the proton on C1 of the carbon ring ($I_{5.1}$).

2.7.4.2 FT-IR of polymers

FT-IR was carried out on starting materials or lyophilised powders to assess the presence of different functional groups. The data presented is the sum of 50 scans after bassline correction.

2.7.4.3 Ultraviolet-visible spectroscopy of polymer and indicator solutions

Aqueous solutions of methacrylated polymers (GC-M and CMC-M, 0.1% w/v) or the photoinitiator 2-hydrox-4'-(2-hydroxyethoxy)-2-methylpropiophenone (Irgacure 2959, I2959) (0.002% w/v) were analysed using UV/Vis spectroscopy to assess the adsorption of light at the wavelength of irradiation.

2.7.4.4 Potentiometric titrations of polyions

Potentiometric titrations were used to find the pK_a and DOS of the functionalised polymers. The system pH was monitored with an InLab micro electrode after calibration with standard buffers. To achieve the fully protonated form of the acidic polymers (CMC and CMC-M) before titration, an ion exchange resin was used. Amberlite resin (H form) was added to a polymer solution (4 mg/mL) in portions and the pH monitored. When the pH reached a minimum value and stopped changing, the protonation was determined to be complete. The resin was removed, and the solution of protonated polymer used for titration directly. Aliquots of the solution were taken prior to titration and lyophilised to calculate the concentration of polymer in the final solution.

GC was purified by dialysis against water and then lyophilised. GC-M was used as formed since the workup stages of the synthesis yield a pure product. GC and GC-M were dissolved in water at 1 mg/mL and adjusted to roughly pH 3 using 2 M HCl to achieve a fully protonated form.

To account for water adsorption by solid NaOH, an NaOH stock was titrated against HCl to determine an accurate concentration. To carry out the polymer titration 10 μL portions of NaOH (0.1 M for GC, GC-M or CMC, and 0.01 M for CMC-M) were added to the polymer solution (10 to 20 mL) with vigorous stirring. After each addition the pH was allowed to equilibrate before being recorded. The titration was continued until the pH plateaued at high pH and each titration was repeated in triplicate.

The resulting plots were analysed using the extended Henderson Hasselbach equation [133]:

$$pH = pK_a - nlog\left(\frac{1-\alpha}{\alpha}\right) \tag{2.22}$$

Where n is a constant relating to the degree of deviation from ideal behaviour and pK_a and α are calculated as follows:

$$pK_a = -log\left(\frac{[conjugatebase]}{[conjugateacid]}\right) \tag{2.23}$$

$$\alpha = \left(\frac{[conjugatebase]}{[conjugateacid] + [conjugatebase]} \right) \tag{2.24}$$

For the GC and GC-M titrations the first equivalence point is due to the titration of excess HCl in solution and thus this can be taken as the point at which the titration of the polymer begins (α = 0). In the case of the CMC and CMC-M the dissolved polymer is in the fully protonated form at the beginning and thus the start point is α = 0. The equivalence point of the polymer occurs when the polymer is fully deprotonated (α = 1). The variation in α with pH was calculated. A plot of pH against $\log\left(\frac{\alpha}{1-\alpha}\right)$ yields the value of n and pK_a from the gradient and y intercept values of the linear region between -0.5 < α < 0.5.

The degree of deacetylation of GC was also calculated from the titration curves. The number of moles of amine in solution was calculated from the number of moles of NaOH required to go from α = 0 to α = 1. Based on the initial concentration of the polymer and the mass of the monomers, the percentage of monomers which had the amine functionality (those which had been deacetylated) was calculated, and used as a comparison with the deacetylation calculated via NMR.

2.7.5 Hydrogel and prototissue formation

2.7.5.1 Photogelation

To aid dissolution, lyophilised methacrylated polymers were first manually pulled apart. Polymers were then stirred in water (concentration 8% w/v) at room temperature for roughly one day, with vigorous manual mixing at intervals. The homogeneous stock solutions were stored in the fridge (2 - 8 °C) until use. The photo initiator I2959 was heated to 70°C in water to dissolve (1 mL of 4% w/v, 178 mM), and then maintained at a temperature of 55 °C in the dark. Fresh I2959 stocks were prepared daily.

To form pre-gel solutions, methacrylated polymer stocks (GC-M or CMC-M) were weighed out into eppendorphs to bypass errors that would occur from pipetting volumes of very viscous solutions. The eppendorphs were placed in the Grant Dry Block Thermostat at 55 °C, this prevented precipitation of I2959 when it was added but also helped to reduce solution viscosity. DI water and I2959 stock were added and the solution vigorously mixed with a pipette to give a pre-gel solution with final concentrations 2% w/v methacrylated polymer and 0.5% w/v I2959. Examples where these concentrations were varied followed the same method and are specifically noted in the results.

All photogelation was carried out using a UV lamp with a 365 nm filter and a and collimator lens. The height of the collimator lens was set at 13 cm from the benchtop in all cases the lamp was set to 100% power.

Initial photogelation tests were carried out using the inversion method. A small volume (10 μL/mL pre-gel solution) of food colouring was added to the pre-gel solution to aid in

visualisation, and the mixture added to a glass vial. Vials were held at an angle and irradiated for 75 s or 150 s as indicated. Vials were placed upright and when samples holding their shape instead of flowing to fill the bottom of the vial indicated gelation.

Controls were carried out where I2959 was omitted from solution, non-methacrylated polymer (glycol chitosan or carboxymethyl cellulose) was used, or the vial was kept in the dark instead of being irradiated. For comparison photogelation was also carried out in an inert atmosphere, by bubbling the pre-gel solution with argon and sealing the vial prior to irradiation.

The process for forming free standing hydrogel pieces via photogelation is shown in Figure 2.8. PMMA moulds were formed using the same design as those described in Section 2.6.2.1. Prior to use all mould pieces were treated using RainX hydrophobic spray, as this facilitated hydrogel removal from the mould. The PMMA frame of desired dimensions was clipped to a PTEG sheet and solution added. A second PTEG sheet was added and clipped on top, taking care to avoid bubbles. The mould was irradiated for the desired length of time (45 to 600 s) to induce hydrogelation.

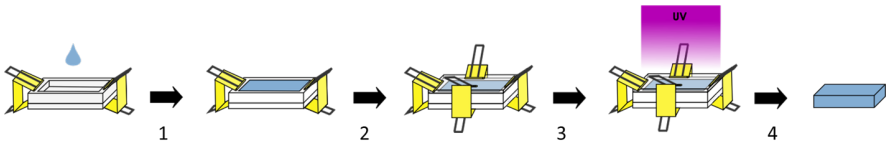

FIGURE 2.8. A scheme of the method used for forming free standing hydrogel monolayers by photogelation. (1) Pre-gel solution is added to the assembled mould. (2) The lid is placed over the solution and clipped in place, with care that no bubbles are formed. (3) The solution is irradiated at 365 nm to induce gelation. (4) The free standing hydrogel is removed from the mould.

As an example of the photopatterning possible with this gelation method, a masking technique was used to create a hydrogel with the Centre for Organised Matter Chemistry logo embedded. The shapes were drawn onto the top PTEG piece using marker to prevent light reaching the pre-gel solution. After irradiation, ungelled solution was removed from the sections under the mask and fresh pre-gel solutions containing different dyes were added to the voids. Further irradiation lead to the formation of a hydrogel with patterned shapes.

2.7.5.2 Formation of bilayer hydrogels

Bilayer hydrogels were formed from adjoined layers of CMC-M hydrogel and GC-M hydrogel as shown by the scheme in Figure 2.9. Pre-gel solutions containing 2% w/v methacrylated polymer and 0.5% w/v I2959 were formed as described in Section 2.7.5. The pre-gel solution of CMC-M was added to a 2.5 x 0.5 x 0.1 mm PMMA mould and irradiated for 10 minutes at 365 nm. The hydrogel piece was then inverted and placed in the bottom of a 2.5 x 0.5 x 0.2 mm PMMA mould.

The GC-M pre-gel solution was added on top and irradiated for 10 minutes to directly gel the two pieces together.

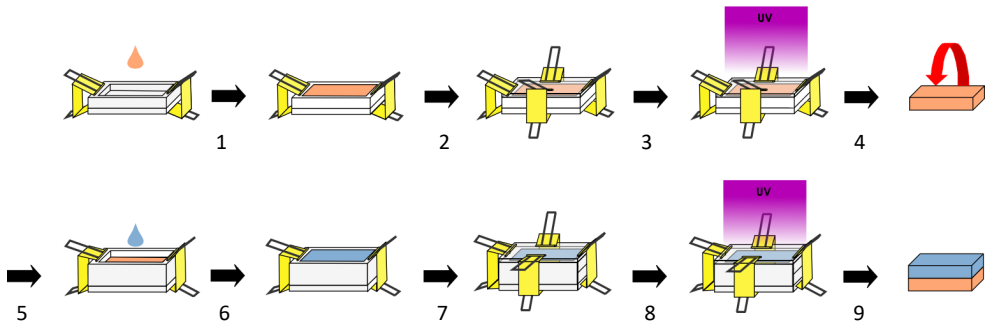

FIGURE 2.9. A scheme of the method used for forming free standing hydrogel monolayers by photogelation. (1) Pre-gel CMC-M solution (shown as orange in the scheme) is added to the assembled mould. (2) The lid is placed over the solution and clipped in place, with care that no bubbles are formed. (3) The solution is irradiated at 365 nm to induce gelation. (4) The free standing hydrogel is removed from the mould. (5) The CMC-M hydrogel is inverted and placed into a 2 mm deep mould. (6) GC-M pre-gel solution (shown as blue in the scheme) is added on top of the CMC-M layer. (7) The lid attached. (8) The mould is irradiated at 365 nm again. (9) The bilayer hydrogel is removed.

2.7.5.3 Formation of prototissues

URS colloidosomes and GOx colloidosomes were formed as described in Section 2.7.1. URS colloidosomes were formed using a solution of 2270 U/mL at pH 4.5 and crosslinked using 15 μL TMOS. GOx colloidosomes were formed using a solution of 2270 U/mL at pH 4 and crosslinked using 15 to 20 μL TMOS. After transfer to water the total sample volume was adjusted to 500 μL. To form hydrogels containing protocells (prototissue monolayers), colloidosomes were combined with initiator and polymer (CMC-M or GC-M) and gently but thoroughly mixed to form the pre-gel solution (final concentration 2% w/v methacrylated polymer and 0.5% w/v I2959). Usually 100 μL colloidosome sample (50 μL of each type) were used in 200 μL pre-gel solution, although in some cases the ratio of the colloidosomes is varied and this is indicated in the results discussion.

The pre-gel solution was placed into the mould (2.5 x 0.5 x 0.1 cm) and immediately irradiated (10 minutes) as before, to prevent sinking of the colloidosomes within the hydrogel. The formation is depicted in Figure 2.10.

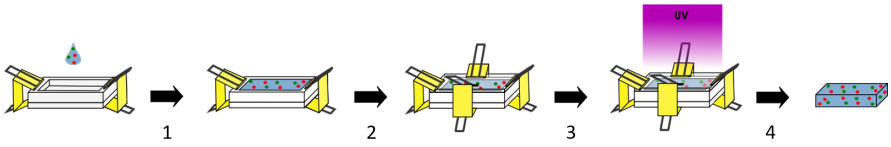

FIGURE 2.10. A scheme of the method used for forming free standing prototissue monolayers by photogelation. (1) Pre-gel solution containing colloidosomes (red and green circles) is added to the assembled mould. (2) The lid is placed over the solution and clipped in place, with care that no bubbles are formed. (3) The solution is irradiated at 365 nm nm to induce gelation. (4) The free standing hydrogel prototissue is removed from the mould.

For the formation of prototissues bilayers, the same procedure described in Section 2.7.5.2 was used, with the CMC-M layer being formed first and the GC-M layer being gelled directly on top (Figure 2.11).

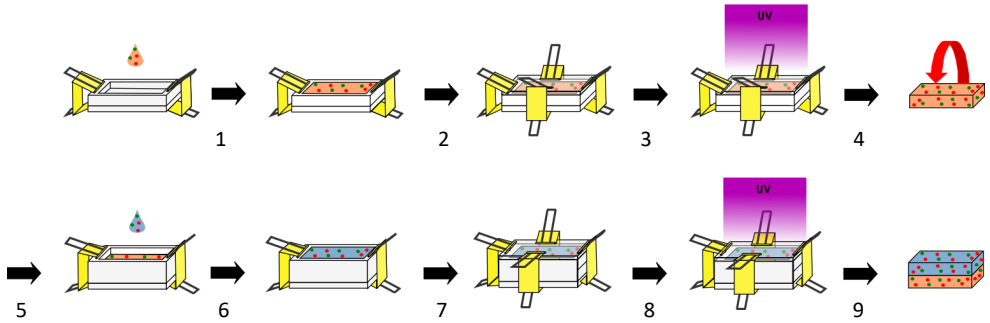

FIGURE 2.11. A scheme of the method used for forming free standing prototissue bilayers by photogelation. (1) Pre-gel CMC-M solution (shown as orange in the scheme) containing colloidosomes (red and green circles) is added to the assembled mould.(2) The lid is placed over the solution and clipped in place, with care that no bubbles are formed. (3) The solution is irradiated at 365 nm to induce gelation. (4) The free standing hydrogel is removed from the mould. (5) The CMC-M hydrogel is inverted and placed into a 2 mm deep mould. (6) GC-M pre-gel solution (shown as blue in the scheme) containing colloidosomes is added on top of the CMC-M layer. (7) The lid attached. (8) The mould is irradiated at 365 nm again. (9) The bilayer hydrogel prototissue is removed.

2.7.6 Photography and RGB measurements

A general method for monitoring colour by measuring RGB values from images and converting to hue angles was outlined in Section 2.3.4.1. To monitor pH changes within hydrogel prototissues universal indicator (UI) was included in the bulk aqueous solution. A pH indicator gives a colorimetric sign of a pH change because its conjugate acid form has a different colour from the conjugate base. Below the pK_a the majority of the molecules are in the acidic form and so the indicator solution is one colour, but as the pK_a is increase to above the pK_a a colour change occurs as the majority of the molecules are in the basic form. Universal indicator is a mixture of several indicators with different pK_as. The overall colour is formed due to the combination of all the colours, meaning that instead of showing two colours, the mixture shows a gradient of colours across a wide pH range.

Reliable measurement of the RGB values required shadow free, constant and homogeneous

illumination. For RGB measurement hydrogels were placed on top of a light board and imaged from above. The lights in the room were kept on throughout imaging and the system was partially enclosed within a box to reduce the impact ambient light changes. The camera was used in manual mode rather than automatic so that the aperture (f7.1), shutter speed (1/40) and ISO (100) could be set to reduce fluctuations in the lighting and colour.

Illumination from the light board appears slightly blue when processed and hence all images were white balanced with a macro (based on code published by V. Bindokas [134] and adapted for use by Dr Stephen Cross from the Wolfson bioimaging facility, University of Bristol). The macro takes measurements from a user specified area of the background and applies the conditions which white balance this, to the whole image. RGB values were measured using the RGB measure plugin on Fiji Image J, and were converted to hue angles as previously described.

Images of hydrogel monolayers and prototissue monolayers which were not used in RGB measurements were taken on a white background with lighting from above (top lighting method). These images were white balanced and brightness adjusted for use in figures.

2.7.7 Hydrogel and prototissue characterisation

2.7.7.1 Measuring hydrogel pH response

Individual GC-M and CMC-M hydrogels or prototissues were formed via photogelation as previously outlined. The final methacrylated polymer concentration was 2% w/v and I2959 was used at 0.5% w/v. Hydrogels were irradiated for 10 minutes in 2.5 x 0.5 x 0.1 cm PMMA moulds. Each hydrogel was cut into three pieces (ca. 0.8 x 0.5 x 0.1 cm) and one piece used for each swelling test.

Acetate buffer (30 mM pH 3, 4, 5 and 6) and Tris buffer (30 mM pH 7, 8 and 9) containing universal indicator (7.5 μL /mL) were adjusted to a calculated ionic strength of 0.03 M using NaCl. In order to calculate the ionic strength of the buffer (for simplicity the ionic strength contribution of the universal indicator solution is ignored but since the amount of indicator used is small this contribution would be small) and thus the amount of NaCl required for each solution, the following equations were used:

$$pH = pK_a + log\left(\frac{A^-}{HA}\right) \tag{2.25}$$

$$I = \frac{1}{2}\sum_i (c_i z_i)^2 \tag{2.26}$$

Where [A^-] is the concentration of the deprotonated species, [HA] is the concentration of the protonated species, I is the ionic strength, and C_i and Z_i are the concentration and valence (charge) of each species. The pK_a values for acetate and Tris buffer are 4.74 and 8.1 respectively.

Hydrogels were weighed after formation and then submerged in 15 mL buffer solution and left to equilibrate at room temperature. After 24 hours the solution was removed, and excess removed from the surface of the hydrogels by wicking with filter paper. The hydrogels were weighed again and the swelling ratio calculated as follows:

$$S_r = \frac{M_f}{M_i} \times 100\% \tag{2.27}$$

Where M_f is the final mass of the swollen hydrogel and M_i is the initial mass of the hydrogel after formation.

For hue angle measurements the swelling experiment was repeated on a single whole gel at each pH. The swollen hydrogels were imaged using the RGB measurement setup described in Section 2.7.6 (back lighting using light board, imaged from above). RGB values were measured at three points within the hydrogel and converted to hue angles. The standard deveiation of the three hue values was calculated. Images taken on the LED board are unrepresentative of hydrogel appearance in the case of single layer hydrogels. To get around this, hydrogels were also were imaged on a white background (top lit) and these images were white balanced and used for figures, but were not used for any RGB measurements.

2.7.7.2 Characterisation of the pH response of bilayer hydrogels

Hydrogel bilayers were formed using the method described in Section 2.7.5.2 and soaked in DI water to remove unreacted species. Bilayers were placed in 25 mL buffer (pH 3 or 5 acetate 30 mM or pH 7 or 9 Tris 30 mM) containing universal indicator (7.5 μL/ mL) which were prepared, and ionic strength adjusted (to 0.03 M) as previously described. Bilayers were left overnight to equilibrate and then imaged on the LED board (back lit) (Figure 2.12).

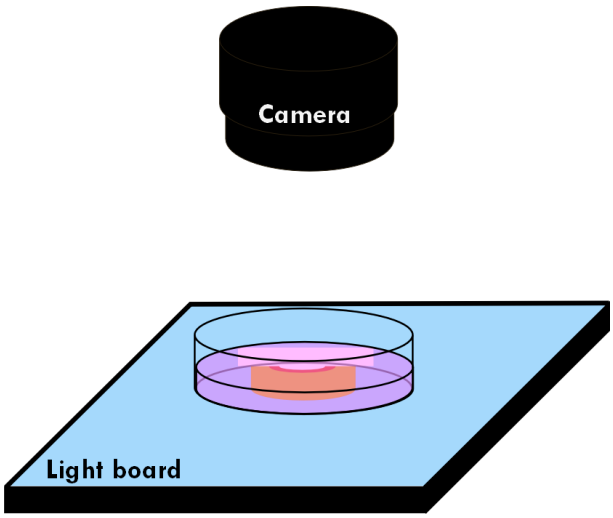

FIGURE 2.12. A scheme showing the method used for imaging bilayer hydrogels by placing them on a light board and imaging from above (referred to as backlit).

The bending of the hydrogel in response to changes in pH was quantified by measuring the curvature, which is defined as:

$$\kappa = \frac{1}{R} \tag{2.28}$$

Where κ is the curvature (in cm^{-1}) and R is the radius of the circle which osculates the curve (in cm)(Figure 2.13). Fiji Image J was used to find the value of R. Three points are marked on the interface of the two layers within the hydrogel and the "fit circle" tool used to create the osculating circle. The area of the circle is measured, and used to find R and thus κ. The experiment was repeated in triplicate and the average values calculated.

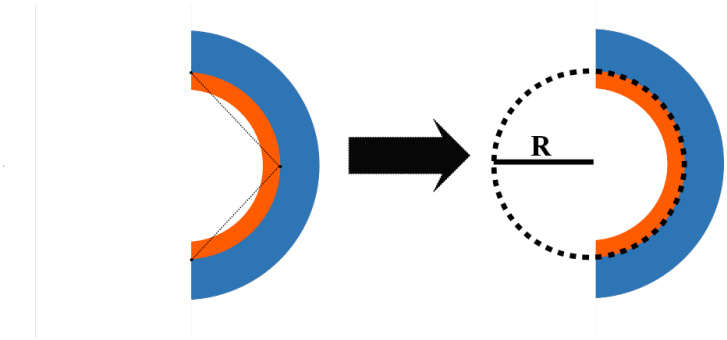

FIGURE 2.13. A scheme showing the method used for finding an osculating circle for the hydrogel curve. Three points are selected along the interface of the two hydrogel layers (GC-M layer shown in orange and CMC-M layer shown in blue) and a circle is fitted to these three points. The radius of the circle (R) is used in the calculation in Equation 2.28.

To show the reversibility of the pH induced actuation, bilayer hydrogels were placed into a petri dish adapted using capillary tubes to hold the hydrogel in place (Figure 2.14). This prevents hydrogel from tipping over when the curvature is 0 and holds them in the same position in the dish. Bilayer hydrogels were first equilibrated overnight with pH 3 acetate buffer (30 mM, I 0.03 M) containing universal indicator. The buffer was replaced with pH 9 Tris buffer (30 mM, I 0.03 M) and the system imaged every 5 minutes on the LED board. After two hours the buffer was removed and replaced with pH 3 and the whole cycle was repeated 3 times. The curvature value of the hydrogel was measured every 20 minutes and the experiment was repeated in triplicate. Some anomalous values where the hydrogel appeared to briefly stick, were removed.

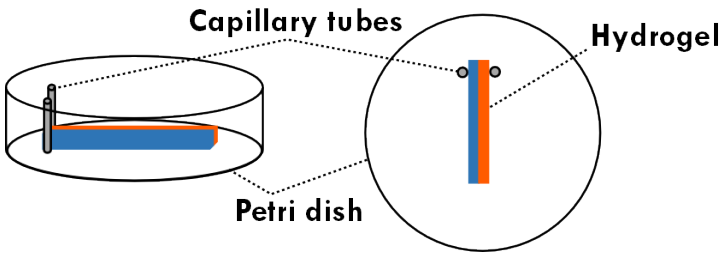

FIGURE 2.14. A scheme showing the holders used for actuation and chemo-mechanical transduction experiments. Hydrogels (GC-M layer shown in orange and CMC-M layer shown in blue) are held in place by two upright capillary tubes in a petri dish.

To characterise the pH response of prototissue bilayers (formed with GOx and URS colloidosomes as described in Section 2.7.5.3), the characterisation used for hydrogel bilayers was extended. Prototissue bilayers were placed in 25 mL buffer (pH 3, 4, 5 or 6 acetate 30 mM or pH 7, 8 or 9 Tris 30 mM) containing universal indicator (7.5 μL/ mL) which were prepared, and ionic strength adjusted (to 0.03 M) as previously described (Section 2.7.7.1). After overnight equilibration the hydrogels were imaged using the backlit setup. Curvatures were calculated and RGB measurements taken for hue angle determination. All experiments were repeated in triplicate and average values of both curvature and hue calculated for each pH. This method was used to calibrate the system so that the hue angle of the GC-M layer (hue_{GC-M}) could be quantitatively linked to pH in later experiments.

2.7.7.3 Fluorescence microscopy of prototissues

GOx and URS colloidosomes were formed with 1 mg/mL fluorescently labelled BSA (FITC-BSA or DL650-BSA) and crosslinked as normal. After transfer to water colloidosomes were used to form individual CMC-M or GC-M prototissue monolayers, which were imaged directly on a widefield fluorescence microscope. Prototissue bilayers formed using the fluorescent colloidosomes were cut to produce a cross section and then soaked in water overnight (to induce bending) prior to imaging.

2.7.7.4 SEM of prototissues

Colloidosomes containing URS and GOx were frozen by adding 50 μL to an SEM stub and placing in a shallow bath of liquid nitrogen. The frozen samples were lyophilised and then placed onto a carbon pad and silver coated.

Hydrogels pieces and bilayers were formed and left to soak for 2 hours in DI water before being cut into thin sections which were dropped directly into liquid nitrogen. Once the pieces were frozen, they were fractured and lyophilised. The fractured surface was placed facing upwards on an SEM stub and silver coated prior to imaging.

2.7.7.5 Rheology

Hydrogels were formed by irradiating solutions containing 2% w/v GC-M or CMC-M and 0.5% w/v I2959 for 10 minutes in 2.5 x 2.5 x 0.1 cm moulds. To form prototissues GOx and URS colloidosomes were included in the pre-gel solution at a concentration of 50 μL each in 200 μL solution. The resulting hydrogels or prototissues were swelled overnight in DI water. Prior to testing the were cut to cylinders of 19 mm diameter using a metal bore cutter so that they approximately matched the geometry of the rheometer. Excess water was wicked off the hydrogel surface using filter paper. A hydrogel disk was placed onto the rheometer baseplate and the 20 mm flat plate geometry lowered until a set force of 1 N was achieved. SAOS strain amplitude sweeps were carried out from 0.1 to 100% using a frequency of 1 Hz. Based on the strain amplitude sweeps a value of 0.1% strain was chosen to run SAOS frequency sweeps between 0 and 25 Hz. Each hydrogel was used for one experiment and all frequency sweep experiments were carried out in triplicate.

2.7.7.6 Polymer permeation into colloidosomes

To study the interaction of GC-M or CMC-M with the colloidosomes they were labelled with fluorescent dyes. Fluorescent labelling of GC-M was achieved using a similar method to that used for protein labelling. A solution of amine reactive dye (FITC, 0.47 mg, 0.0013 mmol, 0.005 eq.) in DMSO was added to a solution of GC-M in pH 8.5 sodium carbonate buffer (5 mL of 10 mg/mL) and the solution stirred for 24 hours. The polymer was then dialysed against water for 24 hours before being lyophilised.

To produce fluorescent CMC-M, another EDC coupling reaction was used. CMC-M (200 mg, 0.98 mmol monomer) was dissolved in DI water (final concentration 5 mg/mL) and the pH was adjusted to 6.5. Solution of EDC (1.8 mg, 0.012 mmol, 0.012 eq.) and fluoresceinamine (4 mg, 0.012 mmol, 0.012 eq.) were added and the pH adjusted to 6.5 again. After 4 hours the pH was raised to 8.5 and the reaction left overnight. To purify the product the solution was dialysed against DI water for several days before being lyophilised.

To calculate the extent of labelling of the polymers, UV/Vis spectroscopy was used. A spectrum was recorded for a solution of known concentration of the labelled polymer. The concentration of fluorescein in the solution was calculated using the Beer-Lambert law:

$$c = \frac{A}{\epsilon L} \tag{2.29}$$

Where c is concentration of the dye, A is absorbance at the wavelength or maximum absorption (λ_{max}) ϵ is the molar absorptivity and L is the path length of the cuvette (1 cm). To calculate a percentage of labelling the following relationship was used:

$$Labelling = \frac{[dye]}{[monomer]} \times 100\% \tag{2.30}$$

Aqueous stock solutions (2% w/v) of labelled CMC-M (F-CMC-M) and labelled GC-M (FITC-GC-M) were formed. Both solutions contained precipitate, which was removed via filtration before use, but for the sake of simplicity the concentration was estimated 2% w/v. The fluorescent polymer stock solutions were mixed with 8% w/v stock of methacrylate polymer to give solutions of approximately 0.5% w/v FITC-GC-M 3.5% w/v GC-M or 2% w/v F-CMC-M 2% w/v CMC-M. The mixtures were equilibrated to 55°C in a Grant Dry Block Thermostat before photo initiator solution, water and colloidosomes were added to form the pre-gel solution (c.a. 2% w/v total GC-M or CMC-M (including fluorescent analogues), 0.5% w/v I2959 and 40 μL colloidosomes per 200 μL pre-gel solution) and the suspension gently mixed. The pre-gel solution was injected into the 2.5 x 0.5 x 0.1 cm PMMA/PTEG mould. The lid was attached, and the mould irradiated for 10 minutes using the previously outlined settings. The resulting hydrogel prototissue monolayers were removed from the mould after gelation and stored in a humid environment in a fridge (2 - 8 °C) until imaging using confocal microscopy.

2.7.7.7 Dye uptake in colloidosome prototissues

GC-M and CMC-M prototissue monolayers were formed using URS and GOx colloidosomes as described in Section 2.7.5.3. Solutions of Rhodamine B (0.01 mg/mL in 5 mM Tris buffer at pH 7.5) and fluorescein (0.01 mg/mL in 5 mM Tris buffer at pH 7.5) were prepared. Small samples of the prototissue hydrogels were submerged in the 5 mL dye solution and left overnight at room temperature in the dark. For comparison, colloidosome suspensions were soaked in the two dyes without the presence of a hydrogel matrix. Colloidosomes (20 μL GOx or URS containing colloidosomes) were added to 100 μL dye solution (Rhodamine B and fluorescein as above) and stored overnight in the dark. Colloidosome and prototissue samples were imaged without further processing on a confocal microscope.

2.7.8 Kinetics of enzyme responsive hydrogel swelling

To test the activity of enzyme-containing colloidosome protocells within hydrogels, individual GC-M or CMC-M hydrogel pieces were formed with URS an GOx colloidosomes, following the method described in Section 2.7.5.3. Immediately after formation the initial mass of the hydrogels was recorded (M_i). The hydrogels were immersed in DI water for 1 hour before being added to aqueous UI solutions that had been adjusted to either pH 4 or pH 9 and left to equilibrate overnight.

The pH of the solutions after overnight equilibration was measured and, particularly in the case of the high pH solution, were found to have changed slightly due to the buffering effect of the hydrogel. Aqueous solutions of urea (25 mM) or glucose (100 mM) with UI were adjusted to roughly the same pH as the equilibrated solution (around pH 4.3 for urea solutions or pH 7.2 for glucose solutions). Hydrogels were removed from the solutions and excess water wicked off

using filter paper. The mass of the hydrogels was recorded ($M_t = 0$) and they were imaged (top lit, images for figures only).

To initiate the enzymatic reactions, hydrogels were submerged in the urea or glucose solutions (those which were left in pH 4 overnight in urea and those in pH 9 in glucose). At predetermined time intervals, the solution pH was measured, and the gels were removed, and the weighing and imaging procedures repeated. The swelling ratio at time t (S_t) was calculated as follows:

$$S_t = \frac{M_t}{M_i} \times 100\% \tag{2.31}$$

Control experiments were carried out using prototissue monolayers formed with plain colloidosomes (containing BSA instead of GOx or URS).

2.7.9 Chemo-mechanical transduction in bilayer prototissues

Prototissue bilayers were formed using the method described in Section 2.7.5.3 and were placed in petri dishes adapted with capillary tubes to act as holders (Figure 2.14). The prototissues were soaked in DI water for 1 hour before the solution was replaced with 15 mL DI water containing 7.5 μL/mL universal indicator. Prototissues were left to equilibrate overnight in the fridge (2 - 8 °C) and were then left to warm to room temperature prior to use. The sample dish was placed on top of an LED lightboard and imaged from above using the manual camera settings previously outlined (Section 2.7.6). To initiate the reaction the solution was replaced with 25 mL DI water containing 7.5 μL/mL universal indicator along with urea or glucose at the desired concentration. Initial experiments utilising just one substrate were carried out over a period of 8 hours. Images were taken every 20 minutes for the course of the experiment. Images were processed as previously described: each image was white balanced in Fiji Image J and the curvature of the bilayer measured.

RGB values were measured in 3 areas of the GC-M layer of the hydrogel and used to calculate hue angles (hue_{GC-M}). Each experiment was carried out in triplicate and average values and standard deviations calculated. One run of each experiment was carried out with a pH probe monitoring the solution pH. The internal pH of the hydrogel (pH_{pt}) is estimated using the calibration graph created in Section 2.7.7.2. Each time the hue_{GC-M} reaches the value which was found to correlate to a certain pH, the hydrogel is assumed to have reached that pH. If the hue_{GC-M} value was reached between two measurement points, the relevant pH was assigned to the time half way between the two measurements. Hue_{GC-M} at pH 9 was lower than pH 8, which went against the trend in the rest of the calibration. To get around this when plotting pH values from hue_{GC-M}, a pH value of 9 was only plotted if the relevant hue value is both preceded and followed by a hue value equivalent to pH 8.

2.7.9.1 Out-of-equilibrium chemo-mechanical transduction using standard prototissues

To create transient pH states and back and forth motion (refered to as A->B->(C->A')), combinations of glucose and urea were used. The experiments were set up as with the single substrate runs, with the prototissue first being submerged in 25 mL of 100 mM glucose. After four hours 1 mL of urea solution was added. The resulting initial urea concentration was calculated assuming a total volume of 26 mL and was varied between 2.5 mM and 25 mM to assess the effect of different substrate concentrations. After the addition the solution was mixed gently by pumping the pipette tip to ensure that the urea distributed evenly. All experiments were run in triplicate and processed using the method described for the single substrate runs.

2.7.9.2 Out-of-equilibrium chemo-mechanical transduction using prototissues with heterogeneous protocell distribution

Prototissues were formed with spatially segregated colloidosome populations. One type of colloidosome was trapped within each layer by including 100 μL of GOx or URS colloidosomes in 200 μL pre-gel solution. Prototissues where the URS colloidosomes were in the GC-M layer and the GOx colloidodomes were in the CMC-M layer are refered to as prototissue$_{Ug-Gc}$ and prototissues where the URS colloidosomes were in the CMC-M layer and the GOx colloidodomes were in the GC-M layer are refered to as prototissue$_{Uc-Gg}$. Patterned prototissues were run using the staggered addition of substrates outlines in Section 2.7.9.1.

Further patterning of colloidosome populations was achieved using photopatterning (to form prototissue$_{NU}$ (Figure 2.15). A CMC-M pre-gel solution was formed with URS colloidosomes (100 μL in 200 μL solution) and was injected into the 2.5 x 0.5 x 0.1 cm mould. The piece of PTFE used to cap the mould was half covered with a mask (Figure 2.15). The solution was irradiated for 2 minutes to induce hydrogelation in in the irradiated section. The cap was removed and the ungelled solution gently removed. Pre-gel CMC-M solution containing GOx colloidosomes (100 μL in 200 μL solution) was injected into the gap left by the photomasking. A fully transparent mask was placed on top and the whole mould irradiated for 10 minutes. The patterned CMC-M gel was inverted and placed into the 2.5 x 0.5 x 0.2 cm mould. GC-M pre gel solution was formed with URS colloidosomes (100 μL in 200 μL solution) and injected into the mould. Again, the mask was placed on top, with the masked section above the URS colloidosome containing region of the CMC-M hydrogel. Once again irradiation was applied for two minutes, and ungelled solution was removed. GOx colloidosomes were used to form a pre-gel solution which was placed into the void left by the mask. The ensemble was irradiated for ten minutes. Chemo-mechanical transduction experiments were carried out using the method described above for non-patterned hydrogels.

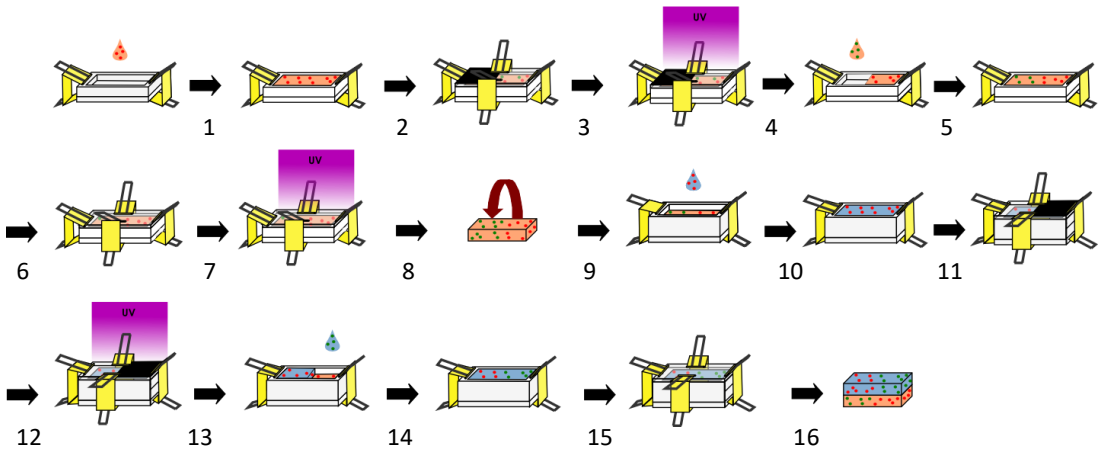

FIGURE 2.15. A scheme of the method used for forming patterned prototissue bilayers by photopatterning. (1) Pre-gel CMC-M solution (shown as orange in the scheme) containing GOx colloidosomes (red circles) is added to the assembled mould. (2) A lid that is half covered by a mask is placed over the solution and clipped in place, with care that no bubbles are formed. (3) The solution is irradiated at 365 nm to induce gelation. (4) Ungelled solution that was covered by the mask is removed from the mould. (5) The empty section of the mould is filled with pre-gel CMC-M solution containing URS colloidosomes (green circles). (6) A lid (no mask) is placed over the solution and clipped in place, with care that no bubbles are formed. (7) The solution is irradiated at 365 nm to induce gelation.(8) The patterned CMC-M hydrogel is inverted and placed into a 2 mm deep mould. (9) GC-M pre-gel solution (shown as blue in the scheme) containing GOx colloidosomes is added on top of the CMC-M layer. (10) A lid that is half covered by a mask is placed over the solution and clipped in place, with care that no bubbles are formed. The masked section of the lid is placed so that it covers the section of the CMC-M hydrogel that contains GOx colloidosomes. (12) The solution is irradiated at 365 nm to induce gelation. (13) Ungelled solution that was covered by the mask is removed from the mould. (14) The empty section of the mould is filled with pre-gel GC-M solution containing URS colloidosomes. (15) A lid (no mask) is placed over the solution and clipped in place, with care that no bubbles are formed. (16) The solution is irradiated at 365 nm to induce gelation, and the bilayer hydrogel prototissue is removed from the mould.

Control experiments were carried out using bilayers containing plain colloidosomes. The

colloidosomes were formed using 100 mM pH 4 acetate buffer with 3 mg/mL BSA and crosslinked as normal. The prototissue bilayers containing these plain colloidosomes were formed using the same method as previously described and chemo-mechanical transduction experiments carried out using the same method as for the standard prototissues. Control were also run using bilayer hydrogels containing free enzyme. Enzyme solutions were first dialysed to remove buffer solutions in the lyophilised powders. To form the pre-gel solutions 100 μL aqueous enzyme solution (URS and GOx, both at 568 U/mL) was added to the polymers and initiator. The standard methodology for creating the hydrogel and running the chemo-mechanical transduction experiments was followed.

CHAPTER 3

RE-EXAMINING THE STRUCTURE OF COLLOIDOSOME PROTOCELLS

3.1 Chapter overview

In this chapter, the structure of silica-based colloidosome protocells is investigated. The previously described model of a hollow capsule with a porous membrane is disproved. Instead the colloidosomes are described as having a silica nanoparticle membrane with a secondary silica network inside, resulting from the condensation of TMOS during the crosslinking procedure. The nature of this silica network is shown to vary with the pH of the aqueous phase used to form the colloidosomes. Investigations into the permeability of the colloidosomes are presented, proving that the membrane is porous. The internal silica network colloidosomes can adsorb molecules from solution and this allows colloidosomes to build up above equilibrium concentrations in their interior and retain molecules inside after the solutions are washed away. The colloidosome membranes are shown to be permeable to large molecules such as proteins, indicating that the molecular weight cut off of the membrane is far greater than has previously been described and based on this a new mechanism for protein entrapment within colloidosome protocells is suggested. The activity of colloidosomes containing the enzyme horseradish peroxidase is investigated.

3.2 Introduction

3.2.1 Formation of silica using sol-gel chemistry

Silica (SiO_2) is an incredibly abundant material, found naturally in both abiotic and biotic contexts [135]. How silica is formed dramatically affects its properties, with structures ranging from hydrogels to crystalline (in materials such as quartz). This discussion focuses of formation of

silica via condensation of monomeric species and the result is always amorphous and formed from interconnected SiO_4 tetrahedra with varied Si-O bond angles and lengths [136]. The formation of silica from a solution of monomers is referred to as the sol-gel processes. Monomers react to give a colloidal solution, which then transforms into an infinite three dimensional (3D) network or gel [135, 137].

To form silica synthetically, silicon alkoxides ($Si(OR)_4$), are often used as precursors because orthosililic acid cannot occur in solution above very low concentrations [135]. The conversion from a solution of precursor to a silica gel shown by the overall equation (Equation 3.1), is described by three processes: hydrolysis (Equation 3.2), alcohol condensation (Equation 3.3) and water condensation (Equation 3.4). In the reactions shown below ≡ indicates bonds to three other groups, Si-OH, Si-OR or Si-O-Si. Note that for the three processes the reverse reactions are also possible. All the steps are affected by a wide range of factors such as precursor identity, concentration, catalyst, temperature, solvent, pH and the presence of other species such as small molecules, ions or biopolymers [136].

$$nSi(OR)_4 + 2nH_2O \rightarrow nSiO_2 + 4nROH \qquad (Overall) \tag{3.1}$$

$$\equiv Si(OR) + H_2O \rightleftharpoons \equiv Si(0H) + ROH \qquad (Hydrolysis) \tag{3.2}$$

$$\equiv Si(OR) + \equiv Si(0H) \rightleftharpoons \equiv Si - O - Si \equiv + ROH \qquad (Condensation) \tag{3.3}$$

$$\equiv Si(OH) + \equiv Si(OH) \rightleftharpoons \equiv Si - O - Si \equiv + H_2O \qquad (Condensation) \tag{3.4}$$

Hydrolysis proceeds via nucleophilic attack of the oxygen in water on the silicon of Si-OR, leading to loss of an alcohol and formation of an Si-OH bond (silanol). The mechanism is bimolecular (S_N2) and the reaction is catalysed by both acidic and basic conditions. In acidic conditions the OR group is pronated making it a better leaving group, whereas in basic conditions OH^- acts as the nucleophile. The rate of hydrolysis varies with pH as shown in Figure 3.1, with a minimum at neutral pH, which increases either side. The rate of hydrolysis is also affected by other factors. Alkyl chain length and branching are important as they can lead to steric hindrance and reduce the hydrolysis rate. Unsurprisingly, the water-to-Si ratio also affects hydrolysis rate with higher water content increasing hydrolysis rates at all pHs. The electron donating and withdrawing characteristics of the silicon alkoxide OR groups are important because they affect the transition state stability, although the consequence of these inductive affects varies with solution pH. Once hydrolysis has occurred, further hydrolysis is possible, leading to species with multiple silanol groups.

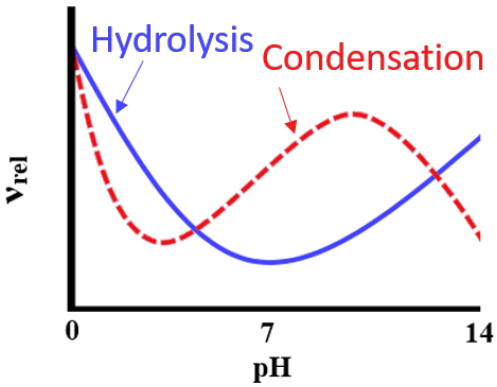

FIGURE 3.1. pH dependence of the rate of the hydrolysis (Equation 3.2) and condensation (Equation 3.3 and 3.4) steps in the formation of silica from siloxanes. The rate of siloxane hydrolysis is shown in blue and the rate of condensation is shown in red. Figure adapted from [138].

Condensation between a silanol (Si-OH) and silicon alkoxide (Si-OR) or another silanol leads to polymerisation through the formation siloxane (Si-O-Si). Like hydrolysis, this occurs via a bimolecular nucleophilic substitution and the process is strongly affected by solution pH (Figure 3.1) [137]. This process is further complicated by the fact that it can involve condensation between species with varying degrees of hydrolysis and the other substituents on silica affect the acidity, and therefore reactivity of the reacting silanol group. In low pH solution condensation rate is low (minimum at pH 2.5, the isoelectric point of silica) and is also essentially irreversible (the depolymerisation step is very slow). Condensation in low pH solutions leads to linear molecules with occasional crosslinking. As the condensation proceeds these linear molecules entangle to form a molecular 3D network (a gel) [137, 138] (Figure 3.2). Under basic conditions condensation is no longer irreversible and depolymerisation reactions occur easily. Polymerisation passes through a series of monomers, dimer, trimers and larger linear and cyclic oligomers eventually forming highly branched clusters [137, 138]. This process involves repeated polymerisation/ depolymerisation steps. Under the right conditions these particles come together to form a gel but at sufficiently high pH gelation is not seen: once they reach a certain size particles are electrostatically stabilised and do not come together to form a network [138]. This stabilisation occurs because although orthosililic acid ($Si(OH)_4$) has a pk_a of 9.8 this decreases as larger oligomers form and silanol groups on the surface of 1 nm oligomers have a pk_a of 6.8 and thus are negatively charged at neutral pH. At intermediate pHs (3 to 8) a series of transitional structures occur [138]. It is worth noting that the water-to-Si ratio is also important in condensation since

higher amounts of water favour the depolymerisation reaction.

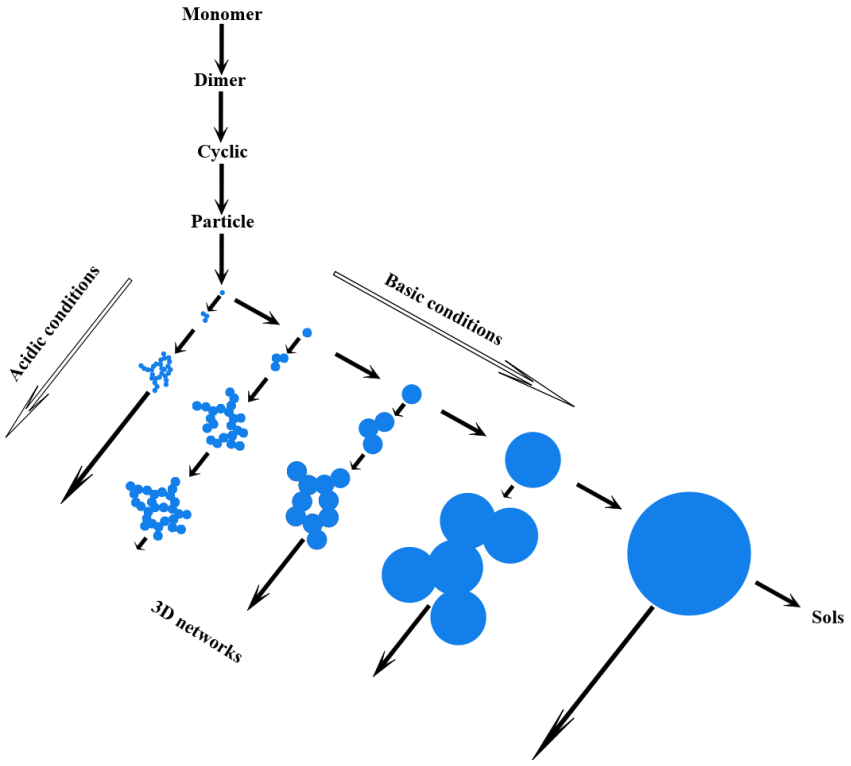

FIGURE 3.2. A schematic depicting the routes of silica format through oligonmers, particles and then aggregates. Under acidic conditions weakly branched structures form, whereas under basic conditions highly branched clusters emerge. Particles come together and form a gel, except at highly basic conditions where electrostatic repulsion between particles prevents gelation. Figure adapted from [136].

3.2.2 Bio-hybrid materials via entrapping or adsorption of proteins with silica

Silica is a commonly used substrate for enzyme immobilisation, via adsorption or covalent binding onto surfaces, entrapment within the material or intercalation in pores. The silica sol-gel chemistry described in Section 3.2.1 can be used for enzyme encapsulation, with enzymes remaining trapped within a silica cage formed around them [139]. As mentioned above alkoxides are commonly used as precursors for silica formation. However, this can be problematic when working with proteins that can be denatured by alcohols and there is a wealth of literature tackling this issue [135]. When trapped in a silica network, protein unfolding under unfavourable conditions (for example pH or temperature) can be reduced, due to the reduced mobility of the enzyme within the confined space [139]. Enzyme reactions can be carried out within silica gels, since they are porous, however, reaction rates may be decreased due to slowed mass transport of substrates through the silica matrix, particularly for bulkier substrates [140, 141]. Leaching

of proteins encapsulated via this method is minimal since the silica is formed around them. When using sol-gel chemistry to encapsulate proteins it should also be noted that the presence of biomolecules can also affect the silica formed. For example, biosilica formation, in species such as diatoms, utilises biopolymers to control the size, structure and shape of silica formed.

Silica can also be utilised to trap enzymes via surface adsorption. Physical adsorption occurs via electrostatic interactions, hydrogen bonding, Van der Waals forces and the hydrophobic effect. Globular proteins are strongly adsorbed to both hydrophobic and hydrophilic surfaces due to the heterogeneous surface distribution of charge and hydrophilic/ hydrophobic groups [142, 143]. The amount of protein adsorbed on a surface is affected by the hydrophobicity, charge, chemical makeup and surface area of the material but also the solution pH, ionic strength, solid to liquid ratio, temperature and the presence of other molecules thath compete to adsorb [135]. Maximum adsorption occurs when the solution pH is equal to the isoelectric point of the protein, as at this point electrostatic repulsion between adsorbed proteins is reduced and thus denser packing can be achieved [135, 143].

Proteins often undergo some degree of structural change when adsorbed onto solid surfaces such as silica nanoparticles and a stronger interaction leads to a greater conformational change [144]. The extent of the structure change is dependent on the nanoparticle size, surface coverage and solution pH. Some proteins are also more resistant to conformational change than others [143]. Loss of structure can in turn cause a loss of activity compared to the native enzyme but there are many examples that show retention of some activity of silica adsorbed proteins [143–146]. The adsorption of protein onto a solid such as silica is often described as irreversible because replacing the protein solution with pure solvent does not usually lead to significant desorption [147]. However, protein desorption is possible and can be induced by factors such as change in pH, ionic strength or by exchange with other surface-active molecules [147].

3.2.3 Crosslinking of emulsions using sol-gel chemistry

Hollow silica micro or nanospheres are of interest in a range of fields, such as micro-reactors or in drug delivery, particularly if they can be designed to allow release of encapsulated molecules only upon a certain trigger [17]. One method for forming such capsules involves the deposition of a silica layer on a sacrificial core, and dissolution of the template particle [148]. Of more interest to the work described in this thesis, however, is the use of sol-gel chemistry to create capsules from emulsions.

Alkoxysilanes such as tetraethyl orthosilicate (TEOS) or tetramethyl orthosilicate (TMOS) are not soluble in water, but upon hydrolysis the species formed are more hydrophilic. As a result, if you form a water-in-oil emulsion and add an alkoxysilane to the oil phase, the hydrolysed species move into the aqueous phase and condense inside. This leads to the formation of a solid silica particles rather than a hollow capsules [149]. Interestingly, when a cationic surfactant is used or a transition metal salt is present, this is not the case: hollow spheres can be achieved. The

silica nuclei or oligomers formed bear a negative charge and thus are attracted to the positive species at the water-oil-interface, resulting in preferential formation of silica here rather than within the aqueous interior [150, 151]. Methods like this do lead to formation of more porous silica and thus alter the permeability of the shell formed.

As described in Section 1.1.1.1, Pickering emulsions are stabilised by solid nanoparticles instead of surfactants. The silica sol-gel methods used for silica sphere formation from surfactant stabilised emulsions can also be applied to crosslink the membrane of silica stabilised Pickering emulsion and allow their transfer to water. The condensation and hydrolysis reactions of the alkoxysilane occur as before but can also include reactions directly with groups at the nanoparticle surface. Just as with surfactant stabilised emulsions, there is the potential for the species resulting from alkoxysilane hydrolysis to move into the droplet interior resulting in formation of silica within the droplet rather than only at the water-oil interface. Jiang et al formed water-in-oil Pickering emulsions from hydrophobised silica nanoparticles with an oil phase of toluene and aqueous solutions of ammonia [17]. The addition of TEOS to the oil phase lead to the formation of a hollow capsule with a distinct and continuous silica shell. They hypothesised that the silica particles at the interface were acting as guides for the sol-gel reactions of the TEOS, although it is unclear why this would happen in this case and not in other examples of silica colloidosomes. The silica shell contained small pores, but the colloidosomes were able to encapsulate small hydrophilic dyes because the hydrophobicity of the silica particles hindered the passing of the hydrophilic molecules.

In the work by Wang et al, silica nanoparticle stabilised Pickering emulsion were crosslinked using hyperbranched polyethoxysilane (PEOS) [152]. This molecule has decreased hydrophilic character when compared to TEOS or TMOS, even after hydrolysis. The hydrolysed species remains at the oil-water interface and thus the resulting capsules have a distinct silica layer. In colloidosomes formed at acidic pH, the silica shell was complete but nanoporous. They extended this work to show that the enzyme Laccase could be encapsulated and would retain activity towards substrates dissolved in the bulk phase [153].

Alkylchlorosilanes can be used as an alternative silica precursor and undergo equivalent hydrolysis and condensation steps. The presence of alkyl groups attached directly to the silica means that after hydrolysis they remain partially hydrophobic. When used to crosslink silica nanoparticle stabilised Pickering emulsions, they stay at the oil water interface and result in a continuous silica shell [154].

As discussed in Section 1.1.1.1, colloidosomes formed via the TMOS crosslinking of silica nanoparticle stabilised Pickering emulsions have been developed for use as protocell models. Evidence of a distinct silica membrane with a hollow core came from the collapse of the structures when imaged dry using SEM, although no direct imaging of the droplet interior was carried out and in fact the structure under SEM imaging conditions is not consistent across papers where different aqueous phase conditions or TMOS concentrations are used [5, 20]. The colloidosome

protocells were found to retain large biomolecules such as enzymes after transfer to water [5]. Enzymes such as alkaline phosphatase remained active after colloidosomes were crosslinked and transferred to water [21]. By functionalising the silica membrane with a pH responsive polymer as well as crosslinking with TMOS, Li et al were able to form a pH responsive membrane [21]. Small charged molecules such as dyes could be gated depending on the pH of the solution in which the colloidosomes were suspended. Inspection of the miscroscope images in this paper show that, in some cases, even under conditions in which the dyes are released from the colloidosomes, small amounts of fluoresence seem to remain inside the colloidosome droplet. This is not to say that the electrostatic gating does not work, but that there is some other factor at play which causes retention of small amount of dye. Furthermore, colloidosomes formed by crosslinking a silica nanoparticle stabilised emulsion often have a nonporous membrane and thus show low permeability and slow diffusion of even small molecules. The rapid diffusion of the dyes or enzyme substrates shown in the colloidosome protocells implies that the silica shell formed is more porous than those seen in other systems.

Fothergill et al showed that when the aqueous phase of the colloidosomes protocells formed is made up of a complex coacervate phase, the addition of TMOS results in particles with a solidified interior [9]. It is believed that the interaction between the positively charged PDDA from the coacervate phase and the silica nanoparticles inhibits the reaction between the TMOS and the nanoparticles. This allows more hydrolysed TMOS species to move into the aqueous phase.

Reviewing the previous work carried out on crosslinking silica nanoparticle emulsions using alkoxysilanes, the question arises as to whether the use of TMOS can really result in a completely hollow, aqueous filled microcapsule. The evidence is thus far inconclusive, and it does seem unlikely the hydrophilic species resulting from TMOS hydrolysis would remain solely at the interface without an additional driving force. Hydrolysed species moving into the emulsion aqueous phase would result in a secondary silica network within the colloidosome rather than a hollow capsule with a distinct crosslinked membrane (Figure 3.3). Since the presence of silica within the capsule lumen has the potential to alter the permeability, uptake and release of molecules and the enzyme activity of colloidosome protocells, this chapter aims to investigate internal structure of colloidosome protocells.

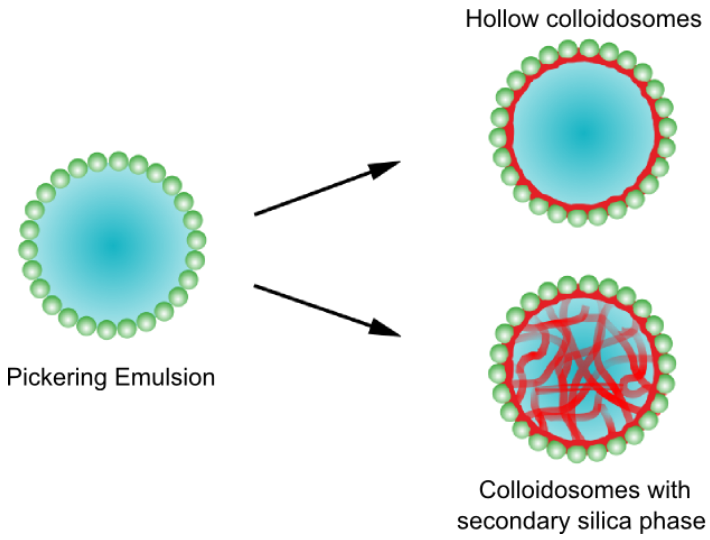

FIGURE 3.3. Schematic depicting the possible structures formed upon crosslinking a silica nanoparticle stabilised Pickering emulsion (left) with TMOS. Localisation of silica condensation at the oil-water or nanoparticle-water interface would lead to formation of a distinct silica layer (in red) inside the nanoparticle membrane and thus a hollow silica capsule (right hand side, top). Permeation of TMOS or hydrolysed TMOS species into the aqueous phase of the emulsion and subsequent condensation would lead to the formation of a secondary silica phase (red) within the colloidosome capsule in the form of a crosslinked silica network (right hand side, bottom).

3.3 Results and discussion

3.3.1 Investigations into the structure of silica colloidosomes

The aim of this chapter was to investigate the internal structure of colloidosome protocells and consider how this relates to their function. As part of the investigation into the structure of TMOS crosslinked silica colloidosomes, the conditions of their formation were varied. Here the results presented focus on variation of aqueous phase pH, as this is known to have a large effect on the hydrolysis and condensation of silica precursors but has not been considered in previous work on colloidosome protocells. Some data relating to variation of other conditions such as mechanism of emulsion formation, presence of protein in the aqueous phase and variation in TMOS concentration is included in Appendix A.1.1 for comparison.

To form colloidosomes, 100 μL aqueous phase at various pHs was added to a suspension of 20 mg silica nanoparticles in 2 mL dodecane. A Pickering emulsion was formed by handshaking for 1 minute and crosslinked with 10 μL TMOS (significantly less than was used in previous works [20]). The aqueous phase was 100 mM acetate buffer (pH 3 to 6) or 100 mM Tris buffer (for pH 7 to 8), containing 3 mg/mL bovine serum albumin (BSA). Crosslinking was carried out at room temperature for 48 hours under continuous rotation. Some previous studies left samples to crosslink for just 24 hours, however for pH 4 with these lower TMOS levels, 24 hours of crosslinking gave samples with very few or no colloidosomes present after transfer to water. An internal aqueous phase of pH 3 yielded no colloidosomes after transfer to water even when the sample was left for 48 hours to crosslink. The reduced crosslinking efficiency at low pH is a consequence of the low rates of silica condensation in an acidic environment. Crosslinking colloidosomes formed at pH 4 with greater volumes of TMOS (20 μL) also yielded spherical colloidosomes after just 24 hours. To allow comparison across samples formed at different pHs, all were formed using 10 μL TMOS and 48 hours crosslinking. The colloidosomes were transferred to water as previously described and bright field microscopy images are shown in Figure 3.4a. All colloidosomes in the remainder of this thesis were imaged after transfer to water.

Colloidosomes formed using FITC- labelled silica nanoparticles show fluorescent membranes but no fluorescence in the droplet lumen (Figure 3.4b). This confirms that the hydrophobic silica nanoparticles form a distinct membrane and do not move into the droplet interior, in agreement with previous work [22]. To investigate the formation of a secondary silica network within the colloidosome lumen, samples were stained with Rhodamine B after transfer to water (Figure 3.4c). After 1 hour incubation in 0.2 mg/mL Rhodamine B, the sample was washed several times to remove free dye. Rhodamine B is a zwitterionic dye known to strongly adsorb to silica and hence is used to visualise all silica in the sample [155]. Confocal microscopy of all the colloidosome samples show fluorescence throughout the interior indicating the existence of internal silica species. Brighter fluorescence at the droplet edge is due to the presence of a denser silica region where the crosslinked nanoparticle shell is. Emulsion formation with an aqueous phase at pH

4 or 7 results in spherical colloidosomes with homogeneous but low internal fluorescence after staining. Colloidosomes formed at pH 5 also show some internal silica formation from Rhodamine B staining, but the majority of colloidosomes show an extremely buckled structure after transfer to water. An aqueous phase at pH 6 gives spherical colloidosomes, though in both bright field images and after staining, the inside of the colloidosome appears to be inhomogeneous due to the presence of large silica aggregates or particles. Bright field microscopy images of colloidosomes formed at pH 8 (Figure 3.4a) show spherical colloidosomes with no membrane wrinkling and inspection of stained samples show that these colloidosomes show significantly higher fluorescence in the colloidosome interior than those formed at pH 4 to 7. This indicates that high pH gives a denser silica network, likely due to the increased rate of silica condensation and more branched nature of the species formed. Colloidosomes formed using increased volumes of TMOS also showed increased internal fluorescence inside implying that internal silica formation increases when more TMOS is used (Appendix A.1.1).

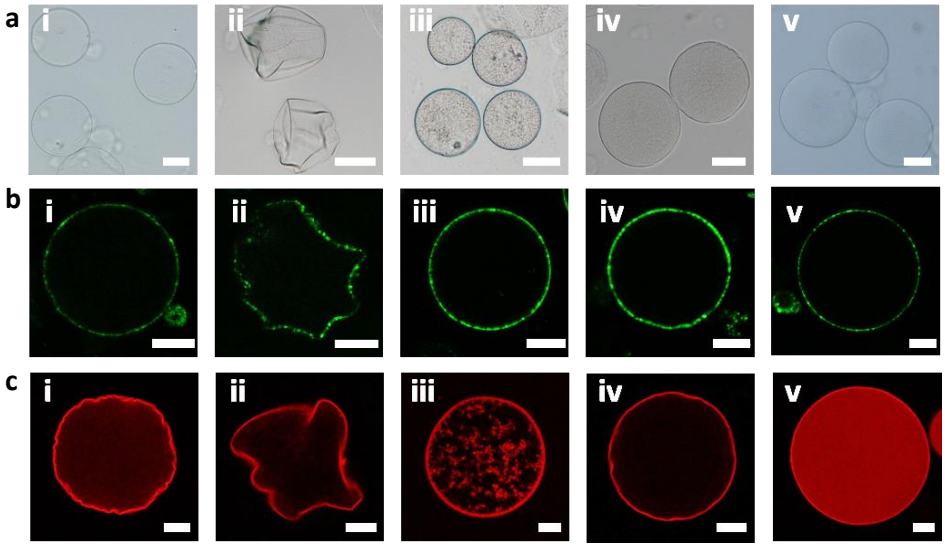

FIGURE 3.4. Images of colloidosomes formed with aqueous phase at various pHs: (i) pH 4, (ii) pH 5, (iii) pH 6, (iv) pH 7, (v) pH 8. All images show colloidosomes after crosslinking with 10 μl TMOS and transfer to water. (a) Bright field microscope images. (b) Confocal microscopy images of colloidosomes which were formed with FITC- labelled silica nanoparticles. (c) Confocal microscopy images of colloidosomes that had been stained using Rhodamine B. To stain them the colloidosomes were incubated with the dye in water and then washed to remove excess before imaging. Scale bars show 20 μm.

Comparing the images in Figure 3.4b and Figure 3.4c shows that all silica inside the

colloidosomes arises due to TMOS condensation and thus can be thought of as a *secondary silica phase*. It should be noted here that other factors, such as ionic strength, buffer identity and the presence of biological molecules or other species, would also impact upon TMOS hydrolysis/ condensation and thus affect colloidosome structure in some way. Some examples of this are shown in Appendix A.1.1 and all show the secondary silica within the capsule, although a full investigation of these factors is beyond the scope of this thesis.

Direct evidence of the internal structure of colloidosomes is found by imaging colloidosomes using electron microscopy, particularly if the capsules can be fractured [152]. Inspection via scanning electron microscopy requires samples to be dry, and during the preparation of samples, dramatic changes in morphology and structure can occur. Various methods of sample preparation were tested, and the most informative are presented here.

To freeze dry colloidosome samples, 50 μL of the aqueous suspension was placed onto a carbon pad on top on an aluminium SEM stub. The stub was then directly placed into a shallow bath of liquid nitrogen. This procedure was used to ensure the sample was frozen as rapidly as possible to minimise ice crystal formation. The frozen sample was lyophilised and subsequently sputter coated with silver prior to imaging. Colloidosomes were significantly distorted by the lyophilisation process, with many appearing as elongated shapes rather than the special form seen in water (Figure 3.5a). This is likely to be due to rapid ice crystal formation exerting a directional force on the colloidosomes. Their shape change under this force implies that the overall structure is soft, as a rigid sphere would not be deformed in this way. The process had also broken and disrupted the samples a lot resulting in a lot of excess silica.

Higher magnification of colloidosomes formed at pH 4 and fractured during the drying process, are shown Figure 3.5b-c. Significant wrinkling of the colloidosome surface is seen in the collapsed structure. The external surface is rough and clearly formed of a shell of nanoparticles, corroborating the evidence shown in figure Figure 3.4b. A transmission electron microscopy (TEM) image of the nanoparticles used in colloidosome formation is shown in Figure 3.5h for comparison. Interestingly the SEM images of the colloidosomes do not seem to show a monolayer as is formed in some Pickering emulsions. Instead the shell is a rough network with clusters seen to protrude from the surface. The smooth surface inside the colloidosome shell is the secondary silica formed via TMOS condensation. However the inside of the colloidosome appears hollow, which seems at odds with the data provided by Rhodamine B staining. Since no silica network can be seen throughout the colloidosome interior it is postulated that the condensation of silica inside formed a polymeric network that has collapsed during drying. The hydrolysis and condensation of silica at low pH is slow meaning that it may be incomplete resulting in a less dense network, but low pH also results in weakly crosslinked polymeric species which could explain why the network formed is not sustained as a 3D structure when the sample is dried.

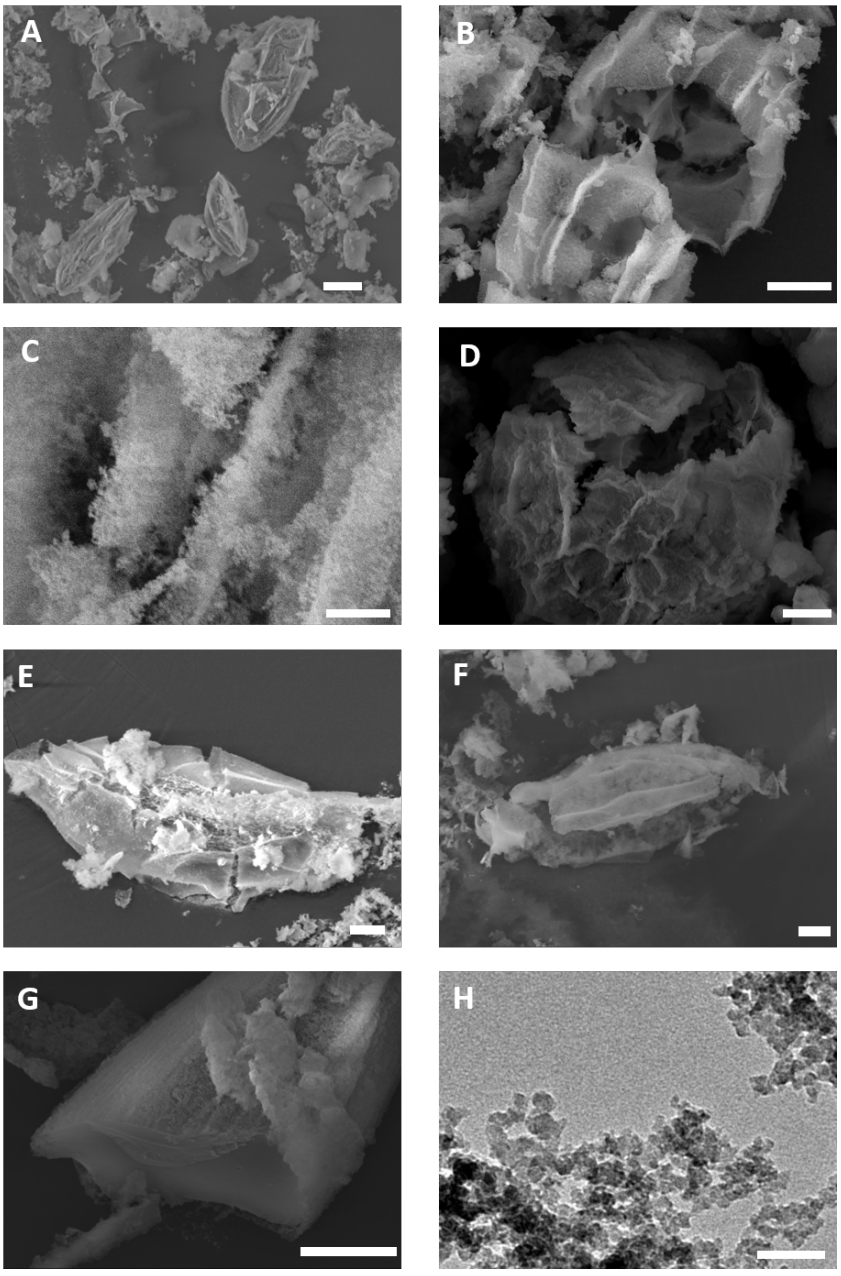

FIGURE 3.5. Colloidosomes were formed via handshaking with various aqueous phase pH. After crosslinking with TMOS and transfer to water, SEM samples were prepared by lyophilisation (a-c and e-g) or freeze thawing and subsequent air drying (d). Colloidosomes which were formed with aqueous pH of 4 and lyophilised are shown at various magnifications in (a), (b) and (c), and the same colloidosomes air dried are shown in (d). Lyophilised samples of colloidosomes formed at pH 5, 7 and 8 are shown in (e), (f) and (g) respectively. Scale bars represent (a) 20 μm , (b and d-g)) 10 μm and (c) 1 μm. (h) Shows a TEM image of the silica nanoparticles used for emulsion formation for compassion (scale bar 50 nm). Some of the images in this figure are reproduced in Appendix A.1.2 at a larger size to improve visualisation.

For comparison SEM images of lyophilised samples of colloidosomes formed at other pHs are included in Figure 3.5e-g. All show a distinct shell of silica nanoparticles on the outside surface. Colloidosomes formed at pH 5 and 7 contain silica structures within, which from these preliminary images seem to be porous even in this collapsed state. Colloidosomes formed at pH 8 show a drastically different internal structure to all other samples. Many colloidosomes in the sample were broken, but unlike colloidosomes formed at other pHs they appeared cracked into pieces rather than torn open. The secondary silica network appeared very smooth and dense indicating that it is significantly more crosslinked that those formed at lower pHs. It is important to note that this is a dried and collapsed structure and the native structure may be more porous. Again, the increased density of the secondary silica phase in colloidosomes formed at high pH can be explained by referring to the silica hydrolysis and condensation chemistry. At basic pHs, condensation rates are increased, and species tend to form more branched and crosslinked networks.

For comparison, colloidosomes which were formed at pH 4 were also prepared for imaging using a different method. The sample was frozen slowly in water (by placing into the freezer), before defrosting and air drying the solution onto a sample stub. The colloidosomes were generally collapsed but have not distorted into elongated shapes in the way that was seen in the lyophilised samples. Some colloidosomes were broken open by the freeze thaw process and Figure 3.5d shows a broken colloidosome with a wrinkled silica nanoparticle membrane and again a smoother network on the inside of the shell.

Based on the observations from the experiments detailed in this section, many of the investigations in the rest of this chapter focus particularly on colloidosomes formed at pH 4. Some experiments were carried out using colloidosomes formed at other pH for comparison, but unless explicitly stated the aqueous phase pH used in formation can be assumed to be 4.

3.3.2 Permeability, sequestration and encapsulation properties

Considering this newly described model of colloidosome protocells as capsules with a secondary silica phase inside, it is logical to assume that the internal silica formed will have some effect on the permeability and encapsulation properties. In fact, the procedure for staining silica with Rhodamine B proves that the colloidosomes can retain small molecules that pass through the porous membrane. Interestingly, the ability of small molecules to pass across the colloidosome membrane backs up previous data on this colloidosome system and highlights a key difference with other colloidosome systems in which small molecules often cannot pass across the membrane [17, 21]. Colloidosomes formed using the method studied in this chapter retain pores in their membrane after crosslinking, a feature which is essential for their use as protocells.

To gain more information on the uptake of small molecules from solution by colloidosomes, they were imaged in solutions of two different dyes. In this case samples were not washed prior to imaging (in contrast with results presented in 3.4 where samples were washed before

imaging to remove unadsorbed dye). Figure 3.6a shows a colloidosome incubated in Rhodamine B solution imaged by confocal microscopy. The high fluorescence intensity in the colloidosome lumen shows that the colloidosome interior builds up above equilibrium concentrations of this small zwitterionic dye. Similar experiments were carried out by incubating colloidosomes with the anionic dye fluorescein. Figure 3.6b shows colloidosomes in fluorescein solution, which are seen as dark circles in the green fluorescent channel. This may imply that fluorescein excluded from the colloidosome lumen to some extent due to electrostatic repulsion between the negatively charged dye and the negatively charged silica. It may also be that the lower fluorescence within the colloidosome is an artefact caused by some light scattering or shadowing due to the silica interior of the colloidosome. (Such effects are known to occur for light adsorbing materials [156].) The solution of fluorescein in water was found to be at pH 8. When the solution was adjusted to pH 3.5 and the experiment repeated, colloidosomes appeared brightly fluorescent compared to the background solution (Figure 3.6c). Reducing the pH means that the fluorescein is no longer negatively charged, and this leads to adsorption onto the secondary silica and build-up of above equilibrium concentrations within the colloidosome.

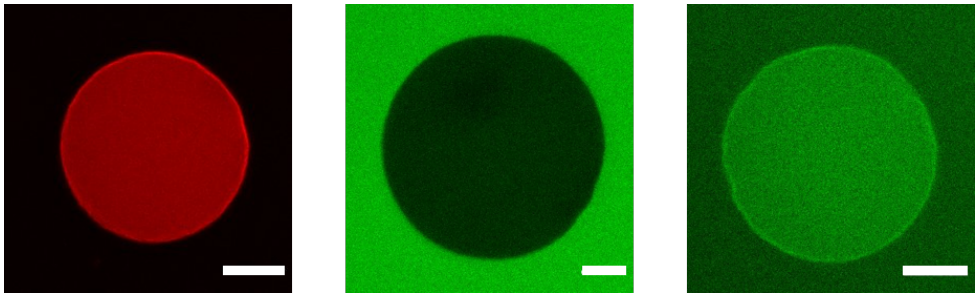

FIGURE 3.6. Confocal microscopy images of colloidosomes in aqueous solutions of (a) Rhodamine B, (b) fluorescein at pH 8 and (c) fluorescein at pH 3.5. Colloidosomes were incubated in dye solutions for one hour at room temperature prior to imaging. Scale bars show 20 μm.

As well as allowing the adsorption/ concentration of small molecules inside the colloidosome, the secondary silica network may affect the permeability of the colloidosomes towards larger molecules. Previous work on colloidosome protocells has shown that they are capable of retaining large molecules such as proteins after transfer to water [18] and this has been attributed to the small pore size of the colloidosome membrane. However, the presence of the secondary silica network may instead mean that large molecules are trapped due to a silica gel forming around them, or due to adsorption onto the silica or reduced diffusion inside the colloidosomes (an alternative form of size selection).

An investigation into the permeability of colloidosomes towards macromolecules was carried out using a method based on that applied with proteinosomes by Huang et al, in which the diffusion of fluorescein isothiocyanate labelled dextran (FITC-dextran) across the membrane is

studied [6]. Colloidosomes were formed using an aqueous phase of 3 mg/mL BSA in pH 4 acetate buffer 100 mM. After crosslinking and transfer to water, colloidosomes were added to aqueous solutions of FITC-dextran of different molecular weights. Samples were incubated for 1.5 hours and then imaged using confocal microscopy, and representative images are shown in Figure 3.7a. Line profiles over droplets were taken to assess the diffusion of the polymer into the colloidosome interior. Complications arise when trying to apply this method for use in colloidosomes, because of the exclusion effects (or shadowing) seen for the small molecule fluorescein. Ideally, to determine permeability and molecular weight cut off (MWCO), a substance that does not interact with the silica would be used. Many substances interact with silica surfaces, and dextran was used because it only weakly interacts. Dextran is a neutral polymer, although the presence of FITC may mean it has a small negative charge and therefore there is a possibility of some repulsion between the silica and the polymer as was suggested for fluorescein. Whereas the application of this method in proteinosomes probes only the MWCO-controlled diffusion across the porous membrane, here there may also be competing effects from interactions with the silica that make the results less accurate.

Even when incubated with the lowest molecular weight dextran (4 kDa), colloidosomes appeared as dark circles, but the relative fluorescence of the interior (compared to external solution) did significantly decrease as the molecular weight of the polymer was increased (Figure 3.7a-b). This indicates a decrease in the amount of polymer that has moved into the colloidosome interior. To calculate an approximate value for the molecular weight cut off (MWCO) of the colloidosomes, the uptake of 4 kDa polymer is assumed to be 100% and the uptake of 250 kDa polymer is assumed to be 0%. The MWCO is the weight at which the membrane is essentially impermeable to the polymer and is defined as the point where 90% of the polymer is excluded from the interior of the capsule [29] (Appendix A.1.3). This analysis gives a MWCO of 150 kDa for colloidosomes formed at pH 4. The MWCO is unchanged if samples are incubated for 24 hours instead of 1.5, which indicates that the decrease in polymer uptake with large molecules may not just be due to slower diffusion of the polymer through the matrix (Appendix A.1.3). Interestingly when this uptake experiment was repeated with colloidosomes formed in basic pH, which have a denser internal silica network, the MWCO appeared to be much lower (around 60 kDa).

Samples incubated with FITC-dextran were washed to remove polymer from solution before reimaging. As shown by Figure 3.7c-d) , fluorescence can still be seen inside the colloidosomes despite the low affinity of dextran for the silica network. The presence of fluorescence tells us that the polymer is not completely excluded from the colloidosome interior. Samples incubated with 250 kDa FITC-dextran showed significantly lower fluorescence inside than those incubated with 20 kDa FITC-dextran.

The calculated value of the MWCO is much greater than the value that has previously been assumed in order to explain the encapsulation of proteins such as BSA (66 kDa). Future studies could use FRAP (Fluorescence Recovery After Photobleaching) to assess the ability of different

molecular weight polymers to cross the membrane, as this may overcome some of the problems observed with the method used here.

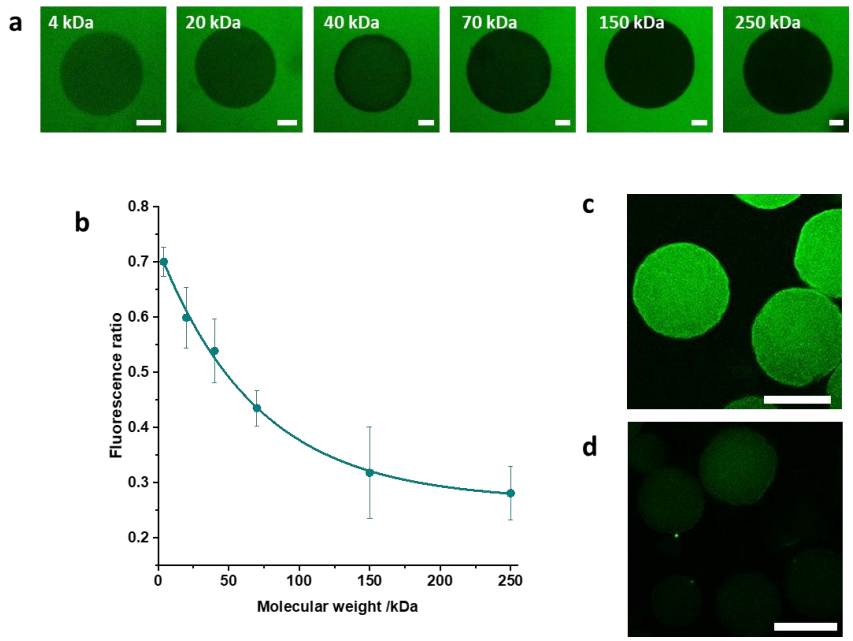

FIGURE 3.7. (a) Confocal microscopy images of colloidosomes incubated in solutions of FITC- dextran of different molecular weights (4 to 250 kDa as labelled on the images). (b) is a plot of the fluorescence ratio of the internal florescence compared to the outside, calculated from line profiles over the colloidosome samples. The data was fitted to a monoexponential decay. (c) and (d) are confocal microscopy images of colloidosomes which were incubated in FITC-dextran solutions (molecular weight 20 kDa and 250 kDa respectively) for 24 hours before beings washed to remove unabsorbed polymer. Scale bars represent 20 μm in (a) and 100 μm in (c-d).

Although the studies with dextran indicate that the MWCO of the colloidosomes is higher than may have previously been assumed, it is important to note that water is a good solvent for dextran and hence the polymer is not compact and globular. Most of the macromolecules which have previously been encapsulated in colloidosomes have been globular proteins that are not accurately represented by a linear polymer of equivalent size. To evaluate the diffusion of proteins across the colloidosome membrane and their interaction with the secondary silica network, colloidosomes were incubated with aqueous solutions of FITC labelled HRP (44 kDa), BSA (60 kDa) and GOx (80 kDa but forms 160 kDa dimers in solution). The proteins were dissolved in water at a concentration of 2 mg/mL and 80 μL added to 20 μL of colloidosomes. Samples were imaged using confocal microscopy after 1.5 hours and again after 24 hours. Unadsorbed protein was then washed away using DI water and the samples imaged again under the same conditions. Figure 3.8 shows typical confocal microscopy images of colloidosomes within the samples. After

just 1.5 hours colloidosomes incubated with FITC-HRP show significantly brighter fluorescence than the background, indicating that the protein has been adsorbed onto the secondary silica network resulting in high internal concentrations when compared to the aqueous solutions. The imaging settings used were adjusted to allow proper imaging of the fluorescence within the colloidosome.As this is higher than the bulk solution the bulk appears black, although there may still be some FITC-HRP remaining in solution. There is little change after 24 hours showing that the sequestration of HRP from solution is a rapid process. Colloidosomes incubated with FITC-BSA show internal fluorescence roughly equal to the external solution implying BSA has been able to move into the droplet interior, although not to such an extent as for HRP. This may be due to a difference in the affinity of the protein for the silica under the conditions used, particularly since there is no increase in fluorescence in the colloidosomes after 24 hours soaking with FITC-BSA. In the case of FITC-GOx the dark circles present in the images at 1.5 hours (Figure 3.8c) imply that protein levels within the colloidosomes are not more than the external solution. However, after 24 hours incubation with FITC-GOx colloidosomes show roughly equivalent fluorescence inside and outside indicating that the protein has moved into the colloidosome interior. This confirms that the MWCO of the colloidosome is large, since even globular molecules of molecular weight 80 kDa (160 kDa dimers in solution) can pass across. The time dependence of the uptake of the larger protein GOx can be explained by slower diffusion through the crosslinked silica membrane or secondary silica network.

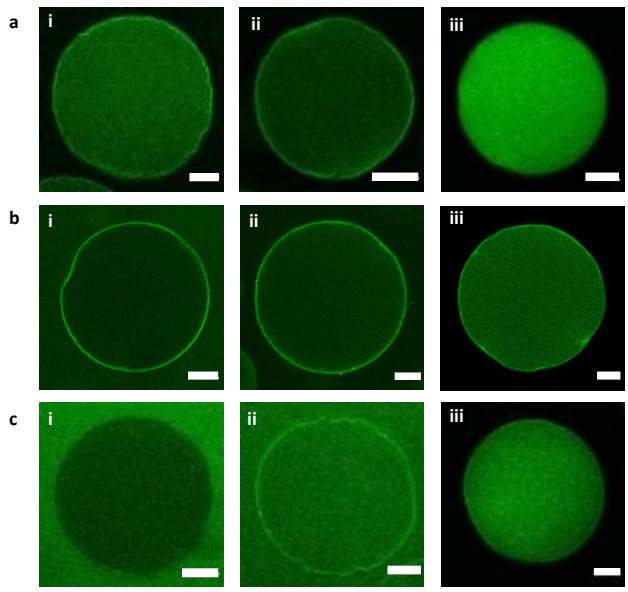

FIGURE 3.8. Confocal microscopy images of colloidosomes incubated with (a) FITC-HRP, (b) FITC-BSA and (c) FITC-GOx. Solutions were images after i) 1.5 hours incubation and ii) 24 hours incubation. (iii) After 24 hours samples were washed with DI water to remove unadsorbed protein and imaged again. All scale bars represent 20 μm.

These protein adsorption experiments were repeated with colloidosomes formed at pH 7 and pH 8 (Appendix A.1.4). As predicted from MWCO calculated using dextran, the large protein GOx does not seem to be able to pass across the membrane of the colloidosomes formed at basic pH. Colloidosomes formed at pH 7 showed similar permeability properties to those formed at pH 4.

The ability of the colloidosomes to build up high (above equilibrium) concentrations of protein, and to retain protein in the interior after the colloidosomes have been washed implies adsorption of the protein onto the secondary silica network. The extent to which this happens reflects the strength of the interaction between the silica and the protein, something which is affected by both the nature of the protein and the pH of the solution. It is interesting to note that these experiments were carried out in water and therefore all the proteins were above their isoelectric point and thus would be negatively charged overall. The incubation with BSA was repeated with solutions adjusted to pH 4 and pH 9 (Figure 3.9). At low pH much greater uptake and retention of the BSA was seen because there is no electrostatic repulsion between the protein and the silica. At higher pH both the silica and BSA are negatively charged, but as the pH is decreased the silica becomes neutral and the protein neutral or positively charged.

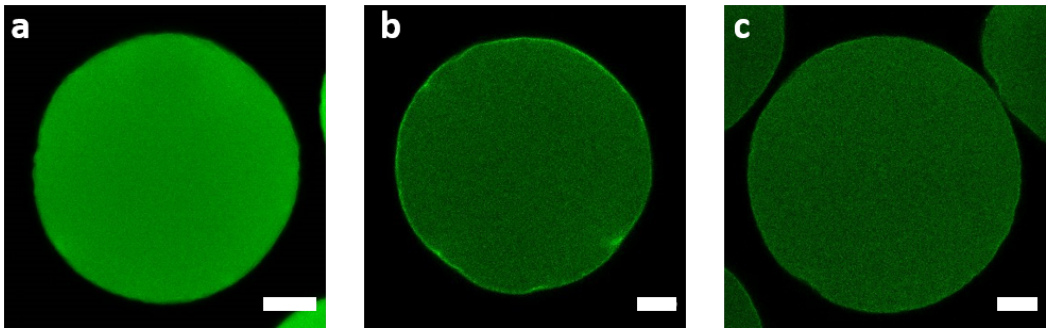

FIGURE 3.9. Confocal microscopy images of colloidosomes incubated with FITC-BSA solutions at (a) pH 4, (b) pH 7 and (c) pH 9. Colloidosomes were incubated for 24 hours and washed before imaging to remove unadsorbed protein. All scale bars represent 20 μm.

Although the pore size of the colloidosome membrane is large enough to allow diffusion of proteins, it has previously been established that proteins included in the aqueous phase upon colloidosome formation tend to be retained within the capsule after transfer to water [11, 22]. To confirm this colloidosomes were formed using a solution of 3 mg/mL FITC-BSA. Figure 3.10 shows confocal microscopy images of the colloidosomes after crosslinking and transfer to water. The samples show fluorescence associated with FITC-BSA inside. Given that BSA can pass across the membrane, there are two possible mechanisms for the retention of protein within the colloidosome interior. Proteins may be trapped by silica condensing around them, a process which has been described in the formation of many bio-hybrid materials previously [139]. Due to the porous or weakly crosslinked nature of the silica formed inside the colloidosomes, particularly at

neutral or acidic pHs, this seems less likely than for silica gels formed in the bulk. Proteins may also be adsorbing onto the secondary silica network within the colloidosome since it is also well known that silica has a tendency to adsorb proteins [145], as shown by the retention of proteins after washing shown in Figure 3.9.

The FITC-BSA colloidosomes in Figure 3.10 were formed with emulsion aqueous phase at either pH 4 or pH 8. Colloidosomes formed at pH 8 have fluorescence associated with FITC-BSA homogeneously throughout the colloidosome, whereas in colloidosomes formed at pH 4 the fluorescence intensity is lower in the lumen than at the membrane. The denser secondary silica network in the pH 8 colloidosomes means more FITC-BSA is adsorbed throughout the interior. In the colloidosomes formed at pH 4, the reduced secondary silica means less of the protein is adsorbed throughout the lumen and the high fluorescence at the membrane is due to adsorption of the protein onto the silica nanoparticles.

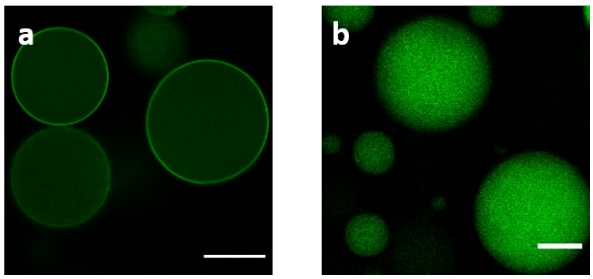

FIGURE 3.10. Confocal microscopy images of colloidosomes formed with FITC-BSA in the aqueous phase of the Pickering emulsion. (a) shows colloidosomes that were formed at pH 4 and (b) shows colloidosomes that were formed at pH 8. All scale bars represent 50 μm.

3.3.3 Enzyme activity in colloidosome protocells

Metabolism is one of the key functions of cells, and functionalising protocells by encapsulating enzymes can mimic this. However, as was discussed in the introduction, conformational changes induced by adsorption of enzymes onto surfaces such as silica can reduce their activity. Li et al showed that crosslinked silica colloidosomes encapsulating alkaline phosphatase (ALP) were capable of enzymatic activity, but that the rate was significantly reduced compared to enzyme in bulk solution [21]. In this study it was assumed that the ALP was trapped in the colloidosome due to the membrane permeability. Based on the new model described in this chapter, experiments

were carried out to confirm that the presence of the secondary silica phase and adsorption of proteins onto it does not necessarily destroy enzyme activity.

Sections 3.3.1 and 3.3.2 showed that the conditions of colloidosome formation affect the capsule structure, secondary silica phase and to a certain extent permeability, as well as affecting the distribution of entrapped protein within the colloidosome and the extent of adsorption onto the membrane. When trapping enzymes within colloidosomes it must also be considered that solution pH can affect enzyme structure and activity. Different enzymes have different ranges of stability, and varied extent of adsorption onto the silica membrane or secondary silica phase may also affect activity. With this in mind, the conditions of formation for colloidosomes containing HRP (from now on referred to as HRP colloidosomes) were refined to optimise structure and enzyme activity. Colloidosomes were formed by adding 100 μL aqueous phase to 2 mL dodecane with 20 mg silica nanoparticles dispersed and shaking for one minute. The aqueous phase contained 740 U/mL HRP in either 100 mM acetate buffer (pH 4,5 or 6) or 100 mM Tris buffer (pH 7). Colloidosomes were not formed at pH 8 because the high levels of silica formed inside colloidosomes at basic pH were undesirable for use as protocell capsules. TMOS (10 μL) was added to crosslink the colloidosomes. After 5 hours rotation at room temperature samples were left in the fridge for ca. 43 hours, as enzyme activity is usually maintained better under refrigeration. Colloidosomes were transferred to water using the same steps of centrifugation as described previously.

Trends in structure across pH range were similar to those seen for BSA. HRP colloidosomes formed at pH 5 and 6 showed the same undesirable features which previously ruled them out in Section 3.2.3 and pH 7 colloidosomes were spherical and didn‘t contain precipitate. The notable difference from samples formed with BSA was that in HRP colloidosomes formed with aqueous phase of pH 4, crosslinking failed and no colloidosomes were seen after transfer to water. As previously discussed, crosslinking is slower at low pH, and this effect seems to be exaggerated by carrying out the crosslinking it the fridge. (BSA colloidosomes were crosslinked at room temperature.) Increasing the TMOS to 15 μL improved the crosslinking at pH 4 and lead to the formation of colloidosomes with a spherical structure and no internal precipitate visible. Thus it was decided that based on structure, a method using an aqueous phase of either pH 4 or pH 7 was preferable. To assess the retention of HRP after transfer to water, colloidosomes were formed at pH 4 and 7 (TMOS 15 μL and 10 μL respectively) with an aqueous phase containing a mixture of HRP and DyLight 650 labelled HRP (DL650-HRP) (2.5 mg/mL each; for unlabelled HRP this is 370 U/mL). Figure 3.11 shows the DL650-HRP colloidosomes after transfer to water. Samples formed at both pH 4 and 7 show homogeneous fluorescence within the colloidosome interior indicating successful retention of the enzyme. As with the FITC-BSA colloidosomes discussed in Section 3.3.2, this implies that the DL650-HRP has been adsorbed onto the internal silica or trapped by silica forming around it, since when added externally it rapidly crosses the colloidosome membrane of samples formed at both pH 4 (section3.3.2) and 7 (Appendix A.1.4). Initial tests into enzymatic activity were carried out by assessing the production of a colorimetric

substrate by eye. Despite successful retention of HRP within the colloidosome interior, samples formed at pH 4 were found to have extremely low enzymatic activity compared to samples formed at higher pH, due to the reduced stability of the enzyme at low pH. HRP colloidosomes were therefore formed with an initial aqueous phase pH of 7 for the remainder of this work.

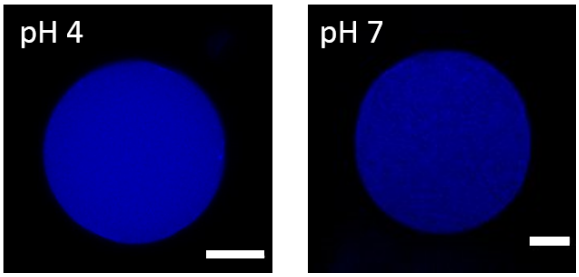

FIGURE 3.11. Confocal microscopy images of colloidosomes containing DL650-HRP which were formed with initial aqueous phase at pH 4 or pH 7. Scale bars show 20 μm.

HRP can oxidise the non-fluorescent molecule *o*-phenylenediamine (*o*PD) to fluorescent 2,3-diaminophenazine (DAP) in the presence of hydrogen peroxide (H_2O_2) [103] (Figure 3.12a) and hence this system was used to assess the activity of HRP colloidosomes. Colloidosomes were suspended in pH 7 Tris buffer and added to the wells of a 96 well plate, where they were allowed to settle before experiments were run. To initiate the reaction *o*PD and H_2O_2 were injected and the mixture gently shaken. The fluorescence intensity (λ_{ex} = 405 - 415 nm, λ_{em} = 520 - 550 nm) was monitored over time. All experiments were repeated in triplicate and averaged, with error bars representing the standard deviation.

The reaction of *o*PD (500 μM) and H_2O_2 (450 μM) in the presence of HRP colloidosomes (50 μL, in 50 mM Tris pH 7) resulted in rapid production of DAP, demonstrating that HRP remains active upon encapsulation (Figure 3.12b). Conversion of the measured fluorescence intensity to concentration of DAP ([DAP]) was achieved by allowing this reaction to run to one hour and measuring the final fluorescence intensity. This was assumed to be equivalent to 225 μM DAP and could be used as a calibration for all other experiments (see (Appendix A.1.5) for detail).

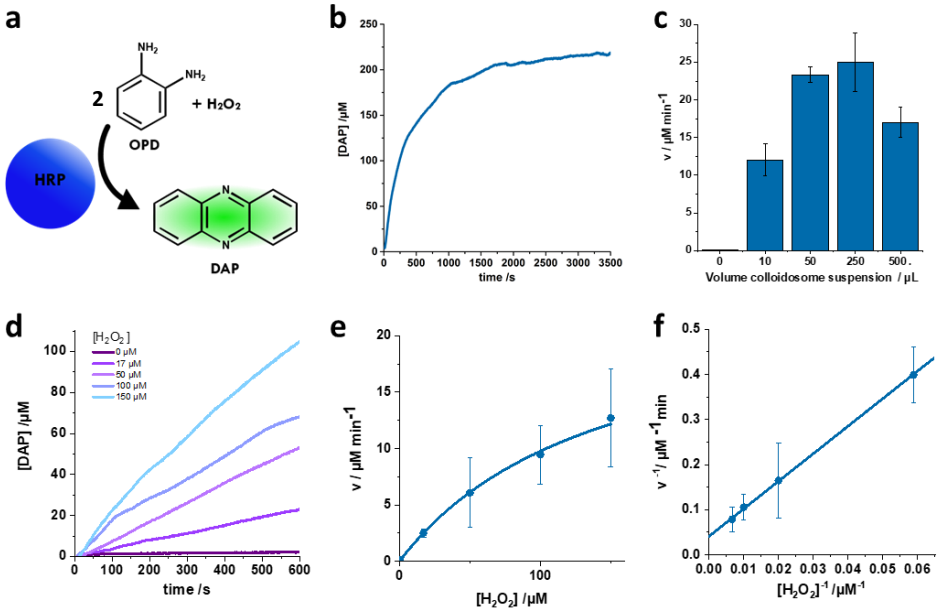

FIGURE 3.12. (a) is a schematic of the conversion of *o*PD to fluorescent DAP by HRP containing colloidosomes. (b) shows increased in [DAP] over time for HRP colloidosomes with initial concentrations of 500 μM *o*PD and 450 μM H_2O_2. (c) is a plot of initial reaction rate as a function of the volume of colloidosomes added to the well. (d) shows the increase in fluorescence over time for reactions with varied initial $[H_2O_2]$ as indicated in the key on the graph. (e) is a Michaelis Menten plot and (f) a Lineweaver Burke plot of the data, with error bars representing standard deviation.

To investigate the effect of colloidosome concentration on enzymatic rate, initial *o*PD and H_2O_2 concentrations were held constant whilst the amount of colloidosomes added was varied. The volume of colloidosome suspension added to the well was varied, and the concentration of the other components was kept constant by varying the amount of water added. The initial rate of reaction (time < 5 minutes), v, for each added colloidosome volume was calculated. Figure 3.12c shows the variation in v with added colloidosome volume. For the increase in added colloidosome volume between 10 μL to 250 μL, an increase in v is seen, although the difference between 10 μL and 50 μL is much larger than between 50 μL and 250 μL. Increasing the added colloidosome volume further to 500 μL appears to cause a decrease in the initial reaction rate. The Pearson correlation coefficient (r) was calculated for this data (whole range of colloidosome volumes) and was found to be 0.4, indicating that there is some correlation between the volume of colloidosomes added and the initial rate. The weak correlation indicated by the r value is due to the break in

the relationship at higher volumes of colloidosomes. At low enzyme concentrations, increased enzyme concentration increases v. At high enzyme concentrations, enzyme concentration is no longer the limiting factor of the reaction and thus little or no change in v is seen when more enzyme is added. This may provide an explanation for some of the observations. However, the observed pattern between 50 μL and 500 μL could instead be due some property of the silica colloidosomes. The fluorescence value after one hour for reactions carried out with a range of colloidosomes (plotted in Appendix A.1.5) may indicate that as the volume of colloidosomes that is added is increased, adsorption of fluorescent molecules is leading to a reduction in observed fluorescence. This could therefore explain the relatively low values of v with higher colloidosome volumes.

To produce the Michaelis-Menten plot in Figure 3.12e, v was calculated from reactions run at a constant initial concentration of *o*PD (500 μM) and varied initial H_2O_2 concentration (0 μM to 150 μM) (Figure 3.12d). The volume of colloidosomes added to the well was held constant at 50 μL, which is in the region where scattering or adsorption would not significantly affect the fluorescence readout. Colloidosomes in suspension show the typical relationship between substrate concentration and rate. At low substrate concentrations rate increases with increased substrate concentration, but at higher concentrations we see the graph begin to plateau as the enzyme becomes saturated. Analysing the data in Figure 3.12d using the Michaelis-Menten equation (Equation 2.16) a Lineweaver burke plot was produced (Figure 3.12f). The intercept and gradient of the linear fit were used to calculate v_{max} and the apparent Michalis-Menten constant (K_M‘), which are shown in table 3.1. The value of the Michalis-Menten constant found is described as an apparent value (K_M‘) since when looking at encapsulated species its value no longer represents the intrinsic affinity of the enzyme for the substrate. These values are used later in this thesis for comparison with hydrogel encapsulated species.

Table 3.1: Calculated kinetic parameters for HRP and HRP colloidosomes

Sample	K_M‘ /μM	v_{max} /μM min^{-1}
Colloidosomes	149 ±12	24 ±2

3.4 Conclusions and future work

TMOS crosslinking of silica nanoparticle stabilised Pickering emulsions was shown to result in colloidosomes with a secondary silica phase throughout the lumen, instead of simple aqueous-filled capsules. This silica phase was demonstrated as being the result of TMOS hydrolysis and condensation only, with silica nanoparticles forming a distinct membrane which can be clearly seen by fluorescent labelling or scanning electron microscopy imaging (SEM). The structure of the colloidosomes and nature of the internal silica network varied with the pH of the initial emulsion aqueous phase.

SEM images of broken colloidosomes revealed the nature of the internal structure. The colloidosomes collapsed during sample preparation by lyophilisation, indicating that they are not completely rigid structures. Colloidosomes formed at pH 8 had extremely dense silica networks inside, whereas those formed at pH 4 appeared hollow indicating that the silica was loosely crosslinked in nature and hence had collapsed against the membrane when samples were dried. Shell et al produced hollow silica capsules that remained spherical under vacuum, and thus the collapse of the colloidosomes produced here indicates that the membrane itself is not completely rigid [152]. In future work, further information of the structure of the membrane and the internal structure of the colloidosomes could be attained by setting the samples in a resin and slicing to allow transmission electron microscopy (TEM) imaging of the structure, as this would avoid the collapsing and deformations observed during drying.

The colloidosome membrane is permeable, and the presence of an internal network of silica allows the colloidosomes to sequester small molecule dyes from solution via their adsorption onto the silica within. The zwitterionic dye Rhodamine B was adsorbed at above equilibrium concentrations within the colloidosomes whereas colloidosomes incubated with the anionic dye fluorescein appeared as dark voids in the fluorescent solution, either due to exclusion of fluorescein form the colloidosome due to electrostatic repulsion or light scattering by the silica matrix. Due to the negative charge of silica surfaces, uptake of fluorescein could be modulated with solution pH.

Considering the silica nanoparticle membrane only, if a perfect monolayer of hexagonally packed nanoparticles were formed, the pore size could be calculated as roughly 15% of the particle diameter, ca. 3 to 4.5 nm. It has therefore previously been assumed that the encapsulation of macromolecules such as proteins within the colloidosome interior after transfer to water is due to their large size prohibiting them from passing through the membrane pores. Investigations into colloidosome permeability showed that the molecular weight cut off was significantly higher than was previously assumed and was particularly high when colloidosomes were formed at pH 4. For more accurate determination of the MWCO of these structures, future studies may want to employ a technique such as FRAP (Fluorescence Recovery After Photobleaching), which would allow direct study of the rate of diffusion of large molecules across the colloidosome membrane. This could also be used to study the diffusion within the colloidosome lumen.

One consequence of the above expected MWCO is that globular proteins can pass across the

membrane. Colloidosomes were able to take up HRP and BSA from solution and due to adsorption onto the silica were able to retain the sequestered protein after washing. Adsorption of GOx was also possible in colloidosomes formed at pH 4, although uptake from solution was slower, possibly due to the increased protein size. In the case of colloidosomes formed at basic pH, BSA and GOx were not taken up by the colloidosome interior even after 24 hours incubation.

Since proteins which were previously described as being encapsulated within colloidosomes, are now shown to be able to pass through the colloidosome membrane, this chapter suggested a new mechanism for protein entrapment within colloidosomes in water. Retention of proteins within colloidosomes is strongly facilitated by interaction with the entrapped silica rather than by physical encapsulation within the membrane. Proteins included in the Pickering emulsion aqueous phase are either trapped by the silica network forming around them or adsorbed onto it. For example, BSA and HRP, which as previously discussed move across the membrane and through the internal silica, can be entrapped within the colloidosome successfully. Colloidosomes stored in water or buffer solution for days to weeks still showed localisation of protein within the colloidosome interior. HRP colloidosomes showed rapid enzyme activity, confirming that the internal silica does not prevent diffusion of the substrate/ product in/out and that adsorption onto the silica doesn‘t rule out protocell function.

The ability of silica colloidosomes formed in this chapter to retain proteins that have molecular weight below their MWCO would be useful for the encapsulation of enzymes for which the substrate is a macromolecule. For systems in which the enzyme is retained in the capsule due to low membrane permeability, such polymeric substrates would also be prevented from crossing the membrane. One example of an enzyme with a macromolecular substrate is glucoamylase (GA), which breaks down starch into glucose and can be used in a three-enzyme cascade reaction with GOx and HRP. Preliminary tests showed that colloidosomes formed with GA inside were able to break down starch even after the substrate had been dialysed to remove lower molecular weight chains, indicating that the macromolecular substrate is able to cross the membrane.

Future work on colloidosomes may focus on creating a capsule with no secondary silica phase and a lower MWCO in order to create a capsule in which macromolecules can be encapsulated due to their size and not due to adsorption onto silica, as was previously believed to be the case. Several studies have shown systems for crosslinking that create a distinct crosslinked membrane and no internal structure. However, due to the silica layer formed during nanoparticle crosslinking, these capsules often show very lower permeability, with even small molecule dyes being trapped inside after transfer to water [17]. The low permeability resulting from these strategies would make the systems unsuitable for use as protocells as substrates and products for enzymes reactions could not easily pass across. Ideally the system would have intermediate pore sizes in the membrane, which would allow easy passage of small molecules but retention of large. One possible strategy for achieving this is to utilise a method used for creating silica capsules from standard emulsions. Inclusion of positively charged species at the oil-water interface causes

silica formation preferentially here due to the attraction of negatively charged oligomers to the positive species. The silica layer formed also tends to be porous, which could give desirable permeability. This could be achieved by doping the Pickering emulsion with cationic surfactants or functionalising the silica with positive species.

This chapter focused on colloidosomes formed via hand shaking and with an oil phase of dodecane. Some applications of colloidosome microcapsules may require smaller or more homogeneous populations of colloidosomes than those formed by this method. Colloidosomes formed using homogenisation instead of hand shaking are less polydisperse and were shown to display similar formation of a secondary silica network upon crosslinking. Colloidosomes can also be formed with an oil phase of mineral oil. Preliminary results showed that these colloidosomes tend to be smaller, no matter what the method of emulsification, and that they form spherical capsules across a wide range of conditions. The mineral oil colloidosomes could be crosslinked using TMOS transferred to water using isopropanol or DMF in place of ethanol (mineral oil is less polar than dodecane and so a less polar solvent is required to dissolve it). The mineral oil colloidosomes exhibited a secondary silica network and similar adsorption and permeability properties to those made with dodecane.

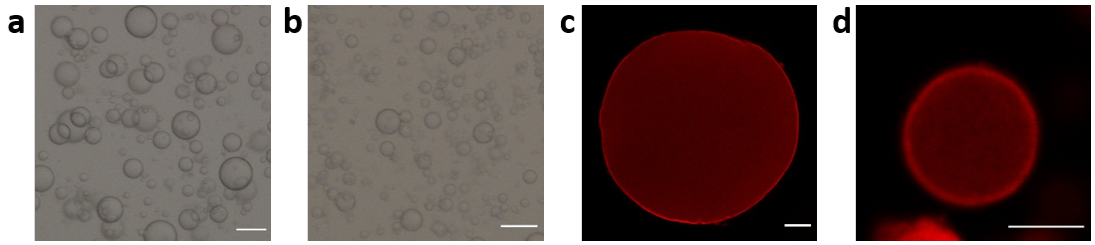

FIGURE 3.13. Bright field microscopy images of silica nanoparticle stabilised Pickering emulsion droplets formed via homogenising using an oil phase of (a) dodecane or (b) mineral oil. Scale bars 50 μm. (c) and (d) Confocal microscopy images of colloidosomes after incubation with Rhodamine B for one hour. Samples were washed prior to imaging. Colloidosomes in (c) were formed via hand shaking and (d) were formed via homogenising, both used an oil phase of mineral oil. Scale bars 20 μm.

All the colloidosomes discussed in this chapter were transferred to water by centrifugation with ethanol solutions. As previously mentioned, many biological molecules are sensitive to the presence of alcohols and thus this may limit the type of molecule that can be encapsulated and hence reduce the application of these colloidosomes for encapsulating biomolecules. Alternative methods for transfer of colloidosomes could be developed to avoid the use of alcohols. Rodriguez-Arco et al have previously shown that silica colloidosomes could be transferred across the water-oil interface of a magnetic Pickering-Emulsion (MPE) droplet in a process mimicking phagocytosis [18]. The transfer of a crosslinked silica colloidosome from the oil phase into the

MPE aqueous phase is mediated by patches of the oil water interface stabilised by oleic acid. The oleic acid forms a monolayer on the colloidosome surface in the oil phase, which becomes a bilayer as the colloidosomes move across the interface into the aqueous phase (Figure 3.14). Preliminary results indicated that this method may be suitable for transfer of colloidosomes to the water phase in bulk systems. Oleic acid was added to crosslinked colloidosomes in dodecane, and the sample placed on top of carbonate buffer. When the pH of the carbonate buffer was high enough, centrifugation lead to transfer of colloidosomes into water.

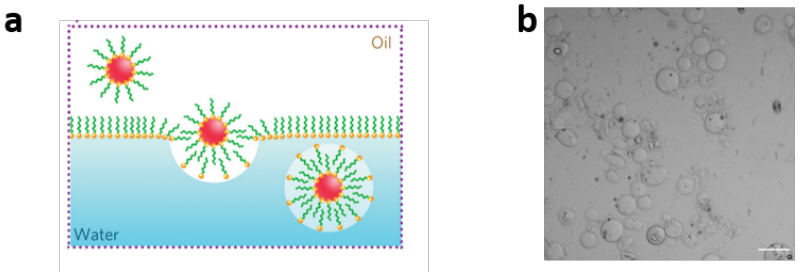

FIGURE 3.14. (a) is a schematic showing the transfer of silica colloidosomes across an oil water interface in the presence of oleic acid (reproduced from [18]). (b) Bright field microscopy image of colloidosomes after transfer to water using the oleic acid method in bulk. Scale bar 100 μm.

CHAPTER 4

A RUDIMENTARY PROTOTISSUE FORMED FROM COLLOIDOSOMES IN AGAROSE HYDROGELS

4.1 Chapter overview

This chapter presents a rudimentary form of prototissue that is created by immobilising colloidosome protocells in polysaccharide hydrogels. The colloidosome-hydrogel prototissues are first characterised to determine the distribution and structure of the colloidosomes within. The activity of enzyme containing colloidosomes in the hydrogel is investigated and this is extended to the use of binary populations for enzyme cascade reactions. A modular system is used to create composite prototissues that have patterned colloidosomes populations. Uniform application of enzyme substrates to the composite prototissues results in patterned enzyme reactions. The patterned appearance of the enzymatic product is shown to be transient, resulting in the in-situ formation of pre-programmed concentration gradients. Investigations into some factors that can be used to manipulate the patterning are carried out.

4.2 Introduction

4.2.1 Hydrogel based prototissues

In Section 1.1.3 the concept of bringing protocells together to form prototissues was introduced. Within living tissues, cells are surrounded by a complex polymeric network called the extra cellular matrix (ECM). In connective tissue in which cells do not show direct cell-to-cell adhesions the ECM is responsible for holding cells together in a tissue [1]. This ECM is a highly hydrated polysaccharide gel of proteoglycans (at low mass, less than 10% w/v) containing fibrous proteins and glycoproteins [1]. The hydrated structure resists compressive forces, providing support and

protection for the cells within, and it also allows rapid diffusion of signalling molecules and nutrients. The ECM helps to regulate cell function and behaviour [1].

In tissue engineering, cells are often embedded within hydrogels that are used to mimic the ECM [42]. Replicating this by embedding protocells within a hydrogel could, therefore, be an interesting mechanism for the creation of a functional prototissue. The hydrogel, mimicking the ECM, could be used to provide structural support or protection and play a role in guiding protocell function. The inherent porosity of hydrogels would facilitate the passage of small molecules and therefore chemical communication between protocells and with the environment. Furthermore, the pore size is usually small compared to microcapsules [157], meaning protocells would be trapped in distinct three-dimensional (3D) arrangements.

Liposomes, GUVs and polymersomes have been encapsulated within hydrogels for purposes such as immobilisation and drug delivery [157–161]. De Hoog et al embedded enzyme loaded polymersomes into a hydrogel to create a reactor system [93]. Trapping the polymersosmes prevented leaching of the enzyme and allowed recycling of the polymersome reactors without the loss of activity that were seen in suspension. They used their system as both a batch and flow reactor and showed that by adding together two polymersome hydrogels tandem enzymatic reactions could be carried out.

Protocells have been shown to be capable of enzyme directed assembly of internal hydrogel networks that mimic the cytoskeleton, and some cases such processes result in the formation of a bulk hydrogel. Akkarachaneeyakorn et al showed that alkaline phosphatase colloidosomes could carry out dephosphorylation of N-fluorenylmethylcarbonyl-tyrosine-(O)-phosphate (Fmoc-TyrP) to Fmoc-TyrOH, resulting in self-assembly to form a hydrogel [22]. Initially this forms a wall around the colloidosomes membrane and then an internal network and if the sample is left to age, a bulk hydrogel with embedded colloidosomes is seen. Krishna Kumar et al created coacervates from poly(diallyldimethylammonium chloride) (PDDA) and deprotonated N-(fluorenyl-9-methoxycarbonyl)-D-Ala-D-Ala (FMOC-AA) [162]. When the pH of the system was gradually lowered to below the pKa of the dipeptide, reconfiguration of the system occurred as it began to self-assemble into fibres. Again, aging of the system resulted in the formation of a bulk hydrogel. Taking this system further Nichols et al used an acoustic trapping device to produce regular 1D or 2D arrays of the coacervate droplet prior to reconfiguration into a hydrogel [103]. The resulting self-standing hydrogel exhibited micropatterned features that, due to the incomplete disassembly of the coacervates, were able to sequester small molecules and enzymes from solution.

Using such a model for prototissue formation is relatively novel. In their modular hydrogel prototissue Bayoumi et al used lipid stabilised aqueous droplets within oil, similar to the system used in previous self-supporting printed tissue models [163]. Lipid containing oil droplets were first injected into the hydrogel and then aqueous droplets formed within these. Lipid bilayers formed at interfaces and thus addition of protein pores allowed electrical and chemical

communication between different droplets.

As well as being of interest to the field of protocell research, hydrogel prototissues represent a new way of instilling functionality to a hydrogel for use in fields such as tissue engineering, drug delivery, biosensors and soft robotics.

4.2.2 Introducing heterogeneity to prototissues

Tissues are complex and often contain multiple cell types in heterogeneous distributions. Within a tissue gradients or variations occur in features bound to the ECM or in soluble chemicals and such gradients are important for achieving variations in cell function or differentiation [1]. Often soluble gradients within tissues are created due to the localised secretion of a signal molecule by a specific group of cells. The molecule diffuses away from the source creating a concentration gradient, affected by the speed of diffusion and the rate of depletion of the molecule [1]. Interactions of the ECM with signalling molecules secreted by cells changes the way they diffuse through the tissues, creating local reservoirs or altering the steepness of a concentration gradient [1]. Considering the heterogeneity and complexity of living tissues it seems appropriate to design prototissues that mimic this. Creating such materials is an interesting exercise for those working in biomimicry or protocell research, but also increases the complexity of function possible for prototissues. For example, the formation of hydrogels that show an anisotropic response to a uniformly applied chemical stimulus would be of great interest in soft robotics [120]. The formation of pre-programmed, patterned chemical gradients within hydrogels would also be desirable for tissue engineering, to mimic the gradients experienced by cells in living tissues.

Some of the prototissue models previously discussed have displayed heterogeneity. Printed droplet networks could be patterned such that only specific pathways allowed communication or contained genetic material [31, 32]. The micro-patterned coacervate hydrogels produced by Nichols et al also show localisation of enzymatic function in certain areas of the gel due sequestration by the coacervates [103]. In this case the product of the enzymatic reaction is also sequestered by the coacervates and so appears in the pattern originally formed.

Chapter 3 (and previous studies [4, 22]), showed that enzymes can be trapped within colloidosomes and retain their function, such that they can be used as a basic representation of cellular metabolism. Herein, is presented a primitive prototissue model created by embedding colloidosomes within a hydrogel matrix. Development of a modular system means that the heterogeneity of living tissues can be mimicked by the spatial isolation of different protocell populations, and thus of different functionalities. This in turn allows the development of transient chemical gradients within the prototissue, in a manner not previously seen.

4.3 Results and discussion

4.3.1 Formation and characterisation of colloidosome-agarose hydrogels

This chapter presents initial investigations into the formation of 3D networks of colloidosomes within hydrogels. Due to the simplicity of hydrogel formation, its wide use in the literature and relatively inert nature, agarose was chosen as the hydrogel ECM mimic. Agarose is made up of repeat units of 1,3-linked α-D-galactopyranose and 1,4-linked 3,6-anhydro-R-L-galactopyranose (Figure 4.1b)[49]. As the temperature of a hot agarose solution is cooled polymer chains associate into double helices that form a network resulting in the formation of a hydrogels. Impurities that are often present can affect the physiochemical properties and are the reason for the weakly ionic character of agarose gels [49].

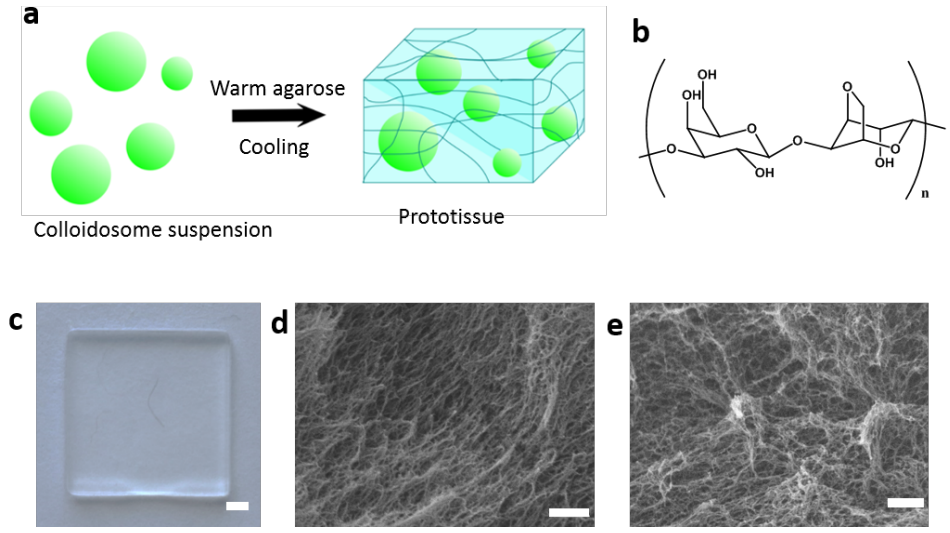

FIGURE 4.1. (a) A schematic showing prototissue formation via the encapsulation of colloidosome protocell suspensions within an agarose hydrogel. (b) A depiciton of the chemical structure of agarose, that is formed from repeating units of the disaccharide agarbiose, formed from 1,3-linked α-D-galactopyranose and 1,4-linked 3,6-anhydro-R-L-galactopyranose. (c) Photograph of an agarose hydrogel with embedded colloidosomes with scale bar 1 cm. (d) and (e) are SEM images of agarose hydrogels without and with encapsulated colloidosomes respectively, showing the similarity of the structure and porosity. Scale bar 1μm.

Agarose solutions (2% w/v) were formed by heating agarose in DI water to 90 °C to dissolve. Solutions were cooled to 55 °C before use to reduce possible damage to biomolecules within the colloidosomes. In order to form agarose prototissues, warm agarose solution was then combined

with a colloidosome suspension (final agarose concentration 1% w/v) and rapidly injected into a PMMA/ glass mould. Moulds were created by clipping a PMMA frame of desired shape and thickness to a glass slide. After the agarose solution was injected a second piece of glass was clipped on top to ensure uniform thickness. Moulds were placed in the fridge (4 °C) for 10 minutes to induce gelation of the agarose. As Figure 4.1c shows, the presence of colloidosomes within the gel network did not prevent bulk gelation. Initial rheological characterisation showed that that the agarose-colloidosome materials showed hydrogel-like mechanical properties (see Appendix A.2 for discussion). Hydrogels appeared more turbid than agarose alone due to the presence of the silica capsules. Scanning electron microscopy characterisation is often used for hydrogel characterisation, but, similar to the work discussed in Chapter 3, sample preparation can be difficult since it causes structural changes. For analysis of agarose hydrogels samples were prepared by solvent exchange to ethanol and then critical point drying. Critical point drying reduces the effect of surface tension, thus retaining more native structure with delicate samples. SEM images of hydrogels formed with or without colloidosomes are shown in Figure 4.1d-e. The hydrogels have a similar morphology and porosity indicating that the presence of colloidosomes and silica has not significantly changed the hydrogel structure.

Colloidosomes formed with an aqueous phase of 3 mg/mL FITC-BSA in 100 mM acetate buffer (pH 4) were used for fluorescence and confocal microscopy characterisation of the hydrogels. After encapsulation within agarose, the fluorescence associated with FITC-BSA remains within the colloidosome interior. Colloidosomes appear unbroken and retain the spherical structure seen in suspension (Figure 4.2d-f). Size analysis was carried out on colloidosomes in aqueous suspension and within the hydrogel matrix (Figure 4.2a-c). To determine the size of colloidosomes within the hydrogel, Z stacks were taken using confocal microscopy and the diameter measured at the midpoint of capsule. Encapsulation within the hydrogel matrix did not cause a significant change in the size distribution or average diameter even in higher agarose concentrations (final concentration 2.5% w/v). Calculation of the Pearsons correlation coefficient ($r = 0.1$) confirmed this as it showed a very weak correlation between the agarose concentration and the size of the colloidosomes. A colloidosome hydrogel was soaked in 2 mg/mL FITC-HRP solution for 1.5 hours and the confocal microscopy image in Figure 4.2f shows that within the hydrogel matrix, the colloidosome still adsorbed the fluorescent protein from solution, indicating that colloidosomes within agarose hydrogels remain permeable, even to large molecules.

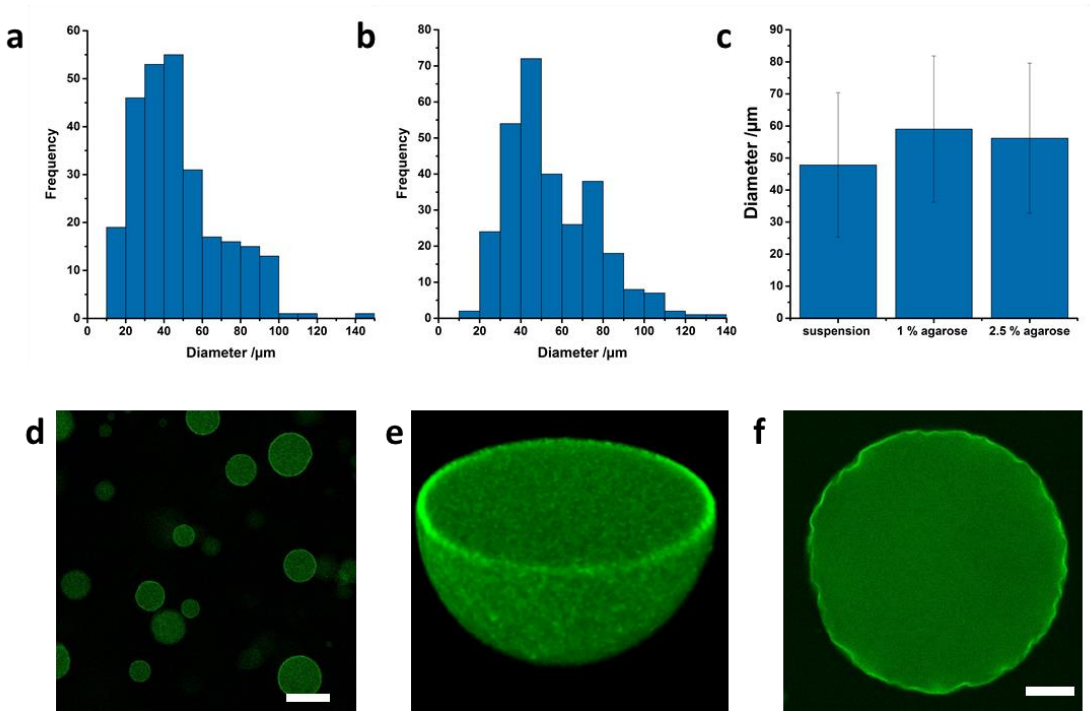

FIGURE 4.2. Histograms of colloidosome diameter in (a) aqueous suspension or (b) 1% w/v agarose. (c) Bar chart depicting the average diameter of colloidosomes in various conditions, with error bar showing standard deviation. (d) Confocal image of FITC-BSA colloidosomes within hydrogel (scale bar 50μm) and (e) Z stack showing the maintained spherical structure. To assess the permeability of the colloidosomes within the agarose matrix, colloidosomes formed with unlabelled BSA were encapsulated in 1% w/v agarose and then soaked in FITC-HRP solution. The confocal microscopy image in (f) shows adsorption of FITC-HRP from solution (scale bar 20μm).

When protocells are placed into the agarose solution, they are being put into a polymer solution that could cause an osmotic pressure and cause collapse of the structure. Permeation of the polymer across the membrane would mean that there is no osmotic pressure difference and could explain the retention of structure of the colloidosomes within the gel. To investigate this agarose was fluorescently labelled with 5-DTAF (5-(4,6-Dichlorotriazinyl) Aminofluorescein) (DTAF). Hydrogels were made with a 1% w/v agarose solution that was doped with DTAF-agarose (total 0.5% w/v). Within the hydrogel colloidosomes appear as dark voids, with low internal fluorescence (Figure 4.3a) indicating that little agarose has passed into the colloidosome lumen. Colloidosomes were also imaged after 1 hour in 0.1% w/v DTAF-agarose (Figure 4.3b). This agarose concentration does not gel, but significant aggregation of the chains does occur, leaving a non-homogeneous background. Fluorescence can be seen inside the colloidosome indicating that agarose can cross the membrane. Though the molecular weight of agarose is such that it may be

able to move across the membrane, it seems unlikely that within hydrogels significant penetration does occur because the hydrogelation is rapid. However, it may be that enough agarose moves across the membrane to prevent osmotic shock collapsing the capsule. The internal structure of the colloidosome may also contribute to them retaining their shape within the hydrogel. Although the collapse of the colloidosomes seen in SEM samples (Chapter 3) shows that the secondary silica network in the colloidosomes is not very rigid, it is possible that it may be providing enough structural rigidity to counteract any initial osmotic pressure or that it is in some way balancing the osmotic pressure and helping maintain the structure.

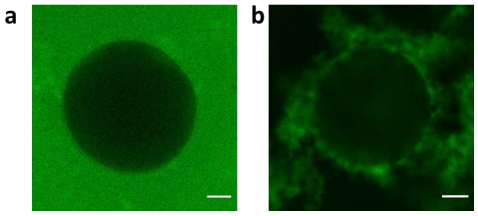

FIGURE 4.3. Confocal microscopy images of BSA colloidosomes (a) in an agarose hydrogel formed using DTAF-agarose or (b) after 1 hour in a 0. 1% w/v solution of DTAF agarose. Scale bars 20 μm.

The concentration of colloidosomes in the hydrogel could easily be controlled by changing the volume of colloidosome suspension added to the agarose. To maintain a final agarose concentration of 1% w/v, colloidosomes were either diluted or concentrated using centrifugation. Hydrogels with higher colloidosome numbers appear more turbid by eye and were more brittle (more easily torn). At all densities colloidosomes are distributed throughout the hydrogel, as shown by the whole gel fluorescence microscopy images in Figure 4.4a-c and the higher magnification images in Figure 4.4d-e that also show that even at high colloidosome densities they do not significantly aggregate. In order to determine the distribution of colloidosomes through the height of the gel, cross sections were imaged (Figure 4.4g-h). Initial attempts to assess the distribution simply by taking Z stacks through the height of the hydrogel showed that when colloidosome density is increased, colloidosomes higher up in the gel cannot be seen, giving a distorted view of the distribution. Using the cross-section method, colloidosomes can be seen throughout the height of the gel. Analysis of colloidosome diameter and position shows even distribution through the height of gel (Figure 4.4i-j) and no relationship between colloidosome diameter and height (Pearson coefficient, r = 0.03 implying extremely weak correlation). This implies that colloidosomes are not sinking within the liquid agarose prior to gelation, likely due to the viscosity of the agarose solution and the rapid gelation.

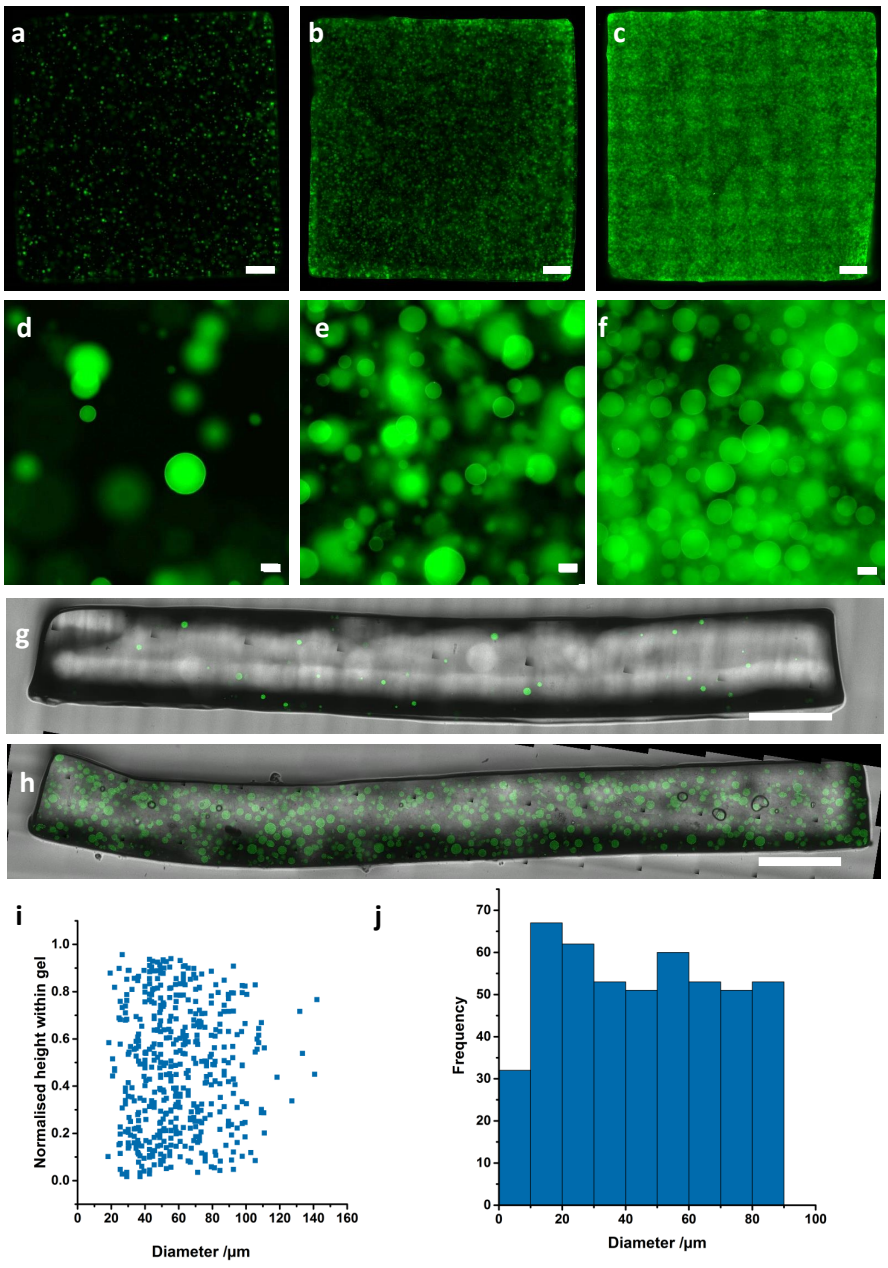

FIGURE 4.4. Fluorescence microscopy tile scan images of whole agarose gel prototissues containing (a) 10 μL, (b) 100 μl and (c) 333μL (concentrated to 100 μL) colloidosome sample per 200μL hydrogel. Colloidosomes were formed with encapsulated FITC-BSA for imaging (scale bars 1 mm) and (d), (e) and (f) are higher magnification images of (a), (b) and (c) respectively (scale bars 50 μm). (g) and (h) are fluorescence and brightfield (overlaid) images of cross sections cut through hydrogels showing distribution through the height of the gel. Hydrogels were formed with 10μL and 333 μL (concentrated to 100 μL) colloidosome sample per 200 μL hydrogel respectively (scale bars 1 mm). (i) is a scatter plot of colloidosome diameter against height within the gel and (j) is a histogram of colloidosome height within the gel.

Other hydrogel shapes can easily be formed by injecting hot agarose solution into different moulds. An example of this is the tube hydrogel shown in Figure 4.5, which was formed by injecting hot agarose into a glass capillary tube and pushing it out using air pressure at the end. Colloidosomes are again evenly distributed through this hydrogel shape.

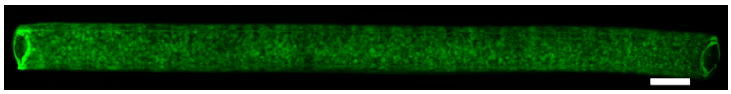

FIGURE 4.5. Fluorescence microscopy image of a colloidosome hydrogel formed in a capillary tube. Scale bar 1 mm.

4.3.2 Protocell function within hydrogels

In order to describe the colloidosome-agarose hydrogels as prototissues, some life-like properties must be mimicked within the system. As shown in Chapter 3, HRP can be contained within colloidosomes providing a basic mimic of metabolism. Confocal microscopy imaging of HRP colloidosomes trapped within agarose showed colloidosomes with a spherical structure and fluorescence associated with the DL650-HRP localised within the colloidosome (Figure 4.6c).

The activity of HRP colloidosomes within the gel was characterised by monitoring the conversion of *o*PD to DAP (Figure 4.6a) using a fluorescence spectroscopy well plate reader, as described for aqueous suspensions of colloidosomes in Chapter 3. Colloidosome hydrogels were directly formed in the sample well by injecting 100 μl warm pre-gel solution into the well and placing in the fridge for 10 minutes. Buffer (Tris pH 7, final concentration 50 mM) was placed on top of the gel and the system allowed to warm to room temperature before measurements were carried out. As for suspension experiments, the substrates *o*PD and H_2O_2 were added automatically and the plate shaken gently to mix before data collection. Fluorescence intensity was monitored over time and converted to [DAP] using the final fluorescence value for gels with 50 μL colloidosomes, 500 μM *o*PD and 450 μM H_2O_2 as was described in Section 3.3.3. The data for suspension colloidosomes is included in some plots for comparison. Trapping colloidosomes within agarose slowed the production of DAP. Comparing the curves in Figure 4.6d we see that whereas in suspension we see DAP being produced immediately, within a hydrogel there is a lag period and the curve takes more of an S shape. The lag period is the period where substrate molecules are diffusing to reach the colloidosomes near the surface, and product is diffusing out to the solution above where it can be detected by fluorescence reader. For initial rate calculations, the lag period is discounted and the slope of the region 100 s to 400 s used.

The Michaelis-Menten plot for gel encapsulated colloidosomes (Figure 4.6f) does not appear to completely plateau at higher substrate concentrations. Inspection of the Lineweaver Burke plot in Figure 4.6g shows that the data for the lowest concentration of H_2O_2 appears to be anomalous. The linear fit with and without this point are indicated by green dashed or solid lines respectively. To calculate the K_M‘ value, the anomalous data is discounted. Despite this, the calculated K_M‘

is 377 ±75 μM, that is more than twice the value calculated for suspension colloidosomes in Chapter 3 (149 ±12 μM). A higher K_M' value implies that that the active site is less available to the substrate, but in the case of enzymes within hydrogels it is also reduced because mass transport of substrates and products to and from the colloidosomes is slowed within the hydrogel. Colloidosomes at the surface of the hydrogel may experience higher substrate concentrations than colloidosomes further within the hydrogel due to the diffusion gradients formed. The surface colloidosomes may also deplete the substrate, further reducing the concentration experienced by colloidosomes further within the hydrogel. Since some colloidosomes within the population are therefore experiencing less than the applied substrate concentration, the Michaelis-Menten curve is shifted to the right and the apparent K_M' rises. The error in the hydrogel value for K_M' is also large. This error was calculated from the standard deviation of three rate measurements using standard error propagation rules, that explains partly why it is magnified compared to the errors in the rate values. However, the large error may also reflect some inhomogeneity in the prototissue hydrogels during formation (in terms of the number of colloidosomes or colloidosome activity).

The v_{max} value for gel encapsulated colloidosomes (18 ±3 μM min^{-1}) is only slightly lower than that for colloidosomes in suspension given the error values (24 ±2 μM min^{-1}). Although this may seem at odds with the obviously delayed increase in [DAP] seen in Figure 4.6d, it is important to remember that the data used to calculate v_{max} discounts the initial lag period, and that might be why the values are more similar than expected. The other value that is often calculated to give an estimate of enzyme activity is K_{cat} (v_{max}/[enzyme]) but this value was not calculated here because it is difficult to accurately determine enzyme concentration within the colloidosome population.

Figure 4.6b shows photographs of cuvettes containing HRP colloidosomes in suspension or in agarose hydrogels, after the addition of *o*PD and H_2O_2, and corroborate the quantitative data from the fluorescence spectroscopy. In suspension, the colour associated with the production of DAP is seen throughout the cuvette. When colloidosomes are trapped within the hydrogel matrix the reaction is localised at the hydrogel surface and, even after an hour, little colour is seen within the hydrogel. Spreading of colour within the solution above the hydrogel is also delayed. Within a bulk hydrogel slowed mass transport means that only some sections of the population may be significantly contributing to the enzymatic rate, as many parts of the population will not be reached by the substrate over short time periods.

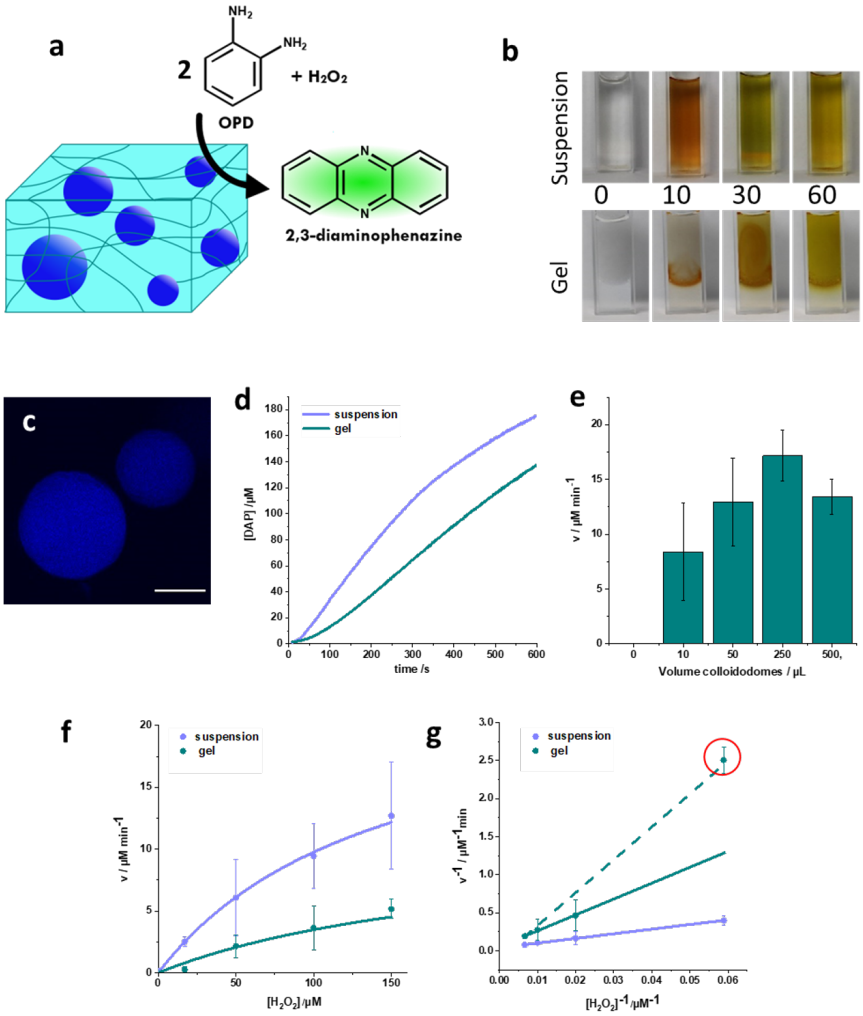

FIGURE 4.6. (a) A schematic depicting the oxidation of *o*PD to fluorescent DAP by HRP colloidosomes within the hydrogel. The reaction was carried out in cuvettes using colloidosomes in suspension and in a hydrogel and imaged over time (b). The elapsed time is indicated in minutes. (c) A confocal microscopy image of DL650-HRP colloidosomes embedded in a 1% w/v agarose hydrogel, scale bar 50 μm. For quantitative analysis of the HRP reaction, the production of fluorescent DAP was monitored and converted to a concentration. In all plots dating relating to colloidosomes in aqueous suspension is shown in blue and that relating to colloidosomes within agarose gel in green. Plot (d) shows the increase in DAP over time when what conditions a sample containing 50 μl colloidosomes was run with 500 μM *o*PD and 450 μM H_2O_2. (e) A chart of the initial rate against the volume of colloidosomes used in the sample. (f) A Michaelis-Menten plot showing the relationship between initial hydrogen peroxide concentration and initial rate of reaction, when *o*PD is held at 500 μM and (g) is the Lineweaver Burke plot that results from converting the data in (f) to the double reciprocal. The linear fit for the hydrogel colloidosome samples was performed with (dashed line) and without (solid line) the value circled. Plot (g) was used to calculate the parameters K_M and v_{max} and the values are shown in table 1.

Chemical communication between the constituent protocells is an important part of prototissue functionality. Binary protocell populations of colloidosomes containing either HRP or glucose oxidase (GOx) were formed. GOx oxidises glucose into gluconolactone and hydrogen peroxide. HRP can then utilise the hydrogen peroxide in the conversion of *o*PD to DAP (Figure 4.7a). The conditions of formation of GOx colloidosomes were again refined to optimise structure and activity. Colloidosomes were formed using an aqueous phase of 2270 U/mL GOx in pH 4 acetate buffer and crosslinked with 15 to 20μL TMOS. Colloidosomes containing FITC-GOx were embedded in agarose hydrogels and showed retention of the fluorescent enzyme and spherical structure (Figure 4.7b).

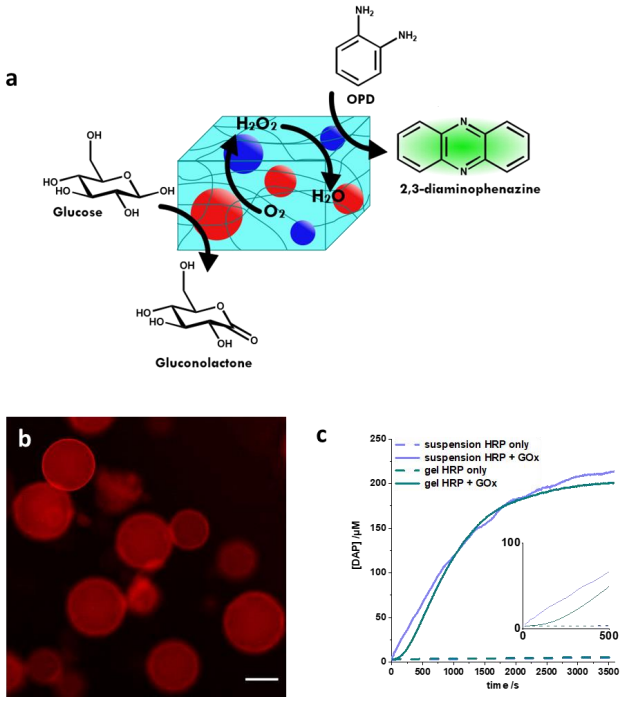

FIGURE 4.7. GOx colloidosomes (red) convert glucose to gluconic acid and produce H_2O_2, as shown by the schematic in (a).HRP colloidosomes (blue) then utilise the H_2O_2 in the oxidation of *o*PD. (b) is a fluorescence microscopy image of colloidosomes formed using FITC-GOx encapsulated within 1% w/v agarose hydrogel. (c) is a plot of DAP concentration over time when glucose is added to colloidosomes in suspension or in gel. Data relating to colloidosomes in aqueous suspension is shown in blue and that relating to colloidosomes within agarose gel in green. Dashed lines are samples run with HRP colloidosomes only and solid lines are samples with a binary colloidosome populations. The inlay shows the same data as the main plot b 0s and 500 s.

Glucose (1 mM final concentration) and *o*PD (final concentration 500μM) were added to GOx/ HRP colloidosome hydrogels and the reaction monitored using fluorescence spectroscopy. The plot in Figure 4.7c shows that only when both colloidosomes populations are present do we see the production of DAP. Again, an initial lag is seen in the production of DAP when the colloidosomes are encapsulated within the hydrogel, but not when they are free in suspension.

The diffusion of hydrogen peroxide from the GOx colloidosomes to the HRP colloidosomes during the cascade reaction is a rudimentary form of chemical communication, as has been described for other protocell models previously [10]. In this case the chemical communication occurs through the polymer matrix around the protocells, as it would through the ECM in a tissue.

4.3.3 Heterogeneity in colloidosome-hydrogel prototissues

Sections 4.3.2 and 4.3.1 showed that by embedding colloidosomes within agarose hydrogels we achieve materials that begin to resemble a prototissue model. However, as mentioned in Section 4.2.2, living tissues are often heterogeneous in features such as cell distribution and function and they also rely on the formation of chemical gradients of soluble materials. In order to mimic this heterogeneity within hydrogel prototissue the simplest route is to create heterogeneous distributions of different colloidosome populations within the hydrogel (colloidosomes are microcapsules so they will not move through the hydrogel structure). Encapsulating different enzymes within these populations would then create hydrogels with heterogeneous distribution of enzymatic function and thus spatially patterned functionality. It should be noted that this heterogeneity cannot necessarily be achieved using free enzyme within the hydrogel since although enzymes are macromolecules, they are often able to diffuse through the porous structure of the hydrogel. Herein, a simple model for the creation of heterogeneous colloidosome hydrogels is developed, creating composite hydrogels by combining different hydrogel pieces.

4.3.3.1 Population patterning in colloidosome hydrogels

Stepwise addition of pre-gel solutions containing different colloidosome populations (FITC-BSA colloidosomes or RITC-BSA colloidosomes) into a capillary tube allows the formation of patterned hydrogel wires, with spatially segregated protocell populations (Figure 4.8). Patterned hydrogel created using this method showed no change in patterning after 48 hours storage, whereas gels created in the same pattern but in the absence of colloidosomes showed mixing of the fluorescently labelled protein and loss of the pattern over time. This indicates that, in order to achieve heterogeneity of function within the hydrogel, enzymes do need to be localised within the colloidosomes.

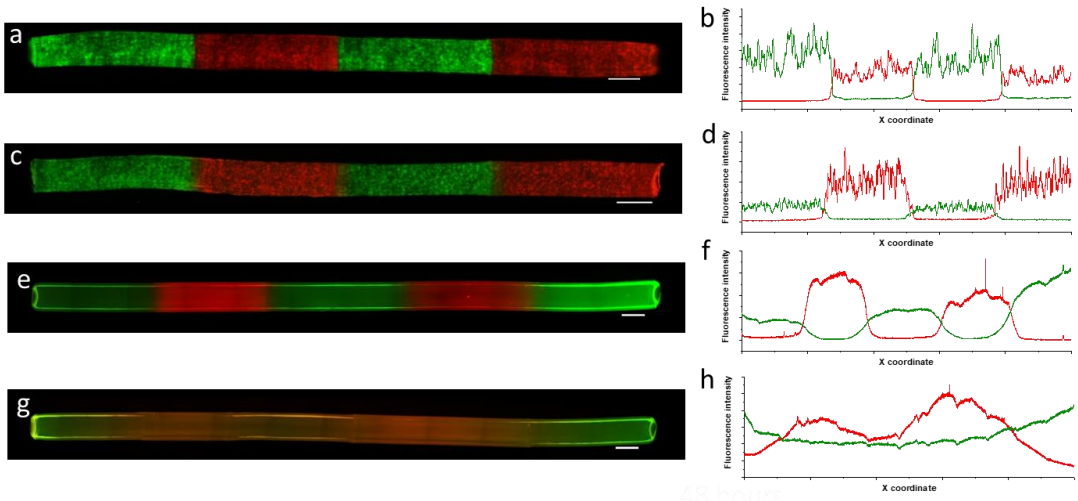

FIGURE 4.8. (a), (c), (e) and (g) are widefield fluorescence microscopy tiles scan images of heterogeneous hydrogels formed using the composite hydrogel method. Red fluorescence shows the presence of RITC-BSA and green fluorescence FITC-BSA. (a) and (e) are images taken immediately after gel formation and show hydrogels formed with protein within colloidosomes or free in solution respectively. Hydrogels were stored in a humid environment for 48 hours and reimaged. (c) shows the gel in (a) after 48 hours and (g) the gel in (e). Scale bars represent 1 mm. (b), (d), (f) and (h) are plots of the fluorescence intensity taken from a line profile along the centre of the capillary hydrogels. Red lines refer to RITC-BSA fluorescence and green to FITC-BSA fluorescence.

In order to increase the complexity of the patterns that can be formed within the agarose-colloidosome hydrogels, a polymer that can be physically gelled by the introduction of a small molecule can be used to bind different gel pieces together, allowing the creation of composite hydrogels. Alginate is a biopolymer made up of guluronic acid and mannuronic acid moieties (Figure 4.9a) that can be gelled via the addition of calcium chloride because the guluronic acid regions chelate Ca^{2+}. One alternative system that was tested was poly(vinyl alcohol)-borax hydrogels, and although the self-healing properties of these gels did allow for the creation of composite hydrogels, it also made the gels more malleable and they lost the moulded shape more easily. In contrast, agarose-alginate interpenetrated network (IPN) hydrogels were more rigid than agarose only gels. Colloidosomes were embedded in an agarose -alginate IPN and as with agarose only gels, they showed retention of spherical structure (Figure 4.9b). Alginate

was labelled using the fluorescent dye 2-(4-Amidinophenyl)-6-indolecarbamidine dihydrochloride (DAPI) and used to form IPN gels containing colloidosomes to assess the permeation of the polymer across the colloidosome membrane. Figure 4.9c shows a confocal microscopy image of a colloidosome within a DAPI alginate hydrogel. Fluorescence intensity is highest at the colloidosome membrane indicating that the alginate interacts with the silica nanoparticles. Although the fluorescence in the colloidosome interior is lower than the bulk of the hydrogel, the difference is not significant indicating that some alginate permeation into the colloidosome lumen does occur. To make heterogeneous composite hydrogels, agarose gels were made in the normal manner, but alginate polymer was included in the pre-gel solution. Multiple agarose hydrogels could then be assembled and pressed together for 30 minutes, to allow some tangling of alginate chains at the surface. $CaCl_2$ (50 mM) was then added causing the alginate to gel. This resulted in a composite hydrogel containing the desired pattern of hydrogel pieces. These gels could be handled as one piece without separating (Figure 4.9d).

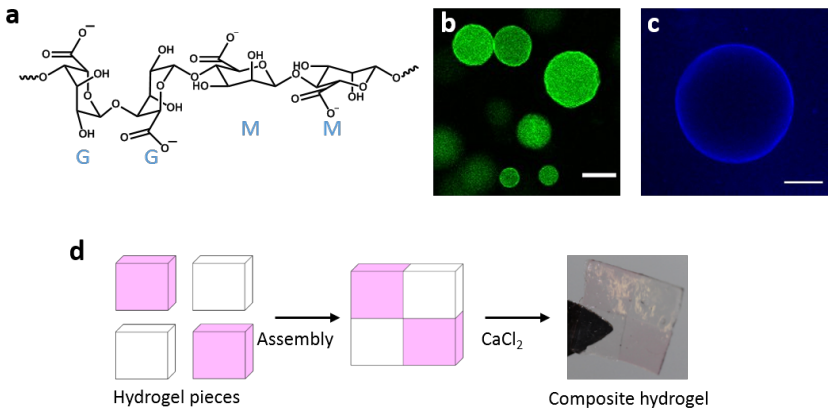

FIGURE 4.9. (a) Chemical structure of alginate, labelled G and M indicating guluronic acid and mannuronic acid respectively. (b) FITC-BSA Colloidosomes distributed within an agarose-alginate IPN hydrogel, scale bar 50 μm. (c) A confocal microscopy image of a BSA colloidosome (non-fluorescent) within an agarose alginate IPN hydrogel formed using 0.5% w/v DAPI labelled alginate. Scale bar 20 μm. (d) Schematic showing the formation of composite gels by the combining of gel pieces. Agarose hydrogel pieces containing ungelled alginate are pressed together in a mould for half an hour before calcium chloride is added, gelling the alginate and joining the neighbouring pieces together to form a composite hydrogel. The resulting hydrogel can be picked up and remains structurally intact, as shown by the photograph.

4.3.3.2 In-situ gradient formation and reaction patterning

The HRP/ GOx enzyme cascade occurs in binary colloidosome populations due to communication between the two types of protocell. It was hypothesised that heterogeneously distributing the two colloidosome populations in a composite hydrogel would create a system that is capable of anisotropic behaviour upon uniform application of a chemical stimulus and tissue-like in-situ formation of chemical gradients through the collective behaviour of the component parts. The colorimetric substrate 2,2'-Azino-bis-(3-ethylbenzothiazoline)-6-sulfonic acid) (ABTS) was used (Figure 4.10). In the presence of H_2O_2, HRP can oxidise ABTS to the radical cation, that has a green/ blue colour and is negatively charged at neutral pH ($ABTS^{\bullet+}$). Disproportionation (slow and thus usually ignored in initial rate experiments) or further oxidation, favoured by excess H_2O_2, results in $ABTS^{2+}$ that is purple/red in colour [164]. The back reaction that converts $ABTS^{\bullet+}$ to ABTS is also very slow [165].

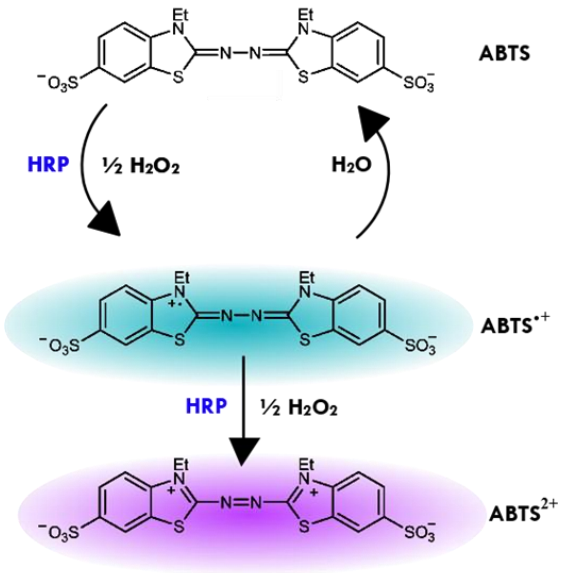

FIGURE 4.10. Oxidation of ABTS by hydrogen peroxide catalysed by HRP forms the coloured compound $ABTS^{\bullet+}$. Under certain conditions this can be further oxidised to $ABTS^{2+}$. A back reaction from $ABTS^{\bullet+}$ to ABTS can occur but is very slow.

A composite prototissue is formed with GOx and HRP colloidosomes co-localised within a section of the hydrogel connected to a section containing no colloidosomes (Figure 4.11a).

Composite hydrogel prototissues were equilibrated overnight with the colorimetric substrate ABTS. In order to initiate the enzymatic reaction, the hydrogels were placed on top of source gels that contained glucose (Figure 4.11b). By imaging the 1 mm thick prototissues from above, the system is treated as pseudo 2D with the substrate applied equally across the hydrogel. Figure 4.11c shows some simple examples of reaction within composite hydrogel prototissues, with fluorescence microscopy images depicting the distribution of colloidosomes. Upon application of glucose to the prototissue, GOx colloidosomes convert glucose to gluconolactone and release H_2O_2. As the H_2O_2 diffuses to the HRP colloidosomes, they convert ABTS to $ABTS^{\bullet+}$. This can be seen in the appearance of blue/ green colouration in the colloidosome containing region of the hydrogel. This pattern is transient; the reaction occurring in one region of the hydrogel sets up a chemical gradient in the other and the point of origin and direction of the concentration gradient is solely controlled by the spatial distribution of the colloidosomes, not by the application of the initial substrate.

RGB values across the hydrogel were measured over time and converted to hue angle and saturation values, which are displayed in the contour map in Figure 4.11d-e. This is not a quantitative measure of the concentration of the species present but is a useful tool for monitoring the spread of the coloured product $ABTS^{\bullet+}$. The hue initially changes within the GOx/ HRP section only and this is accompanied by an increase in the saturation as the concentration of $ABTS^{\bullet+}$ increases. Over time, the blue/green colouration can be seen to spread as $ABTS^{\bullet+}$ diffuses away. The development of the concentration gradient over time can be seen in a gradual change of the hue angle and saturation across the whole gel. The development of the initial pattern relies upon the fact that the reaction occurring is faster than the diffusion of the reporter $ABTS^{\bullet+}$.

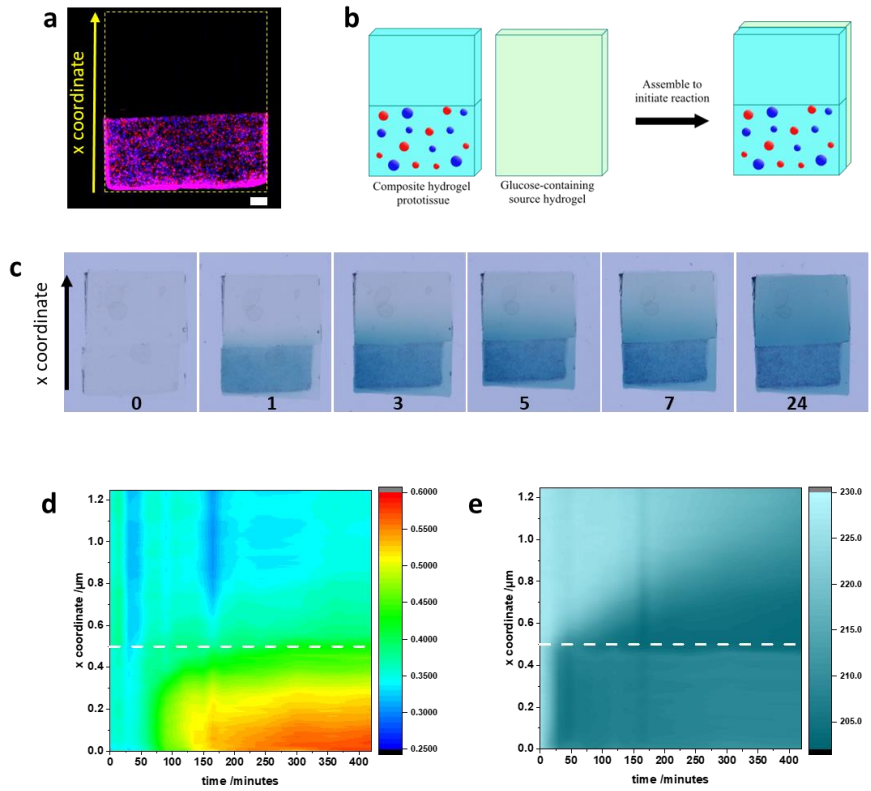

FIGURE 4.11. (a) A fluorescence microscopy image of a composite hydrogel formed from pieces with mixed population (GOx/HRP, 50 μL of each per 200 μL hydrogel) and plain pieces (buffer only). For imaging fluorescently labelled BSA was included in the colloidosome aqueous phase with the relevant enzyme (GOx colloidosomes contained RITC-BSA (red) and HRP colloidosomes contained DL650-BSA (blue)). Pink colouration appears where both colloidosome populations are present. The scale bar represents 1 mm and the yellow dashed line represents the edge of the hydrogel, which cannot be seen due to the lack of fluorescence in some sections. (b) is a schematic of a composite hydrogel where GOx colloidosomes are shown as red and HRP as blue. The schematic also shows how the reaction is initiated by placing the hydrogel on top of a source hydrogel containing glucose. (c) is a series of photographs taken of the composite hydrogel (roughly 1.25 cm x 1 cm) after it was added to a source hydrogel containing 1 mM glucose. The time lapsed is indicated at the bottom of each photograph in hours. Contour plots of the saturation (d) and hue angle (e) over time are shown, with the x coordinate along which the measurements were taken marked on the fluorescence microscopy images and photographs in (a) and (c). The white dashed lines indicate the boundary between the GOx/HRP and plain hydrogel pieces. After the reaction is initiated H_2O_2 released by the GOx colloidosomes diffuses to the HRP colloidosomes, which then convert ABTS to $ABTS^{\bullet+}$. This results in the appearence of blue/ green colouration in the colloidosome containing region of the hydrogel which can be seen in (c), and in increase in saturation and hue shown in (d) and (e). Over time this colouration and increase in saturation and hue spreads across the region of the hydrogel that does not contain colloidosomes, showing that the patterning in transient.

Although after 7 hours the hue angle is uniform across the hydrogel, the saturation shows that there is still a gradient of $ABTS^{\bullet+}$. When the hydrogel is imaged again after 24 hours the whole hydrogel appears the same colour, the system has reached equilibrium. However, closer inspection of the reaction prototissues shows that as the reaction occurs, adsorption of coloured species onto the colloidosomes results in a mottled pattern in the colloidosomes region of the hydrogels, implying that species that interact more strongly with the colloidosomes can be permanently patterned within the hydrogel. It may be that the dark colouration of the colloidosomes is simply $ABTS^{\bullet+}$ adsorbing, however microscope images of gels after reacting (Figure 4.12) seemed to show colloidosomes with purple colouration, which may indicate that the adsorbed species is $ABTS^{2+}$. If present this species would be expected to adsorb more strongly onto the silica colloidosomes as it is neutral overall whereas ABTS and $ABTS^{\bullet+}$ are negative.

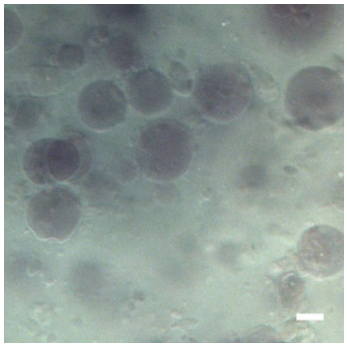

FIGURE 4.12. An RGB bright field microscopy image of a section of colloidosome hydrogel after reaction with ABTS and glucose (scale bar 50 μm).

Assembling more pieces in a heterogeneous composite hydrogel allows the formation of multiple concentration gradients within the bulk sample (Figure 4.13). Again, the GOx/HRP piece becomes coloured first due to the production of $ABTS^{\bullet+}$ by the enzymatic cascade. As the product diffuses away, we see concentration gradients within the non-colloidosome containing pieces, and for the central region, which has a GOx/ HRP region either side, we see a double concentration gradient, with $ABTS^{\bullet+}$ diffusing from both sides. Again, the patterned concentration of $ABTS^{\bullet+}$ is transient; over time the concentration equalises, and the gel becomes uniform in colour. Once again more a permanent patterning due to adsorption onto the colloidosomes can also be seen.

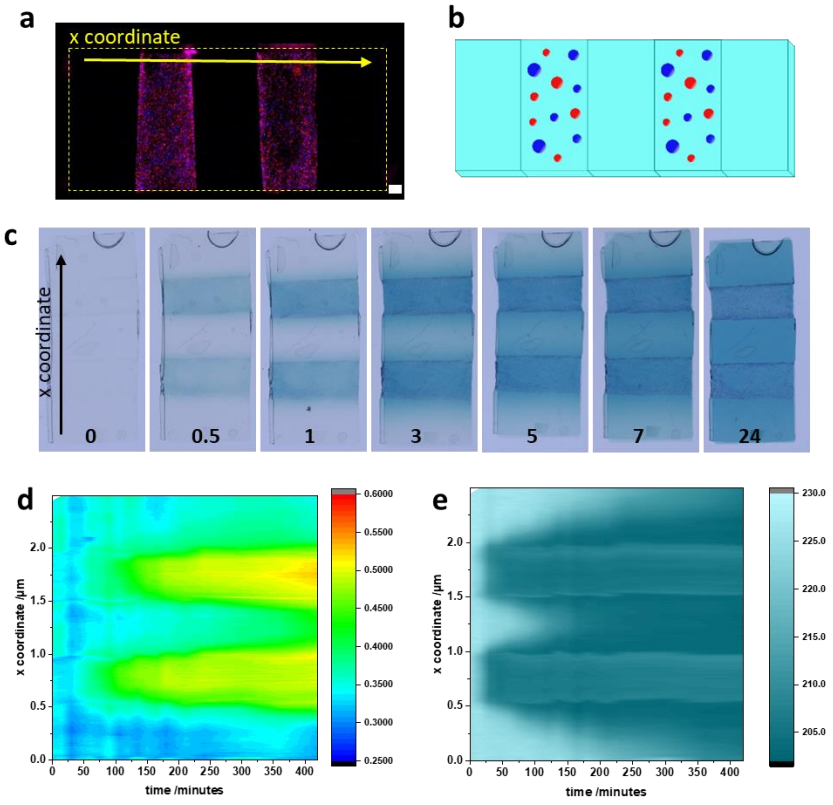

FIGURE 4.13. A fluorescence microscopy image (a) and schematic (b) of a composite hydrogel formed from pieces with mixed population (GOx/HRP, 50 μL of each per 200 μL hydrogel) and plain pieces (buffer only). For imaging fluorescently labelled BSA was included in the colloidosome aqueous phase with the relevant enzyme (GOx colloidosomes contained RITC-BSA (red) and HRP colloidosomes contained DL650-BSA (blue)). In (a) the scale bar represents 1 mm and the yellow dashed line represents the edge of the hydrogel, which cannot be seen due to the lack of fluorescence in certain units. Pink colouration appears where both colloidosome populations are present. In the schematic (b) GOx colloidosomes are shown as red and HRP as blue. (c) is a series of photographs taken of the composite hydrogel (roughly 2.5 cm x 1 cm) after it was added to a source hydrogel containing 1 mM glucose. The time lapsed is indicated at the bottom of each photograph in hours. Contour plots of the saturation (d) and hue angle (e) over time are shown, with the x coordinate along which the measurements were taken, marked on the fluorescence microscopy images and photographs in (a) and (c). After the reaction is initiated H_2O_2 released by the GOx colloidosomes diffuses to the HRP colloidosomes, which then convert ABTS to $ABTS^{\bullet+}$. This results in the appearence of blue/ green colouration in the colloidosome containing regions of the hydrogel which can be seen in (c), and in increase in saturation and hue shown in (d) and (e). The $ABTS^{\bullet+}$ diffuses through the hydrogel resulting in multiple concentration gradients, in a pattern determined by the arrangement of the colloidosome populations.

Composite hydrogel prototissues were created with GOx and HRP colloidosomes spatially segregated (Figure 4.14a-b) and the reaction initiated and monitored using the same method as described above. Within these hydrogels the oxidation of glucose sets up a chemical gradient of H_2O_2 (Figure 4.14c). Since HRP colloidosomes experience different H_2O_2 concentrations according to their position, they produce $ABTS^{\bullet+}$ at different rates. Colour indicative of $ABTS^{\bullet+}$ initially appears at the interface of the GOx and HRP sections. The heterogeneous production of $ABTS^{\bullet+}$ sets up a second chemical gradient within the hydrogel, as well as the gradient of H_2O_2 there is now a gradient of $ABTS^{\bullet+}$. This spreads over time, both through formation of $ABTS^{\bullet+}$ by colloidosomes further from the GOx piece as H_2O_2 diffuses through the gel, and through the diffusion of $ABTS^{\bullet+}$ itself, as can be seen from the saturation and hue plots (Figure 4.14d-e).

The diffusion coefficients of H_2O_2 (1.7×10^{-9} m^2s^{-1}) and $ABTS^{\bullet+}$ (4.5×10^{-10} m^2s^{-1}) in water indicate that H_2O_2 tends to diffuse faster [166, 167]. This is reflected in the way the pattern spreads in the composite hydrogel. If there was no diffusion of H_2O_2 $ABTS^{\bullet+}$ would only be produced at the interface of the HRP and GOx regions and would diffuse outwards from this point symmetrically. It is clear from Figure 4.14d-e that the $ABTS^{\bullet+}$ colouration spreads more rapidly into the section of the hydrogel with HRP colloidosomes than the section with GOx colloidosomes. This is be due to the diffusion of H_2O_2 from the interface through the HRP colloidosome region, which results in $ABTS^{\bullet+}$ production within this section of the hydrogel before $ABTS^{\bullet+}$ produced at the interface would have spread into this region.

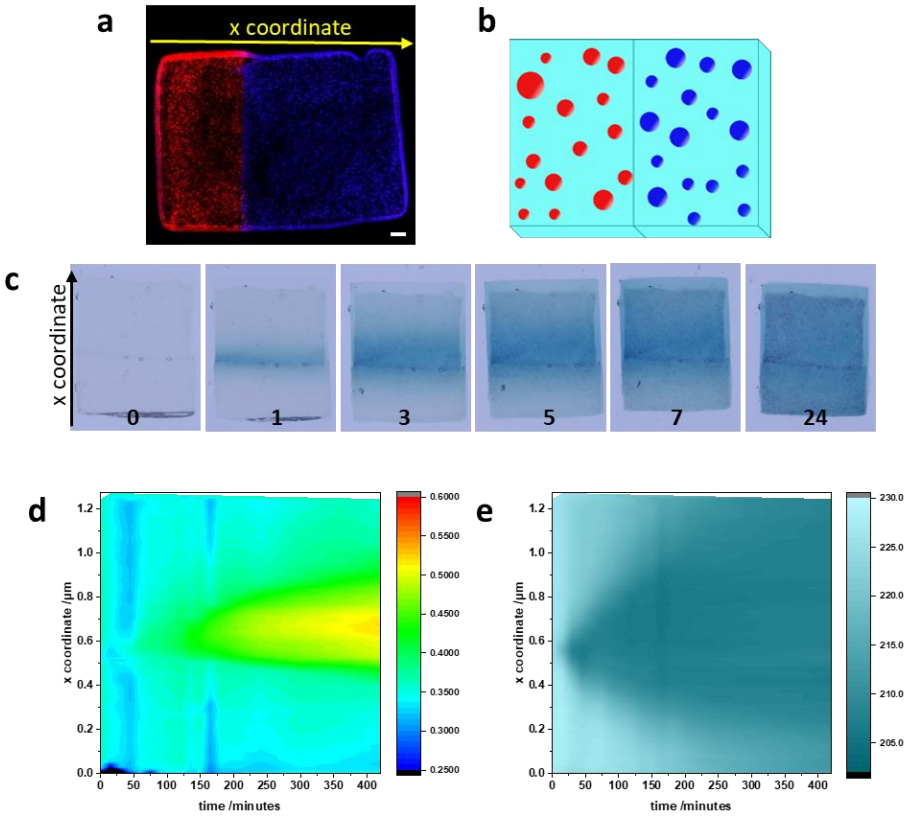

FIGURE 4.14. A fluorescence microscopy image (a) and schematic (b) of a composite hydrogel formed from pieces with GOx colloidosome pieces and HRP colloidosome pieces (both 100 μL of each per 200 μL hydrogel). For imaging fluorescently labelled BSA was included in the colloidosome aqueous phase with the relevant enzyme (GOx colloidosomes contained RITC-BSA (red) and HRP colloidosomes contained DL650-BSA (blue)). In (a) the scale bar represents 1mm. In the schematic (b) GOx colloidosomes are shown as red and HRP as blue. (c) is a series of photographs taken of the composite hydrogel (roughly 1.25 cm x 1 cm) after it was added to a source hydrogel containing 1 mM glucose. The time lapsed is indicated at the bottom of each photograph in hours. Contour plots of the saturation (d) and hue angle (e) over time are shown, with the x coordinate along which the measurements were taken, marked on the fluorescence microscopy images and photographs in (a) and (c). After the reaction is initiated H_2O_2 is produced in the region that contains GOx colloidosomes. The H_2O_2 diffuses into the region of the hydrogel that contains HRP colloidosomes. The colour (c) and increase in saturation and hue (d) and (e) that are indicative of $ABTS^{\bullet+}$ initially appear at the interface of the GOx and HRP sections, but due to the diffusion of H_2O_2 and $ABTS^{\bullet+}$ can be seen to spread through the hydrogel as time progresses. The blue/ green colour and increased hue spread more quickly within the region of the hydrogel that contains HRP colloidosomes than the region that contains GOx colloidosomes, resulting in a nonsymmetrical gradient around the interface of the two regions.

Again, by creating alternating GOx and HRP regions (a pattern described as GHGHG), multiple gradients can be set up. We see transient patterning due to $ABTS^{\bullet+}$ initially forming at the GOx/ HRP interfaces and then diffusing away, with the colour one again spreading faster in the HRP regions than the GOx regions due to the fast diffusion of H_2O_2. The mottled effect due to adsorption onto colloidosomes appears across the hydrogel as the wave of blue/ green colour spreads and is seen across the whole hydrogel uniformly after 24 hours.

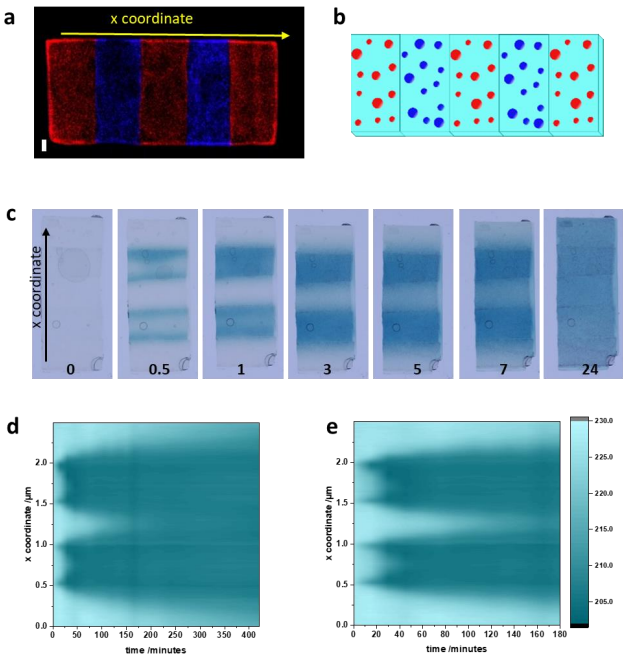

FIGURE 4.15. A fluorescence microscopy image (a) and schematic (b) of a composite hydrogel formed from pieces with GOx colloidosome pieces and HRP colloidosome pieces (both 100 μL of each per 200 μL hydrogel) in the pattern described as GHGHG. For imaging fluorescently labelled BSA was included in the colloidosome aqueous phase with the relevant enzyme (GOx colloidosomes contained RITC-BSA (red) and HRP colloidosomes contained DL650-BSA (blue)). In (a) the scale bar represents 1mm. In the schematic (b) GOx colloidosomes are shown as red and HRP as blue. (c) is a series of photographs taken of the composite hydrogel (roughly 2.5 cm x 1 cm) after it was added to a source hydrogel containing 1 mM glucose. The time lapsed is indicated at the bottom of each photograph in hours. (d) and (e) Contour plots of the hue angle over time are shown, with the x coordinate along which the measurements were taken, marked on the fluorescence microscopy images and photographs in (a) and (c). (e) presents the same data as (d) but over a shorter timescale to allow more detail to be seen. A contour plot of the saturation over time is shown in Figure A.12. After the reaction is initiated H_2O_2 is produced in the regions that contain GOx colloidosomes. The H_2O_2 diffuses into the regions of the hydrogel that contain HRP colloidosomes. The colour (c) and increase in hue (d and e) that are indicative of $ABTS^{\bullet+}$ initially appear at the interface of the GOx and HRP sections, but due to the diffusion of H_2O_2 and $ABTS^{\bullet+}$ can be seen to spread through the hydrogel as time progresses. The blue/ green colour and increased hue spread more quickly within the regions of the hydrogel that contain HRP colloidosomes than the regions that contain GOx colloidosomes, resulting in nonsymmetrical gradients around the interfaces.

Since transient chemical concentration patterns can be formed using composite hydrogel prototissues, it was hypothesised that the development of these patterns over time could be controlled by manipulating certain characteristics of the system. Figure 4.16 shows the result of running the GHGHG patterned hydrogel with 0.5 mM glucose rather than the 1 mM glucose used in Figure 4.15. The initial patterning with high $ABTS^{\bullet+}$ concentrations at the GOx/ HRP interface is maintained for longer.

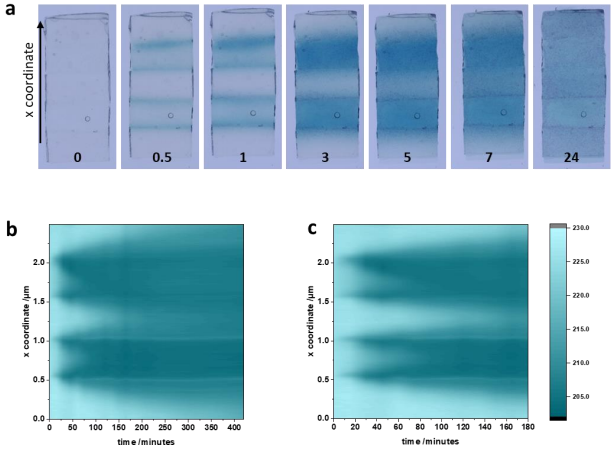

FIGURE 4.16. Composite hydrogels were formed from pieces with GOx colloidosome pieces and HRP colloidosome pieces in the pattern described as GHGHG (see Figure 4.15 for scheme). A hydrogel was formed with GOx colloidosome pieces and HRP colloidosome pieces each containing 100μL colloidosomes per 200μL hydrogel. (a) shows photographs taken of the composite hydrogel (roughly 2.5 cm x 1 cm) after it was added to a source hydrogel containing 0.5 mM glucose. The time lapsed is indicated at the bottom of each photograph in hours. Contour plots of the hue angle (b) and (c) over time are shown, with the x coordinate along which the measurements were taken marked on the photographs in (a). (c) presents the same data as (b) but over a shorter timescale to allow more detail to be seen. A contour plot of the saturation over time is shown in Figure A.12. The colour (a) and increase in hue (b and c) that are indicative of $ABTS^{\bullet+}$ initially appear at the interface of the GOx and HRP sections, and spread more quickly within the regions of the hydrogel that contain HRP colloidosomes than the regions that contain GOx colloidosomes, resulting in nonsymmetrical gradients around the interfaces. The colour (a) and increase in hue (b and c) appear more slowly within the HRP region than in experiments run with higher glucose concentration (Figure 4.15) meaning that the patterning of $ABTS^{\bullet+}$ at the interface regions lasts longer.

A composite hydrogel (GHGHG) with tenfold fewer GOx colloidosomes in the GOx region run with 1 mM glucose shows more exaggerated pattern lifetime than the gel run with 0.5 mM glucose, due to slower production of H_2O_2 (Figure 4.17). Decreases H_2O_2 decrease the rate of

$ABTS^{\bullet+}$ production in general, which would slow the development of the pattern however the H_2O_2 concentration experienced by colloidosomes within the hydrogel is not simply a case of diffusion from the GOx piece. Since HRP colloidosomes will use up H_2O_2 they affect its spread across the hydrogel. Depletion of H_2O_2 by HRP colloidosomes near to the GOx piece reduces the concentration felt by those further away, exaggerating the effect that would be seen due to differences in concentration from simple diffusion profiles. This plays a part in the prolonged patterning seen.

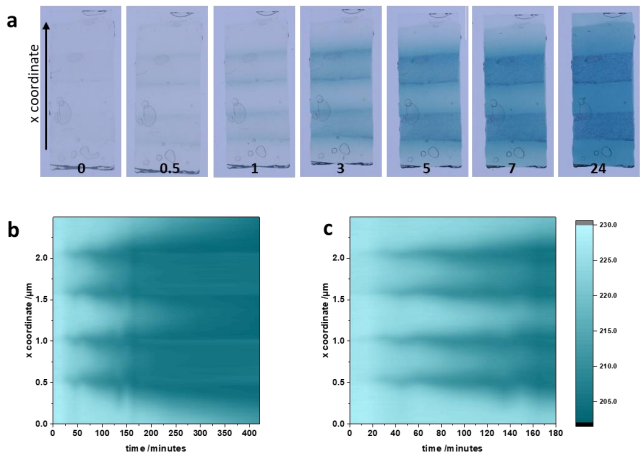

FIGURE 4.17. Composite hydrogels were formed from pieces with GOx colloidosome pieces and HRP colloidosome pieces in the pattern described as GHGHG (see Figure 4.15 for scheme). A hydrogel was formed with tenfold fewer GOx colloidosomes: GOx colloidosome pieces containing 10 μL colloidosomes per 200 μL hydrogel and HRP colloidosome pieces containing 100 μL colloidosomes per 200 μL hydrogel. (a) shows photographs taken of the composite hydrogel (roughly 2.5 cm x 1 cm) after it was added to a source hydrogel containing 1 mM glucose. The time lapsed is indicated at the bottom of each photograph in hours. Contour plots of the hue angle (b) and (c) over time are shown, with the x coordinate along which the measurements were taken marked on the photographs in (a). (c) presents the same data as (b) but over a shorter timescale to allow more detail to be seen. A contour plot of the saturation over time is shown in Figure A.12. The colour (a) and increase in hue (b and c) that are indicative of $ABTS^{\bullet+}$ initially appear at the interface of the GOx and HRP sections, and spread more quickly within the regions of the hydrogel that contain HRP colloidosomes than the regions that contain GOx colloidosomes, resulting in nonsymmetrical gradients around the interfaces. The colour (a) and increase in hue (b and c) appear more slowly within the HRP region than in experiments with higher concentrations of GOx colloidosomes (Figure 4.15) meaning that the patterning of $ABTS^{\bullet+}$ at the interface regions lasts longer.

Figure 4.18 shows a GHGHG patterned hydrogel with tenfold fewer HRP colloidosomes. Since there are fewer HRP colloidosomes there is less depletion of the H_2O_2 and the colouration

indicative of $ABTS^{\bullet+}$ occurs almost simultaneously across the HRP region.

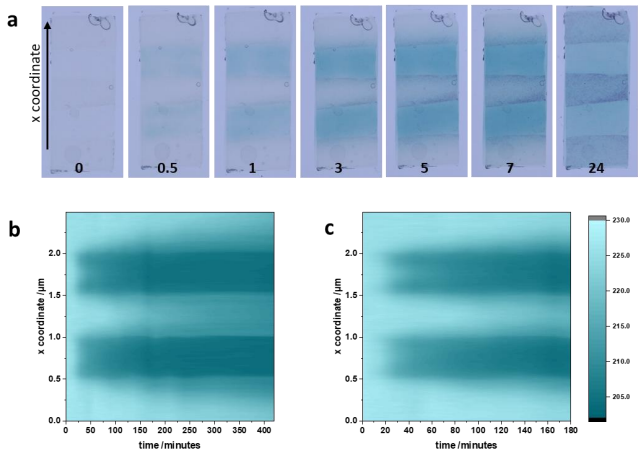

FIGURE 4.18. Composite hydrogels were formed from pieces with GOx colloidosome pieces and HRP colloidosome pieces in the pattern described as GHGHG (see Figure 4.15 for scheme). A hydrogel was formed with tenfold fewer HRP colloidosomes: GOx colloidosome pieces containing 100 μL colloidosomes per 200μL hydrogel and HRP colloidosome pieces containing 10 μL colloidosomes per 200 μL hydrogel. (a) shows photographs taken of the composite hydrogel (roughly 2.5 cm x 1 cm) after it was added to a source hydrogel containing 1 mM glucose. The time lapsed is indicated at the bottom of each photograph in hours. Contour plots of the hue angle (b) and (c) over time are shown, with the x coordinate along which the measurements were taken marked on the photographs in (a). (c) presents the same data as (b) but over a shorter timescale to allow more detail to be seen. A contour plot of the saturation over time is shown in Figure A.12. The colour (a) and increase in hue (b and c) that are indicative of $ABTS^{\bullet+}$ appear across the sections of the hydrogel that contain HRP colloidosomes rather than starting at the interfaces (as was seen in experiments with higher concentrations of HRP colloidosomes (Figure 4.15)). The colour (a) and increase in hue (b and c) spread slowly into the sections that contain GOx colloidosomes, resulting in nonsymmetrical gradients around the interfaces.

A further example of the composite hydrogel prototissues showing spatio-temporal patterning of $ABTS^{\bullet+}$ is shown in Figure 4.19. Multiple GOx/HRP mixed pieces set within a unfunctionalized hydrogel and the density of colloidosomes within each piece altered to vary the rate of $ABTS^{\bullet+}$ production. Where the colloidosome density is higher $ABTS^{\bullet+}$ is formed faster and colour appears first. After 24 hours soluble $ABTS^{\bullet+}$ is uniform across the hydrogel, indicating transient patterning again, but darker mottled purple is seen in the piece with higher colloidosome concentrations.

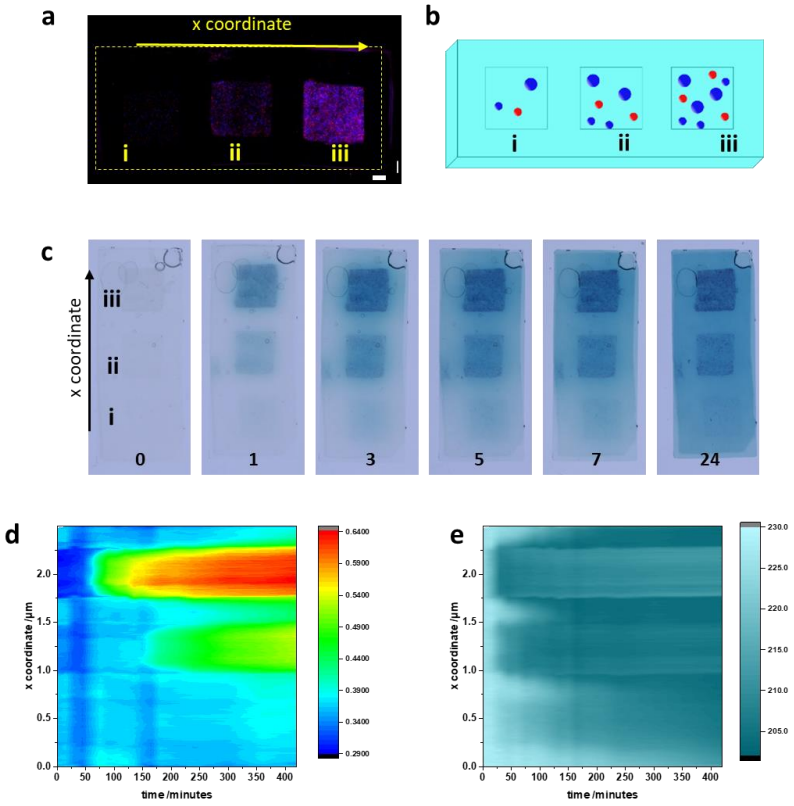

FIGURE 4.19. A fluorescence microscopy image (a) and schematic (b) of a composite hydrogel formed from pieces with mixed population (all GOx:HRP in a 1:2 volume ratio, (i) 15 μL total per 200 μL hydrogel, (ii) 75 μL total per 200 μL hydrogel, (iii) 300 μL total per 200 μL hydrogel) within a bulk plain hydrogel (buffer only). For imaging fluorescently labelled BSA was included in the colloidosome aqueous phase with the relevant enzyme (GOx colloidosomes contained RITC-BSA (red) and HRP colloidosomes contained DL650-BSA (blue)). In (a) the scale bar represents 1 mm and the yellow line represents the edge of the hydrogel. In the schematic (b) GOx colloidosomes are shown as red and HRP as blue. (c) is a series of photographs taken of the composite hydrogel (roughly 2.5 cm x 1 cm) after it was added to a source hydrogel containing 0.5 mM glucose. The time lapsed is indicated at the bottom of each photograph in hours. Contour plots of the saturation (d) and hue angle (e) over time are shown, with the x coordinate along which the measurements were taken, marked on the fluorescence microscopy images and photographs in (a) and (c). After the reaction is initiated blue/ green colouration appears in the colloidosome containing regions of the hydrogel which can be seen in (c), and as an increase in saturation and hue shown in (d) and (e). Colour and increase in saturation/ hue appear most rapidly in section (iii) , followed by (ii) and then (i). Section (iii) reaches a darker colour and greater saturation than section (ii), with section (i) still showing a light blue colour and lower saturation at the end of the experiment.

As a control, a composite hydrogel (GHGHG) was created with enzyme in solution rather than within colloidosomes. When these gels were placed on the glucose source the colouration due to $ABTS^{\bullet+}$ production is seen equally across the hydrogel rather than in the patterns seen for heterogeneous prototissues, as shown by the image in Figure 4.20d which shows the gel after 10 minutes. To confirm that this homogeneity is due to loss of enzyme patterning rather than rapid diffusion of coloured species within non colloidosome hydrogels, composite hydrogels were formed with fluorescently labelled GOx and HRP either free in solution or within colloidosomes. The hydrogels were imaged immediately after alginate crosslinking (Figure 4.20a) and again after being stored overnight in water (Figure 4.20b) (equivalent to the overnight equilibration with ABTS). Both GOx and HRP diffused through the hydrogel matrix over time when not encapsulated in colloidosomes, resulting in loss of the enzyme patterning and therefore loss of the heterogeneous distribution of the function. A second control, in which a composite colloidosome hydrogel (GHGHG) was placed on a source containing buffer only and no glucose, showed no colouration even after 24 hours, proving that the chemical communication between the colloidosome populations is responsible for the formation of the coloured species.

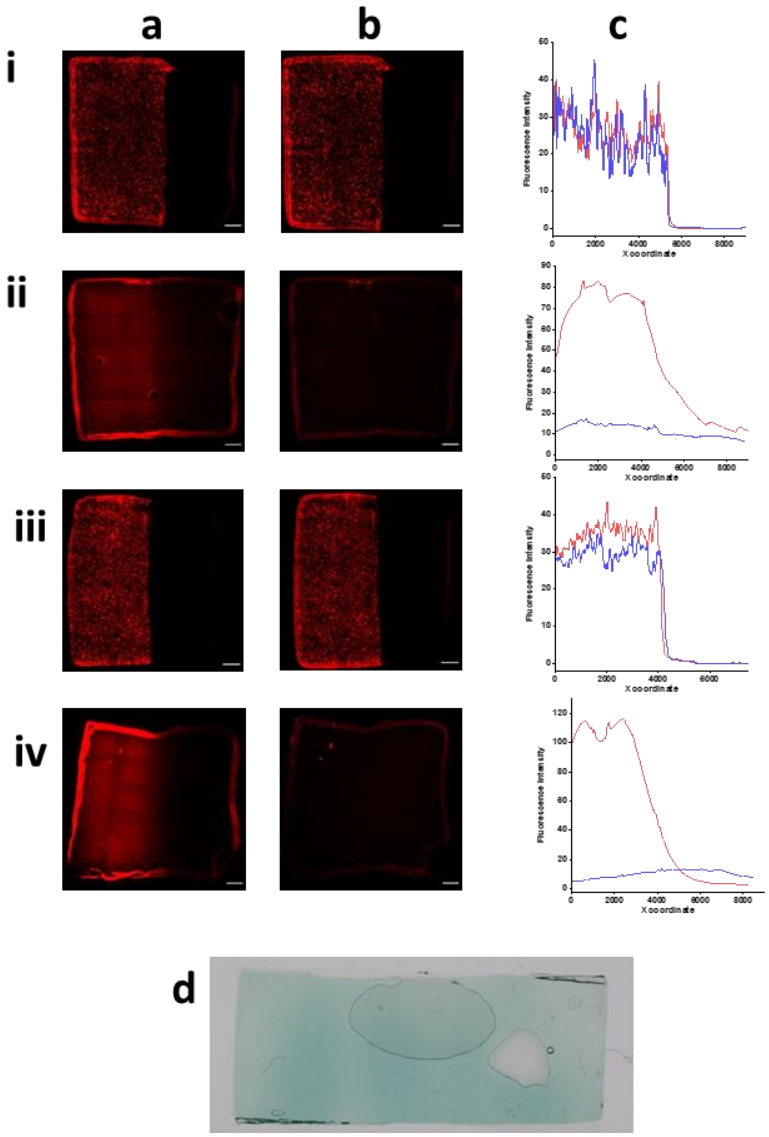

FIGURE 4.20. Composite hydrogels were formed from one piece with protein functionalisation and one plain. Functionalised pieces contained (i) DL650-GOx colloidosomes, (ii) RITC-GOx solution, (iii) DL650-HRP colloidosomes and (iv) DL650-HRP solution. Gels were imaged after crosslinking (a) and overnight equilibration with water (b) and line profile plotted to assess the extent of diffusion (c). Plot of line profiles from (a) are shown in red and from (b) in blue. A composite hydrogel of the pattern GHGHG was formed with free enzyme in solution, equilibrated with ABTS and reacted with a glucose source gel. (d) is an image of this hydrogel after 10 minutes reaction showing that the blue/ green colour indicative of $ABTS^{\bullet+}$ appeared throughout the hydrogel rather than being patterned.

The spatiotemporal patterning discussed so far occurs with hydrogels in air, meaning that all substrate and products are retained within the hydrogels (prototissue and source). If the hydrogel were surrounded by solution (rather than dry), substrate and product could diffuse freely through the water (as well as through the hydrogel). To test if patterns still emerge when the system is run with the hydrogel in water, a GHGHG patterned hydrogel was placed was formed and equilibrated with ABTS as normal. To initiate the reaction 8 mL glucose solution (0.5 mM) was added. The hydrogel was imaged from above, treating it as pseudo 2D again, and the resulting images and plots are shown in Figure 4.21. Despite the exchange with the solution, transient patterning was seen. As with the GHGHG gels run dry, initial colour is seen at the GOx/ HRP interface and this then spreads through the HRP region. Unlike with dry run gels a concentration gradient in the GOx regions is not seen, likely because as it is formed $ABTS^{\bullet+}$ diffuses into the solution and equilibrates throughout, rather than only moving through the hydrogel. Little colour change is seen outside the HRP regions because the overall concentration of $ABTS^{\bullet+}$ is low. The blue colour in the HRP region decreases again because once the production of $ABTS^{\bullet+}$ slows or halts (due to depletion of ABTS) the region reaches equilibrium with the bulk. Purple colouration of the colloidosomes is clearly seen early in the reaction, mostly at the GOx/ HRP interface. Again, over time this covers the whole hydrogel. The purple colouration on the colloidosomes is clearer in this case than the dry gel due to the reduced colour from $ABTS^{\bullet+}$.

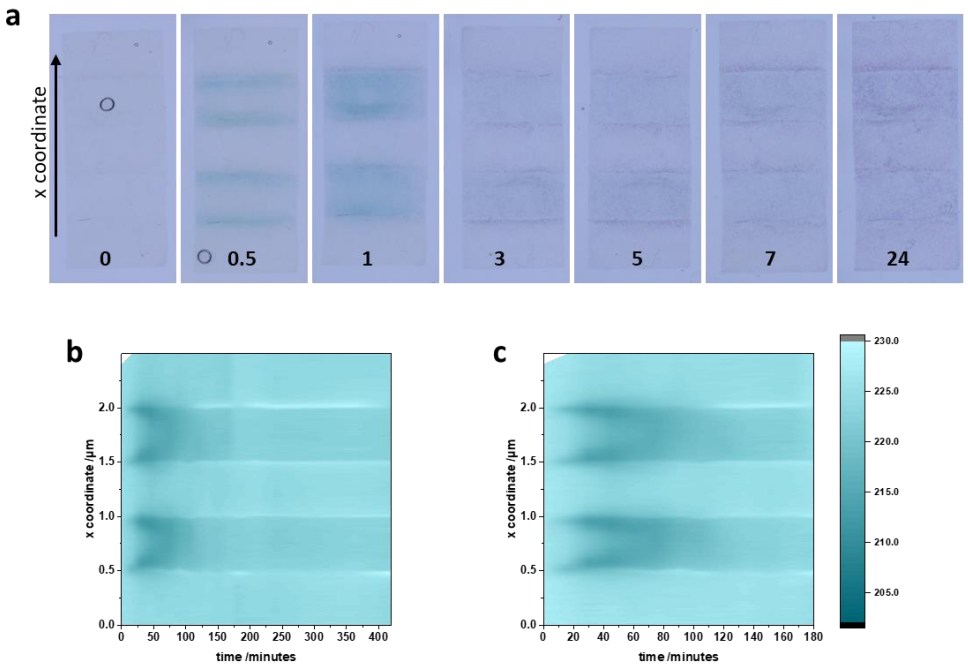

FIGURE 4.21. A composite hydrogel was formed from GOx colloidosome pieces and HRP colloidosome pieces in the pattern described as GHGHG (see Figure 4.13 for scheme) pieces (both 100 μL of each per 200 μL hydrogel) . (a) Photographs taken of the composite hydrogel (roughly 2.5 cm x 1 cm) over time it was added to a solution of 0.5 mM glucose. The time lapsed is indicated at the bottom of each photograph in hours. (b) and (c) Contour plots of the hue angle over time, with the x coordinate along which the measurements were taken, marked on the photographs in (a). (c) presents the same data as (b) but over a shorter timescale to allow more detail to be seen. A contour plot of the saturation is shown in Figure A.12. The colour (a) and increase in hue (b and c) that are indicative of $ABTS^{\bullet+}$ initially appear at the interface of the GOx and HRP sections, and spread more quickly within the regions of the hydrogel that contain HRP colloidosomes than the regions that contain GOx colloidosomes, resulting in nonsymmetrical gradients around the interfaces. The initial appearance of $ABTS^{\bullet+}$ in patterns fades between one and three hours: the colour (a) and hue (b and c) decrease throughout the hydrogel as the $ABTS^{\bullet+}$ spreads throughout the whole solution rather than remaining in the hydrogel.

Embedding colloidosomes within a hydrogel creates a 3D organisation; this can be used to extend the patterning and gradient formation shown here into 3D, which cannot be easily achieved in suspension. As proof of concept, 3D patterns of colloidosomes were created within the hydrogel using the same composite hydrogel method was used as for the pseudo 2D gels, with individual pieces being joined via alginate crosslinking. Composite hydrogels were equilibrated with ABTS solution overnight before being placed into a solution of 5 mM glucose. To capture the 3D development of $ABTS^{\bullet+}$ patterns hydrogels were imaged from above and from the side using a two-camera set up (Figure 2.7).

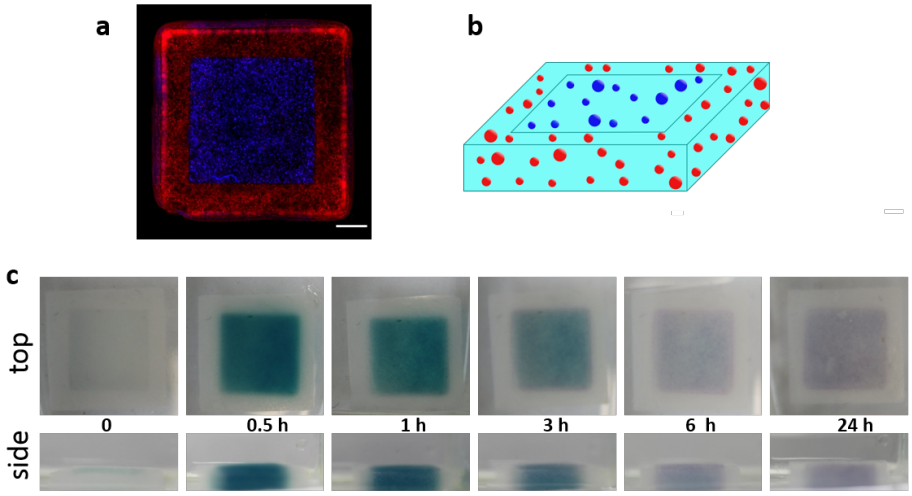

FIGURE 4.22. A fluorescence microscopy image (a) and schematic (b) of a 3D composite hydrogel formed from a HRP colloidosome piece (1 x 1 x 0.4 cm) within a GOx colloidosome piece (1.5 x 1.5 x 0.4 cm) (both 100 μL of each per 200 μL hydrogel). For imaging fluorescently labelled BSA was included in the colloidosome aqueous phase with the relevant enzyme (GOx colloidosomes contained RITC-BSA (red) and HRP colloidosomes contained DL650-BSA (blue)). In (a) the scale bar represents 2.5 mm. In the schematic (b) GOx colloidosomes are shown as red and HRP as blue. (c) is a series of photographs taken of the composite hydrogel after it was added to a solution of 5 mM glucose. Photographs are shown from above and from the side as labelled. The time lapsed is indicated. The photos in (c) show that blue/ green colour appears rapidly throughout the HRP region of the hydrogel after it is placed into the glucose solution. Once production of $ABTS^{\bullet+}$ slows the colour of the HRP region fades because $ABTS^{\bullet+}$ diffuses throughout the whole solution.

A simple composite hydrogel (Figure 4.22) was run to test the 3D patterning. Blue/ green colour appears rapidly throughout the HRP region of the hydrogel. The concentration of glucose

used in these experiments (5 mM) was higher than the pseudo 2D experiments and thus excess H_2O_2 is rapidly produced and diffuses through the HRP region, resulting in colouration of the whole region at once rather than initial intensity at the GOx/ HRP interface. Again, after the initial increase, the colour of the HRP region slowly disappears as $ABTS^{\bullet+}$ formation halts. Once again, the purple colouration on the colloidosomes remains, showing that heterogeneous colloidosome hydrogels can be used for both transient and permanent chemical patterning in 3D.

A more complex pattern is shown in Figure 4.23. The two pieces of HRP hydrogel are positioned at different heights within the GOx containing bulk. Initially the colouration of $ABTS^{\bullet+}$ is seen at the edges of the HRP pieces closest to the solution, as can be seen by the side on image. H_2O_2 produced in the GOx hydrogel can rapidly diffuse through solution. Sections of the HRP hydrogel in which H_2O_2 must diffuse further through the hydrogel matrix become coloured later. Although the overall region where $ABTS^{\bullet+}$ production is eventually seen is controlled by the distribution of the colloidosomes, the point at which the reaction occurs first is, in this case, controlled by the diffusion of the initial substrate. This should be taken into account for such 3D patterning but could be used to add additional complexity to the chemical gradients and patterns formed.

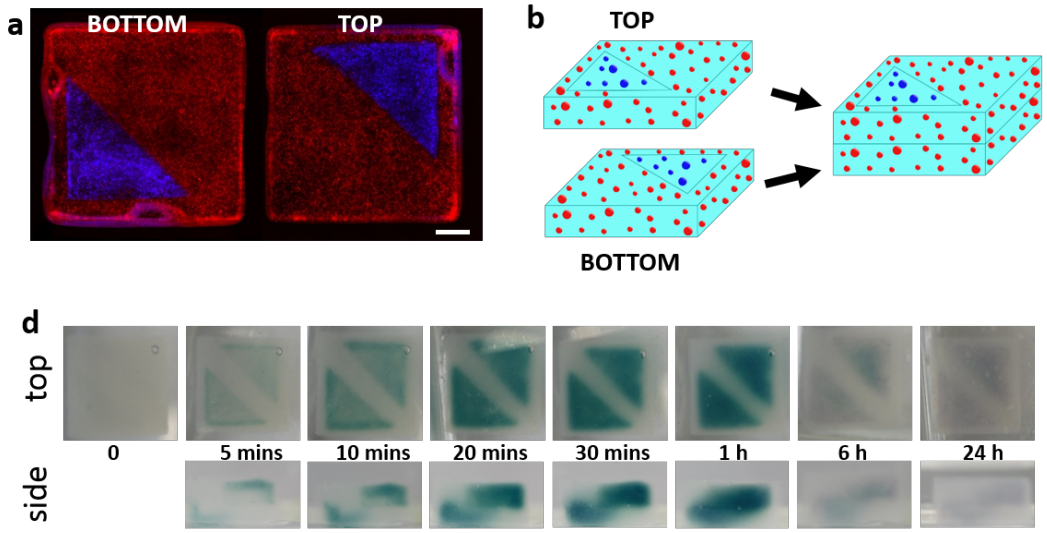

FIGURE 4.23. Fluorescence microscopy images (a) and schematic (b) of a 3D composite hydrogel formed from a HRP colloidosome piece within a GOx colloidosome piece (1.5 x 1.5 x 0.4 cm) (both 100 μL of each per 200 μL hydrogel). Two pieces were combined to give the 3D structure shown in the schematic, and the two individual layers are shown separately in the microscope images (labelled top and bottom). For imaging fluorescently labelled BSA was included in the colloidosome aqueous phase with the relevant enzyme (GOx colloidosomes contained RITC-BSA (red) and HRP colloidosomes contained DL650-BSA (blue)). In (a) the scale bar represents 2.5 mm. In the schematic (b) GOx colloidosomes are shown as red and HRP as blue. (c) is a series of photographs taken of the composite hydrogel after it was added to a solution of 5 mM glucose. Photographs are shown from above and from the side as labelled. The time lapsed is indicated in minutes or hours. The side on photos in (c) show that initially the colouration of $ABTS^{\bullet+}$ is seen at the sections of the interface between the GOx regions and the HRP regions that are closest to the bulk solution. Sections of the HRP hydrogel in which H_2O_2 must diffuse further through the hydrogel matrix become coloured later. Once production of $ABTS^{\bullet+}$ slows the colour of the HRP region fades because $ABTS^{\bullet+}$ diffuses throughout the whole solution.

As an example of an intricate 3D shape that could be utilised for reaction patterning in this system, a silicone mould was used to form a GOx/HRP hydrogel in the shape of a chess piece Figure 4.24. This was embedded within a hydrogel bulk containing no colloidosomes. When the hydrogel was submerged in glucose solution the blue/ green $ABTS^{\bullet+}$ colouration appeared in the

shape of the chess piece. The colour initially appeared at the base of the hydrogel, since here the colloidosome piece is in contact with the solution but over time the 3D structure of the pawn can be seen as coloured. A gradient of $ABTS^{\bullet+}$ can be seen around the chess piece from roughly 2 hours onwards. Due to the large size of the hydrogel, not all the $ABTS^{\bullet+}$ produced will rapidly move into solution. Hence the gradient is seen within the bulk. This proves that complex patterns can be used to generate gradients in different shapes using composite hydrogels.

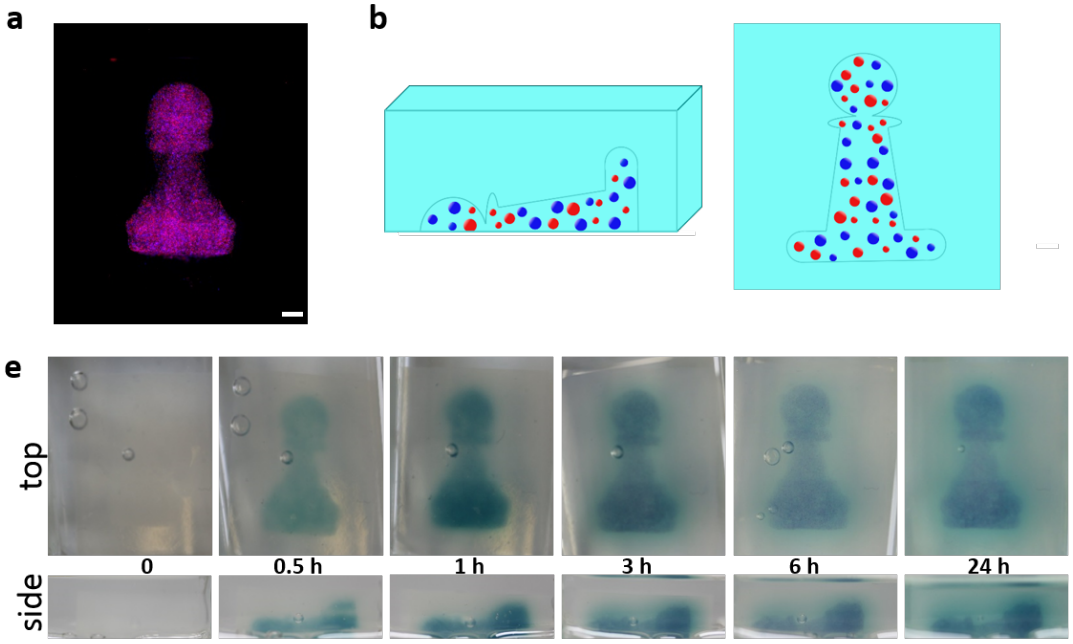

FIGURE 4.24. A fluorescence microscopy image (a) and schematic (b) of a 3D composite hydrogel formed from a piece with mixed population (GOx/HRP, 50 μL of each per 200 μL hydrogel) in the shape of a chess piece within a plain hydrogel (buffer only). For imaging fluorescently labelled BSA was included in the colloidosome aqueous phase with the relevant enzyme (GOx colloidosomes contained RITC-BSA (red) and HRP colloidosomes contained DL650-BSA (blue)). In (a) the scale bar represents 2.5 mm. In the schematic (b) GOx colloidosomes are shown as red and HRP as blue. (c) is a series of photographs taken of the composite hydrogel after it was added to a solution of 5 mM glucose. Photographs are shown from above and from the side as labelled. The time lapsed is indicated in minutes or hours. The photos in (c) show that initially the colouration of $ABTS^{\bullet+}$ is seen at the base of the hydrogel, and as time progresses and $ABTS^{\bullet+}$ is produced further into the colloidosomes containing region the 3D structure of the pawn can be seen.

4.3.3.3 Transient chemical patterning using fluorogenic substrates

Section 4.3.2 showed that HRP colloidosomes can generate the fluorescent product DAP from the non-fluorescent substrate *o*PD. This substrate could also be used in patterning experiments like those in Section 4.3.3.2. Composite gels were formed with *o*PD (0.1 mM) included in the pre-gel mixture and all gelation and compilation steps were carried out in the fridge and in the dark to reduce the oxidation of *o*PD prior to addition of the substrate. A source hydrogel containing glucose (1 mM) was placed on top of the composite hydrogel to initiate the reaction and the assembly imaged on a fluorescence microscope every two minutes to monitor production of DAP (using the tile scan feature). Figure 4.25 shows composite hydrogels with two different patterns run in this way. As with the ABTS patterned reactions, hydrogels in which the colloidosomes are co-localised in regions of the hydrogel between regions that contain no colloidosomnes (Figure 4.25a), show initial product formation across the region with mixed population. The product then begins to diffuse outward through the plain hydrogel stripes creating a chemical gradient of DAP. This spread appears to occur much faster than similar experiments run with ABTS. In the colloidosome containing regions of the hydrogels fluorescence is patchy across the gel because it appears to be associated more with the colloidosomes than the external matrix. DAP is positively charged and so can be expected to adsorb onto the silica of the colloidosomes.

Figure 4.25b shows that with composite hydrogels formed with spatially seperated GOx and HRP colloidosome populations, DAP is initially produced at the interface of the two populations. Chemical gradients are set up like those with ABTS, and eventually the whole hydrogel shows green fluorescence green. The spread into the GOx regions is far more rapid than in the ABTS experiments, with the whole gel being roughly homogeneous in DAP levels after just 50 minutes. This indicates that different substrates can be patterned within the hydrogel matrix but that the development and spread of chemical gradients varies with the nature of the substrate. The reaction of *o*PD with H_2O_2 catalysed by HRP is known to occur more rapidly than the reaction of ABTS. Furthermore, as is discussed in Chapter 1, diffusion within a hydrogel is complex and relies on a variety of factors; the relative rate of patterning spread may also be due to differences in diffusion rate. Although DAP is positively charged (where $ABTS^{\bullet+}$ is negatively charged) and so might be expected to show a stronger interaction with the alginate matrix as well as the silica colloidosomes, it is also smaller than $ABTS^{\bullet+}$ (DAP Mw= 210.24 g mol^{-1}, $ABTS^{\bullet+}$ Mw = 516 g mol^{-1}) which could lead to faster diffusion.

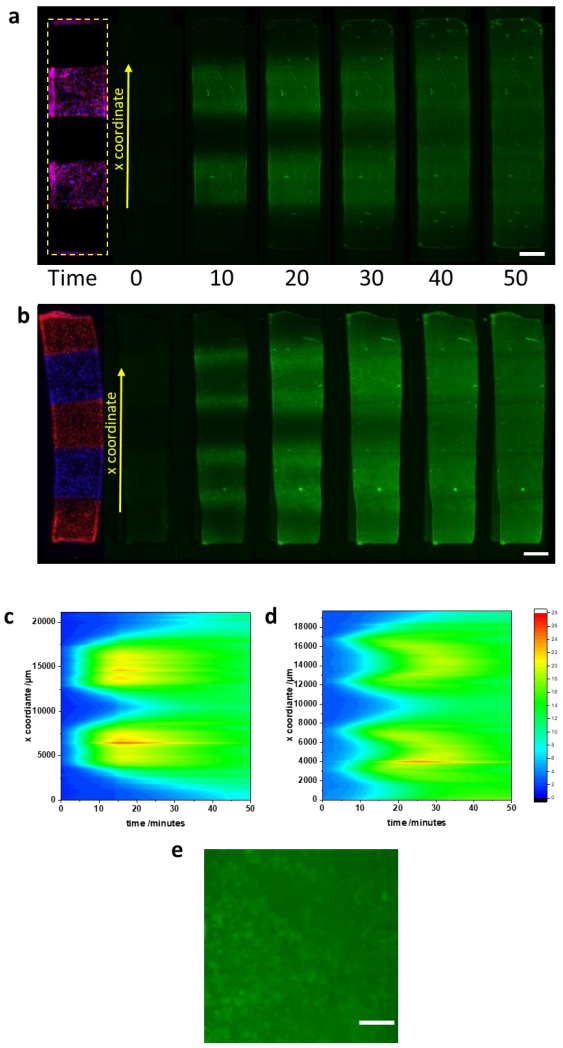

FIGURE 4.25. (a) and (b) are fluorescence microscopy images of *o*PD containing composite hydrogels taken over time (time in marked in minutes). The first image in each series shows the distribution of colloidosomes. For imaging fluorescently labelled BSA was included in the colloidosome aqueous phase with the relevant enzyme (GOx colloidosomes contained RITC-BSA (red) and HRP colloidosomes contained DL650-BSA (blue)). Pink colouration appears where both colloidosome populations are present. The hydrogel in (a) was formed from pieces with mixed colloidosome population (GOx/HRP, 50 μL of each per 200 μL hydrogel) and pieces of plain hydrogel (buffer only) and shows a similar pattern to the ABTS hydrogel in Figure 4.13. The hydrogel in (b) was formed from GOx colloidosome pieces and HRP colloidosome pieces (both 100μL of each per 200μL hydrogel) in a pattern similar to that used for ABTS reactions in Figure 4.15. All hydrogels are approximately 2.5 x 0.5 x 0.1 cm in dimension and the scale bar represents 2.5 mm and in (a) the yellow line represents the edge of the hydrogel. (c) and (d) are contour plots showing the fluorescence intensity across the hydrogels ((a) and (b) respectively) over time, with the x coordinate along which the measurements were taken, marked on the fluorescence microscopy images and photographs in (a) and (b). (e) is a zoomed n image of the hydrogel in (b) after reaction with glucose, scale bar 500μm.

Imaging development of patterns and gradients with the hydrogels using a fluorescent product rather than the colorimetric product of ABTS may in some ways seem preferential. Fluorescence can be easily measured and correlated to chemical concentration within the matrix. Several problems arise that make the application of the *o*PD/ DAP system to this end difficult. At the *o*PD concentration used the fluorescence intensity is low and images must be significantly enhanced to see the patterns emerging by eye. Higher concentrations of *o*PD lead to strange anomalies in the fluorescence; a speckled pattern often merged which is hypothesised to correlate to precipitation of DAP within the matrix and the interfaces of the compiled pieces became very dark over time. Looking at these gels by eye showed that these interface regions in fact showed the greatest colouration implying the greatest concentration of product, and thus possibly precipitation or quenching was leading to lack of fluorescence in the microscope image. Furthermore, *o*PD is a more light-sensitive substrate than ABTS and sometimes hydrogels showed fluorescence prior to being added to the source hydrogel. Over time some fluorescence also began to emerge in control gels (source containing no glucose) due to the irradiation during the imaging process. Although over 50 minutes this level was fairly low, it proved more of a problem in longer experiments, since the appearance of background fluoresce made it hard to track the spread of slow diffusing patterns. When trying to expand the patterning to different arrangements and shapes, larger gels could not easily be imaged on the microscope: the larger the hydrogel the longer each tile scan takes; and at a certain point the first image of the tile scan is taken so long before the latter ones that the compiled image does not give an accurate representation of the hydrogel at a certain time. Using a lower magnification lens (x2.5) reduces the fluorescence intensity and this is already very low for this system.

4.4 Conclusions and future work

In this chapter, a method for embedding colloidosomes within hydrogels to create rudimentary prototissues was outlined. The hydrogel here is acting as mimic of the extracellular matrix, a technique that is regularly used in tissue engineering. Embedding colloidosomes within agarose or agarose-alginate IPN hydrogels had no effect on the size or shape of the colloidosomes, and the agarose-colloidosome hydrogels still showed hydrogel-like mechanical properties. To fully understand the changes to the mechanical properties that come with immobilising colloidosomes in the agaorse hydrogels, further mechanical testing, including SAOS frequency sweeps, should be carried out in the future. Colloidosomes distributed evenly through the hydrogels meaning that this technique allows us to create 3D arrays of the capsules, in a way that is not possible in suspension.

HRP colloidosomes retained their enzymatic function within the hydrogels, and binary colloidosome populations, containing GOx and HRP, could carry out a cascade reaction within the hydrogel thus performing a rudimentary form of chemical communication. Communication, both between the constituent parts and with the external environment, is a key feature of a tissue and so these results indicate that colloidosome hydrogels are a good model for moving towards a prototissue.

To begin to replicate the heterogeneity within living tissues, and thus increase the complexity of the prototissue model, IPN hydrogels of agarose and alginate were formed. The modular system allowed the spatial segregation of different colloidosome populations and therefore of the proteins within them, without the use of complex techniques. The protein patterning persists over time since the colloidosomes are too large to move through the hydrogel matrix. Including enzymes within the different colloidosome populations allowed patterning of different enzyme functionalities within the hydrogel. Uniform application of glucose to such composite prototissues resulted in patterned production of a coloured substrate. The reaction product can diffuse through the hydrogel matrix, and thus the patterning is transient. Chemical gradients of the coloured species occur across the hydrogel, originating from the designed pattern, and over time the system reaches equilibrium with equal distribution of the product. The pattern, and its development over time can be pre-programmed by altering the distribution or number of colloidosomes within the material, as well as the substrate concentration.

Taking advantage of the 3D nature of the colloidosome distribution within the hydrogel matrix, the reaction patterning was also extended to 3D. Soluble gradients in tissues are often formed by the activity of cells in certain locations and thus the work described here is a novel method for the in situ formation of pre-programmed chemical gradients within hydrogels by mimicking the behaviour of living tissues. The patterns that appear rely on communication between protocell populations and interaction with the environment, and are an emergent property of the colloidosome hydrogel prototissues. Future work could increase the complexity of the system by including multiple enzyme cascades or systems that utilise feedback loops.

Although in some cases it has been shown that enzymes can be isolated in a hydrogel simply by including them in the initial solution and that they do not diffuse through the matrix, this is usually not the case. In this chapter it was demonstrated that the enzymes used could diffuse through the hydrogel and that in patterned systems this eventually resulted in loss of the patterning. Trapping enzymes within colloidosomes prior to hydrogel formation prevented this leaching. This result thus opens the door to utilise this type of reaction patterning with a variety of enzymes and hydrogels in which diffusion of free enzyme would otherwise be prohibitive. In the future a variety of different enzymes or hydrogels could be used to engineer systems to show non-uniform response to different stimuli, with different chemicals or molecules being patterned. Immobilisation of enzymes in hydrogels is also used in the formation of biocatalysts and biosensors with a variety of strategies being used to prevent enzyme leaching [91, 92]. The method developed in this chapter could provide a simple alternative, which does not rely on covalent functionalisation of the enzyme and successfully retains enzymes within the hydrogel.

To increase the complexity of the prototissue systems described here patterning techniques could be used to order protocells within the hydrogel on micrometre scale. This could be used in conjunction with the modular system used to create macroscopic patterns resulting in more complex, heterogeneous architectures that would then exhibit more complex reaction patterning and chemical gradients. Such control could be achieved using 3D printing or acoustic patterning.

Future work may also want to build on the studies here and use other membrane bound protocell models in the formation of hydrogel prototissues. As discussed in Chapter 1, different protocells that have been developed have various properties that could be used to tune the prototissue for the desired function. As an initial step towards this, preliminary studies were carried out on the encapsulation of proteinosomes within agarose hydrogels (Figure 4.26). Proteinosomes have a flexible, porous membrane formed from crosslinked protein-polymer nanoconjugates. Embedding proteinosomes within agarose caused them to collapse, presumably because the agarose solution causes an osmotic shock to the capsule. To counteract the osmotic pressure proteinosomes were formed with various polymers encapsulated inside. Interaction between the encapsulated polymers and the protein-polymer nanoconjugate used to form the proteinosome in some cases caused significant aggregation inside, deformation of the structure or increased internal fluorescence intensity (resulting in a less obviously visible membrane) and did not always prevent the collapse. Proteinosomes formed with high BSA (unfunctionalized, not part of a nanoconjugate) or carboxymethyl dextran inside were successfully encapsulated in agarose hydrogels without loss of structure, indicating that these systems show promise for future work building proteinosome-hydrogel prototissues.

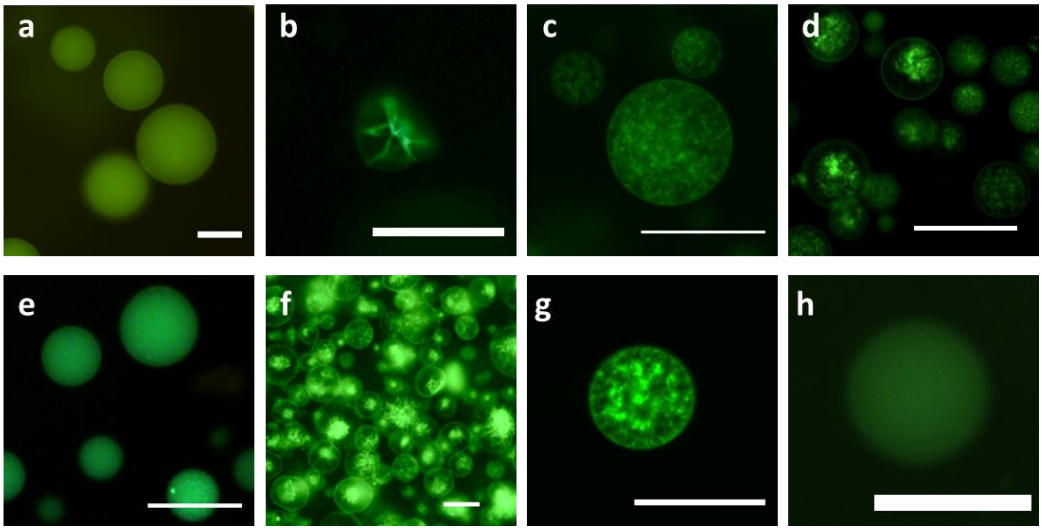

FIGURE 4.26. Fluorescence microscopy images of proteinosomes formed using protein polymer nanoconjugate with FITC-BSA. Proteinosomes formed using the previously reported method [6] after transfer to water (a) and after encapsulation in 1% w/v agarose hydrogels, showing the collapse due to hydrogel encapsulation. Proteinosomes were formed with (c) 17 mg/mL dextran, (d) 60 mg/mL cm-dextran, (e) 17 mg/mL BSA and 5 mg/ mL alginate in the aqueous phase and images were taken after crosslinking and transfer to water. Upon encapsulation in agarose hydrogels cm-dextran (g) and BSA (h) containing colloidosomes showed retention of spherical structure. Scale bars 50 μm.

Gradient hydrogels (or gradients of soluble chemicals within hydrogels) are of interest in tissue engineering; colloidosomes could be used to create heterogeneity and in situ gradients in preprogramed patterns in hydrogels for this purpose. Colloidosomes are too large to be endocytosed by cells and would therefore protect material inside them from engulfment and destruction, allowing the function to continue; they could be used to encapsulate different enzyme or protein systems and thus create gradients of molecules that are used in tissue engineering. Furthermore, patterning of the colloidosomes themselves could be used to create heterogeneous environments, without necessarily utilising encapsulated enzymes. For example, silica is osteogenic, so patterning silica colloidosomes may create heterogeneous cell differentiation.

CHAPTER 5

CHEMO-MECHANICAL TRANSDUCTION IN HYDROGEL-COLLOIDOSOME PROTOTISSUES

5.1 Chapter outline

The aim of this Chapter was to create a prototissue that exhibits chemo-mechanical transduction upon addition of chemical fuels, through the collective behaviour of the component parts. The Chapter first outlines the development of pH changing colloidosome protocells, formed with antagonistic enzymes, and then presents the synthesis and characterisation of a novel, pH-responsive hydrogel bilayer through the photogelation of methacrylated polysacharides. These components are then combined to form the actuating prototissue, and protocell-mediated chemo-mechanical transduciton and out-of-equilibrium behaviour demonstrated.

5.2 Introduction

5.2.1 Actuation and movement

Actuating materials are those that can change shape, moving themselves or their surroundings [168]. Such materials (or tissues) are common within nature, and they often exhibit drastic structural changes under mild conditions and in response to external stimuli [168, 169]. Actuation in nature occurs via a variety of mechanisms. In animals, muscle tissue is a natural actuator and key to its function is the hierarchical, fibrous structure. The presence of calcium ions causes macroscopic contraction [168] through an active process that requires the presence of ATP. Actuation in plants tends to be a passive, swelling based process. This is caused by anisotropic changes in volume where non-uniform structure in the plant lead to differences in water absorption when conditions such as moisture or humidity change [168–170]. For example,

within the scales of a pinecone there is variation in the orientation of cellulose microfibrils within the cell walls. This means that when the humidity changes the cells on the outside of the scale elongate more than those on the inside, resulting in opening or closing of the scales [168].

Actuation in nature occurs through a great variety of elegant mechanisms, but one ubiquitous feature of natural shape changing materials is anisotropy.

5.2.2 Synthetic actuating hydrogels

Researchers working on the design of actuating materials can learn a lot by looking at natural examples, and biomimetic synthetic actuators have been formed from a variety of materials, including hydrogels. Hydrogel actuators are capable of programmed shape changes or mechanical work, and due to the unique properties of hydrogels (Section 1.2) they are of interest in fields such as soft robotics, drug delivery and tissue engineering [59]. Hydrogel actuation is an example of *chemo-mechanical transduction* (the interconversion of chemical and mechanical energy) [171], and thus it can be used to perform work upon application of a stimuli, such as gripping an object [59].

Since anisotropy is a prerequisite in natural soft actuators, it is evident that in hydrogel actuators, anisotropy of the stimuli or the structure is essential [168]. Uniform application of a stimuli to a uniform, responsive hydrogel results in swelling of the whole gel rather than deformation [169]. Like plant tissues, hydrogels actuators are deformed due to asymmetric swelling driven by the uptake or release of water [169, 170].

Physical stimuli such as magnetism or light can be applied anisotropically to cause actuation. However, in many cases this is difficult because stimuli such as temperature or chemical species can transfer through the hydrogel or surrounding solution rather than being isolated in the region to which they are applied. In such cases heterogeneity must instead be built into the material itself to allow actuation [168] . Various approaches can be found in the literature to this anisotropy in hydrogel actuators, including restricting swelling of the material in one direction [168, 169, 172] or creating gradients in properties such as crosslinking, porosity or embedded particles within the hydrogel to produce asymmetric swelling when a stimulus is applied [168, 169]. Alternatively, a bilayer structure can be produced by joining two distinct hydrogel layers that show differing swelling responses [168, 170] such that application of a stimulus causes asymmetry in the swelling of the two layers resulting in a change in shape [170]. Bilayer actuators can be designed with one responsive layer and one inert layer [173, 174] but often to produce bi-directional bending, two layers with opposite response to a stimulus are combined [59]. More complex deformations can be induced by forming the bilayer hydrogel in different geometries, via moulding, photopatterning, assembly of different pieces [173], or introducing dissymmetric shapes [59, 170, 173].

The many stimuli to which hydrogels can be designed to respond were discussed in Section 1.2.7.Utilising those affordances, hydrogel actuators have been designed to respond directly to a

range of stimuli such as pH [173], temperature [172], light [175]), electric current [176]. To create a pH responsive hydrogel bilayer, anionic and cationic hydrogels are used [59, 174]. The change in bending of pH responsive hydrogel bilayers depends on the pK_a of the responsive materials [59, 174], the structure of the hydrogels [59, 174] and extent of crosslinking, number of cation or anionic groups and the size [59, 174] of the hydrogel.

Many of the hydrogel actuators discussed above can be cycled repeatedly through the different states by alternating the stimuli or switching a stimulus on and off [59, 172, 175]. The discussion in Section 1.2.7.7 introduced examples of hydrogel systems that exhibited complex swelling or sol-gel behaviours, such as autonomous behaviour, spatio-temporal patterning or oscillations. For future applications of hydrogel actuators it is interesting to look at ways in which such behaviours could be introduced in actuation, for example to achieve alternating motions without the need for repeated external input. Examples of hydrogel actuators that have achieved this have used living cardiac cells, which undergo repeated cycles of simultaneous contraction and relaxation [177], or the oscillatory BZ reaction (see Section 1.2.7.7) [124]. Another elegant example is seen in one iteration of the SMARTS (self-regulated mechanochemical adaptively reconfigurable tuneable system) platform created by the Aizenberg lab [171]. When the hydrogel actuator were submerged in a cleverly designed liquid bilayer, they were capable of repeated cycles of chemo-mechanical and mechano-chemical transfer through self- regulating feedback loops. Aside from the few examples discussed here, chemo-mechanical transduction in hydrogels tends to be very simple: the applied stimulus causes a change in the most thermodynamically stable state and the system changes shape until it reaches the new equilibrium.

5.2.3 Designing a prototissue for chemo-mechanical transduction

As discussed in sections 5.2.1 and 5.2.2, a plethora of actuating hydrogels responding to different stimuli can be found in the literature and other than a few key examples, these actuators respond directly to an externally applied stimulus, changing shape until they reach equilibrium. In contrast, the work presented in this chapter aims to create a hydrogel actuator that responds indirectly to the applied stimulus, relying on chemical reactions in the hydrogel itself to link the applied stimulus to the chemo-mechanical transduction. Since the chemical species that induce actuation are produced within the hydrogel matrix, it was hypothesized that such a system would exhibit novel properties. In particular, manipulation of the kinetics of the reactions linking the stimulus to the actuation could be used to create more complex forms of motion than the standard move towards equilibrium.

To achieve this goal the system designed was an actuating prototissue, formed from inorganic protocells within a hydrogel matrix. To link biochemical reactions within the enzyme-loaded protocells to the actuation of the hydrogel, their reaction must result in a change in some condition to which the hydrogel is sensitive. It has previously been shown that as they turn over their substrates, some enzymes can cause changes in pH [120, 178] and hydrogels can be designed to

respond to changes in pH. Based on this, enzymatic pH change within a pH responsive hydrogel bilayer was chosen as the mechanism for converting chemical to mechanical energy. The design was based around two colloidosome populations formed using antagonistic, pH changing enzymes because, as discussed in Section 1.2.7.7, manipulating the kinetics of two antagonistic reactions allows the formation of transient pH states [125]. When applied to an actuating hydrogel we hypothesised that this would allow temporal patterning of the chemo-mechanical transduction, with one substrate addition leading to a transient change in shape (a back and forth (A->B->A) motion). The design of the prototissue, which should exhibit chemo-mechanical transduction due to the collective behaviour of the component parts, is shown in the scheme in Figure 5.1.

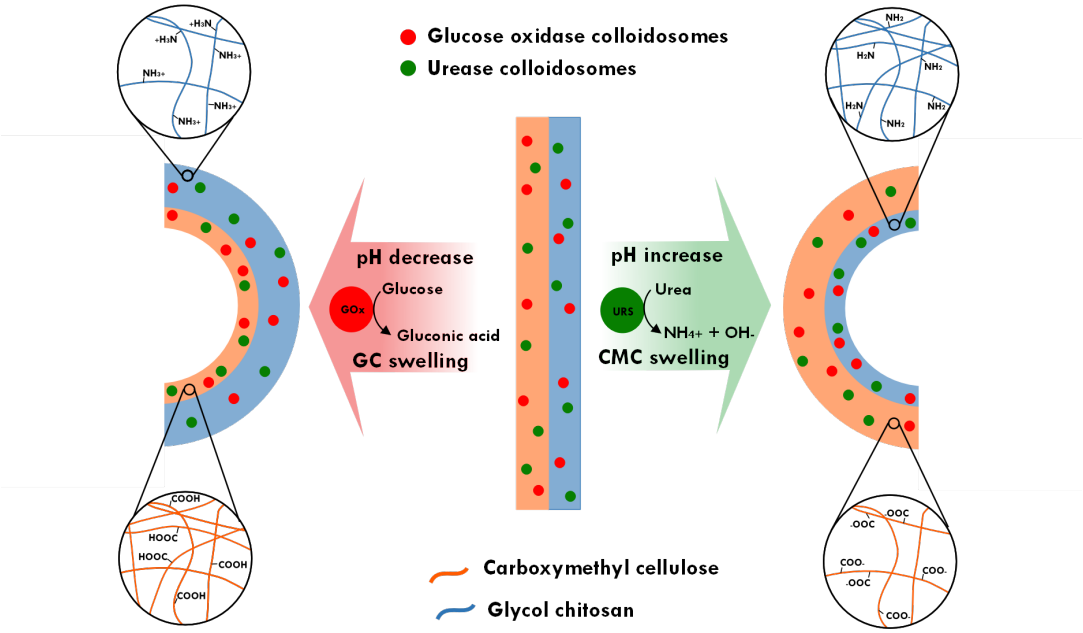

FIGURE 5.1. A schematic of the hydrogel-based prototissue bilayer designed in this project.

5.3 Results and discussion

5.3.1 Formation of pH changing colloidosomes

Earlier in this thesis examples of systems that used antagonistic enzymes to create temporary pH states [125] (Section 1.2.7) were discussed. Similarly, antagonistic enzymes have been used to create a system of self-configurable host guest protocells [178]. The system was based around proteinosomes, containing Glucose oxidase (GOx) and urease (URS), and a solution of pH sensitive fatty acid. GOx oxidises glucose to gluconodeltalacton, which is in equilibrium with gluconic acid and thus, in an unbuffered system, the reaction causes a decrease in pH. In contrast, URS breaks down urea, causing an increase in pH. Taking advantage of this Martin et al used stepwise addition of the two substrates to cause first an increase, and then a decrease in pH. The initial increase in pH caused the pH responsive fatty acid to form coacervates, which captured the proteinosomes. When the pH fell again the system was reconfigured causing the release of the proteinosomes and the formation of fatty acid vesicles in the proteinosome interior.

To create such behaviour in a hydrogel prototissue, two populations of colloidosome protocells were formed. Each population contained one of a pair of antagonistic, pH changing enzymes: GOx which turns over its substrate to cause a pH decrease (Figure 5.2d), and URS which turns over its substrate to cause a pH increase (Figure 5.3d). This initial section of work lays out the development and characterisation of the pH changing colloidosomes.

As discussed in Chapters 3 and 4, the composition and pH of the aqueous phase upon colloidosome formation affects the structure of the colloidosome and the resulting enzymatic activity of encapsulated species. Based on this the pH and conditions of formation were refined individually for both URS and GOx colloidosomes and the discussion is shown in Appendix AA.3. GOx colloidosomes were formed at pH 4 and 2270 U/mL (as in Chapter 4) and crosslinked with 15 to 20 μL TMOS. When colloidosomes were initially formed they appeared yellow due to the high concentration of the enzyme, but after transfer to water the colour was noticeably less strong indicating some protein may be lost during the transfer. Bright field microscopy images (Figure 5.2a) of GOx colloidosomes formed under these conditions showed that they were spherical, and the membrane appears dark and speckled. Colloidosomes were formed using FITC-GOx and imaged using fluorescence microscopy after transfer to water (Figure 5.2b). The enzyme is retained within the colloidosome, with higher concentrations seen at the membrane compared to the lumen, likely due to a strong interaction with the silica nanoparticles upon emulsion formation. An SEM image of lyophilised GOx colloidosomes is shown in Figure 5.2c. The colloidosome exhibited the elongated shape seen in previous samples (Chapter 3), indicating a similar internal structure to the colloidosomes formed using low pH BSA solutions. Interestingly the spots in the membrane that are visible in the bright field microscopy are also seen clearly in the SEM images.

GOx enzymatic activity shows a bell-shaped pH dependence, with an optimal pH of roughly

5.6 and activity over a wide pH range [178, 179]. Since the oxidation of glucose by GOx results in a decrease in pH, the enzyme activity will be altered during the reaction resulting in positive or negative feedback effects, as has been seen for other systems [125] (discussed in Section 1.2.7). To investigate the pH changing capabilities of the GOx colloidosomes a suspension in 1 mM acetate was adjusted to pH 8.5 and the pH was monitored after the addition of glucose (initial concentration 100 mM). As shown in Figure 5.2e the solution pH drops due to the GOx activity. After 12 hours the average pH of the solution (across three runs) was 3.7 ± 0.2. The pH decrease slows when the pH is more acidic, due to substrate depletion and lower enzyme activity in this pH region. Even after 15 hours the solution pH is still dropping, albeit slowly. Some repeats of the pH decrease using GOx colloidosomes showed buffering at intermediate pHs. Control experiments where glucose was added to a suspension of plain colloidosomes (without GOx) or GOx colloidosomes were monitored without the addition of glucose, showed no significant decrease in pH.

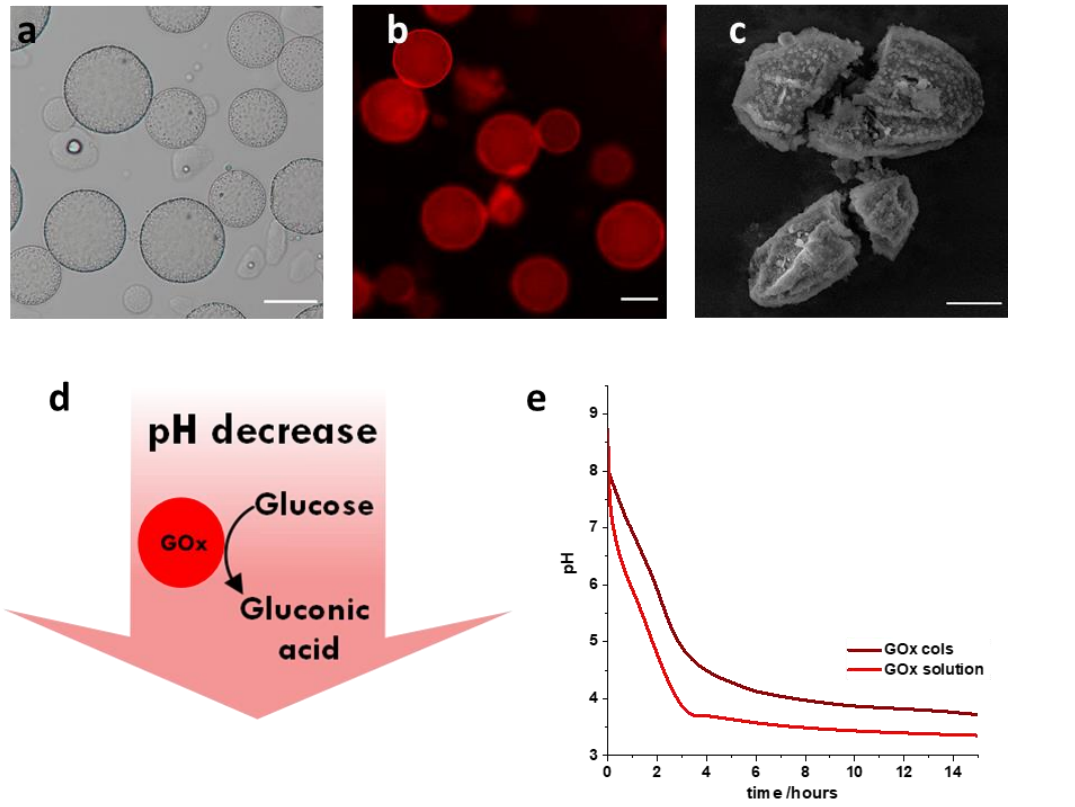

FIGURE 5.2. (a) Bright field and (b) fluorescence microscopy images of GOx colloidosomes and FITC-GOx colloidosomes respectively (scale bars 50 μm). (c) is a scanning electron miscopy image of broken GOx colloidosomes (scale bar 20 μm). (d) is a schematic showing the oxidation of glucose by GOx colloidosomes, resulting in a pH decrease. (e) is a plot of the pH change after addition of 100 mM glucose to a population of GOx colloidosomes or a solution of free GOx at the same theoretical enzyme concentration.

The rate of pH decrease using GOx colloidosomes is slow compared to the same theoretical enzyme concentration free in solution (Figure 5.2). This may be due to some aspect of the encapsulation reducing the enzyme efficiency, but it could also be due to loss of some protein during the transfer of the colloidosomes to water, which would mean the actual enzyme content is lower than the theoretical one. Initial experiments using colloidosomes with lower initial GOx concentrations showed slower pH changes and attempts to create colloidosomes with higher GOx concentrations were unsuccessful. When the GOx concentration was too high no intact colloidosomes were seen after transfer to water indicating that crosslinking had failed.

URS colloidosomes were refined as for the GOx population and for the remainder of this work URS colloidosomes were formed using an initial aqueous solution of 2270 U/mL URS at pH 4.5 and were crosslinked with 15 μL TMOS. A bright field microscopy image of colloidosomes formed using

this method as shown in Figure 5.3a. The colloidosomes were spherical and unbroken and since the pH is similar to that used for the GOx population, the structure of the two populations would be expected to be similar. Storing the colloidosomes in the fridge during crosslinking as for other enzymes caused a decrease in the enzymatic activity and thus for these samples, crosslinking was carried out at room temperature instead. As with GOx colloidosomes, fluorescent labelling of the enzyme prior to colloidosome formation showed that the enzyme is mainly located around the colloidosome membrane (Figure 5.3b). The URS colloidosomes do not show the dark speckled membrane seen for the GOx colloidosomes but aggregation of protein within the colloidosomes could be seen in both bright field and fluorescence images. Tests to reduce aggregation by reducing initial URS concentration also lowered the colloidosome activity and thus the aggregation was determined to be unproblematic. The SEM images of lyophilised URS colloidosomes in Figure 5.3 show deformed elongated structures with wrinkled membranes similar to the images that were seen for BSA colloidosomes formed at low pH, indicating that the internal structure is likely to be a low density porous silica matrix as was seen in Chapter 3.

The breakdown of urea by URS causes an increase in pH (Figure 5.3d) [125]. Like GOx, URS activity shows a bell-shaped pH dependence, although in this case the enzyme activity is seen between pH 4 and 9 and the optimal value is pH 7.1 [180]. Upon addition of 5 mM urea to a suspension of URS colloidosomes at pH 4, the pH rapidly increases, plateauing at a value of roughly pH 9 within 1 hour (Figure 5.3e). Previous systems using the URS/ urea system for pH increases have also reported an upper limit of pH 9, due to the formation of an ammonium buffer [125]. The rate of pH increase was slightly lower than the same theoretical enzyme concentration free in solution, and the free enzyme plateaued at a slightly higher pH.

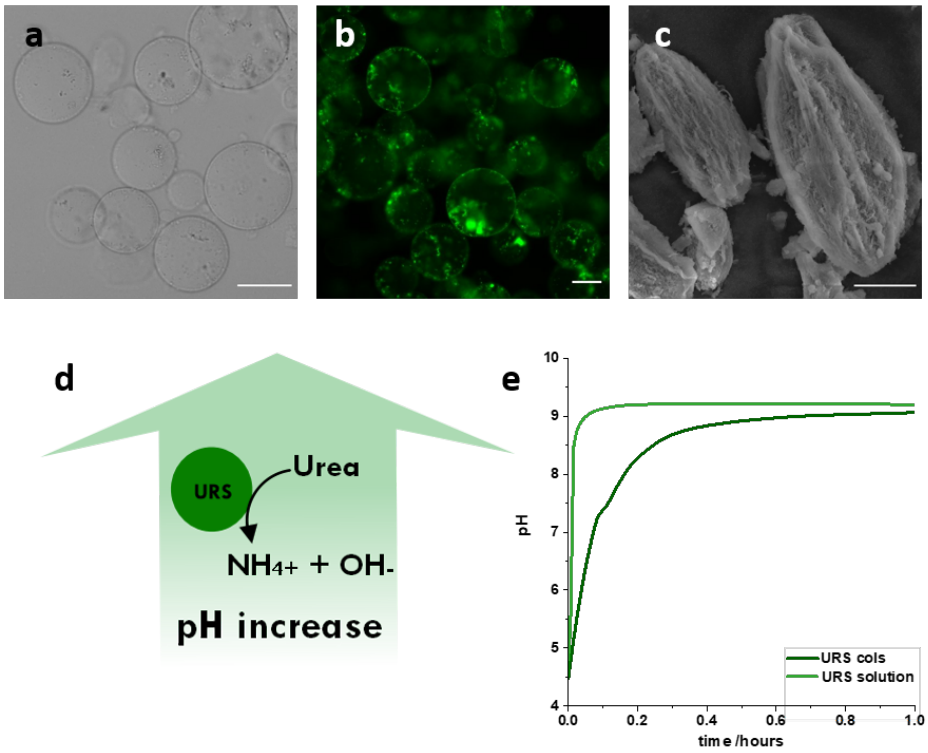

FIGURE 5.3. (a) Bright field and (b) fluorescence microscopy images of URS colloidosomes and DL650-URS colloidosomes respectively (scale bars 50 μm). (c) is a scanning electron microscopy image of URS colloidosomes (scale bar 20 μm). (d) is a schematic showing the breakdown of urea by URS colloidosomes, resulting in a pH decrease. (e) is a plot of the pH change after addition of 5 mM urea to a population of URS colloidosomes or a solution of free URS at the same theoretical enzyme concentration.

One method for creating reversible pH changes using an antagonistic enzyme pair is step-wise addition of the two substrates [178]. However, when there is a difference in the kinetics of the opposing systems, concurrent addition of the two substrates can cause temporary pH changes when the correct substrate ratios are employed. It was predicted that, because of the observed difference in activity between the URS colloidosomes and the GOx colloidosomes, such a result could be achieved by combining the two colloidosome populations with a mixture of glucose and urea. To this end, two suspensions, one containing GOx colloidosomes and urea, and the other URS colloidosomes and glucose, were adjusted to pH 4 and the suspensions were mixed. This mixture contained a one-to-one ratio in the number of colloidosomes and initial concentrations of 100 mM glucose and between 1 and 5 mM urea). After mixing the pH was monitored (Figure 5.4). As predicted, the higher activity of the URS colloidosomes means that despite the excess of glucose compared to urea, the URS/ urea reaction dominates first and the pH increases. The pH increase is less rapid than when only 5 mM urea is added to URS colloidosomes alone because the

slow GOx/glucose system is opposing the change. As the breakdown of urea slows, the production of acidic species from the GOx/ glucose system begins to outweigh the production of basic species, and the pH drops. Experiments carried out using constant initial glucose concentration (100 mM) but varied urea show that changing the substrate ratios affects the timescales and amplitudes of the relative pH states. At higher urea concentrations (5 mM), the pH decrease when the GOx is slow, due to some remaining urea being broken down. Decreasing the urea concentration decreases the amplitude of the initial pH increase but allows for a more rapid decrease meaning that in the timescale studied the pH returns to close to (urea 2.5 mM) or below (urea 1 mM) the starting pH of 4.

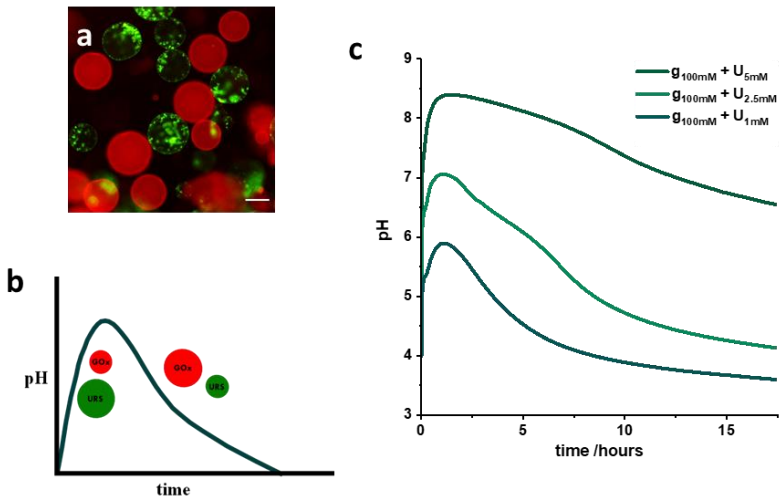

FIGURE 5.4. (a) A fluorescence microscopy image of a mixed population of DL650-URS colloidosomes and FITC-GOx colloidosomes (scale bar 50 μm). (b) A scheme of how the transient pH state is achieved after the addition of a mixture of urea and excess glucose. The URS/ urea reaction dominates initially resulting in a pH increase, but once the urea concentration drops the GOx/glucose reaction dominates and the pH falls. (c) A plot of pH over time after the addition of urea/ glucose mixtures to one-to-one mixture of URS and GOx colloidosomes. The urea and glucose concentrations are indicated in the key.

The successful formation of colloidosome protocells capable of enzyme induced pH increase and decrease that has been demonstrated here is essential to the formation of a pH based prototissue. The differing activities of the antagonistic colloidosome populations allows mixed populations to exhibit transient pH changes when the substrates are added. When included in the final hydrogel based prototissue this should allow reversible, non-equilibrium based motion.

5.3.2 Preparation of pH responsive hydrogel actuators

To form a prototissue that exhibits chemo-mechanical transduction upon addition of urea and glucose, the colloidosome populations described in Section 5.3.1 must be embedded in a pH responsive hydrogel bilayer. In designing the hydrogel bilayer system, several requirements were identified. The method of gelation had to be biocompatible, so that enzyme activity was not destroyed, and rapid, so that colloidosomes did not sink during the process. Additionally, the activity of the colloidosomes limits the pH range that can be used for the system. Based on the pH curves in Figure 5.2 and Figure 5.3 and the enzyme activity seen in the literature, it was determined that a suitable hydrogel must show pH dependant shape changes between pH 4 and pH 9. Systems that require extremes of pH to show significant actuation would not show actuation due to the activity of the enzymes.

With these requirements in mind, a hydrogel bilayer based on the UV induced hydrogelation of two biopolymers was devised. The cationic layer is based on the amine containing polymer glycol chitosan (GC) and the anionic layer on the carboxylic acid containing polymer carboxymethyl cellulose (CMC). The pK_a values for GC and CMC are within the desired pH range indicating that both hydrogels should undergo swelling changes due to the enzyme activity and thus a suitable bilayer could be formed. As discussed in Chapter 1, photogelation can be a rapid method for hydrogel formation which allows the formation of a range of geometries as well as opening up the possibility of photopatterning. Methacrylation of biopolymers has previously been shown to allow their crosslinking using light in the presence of suitable photoinitiations [47, 53, 62, 63] and hence this method was selected for use here. Herein the formation and characterisation of photopolymerised pH sensitive hydrogels and hydrogel bilayers is presented.

5.3.2.1 Synthesis and characterisation of N-methacrylated glycol chitosan

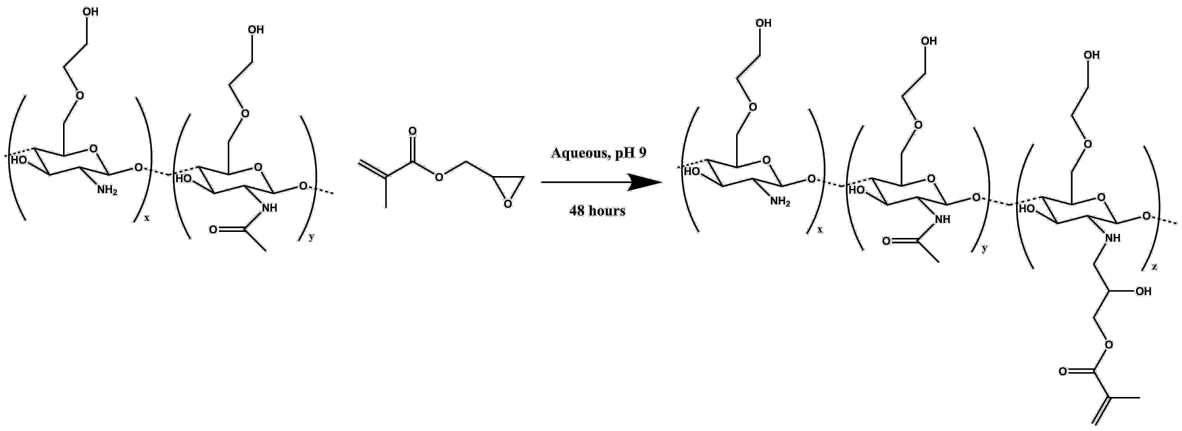

FIGURE 5.5. Reaction scheme for the functionalisation of glycol chitosan with glycidyl methacrylate to produce N-methacrylated glycol chitosan.

N-methacrylated glycol chitosan (GC-M) was synthesised using a procedure adapted from the literature [53]. GC was reacted with glycidyl methacrylate in aqueous solution at pH 9, as shown by the reaction scheme in Figure 5.5. At high pH the amine groups of the chitosan are deprotonated and act as a nucleophile, attacking the epoxide ring of the glycidyl methacrylate. After 48 hours the functionalised polymer was precipitated in acetone before being dissolved in water and dialysed for 24 hours. Precipitate was removed from the solution and it was adjusted to pH 7 using HCl prior to lyophilisation.

Characterisation of the resulting polymer was carried out via FT-IR and NMR. FT-IR of GC and GC-M (Figure 5.6) confirms the introduction of methacrylate onto the polymer backbone via the appearance of a peak at 1710 cm^{-1} corresponding to the C=O of the ester.

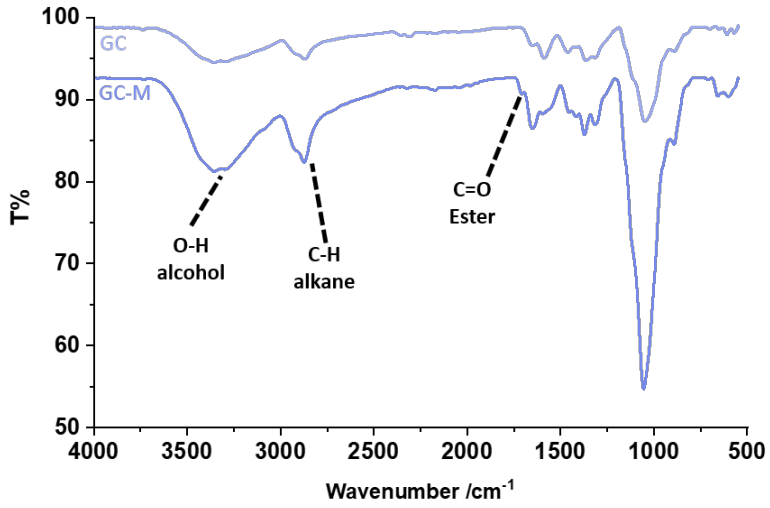

FIGURE 5.6. An FT-IR spectrum of of lyophilised GC and GC-M.

Polymers were dissolved in D_2O at a concentration of 20 mg/mL to allow ^1H NMR analysis. ^1H NMR of GC and GC-M is shown in Figure 5.7, with the important peak assignments labelled. Many of the NMR peaks are broad and hard to resolve, as is common in NMR of large polymers. The ^1H spectrum for GC-M shows the characteristic methacrylate peaks previously reported [53]: two singlets (1H, 5.86 ppm and 1H 6.20 ppm) due to the vinyl protons and a singlet (3H, 2.45 ppm) from the methyl group. These peaks are not observed in unfunctionalized GC and hence indicate that the polymer was successfully functionalised. In both spectra peaks at 5.03 ppm and 5.2 ppm originate from C1 of the sugar ring (acetylated and deacetylated respectively). Incomplete deacetylation during the preparation of GC from chitin leaves some amide groups and can be seen in the singlet at 2.64 ppm.

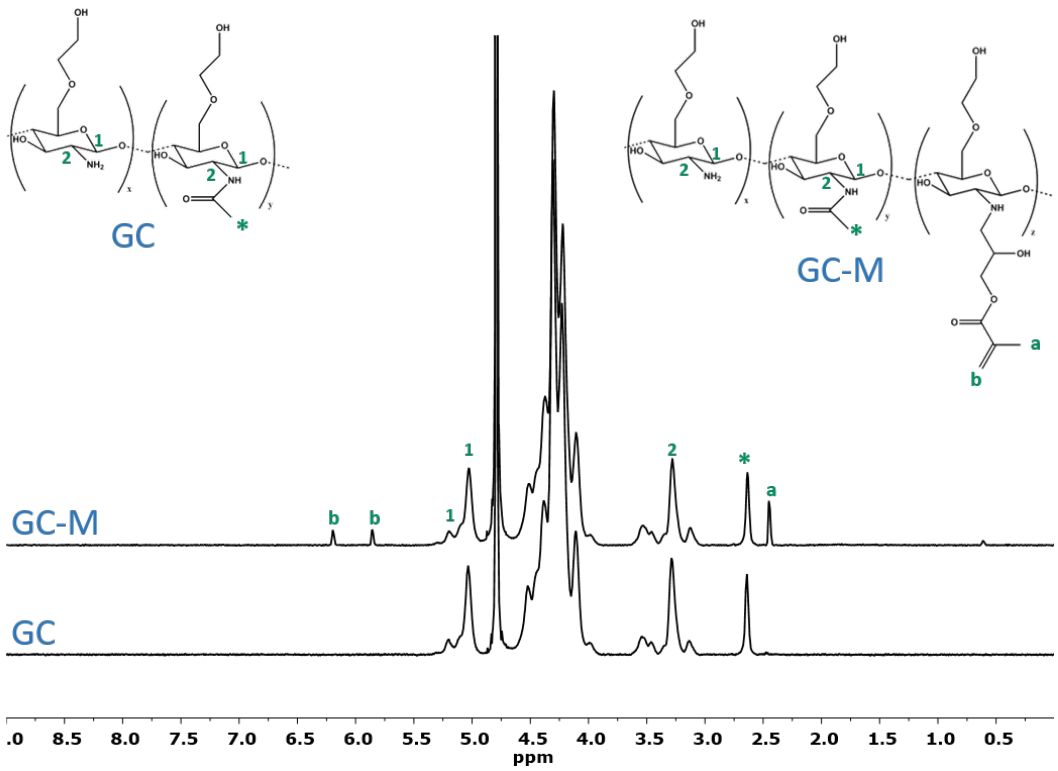

FIGURE 5.7. ^{1}H NMR spectra of glycol chitosan (GC, bottom) and N-methacrylated glycol chitosan (GC-M, top) run at 90 °C. The molecular structures of GC and GC-M are shown are simplified, in reality not every glucose ring with be functionalised with a glycol group.

Amsden et al showed that varying the amount of glycidyl methacrylate used in the synthesis could control the degree of substitution of methacrylate groups onto the polymer chain (DOS)[53]. The DOS affects the properties of the hydrogels formed from a methacrylated polymer because it alters the amount of crosslinking that will occur. Since functionalising the GC with methacrylate also uses up some of the free amine groups it is hypothesised that the DOS will further affect the pH response of the resulting hydrogels, as the amine groups are responsible for the pH sensitivity. Previously reports of the methacrylation of GC have calculated a value for the DOS using integral values from NMR spectra [53]. During the methylation, the degree of acetylation of the glycol chitosan should remain unchanged and hence this was calculated from the ^{1}H NMR as a test of the accuracy of the integral method. The degree of deacetylation was calculated using the integrals of the peaks at 2.64 ppm, 5.03 ppm and 5.20 ppm as detailed in Equation 2.19. Values for GC and GC-M were 81% and 83% respectively. The results are within a reasonable degree of error. Following on from this the integrals of the peaks at 5.86, 6.20, 5.03 and 5.20 ppm were used in the calculation of the DOS using the formula in Equation 2.20 , yielding a value of 4%.

To assess the acid/ base properties of the methacrylated polymer, GC and GC-M were also analysed using potentiometric titration. Prior to the titration, the GC and GC-M solutions were

adjusted to approximately pH 3 using 2 M HCl, so that the polymer was in its fully protonated form. To perform the titration, 0.1 M NaOH was added to a vigorously stirred polymer solution (10 mL of 1 mg/mL) in aliquots of 10 μL. After each addition of NaOH the pH was allowed to equilibrate before being recorded. Figure 5.8a-b shows typical titration plots for GC and GC-M. Two equivalence points are seen because the NaOH initially reacts with excess HCl. The equivalence point of HCl is the point where no excess HCl remains and the polymer is in its fully pronated form, and so data before this point can be discarded. At the HCl equivalence point the degree of dissociation of the ionic groups on the polymer α = 0. The second equivalence point is the point of neutralisation of the ionic groups on the polymer, and hence α = 1. The variation of α with pH was calculated and used to plot $\log(\frac{\alpha}{1-\alpha})$ (Figure 5.8c-d). Using the extended Henderson-Hasselbach equation, these plots were analysed to calculate pK_a values for GC (pK_a = 5.9 ±0.05) and GC-M (pK_a = 5.8 ±0.1). These values are similar, indicating that pK_a is not significantly changed by the methacrylation. The values are in the region that would be predicted for chitosan derived polymers but are slightly lower than expected [181].

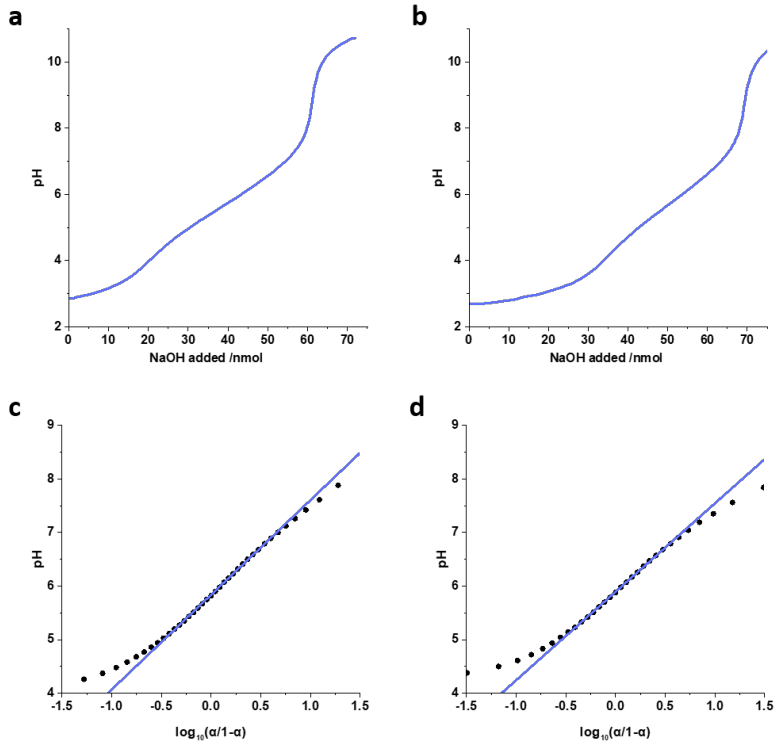

FIGURE 5.8. Potentiometric titration of (a) GC and (b) GC-M using 0.1 M NaOH. The curves were analysed using the extended Henderson Hasslebach equation to produce the plots in (c) and (d) for GC and GC-M respectively.

The amount of NaOH needed to neutralise the amine groups of the GC was also used to calculate the concentration of amine containing monomers in the unfunctionalized polymer (GC).

This gave a value of deacetylation of 77% . This is slightly lower than the value given by the NMR integration method, but the error is low enough to indicate that the NMR integral method gives a good approximate of DOS.

5.3.2.2 Synthesis and characterisation of methacrylated carboxymethyl cellulose

The method for methacrylation of carboxymethyl cellulose (CMC, 90 kDa) was adapted from that by Reeves et al [47]. A carbodiimide coupling reaction was carried out between the carboxylic acid groups of CMC and the amine of aminoethyl methacrylate (AEM) (Figure 5.9). A molar excess of both AEM and N-(3-Dimethylaminopropyl)-N-ethylcarbodiimide (EDC) were used due to the inefficiency of the coupling reaction.

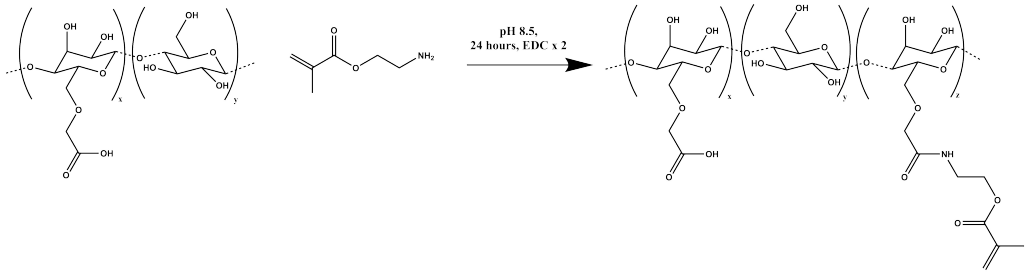

FIGURE 5.9. Reaction scheme for the functionalisation of carboxymethyl cellulose to form methacrylated carboxymethyl cellulose. The functionalisation is carried out by an EDC coupling to aminoethyl methacrylate.

An initial pH of 6.5 was used and addition of AEM to the CMC solution caused some of the polymer to precipitate. Adding the AEM gradually reduced this precipitation somewhat, but attempts to prevent it by using a more dilute solution of AEM, beginning the reaction at pH 8.5 or changing the order of addition of substrates were unsuccessful. After four hours the pH was increased to 8.5 to deprotonate the amine groups and thus allow coupling to the carboxyl groups on the polymer. The reaction was run for a total of 24 hours before being precipitated in acetone. The product was redissolved in DI water but preciipate that did not easily dissolve remained at this stage. The solution was dialysed and then centrifuged to remove remaining precipitate, before being adjusted to pH 7 and lyophilised.

FT-IR of CMC and CMC-M is shown in Figure 5.10. The appearance of peaks corresponding to ester (1702 cm^{-1} C=O stretch) and amide (1666 cm^{-1} and 1537 cm^{-1} C=O stretch) functional groups in the CMC-M spectra confirm successful methacrylation of the polymer. The intensity of these peaks is greater than those seen for the GC-M polymer, implying a higher degree of substitution.

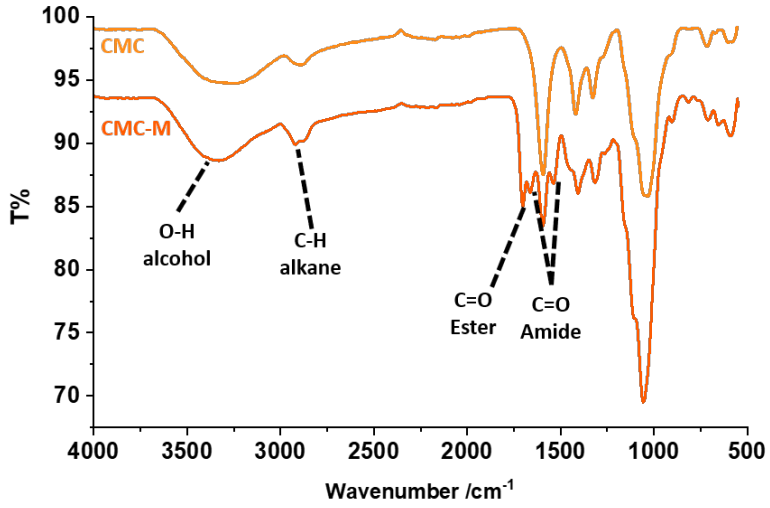

FIGURE 5.10. An FT-IR spectrum of of lyophilised CMC and CMC-M. The most important peaks are labelled.

Once again ^{1}H NMR of the polymers was run at 90 °C using 20 mg/mL solutions. The ^{1}H NMR of CMC-M compared with the starting material CMC in Figure 5.11, confirms that successful methacrylation has occurred. Characteristic methacrylate peaks from the vinyl protons can be seen as singlets at 6.3 ppm and 6.7 ppm. The presence of additional sharp peaks in the NMR spectrum indicate there may be some of the urea biproduct that forms during the EDC coupling reaction, remaining as an impurity in the system.

The DOS for CMC-M can be calculated from the ^{1}H NMR by comparing the integral of the methacrylate peaks to a peak on the sugar backbone (Equation 2.21. Based on peak assignments in previous literature the broad peak at 5.1 ppm can be attributed to the proton at position one on the glucose ring [47]. A molar ratio of free carboxylic acid groups to AEM/EDC of 1 to 1.75 gave a DOS of 9% ±2%. This polymer was used for all characterisation described here. Some samples of CMC-M were formed using less of an excess of AEM and EDC and this resulted in lower DOS values. These samples were used for some hydrogelation experiments

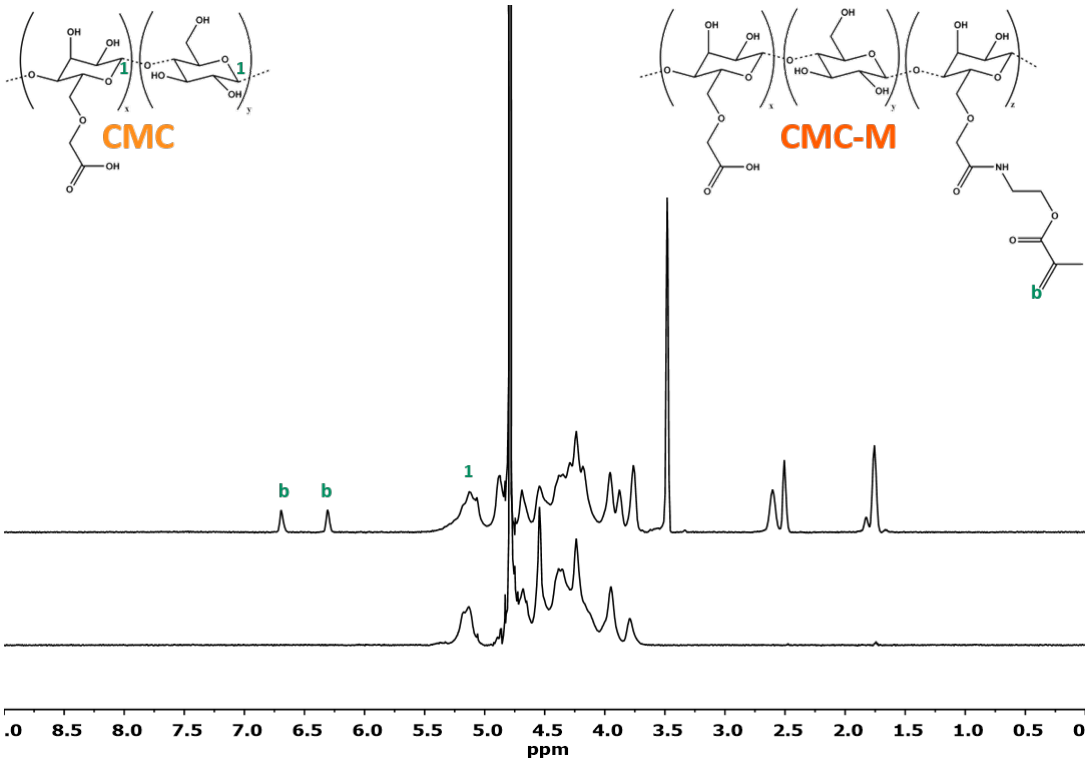

FIGURE 5.11. ^{1}H NMR spectra of carboxymethyl cellulose (CMC) and methacrylated carboxymethyl cellulose (CMC-M) run at 90°C. The molecular structures of CMC and CMC-M are shown on the left and right respectively. The structures are simplified in that not every glucose ring with be functionalised with a carboxymethyl group, and the functionalisation can occur on any of the three alcohols on the ring.

CMC and CMC-M were analysed using potentiometric titration to find pK_a values. An ion exchange resin was used to convert the polymers to their fully protonated form. The method that was used for titrating GC and GC-M, where HCl was used to convert the polymer to the fully protonated form, did not work in this case as no titration peak for the excess HCl could be seen. After treatment with the resin the polymer solutions were used directly for titration and an aliquot of the polymer solution was taken and lyophilised to determine the concentration of polymer, which was around 1 mg/ mL for CMC and around 0.1 mg/mL for CMC-M. The lower concentration of the CMC-M solutions is because there is more precipitate present in the solution prior to treatment with resin, and this is lost during the removal of the resin beads. The titration was carried out using the same method as for GC and GC-M, although due to the lower polymer concentration, CMC-M was titrated using 0.01 M NaOH instead of 0.1 M. Typical titration curves are shown in Figure 5.12. Based on the fact that $\alpha = 0$ at the start of the titration and $\alpha = 1$ at the equivalence point, the variation of α with pH was calculated. Using the plot of $\log(\frac{\alpha}{1-\alpha})$ shown in Figure 5.12, pK_a values for carboxymethyl cellulose and CMC-M were calculated as

pK_a(CMC) = pK_a(CMC-M) = 4.5 ±0.1. The value is unchanged due to methacrylation and in the range previously reported for CMC [182].

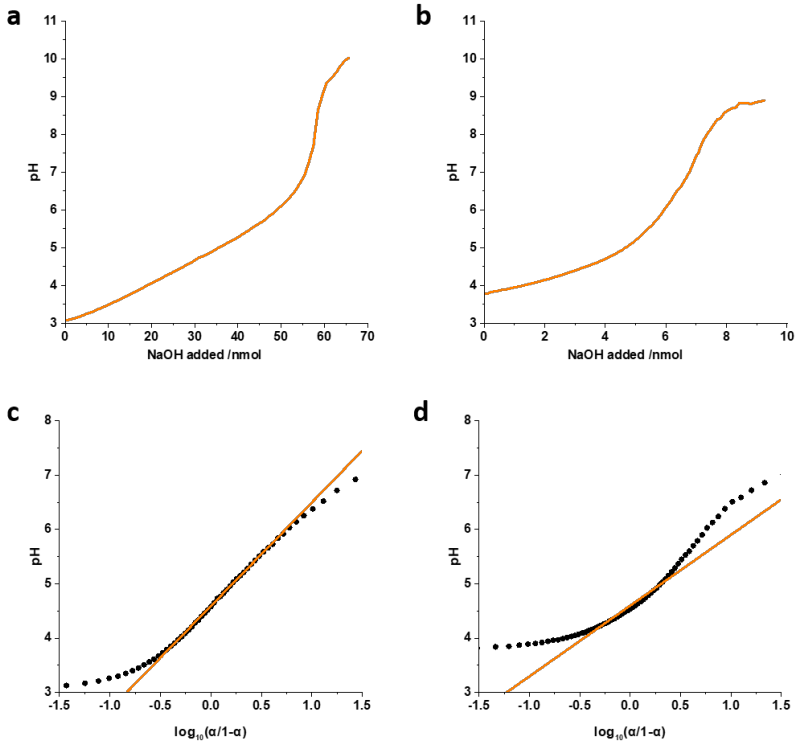

FIGURE 5.12. Potentiometric titration of (a) CMC using 0.1 M NaOH and (b) CMC-M using 0.01 M NaOH. The curves were analysed using the extended Henderson Hasslebach equation to produce the plots in (c) and (d) for CMC and CMC-M respectively.

Reeves et al found that CMC-M with a molecular weight of 90 kDa did not form stable hydrogels when irradiated with a photoinitiator but that higher molecular weight CMC-M (700 kDa) did [47]. Based on this observation, 250 kDa CMC was methacrylated using the same procedure described above. Addition of AEM to initiate the coupling caused significantly more precipitation using the 250 kDa polymer than the 90 kDa, but the synthesis of CMC-M was successful. Solutions of this higher molecular weight CMC-M were very viscous, particularly when compared to the lower molecular weight equivalent.

^{1}H NMR and FT-IR results showed that both GC and CMC were successfully functionalised with methacrylate groups, based on procedures from the literature. The DOS of both polymers was low, meaning many of the pH responsive groups remain unfunctionalized and hence these polymers should be suitable for the formation of pH responsive hydrogels via photopolymerization.

5.3.2.3 Photogelation of methacrylated polymers

Methacrylated bio-polymers can be crosslinked using radical initiators (Figure 5.13a). A procedure for forming GC-M and CMC-M hydrogels via UV irradiation, was developed based on examples from the literature. The photoinitiator 2-hydroxy-4-(2-hydroxyethoxy)-2-methylpropiophenone (I2959) forms radicals upon irradiation with UV light, as shown in Figure 5.13c. When combined with methacrylated polymers this results in crosslinking as the radicals attack the methacrylate double bond and initiate the radical cascade (see Section 1.2.1.5). I2959 absorbs most strongly around 280 nm as can be seen from the UV/Vis spectrum of a dilute solution in Figure 5.13b. When using biological material (such as enzymes) within a hydrogel, using this wavelength is undesirable because it corresponds to the region where proteins absorb and therefore can cause denaturation. Instead, a wavelength of 365 nm was selected for use here. Although the absorption here is relatively low I2959 can successfully form radicals when irradiated at this wavelength. The UV spectra shown in Figure 5.13b confirms that the methacrylated polymers show no absorption at the wavelength of irradiation and so should not prevent the formation of radicals.

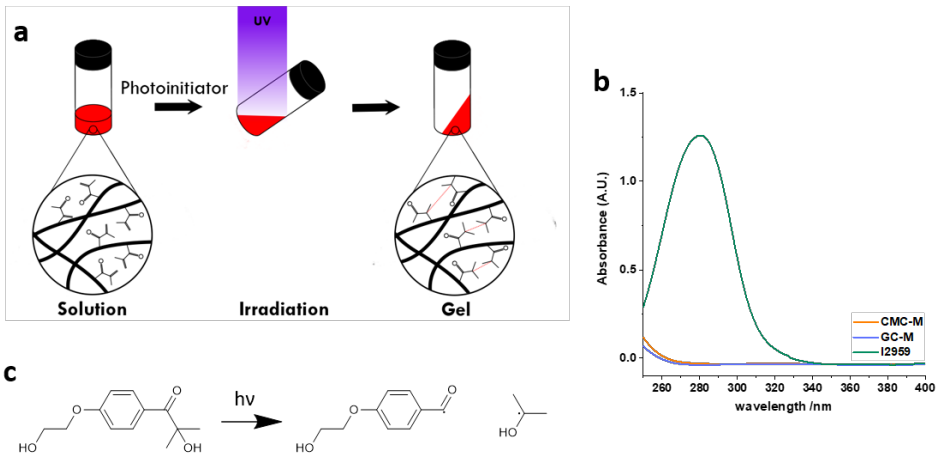

FIGURE 5.13. (a) A schematic showing the photogelation of a methacrylated polymer solution. Due to gelation the shape is maintained in the vial after the sample is returned to upright. (b) UV/Vis spectrum of photoinitiator (I2959), CMC-M and GC-M. (c) A reaction scheme showing the formation of radicals when I2959 is irradiated.

An aqueous solution I2959 (4% w/v) was first formed by adding I2959 to water and heating to 70 °C to dissolve. The stock solution was then kept in the dark at 55 °C until use. To form hydrogels I2959 solution was added to an aqueous solution of GC-M or CMC-M (final concentrations of 2% w/v polymer and 0.5% w/v I2959) at 55 °C. The pre-gel solution was irradiated with 365 nm light, with the lamp power and distance to the sample held constant for all experiments. To test the photogelation the vial inversion method was used, and red food colouring included in the pre-gel solutions to aid in visualisation.

Hydrogels that appear homogneeous are formed at 2% w/v N-methacrylated glycol chitosan (DOS 4% w/v) with 0.5% w/v photoinitiator after 1.25 minutes irradiation and controls showed no gelation (Figure 5.14a). Radical polymerisation often requires an inert atmosphere since oxygen is known to quench the reaction. Although gelation in a sealed argon environment appeared marginally faster, it also made the process more difficult to carry out and since photogelation in all cases was so rapid it was deemed unnecessary.

Hydrogel pieces could be rapidly formed by irradiating the GC-M solution in moulds (Figure 5.14b). For gels formed in 1 cm x 1 cm x 0.4 cm acrylic moulds, after 45 seconds large amounts of ungelled material was seen but upwards of 75 seconds homogeneous, freestanding gels formed (Figure 5.14c-f). Increased irradiation time lead to increased rigidity/ improved mechanical properties of the gels due to increased crosslinking. GC-M with increased DOS, which was formed by increasing the amount of glycidyl methacrylate during the synthesis (GC-M(DOS 13%)), showed a little improvement of the mechanical properties compared to GC-M(DOS 4%) but appeared far more prone to syneresis, visibly shrinking due to expulsion of water when stored in the fridge after formation. If GC-M(DOS 13%) hydrogels were irradiated longer periods of time they exhibited such syneresis during formation and were significantly smaller than the mould upon removal from it. This syneresis is a result of decreasing hydrophilicity. Since decreased crosslinking and increased amine concentration should give improved swelling and pH response, GC-M(DOS 4%) hydrogels were used for the remainder of this thesis.

Rheological characterisation in the form of SAOS strain amplitude and frequency sweeps was carried out to confirm the formation of GC-M hydrogels. Hydrogel pieces were soaked overnight in DI water and cut into to 19 mm disks. For each experiment a disk was removed from solution and excess water wicked off, before it was placed on the rheometer. The top geometry was lowered to exert a pressure of 1 N throughout the experiment. SAOS strain amplitude sweeps were carried out using a frequency of 1 Hz. The strain sweep in Figure 5.14g demonstrates the behaviour expected from a hydrogel, with a linear visco-elastic (LVE) region at low strain, where G' > G" indicating solid like behaviour [73]. Based on the strain amplitude sweeps a value of 0.1% strain (within the LVE limit) was chosen to run SAOS frequency sweeps between 0 and 25 Hz. Each frequency sweep experiment was repeated in triplicate and the plot in Figure 5.14h shows the average G' value. Again, the frequency sweep confirms the successful gelation due to the low frequency plateau of the SAOS frequency sweep which is associated with the presence of

a hydrogel. As is expected for a hydrogel G" was smaller than G' in this low frequency region, however G" is not plotted in Figure 5.14h because its low value made measurement unreliable (as is often the case for hydrogels [73]).

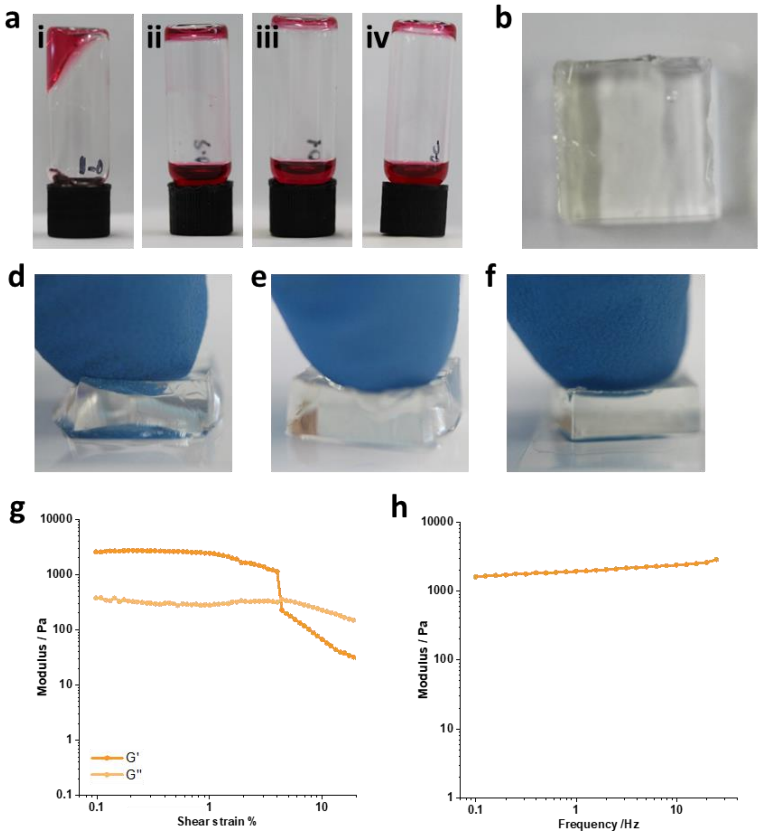

FIGURE 5.14. (a) 2% w/v solutions of GC-M after 1.25 minutes irradiation with 365 nm light under the following conditions: (i) 0.5% w/v I2959, (ii) 0.5% w/v I2959 no irradiation, (iii) 0% w/v I2959. (iv) is a 2% w/v solution of unfunctionalized glycol chitosan with 0.5% w/v I2959 after 1.25 minutes irradiation. (b) A hydrogel (dimensions 1 x1 x 0.4 cm) formed via the irradiation of 2% w/v GC-M solution for 5 minutes. (c), (d) and (e) are hydrogels formed via irradiation of 2% w/v GC-M for 75 s, 150 s and 300 s respectively. Gentle pressure application using a finger demonstrates the increase in rigidity of the gel with longer irradiation time.(g) SAOS strain amplitude sweep and (h) frequency sweep for GC-M hydrogels. The plot in (h) shows the value of G' only as the low value of G" made its measurement unreliable.

Photogelation of CMC-M (90 kDa, DOS 9%) was carried out using the same method described

for GC-M. Irradiation of 2% w/v CMC-M in the presence of 0.5% w/v I2959 produced homogeneous gels (Figure 5.15a). Stocks of CMC-M were turbid and hence so were the hydrogels. Irradiation of CMC-M in moulds rapidly produced free-standing hydrogels. Using the 1 x 1 x 0.4 cm mould again 5.15b shows that at 45 s ungelled material remained but from 75 s onwards homogeneous hydrogels are seen. CMC-M hydrogels were softer and appeared more elastic than those formed from GC-M. CMC-M with lower DOS (3%) did not undergo hydrogelation well upon irradiation. Although crosslinking did occur, the resulting species were extremely soft and did not hold their shape.

Rheological characterisation was carried out to confirm the formation of CMC-M hydrogels. Hydrogel pieces formed by irradiating a solution of 2% w/v CMC-M (90 kDa, DOS 9%) and 0.5% w/v I2959 for 10 minutes were soaked overnight in DI water. The method described for the rheological testing of GC-M hydrogels was repeated. The presence of the LVE region (with G' > G") at low strain values in the SAOS strain amplitude sweeps in Figure 5.15c, and the low frequency plateau in the frequency sweep shown in Figure 5.15d confirm hydrogelation of CMC-M as these are characteristic behaviours of hydrogel materials.

Previous work by Reeves et al stated that under the conditions they used 90 kDa CMC-M did not form stable hydrogels [47]. Under the conditions used in this thesis this is not the case, and usable hydrogels were achieved. However, hydrogels formed from 90 kDa CMC-M were not very strong and thus higher molecular weight CMC-M was tested. CMC-M(250 kDa) again formed free standing hydrogels upon irradiation. There appeared to be some improvement in the mechanical properties, but the pre-gel solution with this higher molecular weight polymer was very viscous. This increased viscosity would make mixing in colloidosomes and injecting into the mould without trapping bubbles into the solution significantly more difficult, so for the remainder of this work 90 kDa CMC-M (DOS 9%) was used.

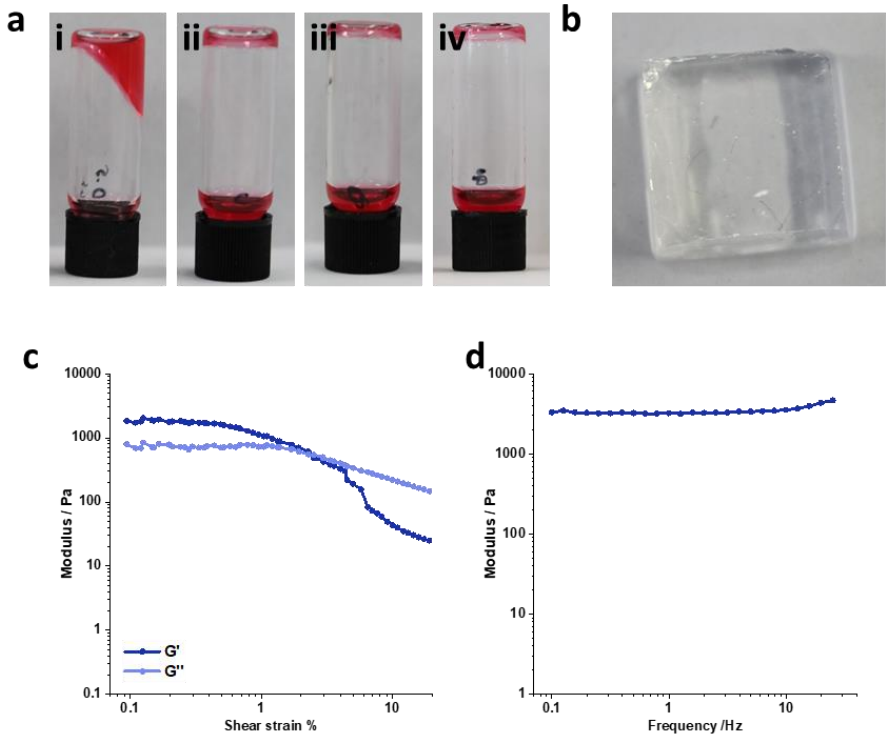

FIGURE 5.15. (a) 2% w/v solutions of CMC-M after 2.5 minutes irradiation with 365 nm light under the following conditions: (i) 0.5% w/v I2959, (ii) 0.5% w/v carboxymethyl cellulose with 0.5% w/v I2959 after 2.5 minutes irradiation. (b) A hydrogel (dimensions 1 x1 x 0.4 cm) formed via the irradiation of 2% w/v CMC-M solution for 5 minutes.(c) Rheological SAOS strain amplitude sweep and (d) frequency sweep for CMC-M hydrogels. The plot in (d) shows the value of G' only as the low value of G" made its measurement unreliable.

For SEM imaging hydrogels were prepared by irradiating pre-gel solution for 10 minutes in 2.5 x 0.5 x 0.1 cm moulds. The resulting hydrogels were soaked in water for 1 hour to remove unreacted species and then cut into strips and dropped directly into liquid nitrogen to induce rapid freezing. The strips were fractured to reveal cross sections and then lyophilised. SEM images of the samples after silver coating are shown in Figure 5.16. The structure of both CMC-M and GC-M after irradiation appears porous, as would be expected for a hydrogel, and both show some fibres as well as continuous sheets, likely due to the low polymer concentration. In the GC-M hydrogel there are regions with much a much more fibrous structure. Without further inspection it is difficult to say whether the appearance of these structures in some regions and not others is due to inhomogeneity in hydrogel formation or some artefact of the SEM samples preparation. There also appears to be some directionality in the pore structure in both hydrogels that is likely an artefact of sample preparation. The low polymer concentration and soft nature of the hydrogels make them difficult to handle after the lyophilisation process. Future work

should attempt to prepare samples for SEM analysis through critical point drying to see if the deformation of the hydrogel structure can be avoided.

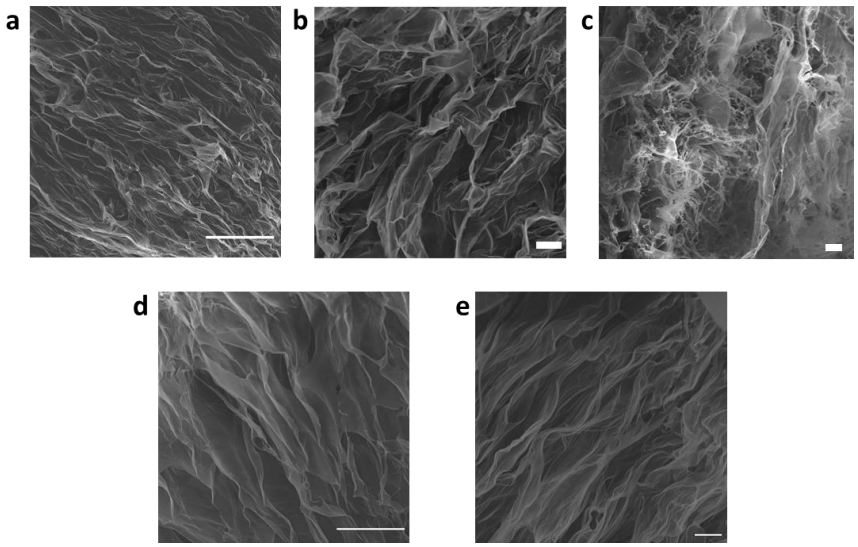

FIGURE 5.16. (a), (b) and (c) are SEM images of GC-M hydrogels (scale bars (a) 100 μm, (b and c) 10 μm). (d) and (e) are SEM images of CMC-M hydrogels (scale bars (d) 100 μm, (e) 10 μm).

The rapid gelation of GC-M and CMC-M upon irradiation in the presence of I2959 highlights some of the benefits of photogelation. A further benefit of photogelation is the ease at which patterns can be formed in the resulting hydrogels using masking. As an example of this a hydrogel was formed with a replica of the Centre for Organised Matter Chemistry logo (Figure 5.17b). The initial pre-gel solution contained methylene blue, although a lot of the colour of this species was lost upon irradiation. The PTEG piece used to seal the mould for the first gelation step, had the desired pattern blacked out and so after irradiation voids were seen in the bulk hydrogel, where light was unable to reach the pre-gel solution. Ungelled solution was removed and the voids filled with new pre-gel solutions containing no dye, rhodamine b or methyl orange. A second irradiation step formed a hydrogel with inset coloured triangles (Figure 5.17a). In the context of the work in this thesis, such photopatterning opens up the opportunity to pattern different populations within the bulk prototissue, in a manor resembling that in Chapter 2.

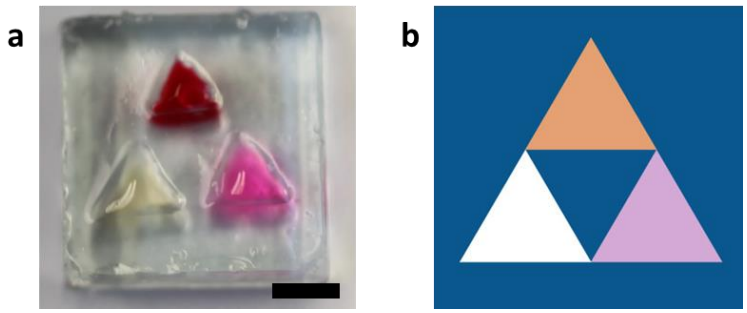

FIGURE 5.17. (a) A patterned GC-M hydrogel replicating the logo shown in (b). The hydrogel was formed by irradiating a solution of GC-M (with blue food colouring) in a square mould, with a mask on top preventing the gelation of the three triangular areas. After this gelation step the ungelled solution was removed from the triangles and replaced with GC-M solutions with different colourings. The hydrogel was then irradiated again resulting in gelation of the new GC-M solutions and a patterned hydrogel. Scale bar shows approximately 0.5 cm.

5.3.2.4 Characterisation of the pH response of hydrogels

Section 5.3.2.3 showed that hydrogels could rapidly be formed from both GC-M and CMC-M using UV light. The DOS of both polymers was relatively low, which has previously been shown to increase equilibrium swelling ratio [53]. To use these hydrogels in the formation of a pH responsive actuator, their swelling response to changes in pH was first investigated. Since the system presented here relies on pH changes generated within the hydrogel, a pH indictor was included so that the internal hydrogel pH could be monitored.

Section 1.2.7.7 discussed examples from the literature where a pH indicator was included in a hydrogels to monitor the internal pH during an enzymatic pH change [120]. The system was calibrated by measuring RGB values in images of hydrogels at specific pHs, and converting them to hue angles. Although this system is elegant, it is limited by the fact that using a single pH indicator only allows pH monitoring around the pK_a of said indicator, outside the indicating range the colour will not change further. Universal indicator is a mixture of several pH indicators and thus shows gradual colour change over a wide pH range. This is shown in 5.18 as a gradual change in the calculated hue angle. Each indicator in the mixture will have a unique partition coefficient in each hydrogel, which will vary with the pH of the solution and the ionic strength. It was hoped that including universal indicator in the final system would allow RBG values of the system components to be measured from photographs, and a hue angle plotted to monitor the pH.

Based on this, universal indicator was included in the buffers used to investigate the hydrogel pH response so that both swelling and colour change could be investigated.

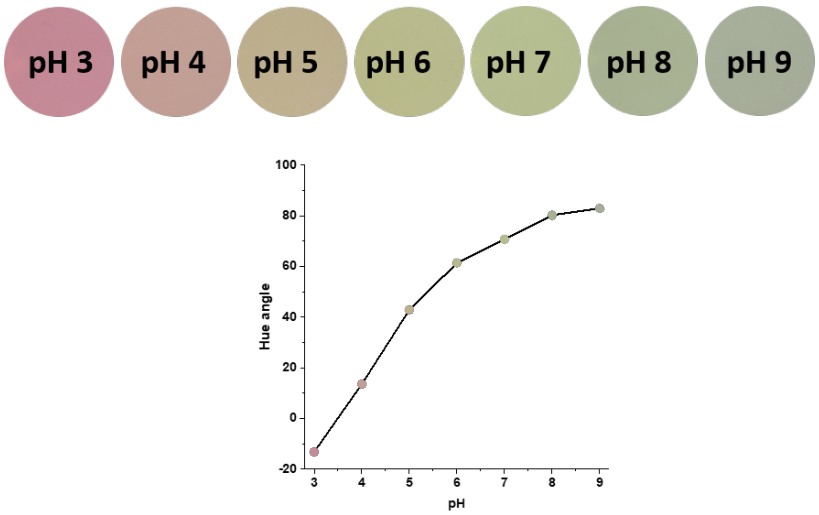

FIGURE 5.18. The circles along the top are photographs of universal indicator solution at the pHs indicated. The RGB values were measured from the images and converted to hue angles, which are shown in the plot.

In order to assess the pH dependant behaviour of the GC-M and CMC-M hydrogels, their swelling in buffers of various pH was assessed (Figure 5.19a). The swelling of pH responsive hydrogels is reduced in solutions with increased ionic strength. The chemo-mechanical transduction experiment later in this thesis had to be carried out in unbuffered solution and so low ionic strength solutions were selected for use in swelling characterisation. To give an accurate representation of pH response the buffer must also be capable of maintaining the pH after addition of the hydrogel. Buffer solutions show maximum buffering capacity around their pK_a and hence mixed buffers or combinations of buffers are required to cover the full range. Phosphate buffer is commonly used in hydrogel swelling experiments due to its three different pK_a values, but it was found that at the low concentrations required here, it did not buffer the solution enough. Instead acetate buffer (pH 3 to 6, 30 mM) and Tris buffer (pH 7 to 9, 30 mM) were used. The ionic strength of the buffer solutions (ignoring any contributions from the indicator for simplicity) was adjusted to 0.03 using sodium chloride prior to use.

Pre-gel solutions containing 0.5% w/v I2959, and GC-M or CMC-M (2% w/v) were injected into 2.5 x 0.5 x 0.1 cm moulds. Photogelation was carried out by irradiating at 365 nm for 10 minutes. The resulting hydrogels were cut into pieces roughly (0.8 x 0.5 x 0.1 cm) for swelling ratio tests. Each piece was weighed and submerged in 15 mL buffer solution containing 7.5 μL /mL universal indicator (from hereon referred to as UI buffers). The hydrogels were left for 24 hours to reach

equilibrium before the solution was removed. Excess was removed from the surface by wicking with filter paper and the hydrogels were weighed.

The swelling ratio was calculated (Equation 2.27) using the initial (M_i) and final masses (M_f) and its variation as a function of pH is shown in Figure 5.19. As expected, pH sensitivity is seen for both hydrogels, as can be seen by the photographs in Figure 5.19e. Cationic hydrogels (GC-M) showed maximum swelling at low pH, when the amine groups are protonated, and minimum swelling at high pH when the amine groups are deprotonated (Figure 5.19b). Conversely, anionic hydrogels (CMC-M) showed maximum swelling at high pH, when the carboxylic acid groups are deprotonated, and minimum swelling at high pH when the carboxylic acid groups are protonated (Figure 5.19b). Rather than the sharp change in swelling seen around the pK_a for GC, CMC-M hydrogels show a gradual increase in swelling with pH across the range studied. Previous examples of pH responsive CMC hydrogels did seem to plateau at higher pH [59].

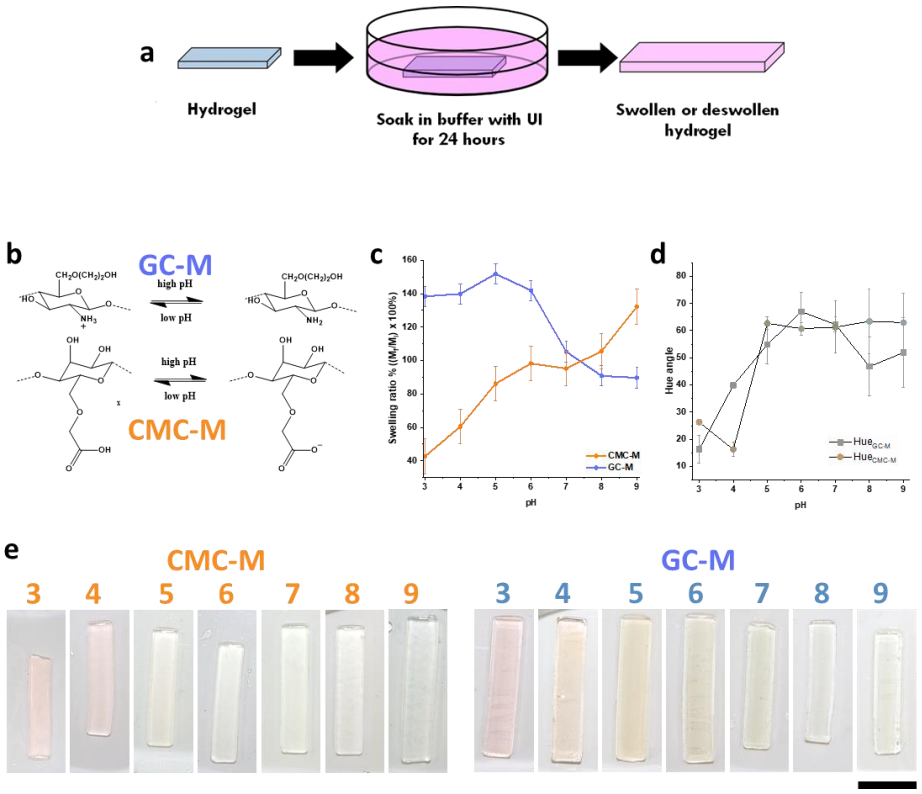

FIGURE 5.19. (a) A schematic showing how the pH response experiments were carried out. A hydrogel piece was placed into a buffer solution of the desired pH, along with universal indicator. After 24 hours the hydrogel was removed and swelling and dye uptake had occurred. (b) The simplified chemical structures of the methacrylated polymers showing how they are altered as the pH changes. (c) A plot of curvature against pH for CMC-M and GC-M hydrogels. (d) RGB measurements were taken from backlit images of swollen hydrogels and used to calculate hue angles at each pH. (e) Photographs GC-M and CMC-M hydrogels after 24 hour equilibration in universal indicator buffer. The pH at which each gel was equilibrated is shown above its photograph. The scale bar shows 1 cm.

The photographs of whole hydrogels after swelling in UI buffers at various pH show that as well as showing variation in size (swelling) at the different buffer pHs, the hydrogels show variation in colour due to the pH indicator (Figure 5.19). By eye variation in colour can be seen across the pH range for GC-M hydrogels but for CMC-M hydrogels little colour is visible above pH 5. The universal indicator solution is supplied only in the buffer solutions, and so colouration of the hydrogel itself relies on components of the indicator mixture moving into the hydrogel during equilibration. The uptake of each component from solution will vary according to the nature of the indicator molecule, the nature of the hydrogel, the pH and the ionic strength. The colour variation of the hydrogels is therefore related to all these factors, and can vary from the simple colour change seen by indicator solutions. Preliminary tests for pH response which were

carried out in buffer of higher ionic strength, showed less uptake of indicator solution and more weakly coloured hydrogels.

For RGB measurement the whole swollen hydrogels were imaged on an LED lightboard (backlit) and the images were white balanced. RGB values were measured using the RGB measure plugin on Fiji Image J. For a more detailed discussion of RGB values and measurement see Chapter 2. The RGB values were converted to hue angles and used to create a plot of the variation of hue angle with pH (Figure 5.19d). Variation of hue angle with pH is seen in both types of hydrogel to an extent, but it appears to plateau at higher pHs or in the case of GC-M show a decrease. High pH measurements also how higher errors and both these findings are likely due to the decreasing dye uptake of the hydrogel with increasing pH.

5.3.2.5 Preparation of pH responsive hydrogel bilayers

Investigation into the pH responsive properties of the CMC-M and GC-M hydrogels showed that they show opposite swelling responses to changes in pH, meaning that it should be possible to use them create a bilayer hydrogel that exhibits pH responsive curvature changes. Additionally, both hydrogels showed changes in swelling in the pH range 4 to 9, meaning they are suitable for use within the range that can be achieved using enzymes. In order to create actuating hydrogel bilayers, CMC-M pre-gel solution was irradiated for 10 minutes in the 2.5 x 0.5 x 0.1 mould. The resulting hydrogel was inverted and placed into a 2.5 x 0.5 x 0.2 cm mould. A GC-M pre-gel solution was added on top and the system irradiated again. During photogelation the GC-M adhered to the CMC-M layer below, likely because there are remaining methacrylate groups on the CMC-M that can react with the GC-M. The layers remain as one piece when the hydrogels are placed into water, indicating that bonds are formed between the two. In unusual cases the two layers can be seen to come apart very slightly at some places (delamination), these gels were not used for characterisation or data collection.

Characterisation of the pH responsive bending of the formed bilayers was carried out using the same UI buffers described for the swelling tests. Bilayers were soaked in DI water to remove unreacted species and then placed into 20 mL UI buffer solution (pH 3 to 9, 30 mM acetate or tris buffer, 7.5 μL /mL universal indicator) and left overnight to equilibrate. The hydrogels were placed on a light board and imaged from above (now using manual camera settings) and the photographs are shown in Figure 5.20. At low pH the GC-M layer is its most swollen state and the CMC-M layer is in its most deswollen state. The difference in the swelling of the two layers exerts a mechanical force on the interface and causes the bilayer to bend. The state where the GC-M layer is more swollen than the CMC-M layer is defined as negative curvature. At high pH, the bilayer bends in the opposite direction (positive curvature) because the CMC-M layer is more swollen than the GC-M layer. The absolute value for the curvature a pH 3 is greater than that at pH 9. Higher curvatures might be possible in the system should the pH be dropped below 3 or raised above 9, but this would not be relevant for use with enzymes due to their limited

range of stability and activity. The curvature of the bilayer hydrogel goes from strongly negative to strongly positive in the range pH 4 to pH 9, and the bilayer should therefore respond to pH changes caused by the pH changing protocells that work within this range.

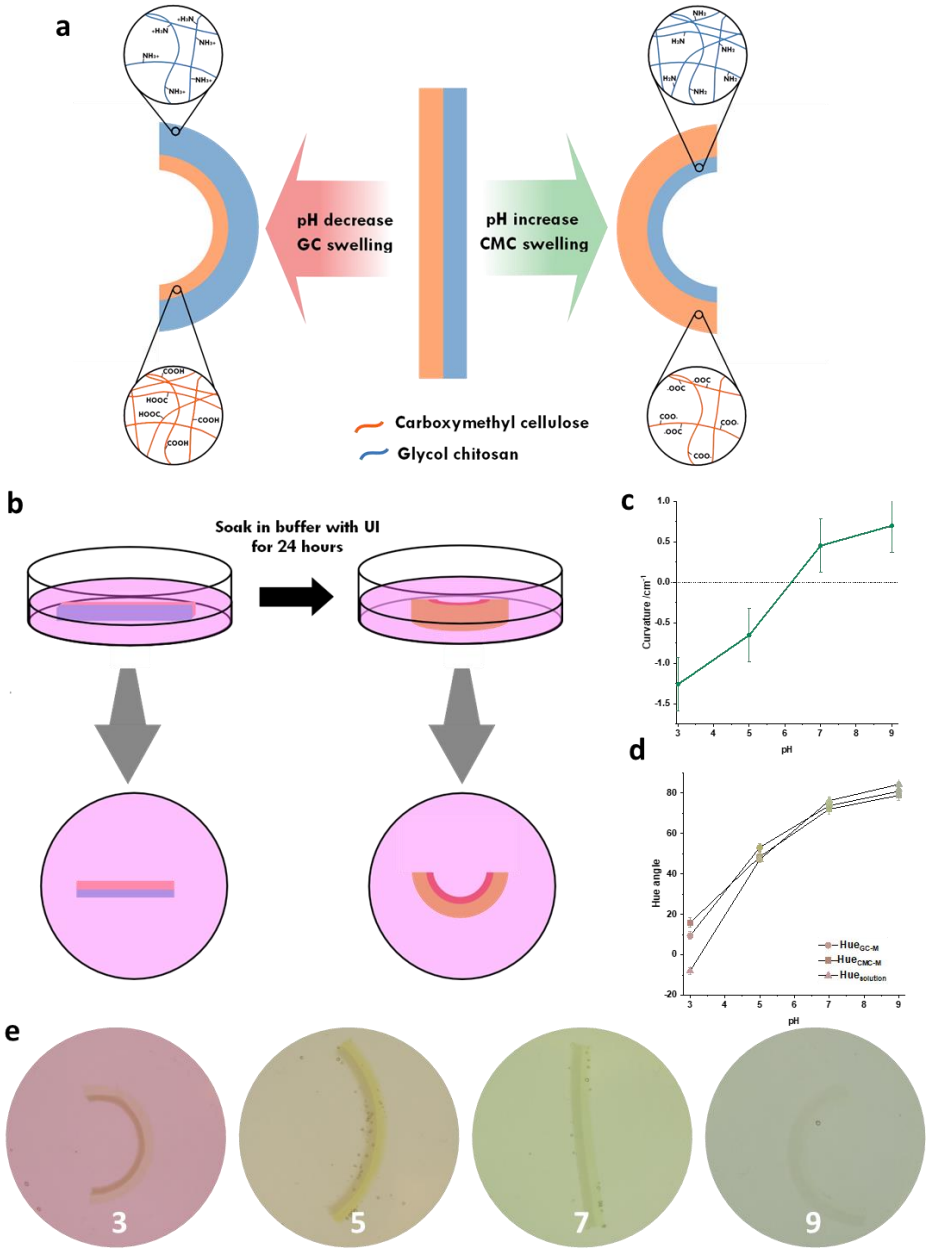

FIGURE 5.20. (a) A schematic showing the pH responsive curvature of the hydrogel bilayer. Hydrogels were equilibrated in UI buffers of various pH and imaged after 24 hours (b). Plots of (c) curvature and (d) hue angle of the hydrogels against pH of the bulk solution. (e) shows the photographs of the bilayers after equilibration, with the solution pH marked onto each photo. Scale bar shows 1 cm.

The images show more intense colouration than those seen for the individual hydrogel pieces out of solution. This is partly due to an increase in the thickness seen through the gel due to the differing orientation. The hydrogels are also within the coloured indicator solution, and this will effect the overall colour seen, particularly at high pH where the hydrogels themselves have little colouration. The RGB values of the solution and of each layer (GC-M or CMC-M) of the bilayer gel were measured from the white balanced images and used to calculate hue angles. Variation in the hue angle of the GC-M layer (hue_{GC-M}), the CMC-M layer (hue_{CMC-M}) and the solution (hue_{sol}) are shown in Figure 5.20. All three plots show an increase in hue angle with pH.

To demonstrate reversible bending of the hydrogel bilayers several cycles of pH change were tested. Hydrogel bilayers were placed in petri dishes between two glued capillary tubes that acted as stabilisers, holding the gels in position and upright. In these holders, hydrogels were equilibrated overnight in pH 3 acetate buffer (30 mM, I 0.03M) before the buffer was removed and replaced with 20 mL pH 9 Tris buffer (30 mM, I 0.03M). The hydrogels were imaged over time to assess the change in curvature. After two hours the buffer was removed and replaced with pH 3 buffer and this cycle was repeated several times to give the oscillations in curvature shown in Figure 5.21. The change in curvature is reversible and reproducible.

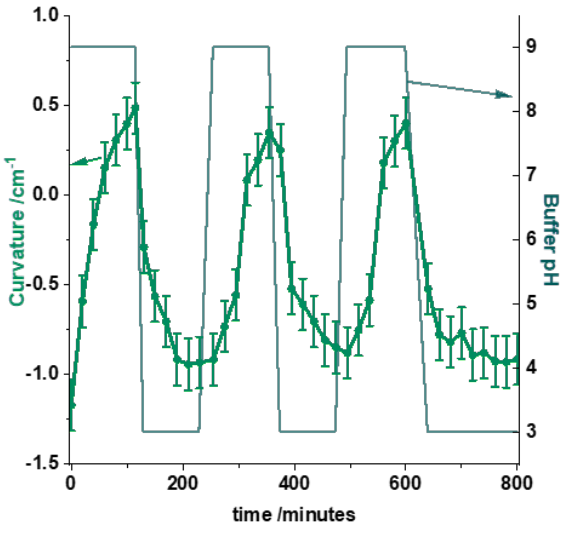

FIGURE 5.21. A plot of the change in curvature over time for hydrogels that were subjected to repeated changes in pH of the bulk solution. The solution pH is also shown on the plot. Anomalous values resulting from interaction between the petri dish and the hydrogel were removed before the average value was calculated.

The prototissue actuator designed in this chapter relies upon a pH responsive hydrogel

actuator which can respond to the protocell-mediated pH changes. As shown here, bilayer hydrogels based on GC-M and CMC-M are suitable for use in the prototissue actuator because they can be formed under biocompatible conditions and show reversible, pH induced changes in curvature within the pH range that can be achieved using enzymes.

5.3.3 Formation of prototissues capable of chemo-mechanical transduction

5.3.3.1 Monolayer prototissue formation and characterisation

Sections 5.3.1 and 5.3.2 presented the development of the key components needed to build a prototissue capable of chemo-mechanical transduction: colloidosome populations capable of pH change, and a pH responsive hydrogel bilayer. To characterise the system hydrogel prototissue monolayers (GC-M or CMC-M) were formed. GOx and URS colloidosomes were mixed into the pre-gel solution and the hydrogelation carried out using the methods described in Section 5.3.2.3, either in a vial or in a mould. Although hydrogels were visibly more turbid upon inclusion of colloidosomes, the presence of colloidosomes did not appear to prevent gelation (Figure 5.22a) and this was confirmed by rheological testing. Prototissues were formed via irradiation of pre-gel solutions containaing URS and GOx colloidosomes along with 2 % w/v solution of methacrylated polymer with photoinitiator. The prototissues were soaked overnight in DI water and cut into to 19 mm disks. The method for rheological testing that was described for GC-M hydrogels in Section 5.3.2.3 was repeated for the prototissues. The SAOS plots in Figure 5.22d to f show the characteristic behaviours expected of a hydrogel, with G' > G" in the LVE in the strain sweeps, and a low frequency plateau in G' in the frequency sweeps.

GOx and URS colloidosomes were formed with FITC-BSA or DL650-BSA respectively, to allow imaging within the hydrogel matrix. Colloidosomes were found to retain their spherical structure within the prototissue and distributed across the whole hydrogel piece (Figure 5.22b and c).

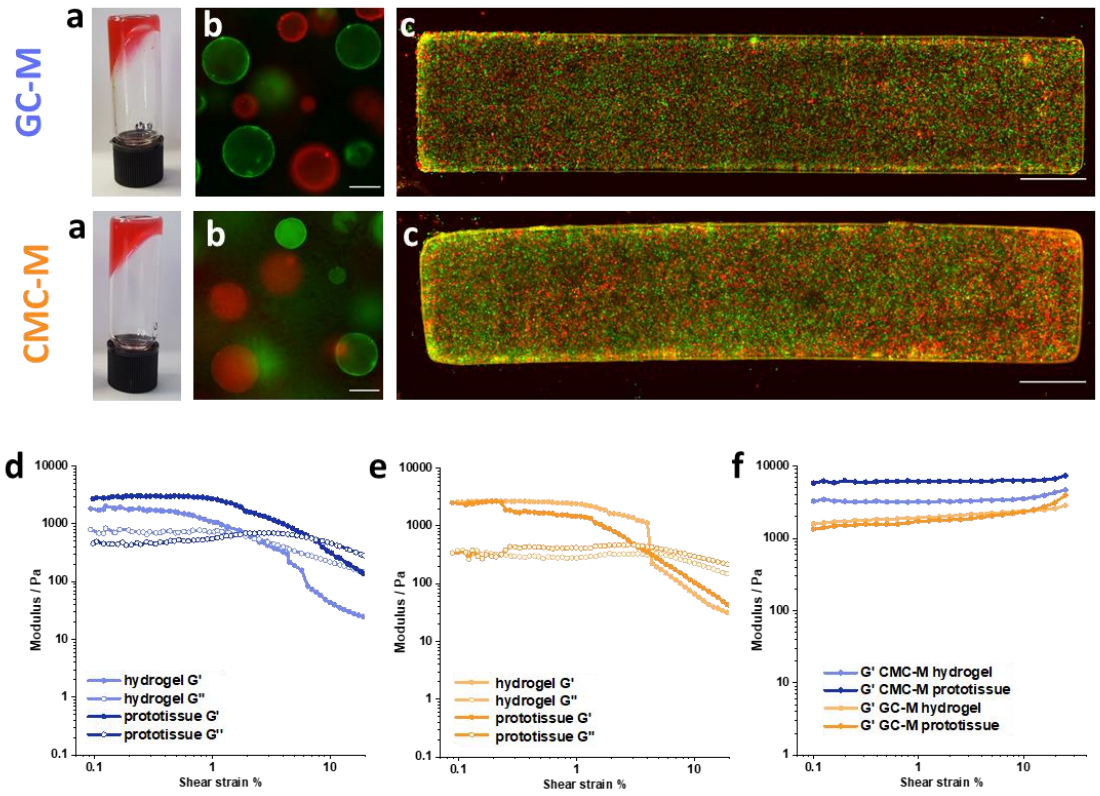

FIGURE 5.22. The top three images are hydrogels formed from GC-M and the bottom three are hydrogels formed from CMC-M. (a) Hydrogels formed by irradiation of a 2 % solution of methacrylated polymer with colloidosomes in the solution. (b) and (c) Fluorescence microscopy images of monolayer hydrogel prototissues containing GOx colloidosomes (with FITC-BSA, red) and URS colloidosomes (with DL650-BSA, green). Scale bars are (b) 50 μm and (c) 1000 μm. Rheological characterisation of hydrogel prototissues is shown in (d), (e) and (f). SAOS strain amplitude sweeps of (d) CMC-M hydrogels and hydrogel prototissues and (e) GC-M hydrogels and hydrogel prototissues. (f) Frequency sweeps for CMC-M and GC-M hydrogels and prototissues. The plot in (f) shows the value of G' only as the low value of G" made its measurement unreliable.

To assess the permeation of the methacrylated polymers into the colloidosomes, fluorescently labelled analogues were produced. GC-M and CMC-M were fluorescently labelled with fluorescein. GC-M was functionalised using FITC and CMC-M was labelled via EDC coupling to fluoresceinamine. UV/Vis spectroscopy showed successful labelling had occurred, with the percentage labelling at 0.002% for FITC-GC-M and 0.005% for F-CMC-M. The fluorescent polymers were used in the formation of colloidosome containing hydrogel pieces. The pre-gel solutions were irradiated for 10 minutes. Pre-gel solutions were visible green/ yellow due to the fluorescein. After irradiation to form hydrogels the colouration had significantly decreased,

indicating that the dye had photobleached. Although the fluorescein absorbed some of the UV light, the hydrogel pieces still successfully formed. Fluorescent polymer prototissues were imaged using confocal microscopy and the images are shown in Figure 5.23. The general background fluorescence of the FITC-GC-M prototissue is low but high fluorescence around colloidosomes and silica debris shows a strong interaction with the polymer. Many of the colloidosomes show high fluorescence intensity at the membrane, as if they are coated with the polymer, but some show fluorescence throughout. It is unclear if this difference is between the GOx and URS colloidosomes or if it occurs across both species. The images of the F-CMC-M prototissue are strikingly different. In the wider image (Figure 5.23c) few colloidosomes are seen, implying less interaction between the colloidosomes and the fluorescent polymer. Instead, the fibrous structure of the hydrogel can be seen. At higher magnification (Figure 5.23d) it is apparent that colloidosomes have fluorescence throughout and at a similar intensity to the background. The increased interaction between the polymer and colloidosomes seen in FITC-GC-M hydrogels compared to F-CMC-M occurs because the FITC-GC-M is positively charged in solution so interacts strongly with the negatively charged silica.

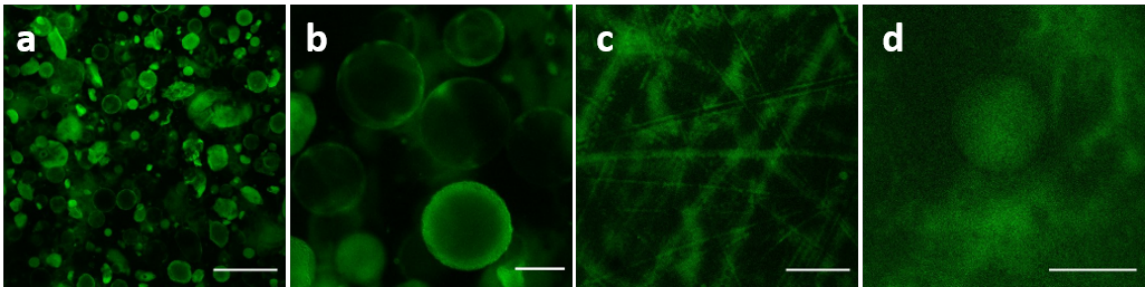

FIGURE 5.23. Confocal microscopy images of monolayer prototissue formed from (a and b) FITC-GC-M or (c and d) F-CMC-M, with mixed GOx colloidosomes and URS colloidosomes. Scale bars show (a) and (c) 200 μm or (b) and (d) 50 μm.

Colloidosome containing hydrogels were prepared for SEM via cryo-fracturing as previously described. SEM images are shown in Figure 5.24 and both hydrogels can be seen to retain a porous structure upon inclusion of silica colloidosomes. The structure of the hydrogel appeared less homogeneous under SEM when colloidosomes were present. In the case of CMC-M the pores appeared smaller in colloidosome containing gels, but it is hard to draw conclusions on this due to the distortion that occurs under SEM preparation. Within the hydrogel most colloidosomes appeared broken and deformed, although interestingly they did not show the elongated structure seen when colloidosomes were lyophilised alone. Figure 5.24 b-f shows some colloidosomes within CMC-M and GC-M hydrogels. The colloidosome in Figure 5.24b and c is broken open, displaying the porous silica matrix inside the colloidosome. In both the CMC-M and GC-M hydrogel the polymer matrix can be seen coating the colloidosomes and interacting with the surface.

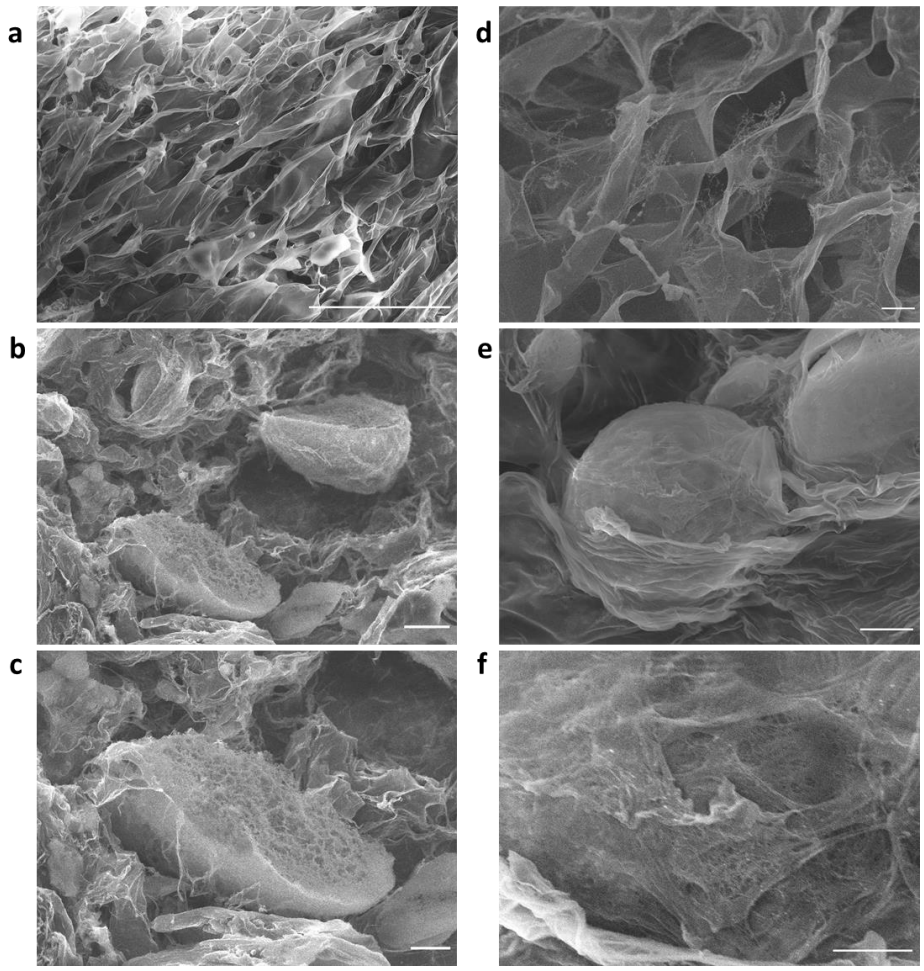

FIGURE 5.24. SEM images of (a-c) CMC-M hydrogels and (d-f) GC-M hydrogels containing mixed colloidosome populations. Images (c) and (f) are expanded regions of (b) and (e) respectively. Scale bars show (a) 100 μm (b) 20 μm (c) 10 μm (d) 10 μm (e) 10 μm (f) 5 μm.

In Chapter 3 it was demonstrated that due to their silica membrane and interior, colloidosome protocells can interact with or uptake small molecules under the right conditions. To explore this property within prototissue layers, GC-M and CMC-M prototissues containing mixed colloidosome populations were created and submerged in solutions of Rhodamine B or fluorescein (both

0.01 mg/mL, Tris buffer 5 mM pH 7.5). The hydrogels were equilibrated with the dyes overnight before being imaged using confocal microscopy (Figure 5.25). For comparison the experiments were also carried out with GOx and URS colloidosomes in suspension. As was demonstrated in Chapter 3, the positively charged Rhodamine B stains the secondary silica network inside the colloidosomes and in the presence of fluorescein the colloidosomes appear as dark circles. When either dye is added to CMC-M and GC-M hydrogels that do not contain colloidosomes, the fluorescence is uniformly distributed. When colloidosomes are present within the hydrogel matrix, they interact with the Rhodamine B to give regions of increased concentration, although unlike the images for free colloidosomes, the background fluorescence levels are still high and the colloidosome internal fluorescence is lower. Unlike the free colloidosomes, colloidosomes within GC-M or CMC-M hydrogels appear to take up fluorescein, causing regions of increased concentration instead of the dark circles seen in free suspension. Further investigation is needed to understand why this occurs.

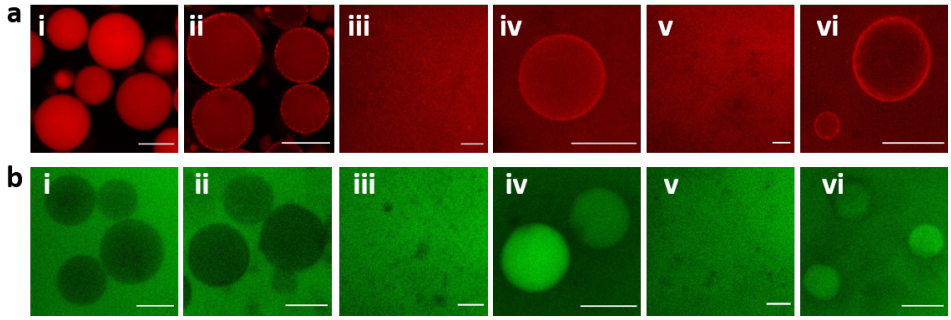

FIGURE 5.25. Confocal microscopy images investigating the uptake of (a) Rhodamine B and (b) fluorescein by colloidosomes or colloidosome hydrogels. The samples were as follows: (i) URS colloidosomes, (ii) GOx colloidosomes, (iii) plain GC-M hydrogel, (iv) mixed colloidosomes in GC-M, (v) plain CMC-M hydrogel, (vi) mixed colloidosomes in CMC-M.Scale bars show 50μm

Characterisation of the pH response of the colloidosome prototissues in was carried out using the same method described in Section 5.3.2.4. The swelling ratio as a function of pH is shown in Figure 5.26. The pH sensitivity of the hydrogel remains upon inclusion of colloidosomes.

Again, the two hydrogel types show opposite swelling pattern with change in pH, with the GC-M prototissue monolayer exhibiting maximum swelling at low pH and CMC-M prototissue monolayer showing maximum swelling at high pH. As well as showing the same general trend in swelling ratio, the swelling value at each pH is similar to that of the plain hydrogel (without colloidosomes), indicating that inclusion of colloidosomes does not affect the swelling of the hydrogel.

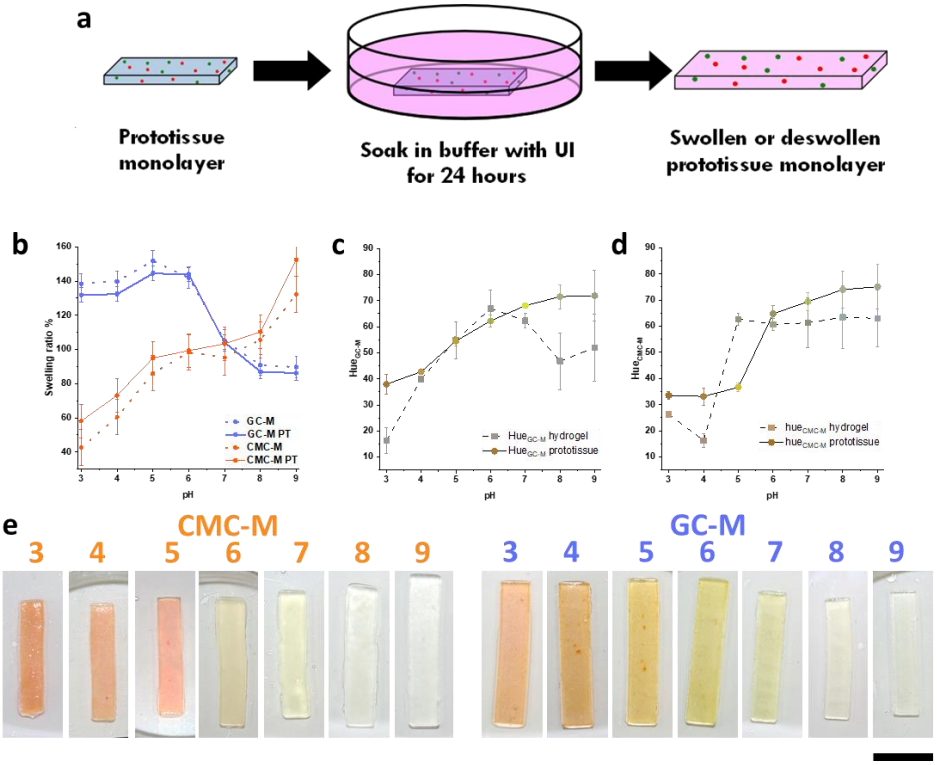

FIGURE 5.26. (a) A scheme showing the equilibration of monolayer prototissues with various pH UI-buffers overnight. (b) shows the variation in swelling ratio with pH of prototissues compared to the plain hydrogels. (c) and (d) are plots of hue angle against pH for GC-M and CMC-M prototissues respectively, again the plain hydrogel data is included for comparison. (e) Photographs of CMC-M and GC-M prototissues after incubation with the buffer solutions. The pH of the buffers is noted above the images. The scale bar represents 1 cm.

Figure 5.26d shows whole GC-M and CMC-M prototissue monolayers after equilibration with the UI buffers. The colour in these prototissue monolayers is easier to see than the plain hydrogels, particularly for pHs below 8. As described in Chapter 3, silica colloidosomes show adsorptive properties that vary with pH and nature of the adsorbing species. Once again hue angles were calculated using RGB values measured from white balanced images and they are shown in Figure 5.26c. GC-M prototissue monolayers show a gradual increase in hue across the

pH range 3 to 9 whereas the CMC-M prototissue monolayers show a gradual change at high and low pHs with a large jump in hue angle between pH 5 and 6. The magnitude of the hue angle change across this range of pHs is lower than is seen for the indicator alone and this can be seen by eye in the orange colouration of the hydrogels at low pH compared to the distinct pink colour of the indicator. It may be that adsorption onto the silica at low pH causes some structural alteration in some of the indicator molecules, for example by favouring one form over another, or it may be that the partition coefficient of some of the indicators within the mixture is different to other.

Single substrate experiments were carried out to demonstrate enzyme induced pH and swelling changes within the prototissue monolayers. Prototissue monolayers were formed from GC-M or CMC-M with mixed populations of URS and GOx colloidosomes. Immediately after formation the mass of each prototissue monolayer was recorded and they were placed into DI water for 1 hour. The prototissue monolayers were placed in UI solution (pH 4 or pH 9, depending on the substrate to be used) and equilibrated overnight in the fridge. The UI solutions were in water only, not buffer and thus the buffering effect of the hydrogel changed the solution pH overnight. The prototissue monolayers were removed from the solutions and excess water removed using filter paper. The mass was recorded and the prototissue monolayers imaged. UI solutions containing urea (25 mM) or glucose (100 mM) were adjusted to roughly the same pH as the bulk solution from the overnight prototissue equilibration (around pH 4.3 for urea solutions or pH 7.2 for glucose solutions). Prototissue monolayers were submerged in the relevant substrate solution (urea for gels equilibrated at low pH and glucose for those equilibrated at high pH) to initiate the reaction. At regular time intervals over an 8 hour period, the hydrogel pieces were removed from the substrate solutions and the weighing and imaging procedures repeated. The recorded masses were used to calculate a swelling ratio at each time using Equation 2.31. Upon addition of glucose to the bulk solution around GC-M or CMC-M prototissues, the solution pH decreased (Figure 5.27a) to around pH 4 over several hours due to the GOx/glucose reaction in the protocells. The swelling ratios of the hydrogels show opposite trends over time as would be expected from their earlier characterisation, with the GC-M hydrogel swelling and the CMC-M hydrogel deswelling (Figure 5.27b). The bulk solution pH decreases more rapidly in the case of the CMC-M prototissues, although the rate of swelling change does not appear to be significantly different.

Breakdown of urea by URS colloidosomes within GC-M prototissues resulted in a rapid decrease in swelling ratio over a period of 1 hour followed by a more gradual decrease was seen for the remainder of the measurement period (Figure 5.27b). The solution pH rose to around 9 over a period of a few hours, lagging slightly behind the rapid change in swelling ratio. Based on the pH responsive swelling of the CMC-M hydrogels, it was predicted that the pH change resulting from addition of urea to the prototissue would cause an increase in swelling ratio. However, in stark contrast to the rapid activity of URS colloidosomes within GC-M hydrogels,

within CMC-M hydrogels the colloidosomes appear to be inactive and no pH change is seen when urea is added. The swelling ratio of the CMC-M prototissues after urea addition does not increase, and instead a slight decrease is seen, probably due to a slight pH or ionic strength difference in the substrate solution compared to the equilibration solution.

Responsive hydrogels are often used in triggered substrate release, and so we hypothesise that the prototissue monolayers show decreased reaction rate when starting from an uncharged, deswollen state due to changes in the uptake of the substrate. In the case of CMC-M it appears that at low pH there is no urea uptake and thus no enzymatic reaction. Comparing the reaction of GC-M or CMC-M prototissue monolayers with glucose, it seems that glucose uptake may be reduced in the deswollen GC-M prototissue monolayers compared to the CMC-M prototissue monolayers, although this effect is much less dramatic than that seen for urea.

Addition of urea or glucose to control hydrogels formed with plain colloidosomes (no enzyme) resulted in no pH change and no change in swelling (Figure 5.27c), proving that the enzymes within the colloidosomes are essential to the prototissue function.

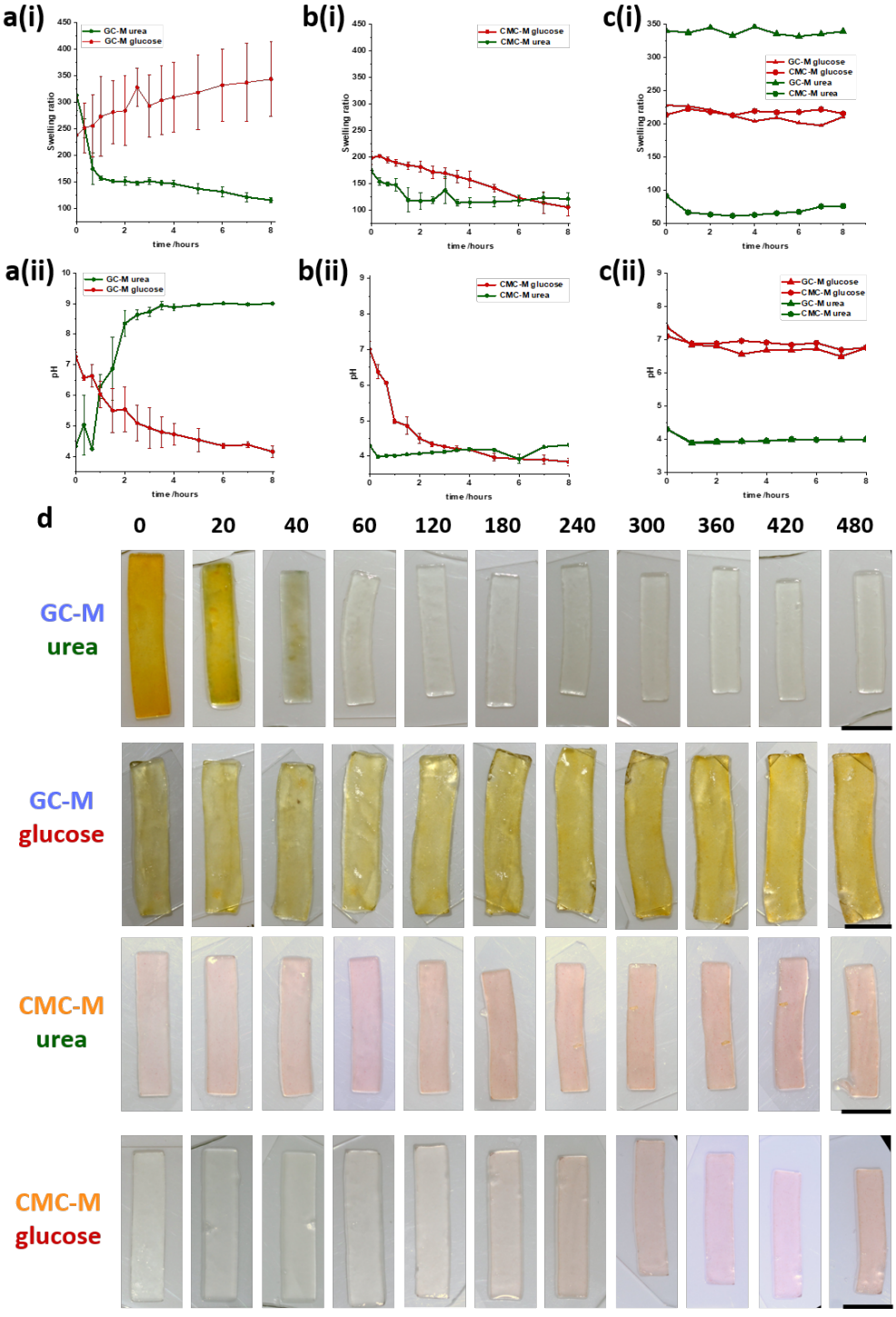

FIGURE 5.27. Monolayer prototissues formed from mixed colloidosome populations in (a) GC-M or (b) CMC-M were submerged in either 25 mM urea or 100 mM glucose (as labeled on the individual plots). Control experiments were run using hydrogels formed with plain colloidosomes (c). The hydrogels were periodically removed from the substrate solution to be imaged and weighed. (i) are plots over of the change in swelling ratio and (ii) are plots of the bulk solution pH. (d) Photographs of monolayer prototissues after the addition of urea or glucose as indicated. The lapsed time in minutes is shown at the top of the image.Scale bar shows 1 cm.

5.3.3.2 Formation of prototissue bilayers

Monolayer prototissues formed by embedding colloidosome protocells in GC-M and CMC-M showed swelling changes when enzymatic substrates were added. For the protocell induced pH changes to results in actuation the protocells must be used in a prototissue bilayer. Prototissue bilayers were first formed and characterised for comparison with plain bilayer hydrogels.

Prototissue bilayers were formed by including URS and GOx colloidosomes (50 μL each in total 200 μL solution) in the GC-M and CMC-M pre-gel solutions and following the method described for the formation of plain hydrogel bilayers. The two layers adhered to form the prototissue bilayer, which appeared turbid due to the presence of the colloidosomes. GOx and URS colloidosomes containing fluorescently labelled BSA were again used for imaging the protocells within the hydrogels. Widefield fluorescence images of the whole prototissue bilayer after soaking in water shows colloidosomes distributed through the two layers of the hydrogel (Figure 5.28c-d). The fluorescence appears brighter in the CMC-M layer, likely because the deswollen state of the gel means the fluorescent colloidosomes are packed into a tighter space. Figure 5.28a is an SEM image of a section of a prototissue bilayer was obtained via the cryo-fracturing method. The porous structure of both layers is visible, and broken colloidosomes can be seen within. Interestingly the colloidosomes in this image seem to be mainly located around the interface of the two layers, implying that despite the rapid gelation some colloidosomes might sink within the solution prior to complete gelation. More rigorous analysis of the form carried out in Chapter 4 could be carried out in future studies to get clearer information on this.

The response of the prototissue bilayers to changes in external pH was characterised. Prototissue bilayers were placed into UI buffers of various pH and equilibrated for 24 hours before being imaged. Figure 5.28e shows the typical photographs and the variation in curvature with pH is shown in Figure 5.28f. The prototissue bilayers show pH dependent curvature switching from negative curvature to positive as the pH increases.

The change in colour with pH is seen clearly for both GC-M and CMC-M. Once again, hue angles were calculated from the white balanced images and the average values are shown in Figure 5.28g. Here, three measurements were taken from each section in an image, and the process was repeated across three samples to give an average. Both the hue angle of the GC-M layer (hue_{GC-M}) and of the CMC-M layer (hue_{CMC-M}) increase with increased pH. The plot of hue_{GC-M} acts as a calibration curve that is used later in this work to estimate internal hydrogel pH from RGB measurements. This calibration curve is applied using hue_{GC-M} only since the GC-M layer of the prototissue bilayer showed more intense colouration and should therefore be less affected by changes in colour of the bulk solution than the CMC-M hydrogel.

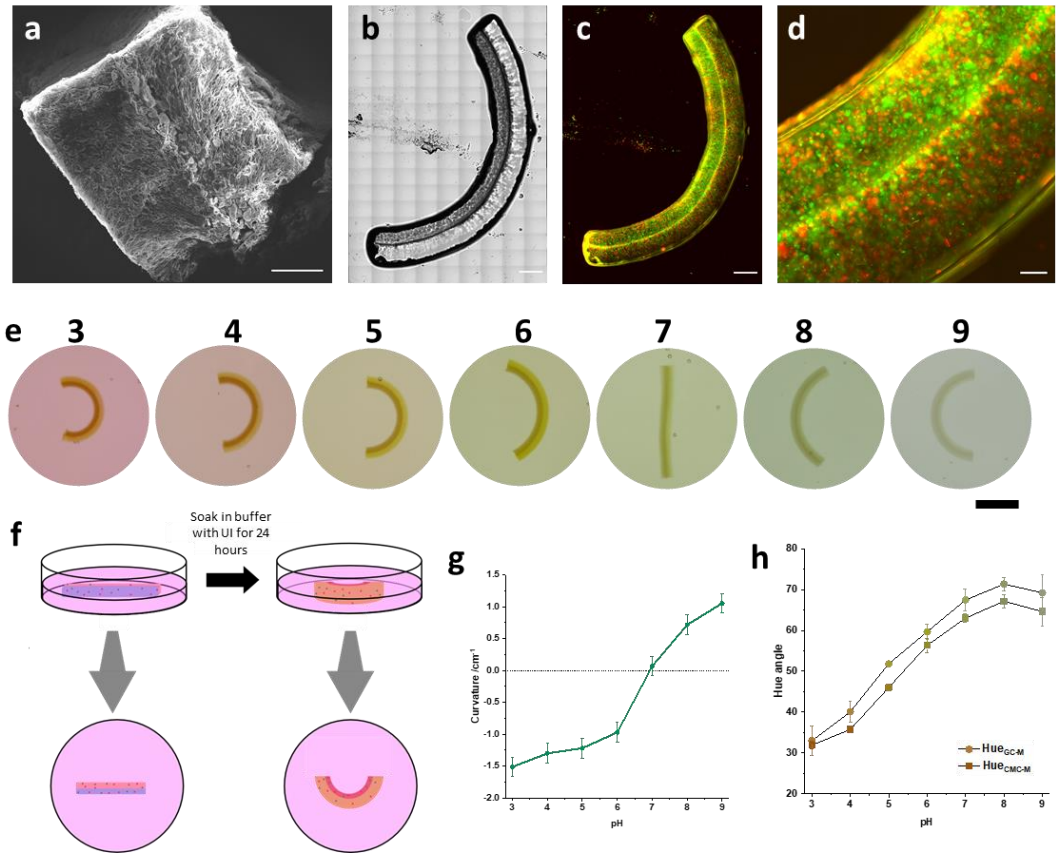

FIGURE 5.28. (a) An SEM image of a prototissue bilayer (scale 500 μm). (b) Bright field and (c and d) fluorescence microscopy images of a prototissue bilayer after swelling in DI water. The bilayer was formed using GOx colloidosomes (with FITC-BSA, red) and URS colloidosomes (with DL650-BSA, green). Prototissue bilayers were submerged in buffers of various pH with universal indicator. The images taken after 24 hours are shown in (e) and a scheme of how the experiment was carried out is in (f). Plots of average curvature and hue angles are shown in (g) and (h) respectively.

5.3.4 Prototissues capable of chemo-mechanical transduction

5.3.4.1 Single substrate experiments

The work in this chapter so far has demonstrated the successful formation of pH responsive prototissue bilayers and also shown that the protocell populations can carry out enzymatic reactions to alter pH both in suspension and within a hydrogel matrix. Adding the enzymatic substrates to prototissue bilayers should therefore result in protocell mediated chemo-mechanical transduction.

Prototissue bilayers containing uniformly distributed GOx and URS colloidosomes (standard

prototissue, Figure 5.29) were placed in holders and soaked in DI water for one hour, before being equilibrated in UI solution overnight in the fridge. The next day the UI solution was removed and 25 mL fresh UI solution containing the desired substrate (100 mM glucose or 5 mM urea) was added. The system was imaged every 20 minutes for 8 hours. Each experiment was repeated in triplicate, and during one run of each a pH electrode was used to monitor the bulk solution pH.

For each image the hue angle of the GC-M layer (hue_{GC-M}) was calculated from measured RGB values and used to estimate the internal hydrogel pH (pH_{pt}) using the calibration curve in Figure 5.28. The average hue_{GC-M} values were compared to the calibration graph and when value reached the average hue_{GC-M} that corresponded to a particular pH on the calibration graph, pH_{pt} was estimated to be at that value. Where hue_{GC-M} reached a calibration value between two measurements, the time at which that pH was reached was estimated as half way between the two measurements. Furthermore, due to the decrease in hue_{GC-M} upon pH increasing from 8 to 9, a pH value of 9 is only plotted if the relevant hue_{GC-M} value is both preceded and followed by a hue_{GC-M} value equivalent to pH 8

Photographs of a prototissue bilayer after addition of 100 mM glucose solution are shown in Figure 5.29. Oxidation of glucose by the GOx colloidosomes caused a decrease in pH, which is seen by both the direct solution pH measurement (Figure 5.29e) and the decrease in hue_{GC-M} (Figure 5.29d). Initially the hue_{GC-M} value indicates pH_{pt} between 4 and 5. After the addition of glucose hue_{GC-M} falls, indicating a decrease in pH_{pt}, but it does not reach the value which would indicate $\text{pH}_{pt} = 4$. As the pH decreases the GC-M layer swells and the CMC-M layer de-swells causing the prototissue to gradually change shape, with the curvature to becoming increasingly negative (Figure 5.29f).

Figure 5.29c shows the chemo-mechanical transduction response of a prototissue bilayer which was subjected to 5 mM urea solution. Prototissues showed an increase in bulk solution pH and pH_{pt} due to the turnover of urea by the URS colloidosomes. The enzymatic reaction occurs within the prototissues and hence pH_{pt} rises faster than the bulk solution pH, with the hue_{GC-M} indicating $\text{pH}_{pt} = 8$ after just 1 hour and remaining above this value for the remainder of the experiment. The pH increase causes the prototissue bilayer to change shape, switching from negative to positive curvature over the course of several hours (Figure 5.29f). The increase in pH_{pt} that is seen in the first hour is accompanied by the period of most rapid curvature change and after this, the change in curvature occurs gradually over the remainder of the experiment. The initial period of rapid pH change plays a role in the rapid initial curvature change. However, consideration of the curvature plot in Figure 5.28 shows that the difference in curvature between pH 6 and pH 8 is much greater than for pH variation outside these bounds, meaning that the same pH change would cause a greater curvature change in this region, and this likely contributes to the rapid curvature change.

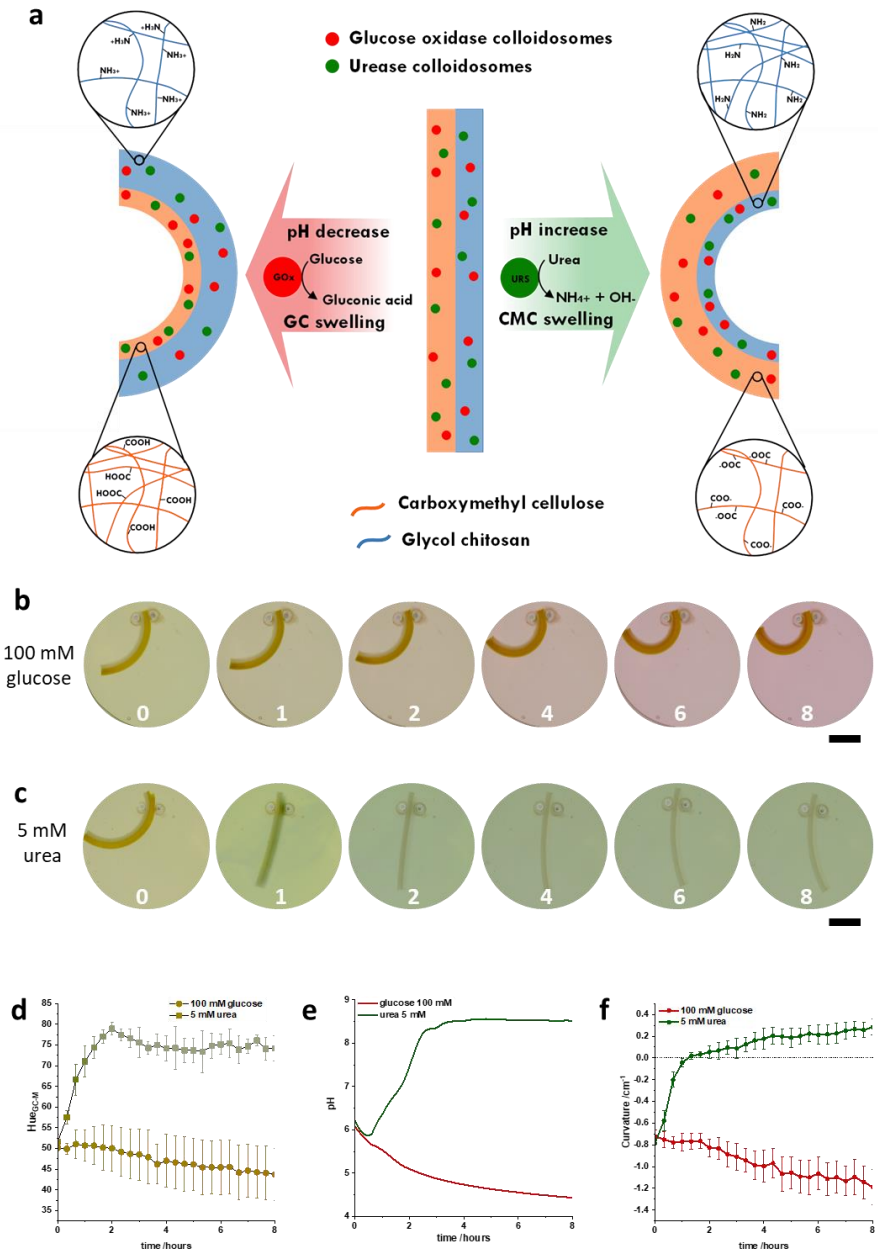

FIGURE 5.29. (a) A schematic showing how the prototissue actuation response occurs upon addition of urea or glucose. Photographs of a prototissue bilayer after addition of 100 mM glucose (b) or 5 mM urea (c). The time is shown in hours on each image and the scale bars show 1 cm. The photographs were processed and the average hue_{GC-M} angles (d) and curvature (f) across three repeats plotted. (e) is a plot of the measured solution pH over time.

These experiments show that addition of either glucose or urea to the prototissue successfully results in chemo-mechanical transduction over a period of several hours. As would be expected

from results discussed earlier in this chapter, the change in curvature is more rapid when urea is used going from -0.79 ±0.005 cm^{-1} to 0.18 ±0.097 cm^{-1} in four hours, compared to prototissues that go from -0.72 ±0.059 cm^{-1} to -1.0 ±0.14 cm^{-1} in the same period of time after addition of glucose. The curvature values seen are generally lower in magnitude than may be expected from the characterisation plot in Figure 5.28. The characterisation of the pH response was carried out in low concentration buffer, meaning that the ionic strength was higher in the characterisation than in the experiments here. This difference in ionic strength likely the cause of the differences in curvature magnitudes. As has been previously mentioned, pH responsive hydrogel bilayers can be slow to respond since the swelling change occurs via diffusion. In this case the rate of curvature change is also controlled by diffusion of substrates into the hydrogel and the rate of the enzymatic reaction. Although the change here is slow, manipulating the enzymatic systems used and the nature of the hydrogels could significantly increase the speed for future applications. For the purpose of the proof of principle work discussed in this thesis, the gradual nature of the change is acceptable, since the chemo-mechanical transduction is still an example of an emergent property and the system is therefore functioning as designed. This is highlighted by the controls shown in Figure 5.30, where hydrogel bilayers formed with plain colloidosomes (no enzyme) were placed into glucose or urea solutions and monitored. In these cases, no significant change in hue angle or curvature is seen over time.

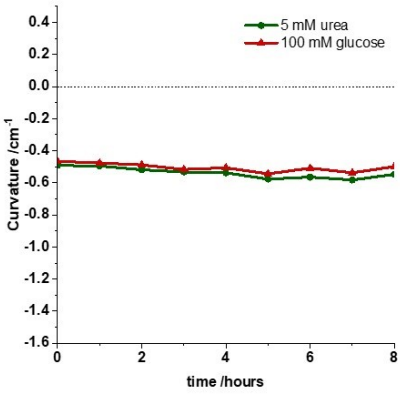

FIGURE 5.30. A plot showing the change in curvature over time after addition of urea or glucose to the bulk solution around a control prototissue bilayer formed with colloidosomes containing no enzyme.

5.3.4.2 Out-of-equilibrium behaviour in chemo-mechanically transducing prototissues

Section 5.3.4.1 showed that prototissue bilayers are capable of prototcell mediated chemo-mechanical transduction due to the collective behaviour of the component parts. Addition of a single substrate (either urea or glucose) caused change in curvature in one direction as the system moved towards equilibrium. Section 5.3.1 showed that the mismatch in kinetics between the antagonistic colloidosome populations in suspension resulted in transient pH changes upon concurrent addition of the two substrates. It was hypothesised that taking advantage of such a transient pH change in a prototissue should allow temporal patterning of the chemo-mechanical transduction, meaning that having both substrates in solution at once could result in first a shape change in one direction, and then the reversal of that shape change (a back and forth motion) without the addition of another substrate.

To achieve out-of-equilibrium chemo-mechanical transduction (i.e. temporally patterned chemo-mechanical transduction) prototissue bilayers were prepared as described for the initial experiments. After overnight equilibration with UI solution, prototissue bilayers were set up for imaging and substrate solution added. Several different methods for applying the two substrates were tested, but the final method used was based on staggered addition of the substrates. Glucose (100 mM) was used in the first stage, as this reduced the pH and the prototissue became increasingly bent (negative curvature) (Figure 5.31). As in the glucose only experiments shown in Figure 5.29, pH_{pt} begins between 4 and 5, and although the hue_{GC-M} implies that it falls, it does not reach 4.

After 4 hours, 1 mL urea solution was added (initial concentration upon mixing 5 mM) and the solution gently mixed. Upon addition of urea, the URS/ urea reaction dominates due to its rapid kinetics compared to the GOx/ glucose system. Consequently an increase in pH_{pt} and, more slowly, bulk solution is seen (Figure 5.31d). In the first few hours after urea is added, indicator leaves the hydrogel as the change in pH changes the partition coefficient of the indicator molecules. The increase in pH caused by the URS dominance is accompanied by an increase in curvature, reaching a maximum value of 0.5 $\pm$0.1 cm^{-1} 5 hours and 20 minutes after the addition of the urea. Once again, this value is lower in magnitude than the value that might be predicted at this pH when looking at the characterisation plot in Figure 5.29.

The urea concentration fell over the initial reaction period as it got used up and the reduced concentration caused a decrease in the URS/ urea reaction rate. The GOx/ glucose reaction became dominant, resulting in a fall in pH_{pt} and pH. Consequently the curvature also decreased, although pH_{pt} reached a maximum value and began to fall before the maximum curvature was achieved. This lag period is due to the time it takes for hydrogel swelling and deswelling to occur.

Overall the addition of urea caused the pH_{pt} to increase beyond that seen for the bulk solution pH. The hue_{GC-M} indicates that pH_{pt} reaches pH 8 at roughly 7.3 hours, whereas the solution measurement never increases above pH 6.7. The disparity in the pH values is because the URS/

urea reaction occurs within the hydrogel network and due to the time it takes for the pH change to spread to the bulk solution, the pH_{pt} begins to fall before the solution pH would have time to reach the maximum value.

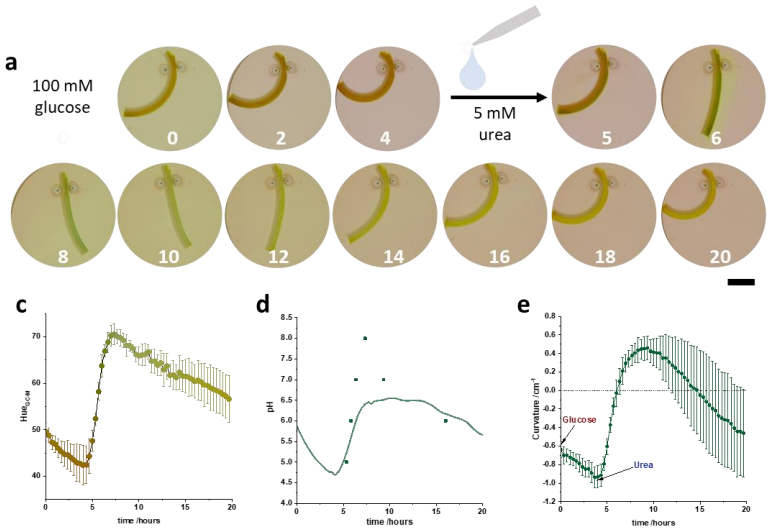

FIGURE 5.31. (a) Photographs of a prototissue bilayer after addition of 100 mM glucose followed by 5 mM urea after four hours. The time is shown in hours on each image and the scale bars show 1 cm. The photographs were processed and the average hue_{GC-M} angles (c) and curvature (e) across three repeats plotted. The hue_{GC-M} angles were used to estimate the internal hydrogel and the results are shown along with the plot of measured solution pH in (d).

The actuation that is shown via the staggered addition of the two substrates can be described as A->B->(C->A‘) chemo-mechanical transduction. The initial addition of glucose causes an increasingly negative curvature (A->B). When urea is added a transient pH increase occurs. This results in a change from negative to positive curvature and then without further addition of a substrate a return to negative curvature of similar value to that at the start of the experiment (B->(C->A‘)). The (B->(C->A‘)) section of this motion is a novel example of out-of-equilibrium behaviour. This has not been seen in a bilayer hydrogel actuator before, since it is not possible in a system that reacts to a change in stimulus by simply reaching an equilibrium value.

5.3.4.3 Controlling the chemo-mechanical transduction in prototissues

Due to the rapid reaction kinetics of the URS/ urea colloidosomes, addition of a small amount of urea to a system that has been supplied with an excess of glucose some time before, resulted in a transient pH increase. This led to protocell mediated A->B->(C->A‘) chemo-mechanical transduction. The mismatch on of the kinetics that is achieved using the URS and GOx

colloidosomes is necessary to create this novel actuation response. Enzyme kinetics are sensitive to changes in substrate concentration, and thus experiments were carried out to demonstrate that A->B->(C->A') chemo-mechanical transduction of the prototissue bilayers could be controlled by varying the concentration of one of the substrates. The initial addition of glucose was kept constant at 100 mM but the concentration of urea used in the second step was either 2.5 mM or 25 mM. Photographs of such experiments are shown in Figure 5.32a-b.

Increasing the initial urea concentration from 5 mM to 25 mM caused a more rapid increase in both pH_{pt} and bulk solution pH (Figure 5.32d). The change in curvature from negative to positive (Figure 5.32e) and once again the maximum curvature was reached at around 9 hours, with a delay between maximum pH and maximum curvature as was observed for the 5 mM urea experiments. After reaching a maximum, the solution pH falls but the pH_{pt} shows a much more gradual decrease than for the experiment run with 5 mM urea, as does the curvature. The increased initial urea concentration may result in more urea remaining in solution and thus the continuation of the URS/ urea reaction retards the rate of pH decrease by the GOx/ glucose system. Alternatively the gradual pH decrease may indicate reduction in GOx activity. The increased urea concentration may have caused pH_{pt} to reach a higher value than was achieved upon addition of 5 mM urea and based on the bell shaped activity curve of GOx it may be that it reaches a value where it shows very low activity, or high pH could also structurally damage the enzyme.

One issue that can be observed in the experiment run with 25 mM urea is the colour seen for the hydrogel after it has reached maximum hue_{GC-M}. The colour looks different from that seen at similar hue_{GC-M} values before the maximum. This may result from issues with diffusion of indicator molecules in and out of the prototissue or solution colour interfering with the hue_{GC-M} measurement. Regardless of this the hue_{GC-M} clearly shows that pH_{pt} reaches a higher value than bulk solution pH. The complications and possible solutions that could be used in future are discussed in the chapter conclusions.

When the initial urea concentration is reduced to 2.5 mM only a slight increase in pH and curvature is seen before both begin to fall again. The low concentration of urea results in a lower URS/ urea reaction rate. Interestingly the maximum curvature occurs at roughly the same time as for experiments run with 5 mM or 25 mM urea, and this is something that may be interesting to explore in future studies.

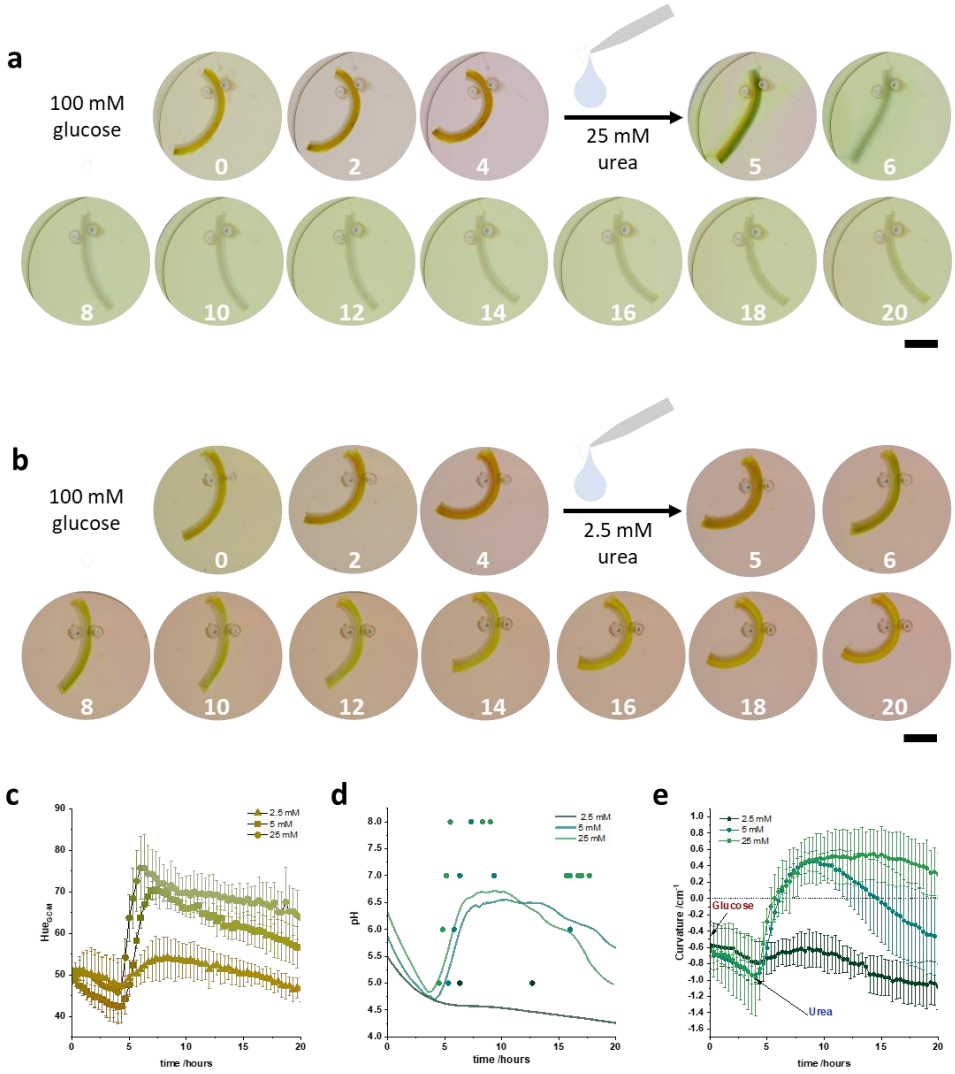

FIGURE 5.32. Photographs of a prototissue bilayer after addition of 100 mM glucose followed by (a) 25 mM urea or (b) 2.5 mM urea after 4 hours. The time is shown in hours on each image and the scale bars show 1 cm. The photographs were processed and the average hue$_{GC-M}$ angles (c) and curvature (e) across three repeats plotted. The hue$_{GC-M}$ angles were used to estimate the internal hydrogel pH and the results are shown along with the plot of measured solution pH in (d). The data from the experiment run using 5 mM urea that was shown in Figure 5.31 is included here for comparison.

5.3.4.4 Out-of-equilibrium chemo-mechanical transduction in prototissues with heterogeneous protocell distribution

Varying the initial urea concentration used provided some temporal control over the A->B->(C->A‘) chemo-mechanical transduction of the standard prototissue bilayer. The prototissue monolayer kinetics experiments discussed in Section 5.3.3.1 showed that the two different colloidosome populations displayed varied reaction kinetics depending on the type of hydrogel in which they were embedded. It was therefore hypothesised that creating heterogeneously distributed colloidosome populations within the prototissue bilayer would affect the chemo-mechanical transduction. Figure 5.33a shows schematics of prototissues created with URS colloidosomes in the GC-M layer only and GOx colloidosomes in the CMC-M layer only (prototissue$_{Ug-Gc}$), or with the reverse distribution (prototissue$_{Uc-Gg}$). The same overall concentration of each colloidosome species was present in the prototissue as for the prototissue bilayer with homogeneously distributed mixed populations (standard prototissue). Prototissue bilayers were prepared and equilibrated with UI solution as previously described. Once again staggered addition of the two substrates was used to instigate A->B->(C->A‘) chemo-mechanical transduction. The prototissue was submerged in 100 mM glucose and after four hours 1 mL urea solution was added to give a concentration of 5 mM.

As Figure 5.33b-f shows, little difference was seen between the initial glucose only reaction with prototissue$_{Ug-Gc}$ and prototissue$_{Uc-Gg}$ when compared to a standard prototissue, which reflects the fact that GOx colloidosomes showed only a slight difference in rate when encapsulated in GC-M hydrogels or CMC-M hydrogels. Upon addition of urea dramatic differences are seen because URS colloidosomes are essentially non-functional when encapsulated within CMC-M hydrogel, but they show high urea turnover when encapsulated within GC-M. When 5 mM urea was added to a prototissue$_{Ug-Gc}$, the URS/ urea reaction occurred rapidly and the curvature increased. The pH and curvature plots in Figure 5.33 are similar to those seen for a standard prototissue with increased (25 mM) urea concentration was used. In a standard prototissue half of the URS colloidosomes are in an environment that renders them non-functional, meaning that in a prototissue$_{Ug-Gc}$ there are twice as many active URS colloidosomes and therefore an increased rate of URS/ urea reaction. The gradual decrease in pH$_{pt}$, seen in the later stages of the experiment, may once again be due to sustained URS/ urea reaction, but may instead be caused by reduction of GOx activity due to a high pH$_{pt}$.

Due to the non-functionality of URS colloidosomes within CMC-M, prototissue$_{Uc-Gg}$ shows no pH increase and no increase in curvature upon addition of urea. In the later stages of the experiment delamination of the GC-M and CMC-M hydrogel layers is seen, indicating that the sustained low pH has caused a large difference in size between the two layers and the mechanical force has overcome the bonding between the two hydrogels. This type of delamination is something that has been reported previously for some hydrogel bilayers but stronger interactions between the two hydrogel layers could be introduced in future work to overcome this issue [59].

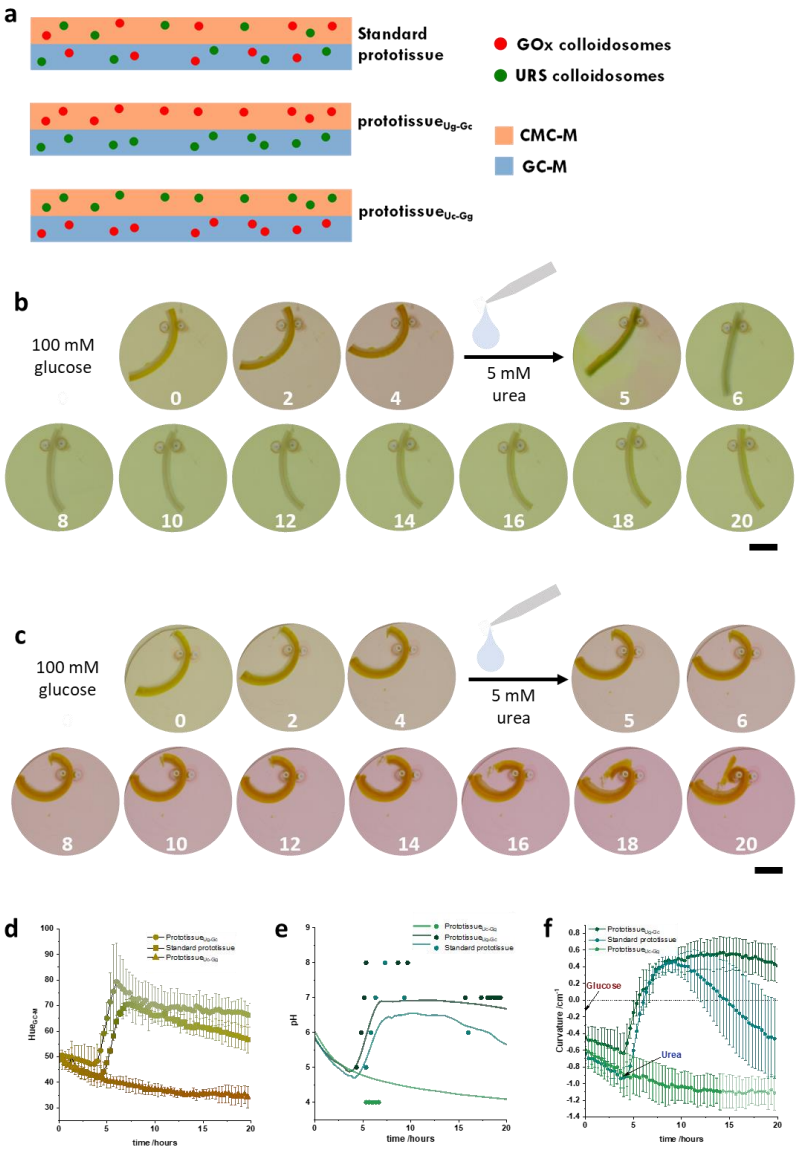

FIGURE 5.33. Prototissue bilayers were formed with different arrangements of colloidosome populations as shown by the scheme in (a). The photographs in (b) and (c) show the chemo-mechanical transduction seen when the staggered addition of glucose (100 mM) and urea (5 mM, at four hours) is used on prototissue$_{Ug-Gc}$ or prototissue$_{Uc-Gg}$ respectively. The time is shown in hours on each image and the scale bars show 1 cm. The photographs were processed and the average hue$_{GC-M}$ angles (d) and curvature (f) across three repeats plotted. The hue$_{GC-M}$ angles were used to estimate the internal hydrogel pH and the results are shown along with the plot of measured solution pH in (e). The data from the experiment run using a standard prototissue which was shown in Figure 5.31 is included here for comparison.

5.3.4.5 Spatial patterning of out-of-equilibrium chemo-mechanical transduction in prototissues with heterogeneous protocell distribution

A hydrogel bilayer with uniformly applied stimulus responds with an overall change in curvature. As discussed in Section 5.2.1, there have been various examples of hydrogels with varied geometry and different distributions of the hydrogel layers that cause different changes in shape. The prototissue bilayers presented in this thesis do not respond directly to the stimulus that is uniformly applied (the chemical fuel, urea or glucose), but to the protocell induced pH change happening within the hydrogel matrix. Chapter 4 showed that patterned colloidosome populations within a hydrogel matrix could result in non-uniform production of an enzymatic substrate. It was predicted that applying this principle to the prototissue bilayers would result in heterogeneous pH changes upon uniform application of the chemical fuels, and that this in turn would produce asymmetric changes in shape despite a simple bilayer arrangement of the two hydrogel types. Such behaviour would build upon the temporal patterning shown in Sections 5.3.4.2 to 5.3.4.4, demonstrating spatio-temporal patterning of the protocell mediated chemo-mechanical transduction.

Patterned hydrogel populations within a prototissue (prototissue$_{NU}$) were achieved using the photo masking method. The simple pattern shown in Figure 5.34a was used to demonstrate the principle. One section of the hydrogel contained URS colloidosomes in GC-M and GOx colloidosomes in CMC-M (section$_{Ug-Gc}$), and the other section of the hydrogel had the opposite colloidosome distribution (section$_{Uc-Gg}$). Staggered addition of 100 mM glucose and 5 mM urea was once again used to induce the chemo-mechanical transduction and photographs are shown in Figure 5.34b. After addition of glucose the overall curvature of the hydrogel increases as the pH falls and the GC-M layer swells. This occurs in both section$_{Ug-Gc}$ and section$_{Uc-Gg}$ because the GOx colloidosomes are active in both sections. The URS colloidosomes are only active in GC-M and so when urea is added to the system, a dramatic change in curvature and colour is only seen in section$_{Ug-Gc}$. As the curvature of the two sections deviates after the addition of urea, the prototissue transforms into an S shape. Addition of urea causes section$_{Ug-Gc}$ to change from negative to positive curvature and pH$_{pt}$ in this section increases. The curvature of section$_{Ug-Gc}$ reaches a maximum and after this point shows a gradual decrease, similar to prototissue$_{Ug-Gc}$. In contrast, section$_{Uc-Gg}$ shows only a small pH$_{pt}$ change that results in a slight curvature change. The slight changes that occur in section$_{Uc-Gg}$ are not due to URS/ urea reactivity in this section. The pH$_{pt}$ changed initiated within section$_{Ug-Gc}$c gradually spreads resulting a slight pH$_{pt}$ increase in section$_{Uc-Gg}$.

Interestingly, the colour of the bulk solution seems to indicate that its pH never increases to the extent that is seen in the case of a standard prototissue under the same conditions, despite in theory having the same number of URS colloidosomes in an active environment (i.e. within GC-M). Further repeats and experiments would be needed to draw a firm conclusion on this. One possible explanation is that the activity of the GOx colloidosomes in prototissue$_{Uc-Gg}$ is

higher after the addition of urea than it is in the standard prototissue. Since the pH_{pt} of this section is not rapidly increased when urea is added the pH may remain in the region of the bell shaped GOx activity curve that corresponds to higher activity. This increased GOx activity would reduce the overall pH increase of the solution and would also further account for the low change in curvature seen in section$_{Uc-Gg}$ during these experiments.

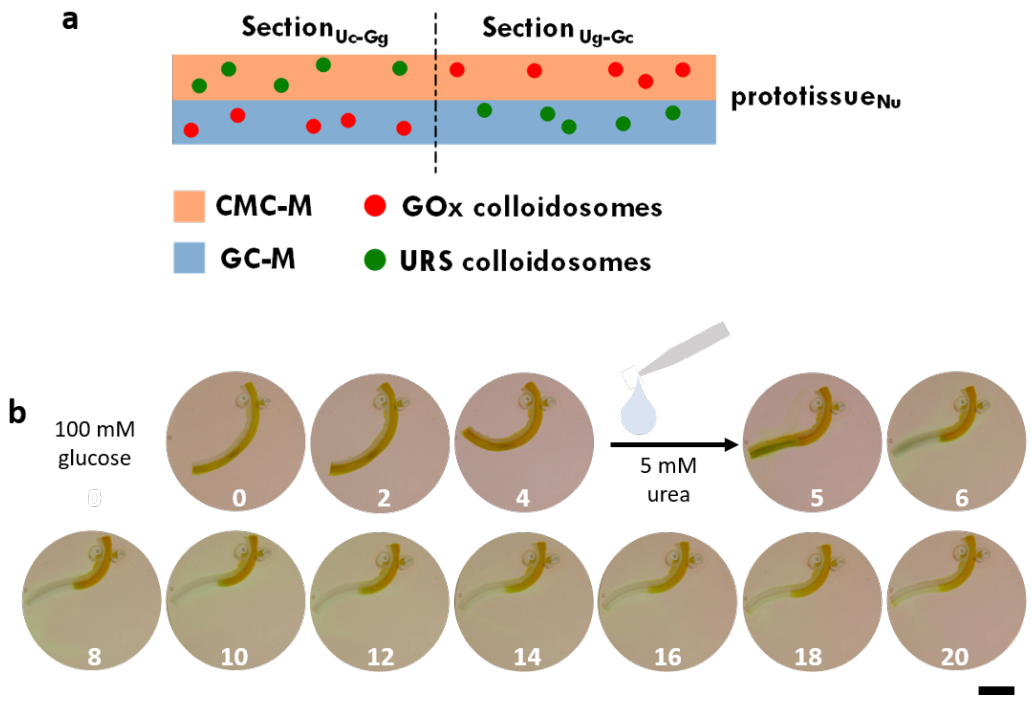

FIGURE 5.34. (a) A schematic of the non-uniform shape change resulting from the addition of substrates to prototissue$_{NU}$. The photographs in (b) show the chemo-mechanical transduction seen when the staggered addition of glucose (100 mM) and urea (5 mM, at four hours) is used with prototissue$_{NU}$. The time is shown in hours on each image and the scale bars show 1 cm.

Patterning colloidosome populations within the prototissue bilayers created a system that showed normal increase in curvature in response to one chemical fuel, but transition to an S shaped geometry upon uniform application of another. Previous examples of hydrogel actuators that show different geometries in response to a chemical stimulus have relied upon heterogeneous mechanical properties or altering the distribution of the hydrogel species, and these systems would not display the two differing responses shown here.

5.3.4.6 Assessing the role of the colloidosomes in the chemo-mechanically transducing prototissues

Figure 5.35a shows a control experiment that was carried out using a hydrogel bilayer with URS and GOx free in the hydrogel rather than encapsulated within colloidosomes. The bilayer was formed using the method described for the standard prototissue bilayer, but the colloidosome suspension was replaced with aqueous enzyme solution at the same theoretical concentration. The experiment was carried out using staggered addition of 100 mM glucose and 5 mM urea. An increase in curvature is seen upon addition of glucose indicating that enzyme remains in the system despite the washing step and overnight equilibration with UI solution. Addition of urea in the second step caused little change in curvature or colour, whereas in the standard prototissue it lead to the back and forth motion.

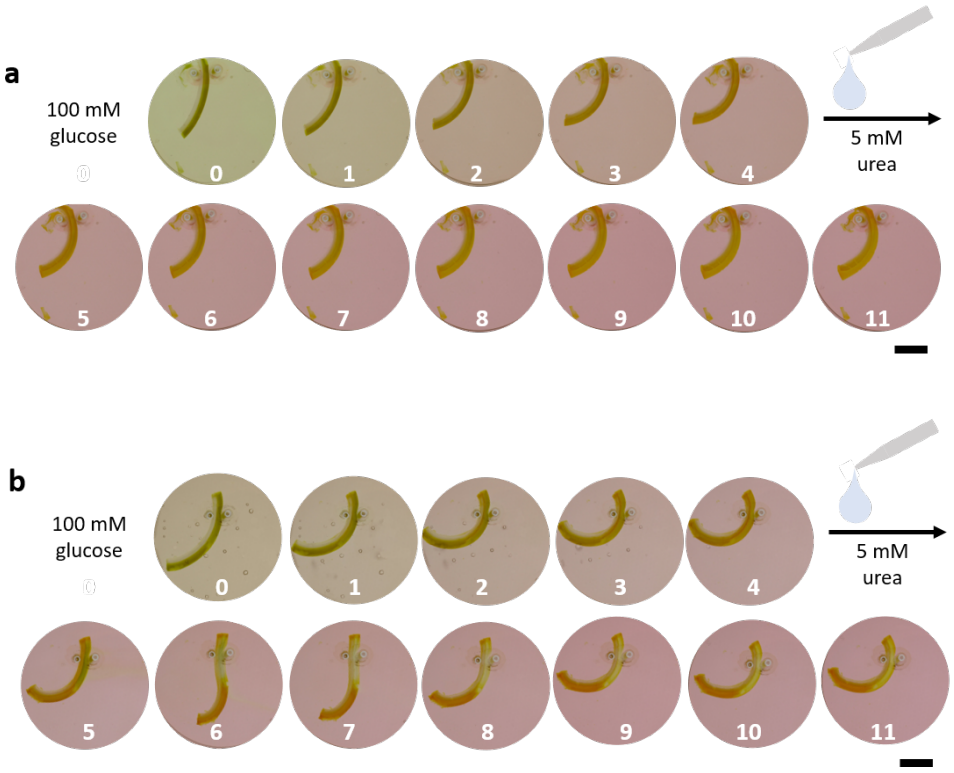

FIGURE 5.35. Experiments carried out using bilayer hydrogels formed with free enzyme solutions (a) evenly distributed throughout (equivalent to a standard prototissue) or (b) patterned (equivalent to prototissue$_{NU}$). Photographs show the result of adding 100 mM glucose followed by 5mM urea after 4 hours. The time is shown in hours on each image and the scale bars show 1 cm.

Photopatterning was used to form a hydrogel bilayer equivalent to a prototissue$_{NU}$ but the heterogeneous distribution of the enzymes was reproduced using free enzyme solutions in place of the enzyme containing colloidosomes. Again, the experiment was carried out using the same

staggered substrate method and the initial step involving the addition of glucose resulted in an increase in curvature across the whole hydrogel. Addition of 5 mM urea resulted in a change in hue_{GC-M} and curvature in section_{Ug-Gc} but little change in section_{Uc-Gg}. This mirrors what was seen when this experiment was carried out using the colloidosome prototissue. However, the hydrogel never reaches the full S shape seen in the patterned prototissue. Instead the curvature of section_{Ug-Gc} reaches around 0 and begins to decrease again. Eventually the hydrogel returns to a roughly uniform curve.

These controls indicate that, despite overnight soaking, both URS and GOx are present in the system and are not fully washed out of the hydrogel in the absence of colloidosomes. The slow reaction of the GOx colloidosomes in comparison to the URS colloidosomes is essential for creating a system where the URS/ urea reaction dominates when both substrates are present, resulting in a pH increase. Section 5.3.1 showed that free GOx is significantly more reactive than the GOx colloidosomes. The differences that occur in these free enzyme controls compared to the prototissues are in part due to increased reactivity of GOx reducing the dominance of the URS/ urea reaction.

The shape change of the patterned free enzyme hydrogel confirms that at least in the case of the URS, some of the enzyme is fixed in the hydrogel matrix. This means that enzyme encapsulation in the colloidosomes is not essential for producing enzymatically active and patternable hydrogels. However, these experiments do not prove that enzyme leaching does not occur over longer time periods and they do not prove that some leaching of free enzyme is not causing reaction to occur outside the hydrogel as well. Further work on this system should involve a greater investigation of these free enzyme hydrogels, however it could also take advantage of other properties that could only be achieved using enzymes within protocells, such as heterogeneous substrate concentrations due to interaction with the protocells or membrane gating.

5.4 Conclusions and future work

This chapter outlined the design and development of an actuating prototissue that utilised protocell mediated pH changes to convert enzymatic substrates into hydrogel actuation. To achieve this the individual components (pH changing protocell populations and a pH responsive hydrogel bilayer) were first synthesised and characterised before being combined to form the prototissue system.

Two populations of colloidosome protocells were formed using the antagonistic, pH changing enzymes GOx and URS. The protocells exhibited enzymatic activity, increasing (URS) or decreasing (GOx) the pH upon addition of the relevant substrate. Furthermore, concurrent addition of 2.5 mM urea and 100 mM glucose to a mixed population of GOx and URS colloidosomes (one-to-one ratio) resulted in a transient pH increase. Control over kinetics is required to achieve such behaviour using two opposing reactions, and an inherent difference in activity of the two protocell populations provided this .

The pH responsive bilayer hydrogel actuator was based on methacrylated carboxymethyl cellulose (CMC-M) and N-methacrylated glycol chitosan (GC-M). Photogelation was used because it is biocompatible, fast and it affords photopatterning. The methacrylated polymers rapidly gelled upon irradiation at 365 nm in the presence of I2959 photoinitiator, resulting in pH responsive hydrogels. Sequential photogelation of a CMC-M layer and a GC-M layer was used to form a novel, polysaccharide-based, hydrogel bilayer. Reversible, pH dependent changes in bilayer curvature were demonstrated within the range that can be achieved using enzymes, making this system suitable for use in the prototissue design.

Combining the synthesised components, binary colloidosome populations (URS and GOx) were included in methacrylated polymer solutions prior to gelation to colloidosome-containing GC-M or CMC-M hydrogels, which were referred to as prototissues. The prototissues exhibited similar pH responsive properties to the corresponding hydrogels without colloidosomes. Addition of glucose to prototissue monolayers formed using either GC-M or CMC-M resulted in a protocell-mediated pH decrease within the hydrogel matrix, and as a result, changes in prototissue swelling over time. In contrast, addition of urea to prototissue monolayers resulted in protocell-mediated pH increase and change in hydrogel swelling only in prototissues formed using GC-M. The protocell-mediated hydrogel swelling achieved in response to glucose or urea is an emergent property of the system, since the hydrogels themselves do not respond to these molecules.

Addition of urea or glucose to prototissue bilayers resulted in protocell mediated chemo-mechanical transduction: the chemical fuel was broken down by the protocells within the hydrogel matrix, leading to a change in pH and hydrogel actuation. The collective behaviour of the components of the prototissue converted the chemical energy of the fuel to mechanical energy causing a change in shape. The actuation process occurred over a period of several hours and was quicker in response to urea than glucose, as would be expected due to the faster activity of the URS colloidosomes. The protocell-mediated pH changes within the hydrogels were monitored by

using hue angle as a quantitative measure of the colour of universal indicator that was added to the system.

The application of a stimulus to a hydrogel actuator results in a gradual change in shape as the system shifts to the most thermodynamically stable state. Concurrent addition of two opposing stimuli still results in a single change in shape as the system simply reaches equilibrium. In contrast to this standard response, it was hypothesised that the prototissue actuator presented in this chapter would be capable of transient (out-of-equilibrium) shape changes in response to the concurrent application of two opposing chemical fuels. The system was designed to achieve this novel behaviour by relying on protocell-mediated chemo-mechanical transduction. Using the bio-chemical reactions within the protocells allowed the kinetic control that is essential to achieving such out-of-equilibrium behaviour.

The method that was developed to demonstrate this out-of-equilibrium chemo-mechanical transduction involved staggered addition of the two substrates, with glucose in excess. The initial addition of 100 mM glucose resulted in a pH decrease and an increasingly negative curvature (A->B). Subsequent addition of 5 mM urea caused a transient increase in pH, which was accompanied by a transient change in shape (B->(C->A‘)). This protocell-mediated A->B->(C->A‘) chemo-mechanical transduction is a demonstration of the novel, out-of-equilibrium behaviour for which the system was designed. The magnitude and pattern of the protocell-mediated chemo-mechanical transduction could be altered simply by changing the concentration of urea added in the second step or heterogeneously distributing the two colloidosome populations between the two layers.

In Section 1.2.7.7 complex hydrogel behaviours resembling self-regulation or autonomy were introduced as an important step towards intelligent, lifelike hydrogel materials that are of great interest in fields such as soft robotics and tissue engineering. Such behaviour has previously been shown in sol-gel transitions of small molecule gels or in swelling changes in microgel beads [87, 122]. However, aside from the unique example of the oscillating BZ reaction, the work presented in this chapter is the first example of such behaviour linked to hydrogel actuation. Furthermore, including the protocells within the hydrogel matrix to form a prototissue created a hydrogel actuator that displays novel, unique behaviours in response to the non-toxic, simple molecules urea and glucose, making this system an interesting step towards autonomous behaviour in soft materials.

Building on the work in Chapter 4 of this thesis, it was also demonstrated that heterogeneous distribution of protocells within the prototissue actuator lead to novel shape changes upon uniform application of the chemical fuels. Such changes in shape would not be possible using standard hydrogel actuators, and this feature should be explored further to allow new and more complex forms of hydrogel actuation.

Future work on this prototissue actuator should focus on improving the mechanical properties of the hydrogels used as well as increasing the rate of the protocell-mediated pH change and

the rate at which the hydrogel responds to changes in pH. The protocell-mediated pH change might be improved using different enzymes or other protocell models. Strategies that can be used to increase the response rate of hydrogels were discussed in Section 1.2.1.9, but future work utilising these principle must ensure that the hydrogel and its synthesis meet the criteria that were previously discussed to allow it to be used as a matrix to encapsulate protocells. Future work into this prototissue actuator system should also attempt to induce further cycles of actuation by adding further substrates after a first transient shape change has occurred, since initial attempts to achieve this during this project were unsuccessful.

In the agarose prototissues developed in Chapter 4, free enzymes freely diffused through the hydrogel matrix and thus heterogeneous enzyme distribution was only achieved when the enzymes were within the protocells. In the hydrogels shown here, initial experiments showed that enzyme activity and patterning (of URS) could be achieved by including free enzyme in the pre-gel solution, although the balance of kinetics between the antagonistic reaction is distorted. Further investigation is required to determine whether all the enzyme activity for both species is occurring within the hydrogel or whether GOx has leeched out and is reacting in the bulk solution. Due to the charged nature of the polymers used and the surface charge of proteins in solution (along with the low polymer concentration and large pores of the hydrogels), it may be that the proteins are held within the hydrogel by electrostatic interactions, which would limit their use in certain conditions. Future investigations should determine the stability of these free enzyme systems for comparison with the prototissues. Despite the possibility of creating these actuators without the use of colloidosomes, there are reasons why future work may want to utilise the prototissue model. It was shown that colloidosomes within the prototissue take up fluorescent dyes from solution, increasing their concentration relative to the outside. This ability for substrate concentration, is one example of a feature of protocells that could be used to increase the behavioural complexity of the system that could not be achieved using free enzymes. Additionally, protocell models that exhibit features such as stimuli responsive membrane gating or encapsulation of cell free gene expression systems could be used .

The weaknesses that were highlighted in the method for monitoring internal hydrogel pH using hue angle measurements could be overcome by developing ways to fixed mixed indicator systems within the hydrogel matrix rather than having them in the bulk solution. This could be achieved by methacrylation of the pH indicator molecules so that they copolymerise with the polymers during the hydrogelation. Initial investigations carried out into the methacrylation of two indicators (phenol red and alizarin red S) showed that they could be successfully functionalised with the methacrylate moiety and that polymers could be formed. Although further investigation is needed to achieve incorporation into hydrogels, these novel species show great potential for future work in this project and more generally in new pH detecting materials.

In summary, this chapter presented new pH changing protocells systems, a novel, biocompatible, photogelated polysaccharide bilayer, and successfully demonstrated a

prototissue actuator capable of protocell-mediated chemo-mechanical transduction and novel out-of-equilibrium transient shape changes. The work in this chapter further serves as a proof of principle study with potential applications in a variety of contexts, including protocell research and soft robotics.

CHAPTER 6

THESIS CONCLUSIONS

Bottom-up synthetic biology has produced many elegant and increasingly complex protocell models, but there are few examples so far of multi-protocellular communities that exhibit emergent behaviours. The aim of the research reported in this thesis was to design and produce rudimentary synthetic prototissues by embedding colloidosome protocells within polysaccharide hydrogels.

Colloidosome protocells have previously been assumed to be hollow, aqueous-filled capsules that can encapsulate large biological molecules due to their semi-permeable membrane. This research showed that in fact, the TMOS crosslinking of the Pickering emulsion results in secondary silica phase within the colloidosome lumen. The MWCO of colloidosomes was shown to be above the molecular weight of many proteins used in protocell work, and thus it was concluded that the encapsulation of proteins in colloidosome models, which is essential to their function as protocells, is often due to adsorption of the proteins onto the secondary silica network, rather than the permeability of the membrane.

Immobilising colloidosome protocells within hydrogels to form rudimentary prototissues did not perturb the hydrogelation or alter the structure of the colloidosomes. Protocells retained enzymatic activity within the prototissue in most cases, because like the natural ECM, the hydrogel allows passage of small molecules. Due to their large size, colloidosomes are trapped in the hydrogel matrix and can be distributed in patterns. Patterning of colloidosome populations in the hydrogels mimics the heterogeneous nature of living tissues. Non-uniform application of enzyme substrates to hydrogels that contain heterogeneously distributed colloidosome populations resulted in patterned enzymatic reactions.

Prototissues formed from agarose and alginate were used in a modular system to pattern colloidosomes within the hydrogel. Chemical communication between binary protocell populations

resulted in patterned enzymatic reactions that could be extended to shapes in 3D. The enzymatic product appeared in transient, pre-programmed patterns and lead to the in-situ formation of chemical gradients.

A more complex prototissue model was created by embedding colloidosomes within a novel pH responsive polysaccharide hydrogel bilayer. The result was an actuating prototissue, that utilised protocell mediated pH changes to convert enzymatic substrates into hydrogel actuation. Two antagonistic protocell populations were used, and due to differences in the kinetics of the opposing reactions, transient changes in shape were achieved. The protocell-mediated chemo-mechanical transduction and novel out-of-equilibrium behaviour occurred due to the collective behaviour of the components. Such behaviours cannot be achieved by the direct application of a stimulus to a normal hydrogel actuator, and are a step towards autonomous, life-like hydrogels.

The work presented in this thesis is part of a new trend within synthetic biology that makes use of interactions between protocell populations, and the results here demonstrate that brining protocells together within prototissues allows you to achieve complex emergent behaviours, even when using a basic protocell model. Although the colloidosome protocells used here are not designed to be prebiotically relevant, it is also interesting to reflect upon this in the context of the origin of life: even systems of simple abiotic droplets or early cells could have exhibited complex behaviours as emergent properties, arising from simple features such as the diffusion of molecules between droplets (communication), spatial segregation of two populations, or a mismatch in kinetics between populations carrying out opposing reactions.

For those outside the field of protocell research, the use of protocells within the hydrogel matrix is also a novel way of building new functional soft materials. Smart hydrogels, particularly those that show more complex behaviour such as non-uniform response to a stimuli, actuation, or out-of-equilibrium behaviour, are of great interest to a variety of fields. This thesis shows that hydrogel prototissues can be designed that are capable of such behaviours, but there is great potential for this to be developed further in future work. This thesis made use of colloidosome protocells, but other protocells such as proteinosomes, coacervates or lipid vesicles could be used instead. Protocell models have been designed that are capable of a huge range of behaviours, including many different chemical and biochemical reactions, replication, stimuli responsive gating, gene directed protein synthesis and various responses to both chemical and physical stimuli. Similarly, hydrogels can be designed to show many unique properties, including biocompatibility, and response to many different stimuli. Given the variety of properties that it is possible to achieve in both hydrogels and protocells, hydrogel prototissues that combine these properties and exhibit collective behaviour between the component parts, are an exciting new option for the creation of smart soft materials.

APPENDIX A

A.1 Appendix to Chapter 3

A.1.1 Colloidosome structure

Figure A.1 shows colloidosomes formed via homogenisation. After addition of the aqueous phase to the silica nanoparticles in oil, the samples were homogenised at 10 krpm for 30 s to form the emulsion. Samples were crosslinked, transferred to water and then stained with Rhodamine B using a similar procedure to that described in section 3.3.1. All samples show Rhodamine b adsorption inside indicating the presence of a secondary silica network. Comparing Figure A.1a and Figure A.1b it is apparent that increased TMOS used for crosslinking increases the internal fluorescence intensity implying that there is more dye adsorbed and likely an increase in the density of the secondary silica.

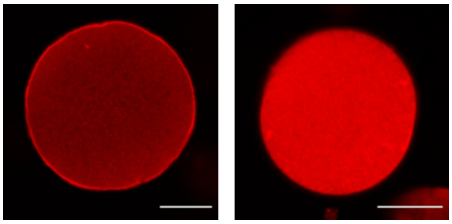

FIGURE A.1. Colloidosomes formed with an aqueous phase of pH 7 containing no dissolved protein. Samples were formed with dodecane as the oil phase and the emulsion was formed via homogenisation. The sample in (a) was crosslinked using 10 μL TMOS and (b) used 20 μL. Samples were transferred to water and incubated with Rhodamine B solution. The excess dye was washed away prior to imaging and fluorescence indicates the presence of silica due to adsorption of the dye. Scale bars 20 μm.

A.1.2 Colloidosome SEM

Figure's A.2 to A.7 are enlarged versions of images included in Figure 3.5.

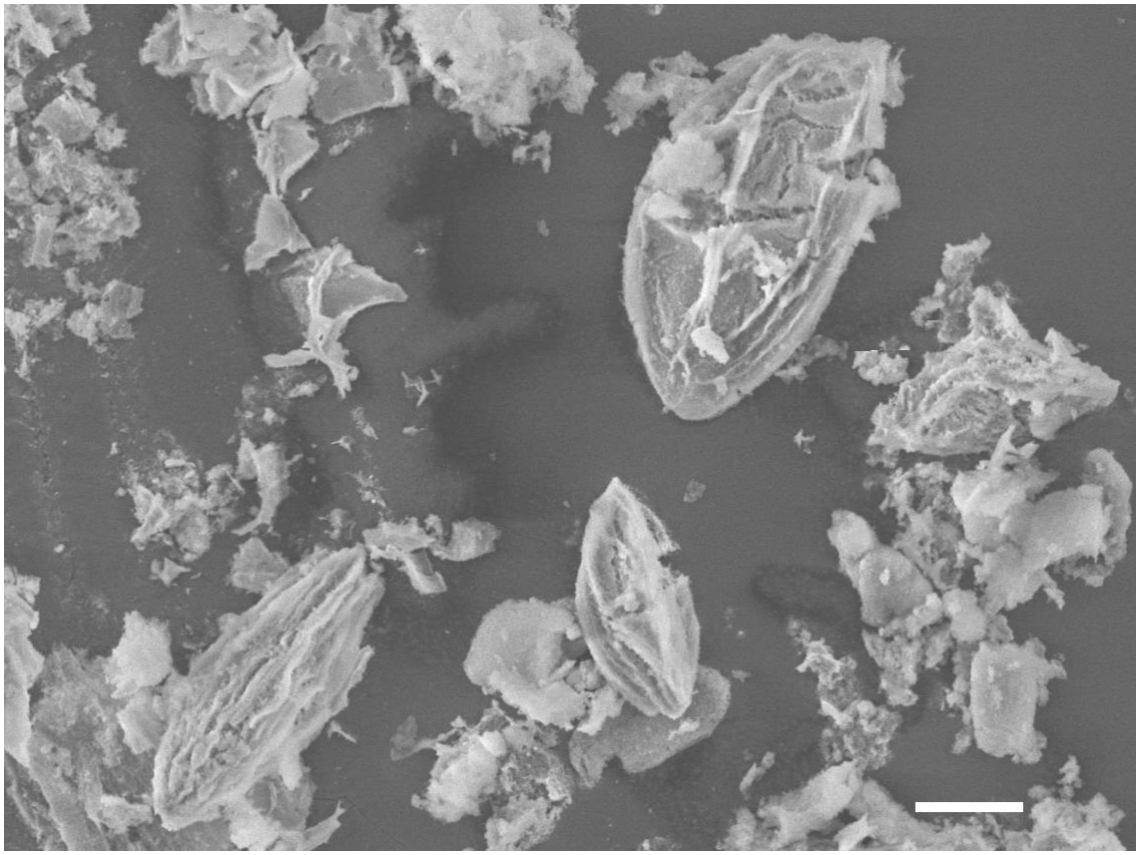

FIGURE A.2. Colloidosomes were formed via handshaking with aqueous phase pH 4. After crosslinking with TMOS and transfer to water, SEM samples were prepared by lyophilisation. Scale bar shows 20 μm.

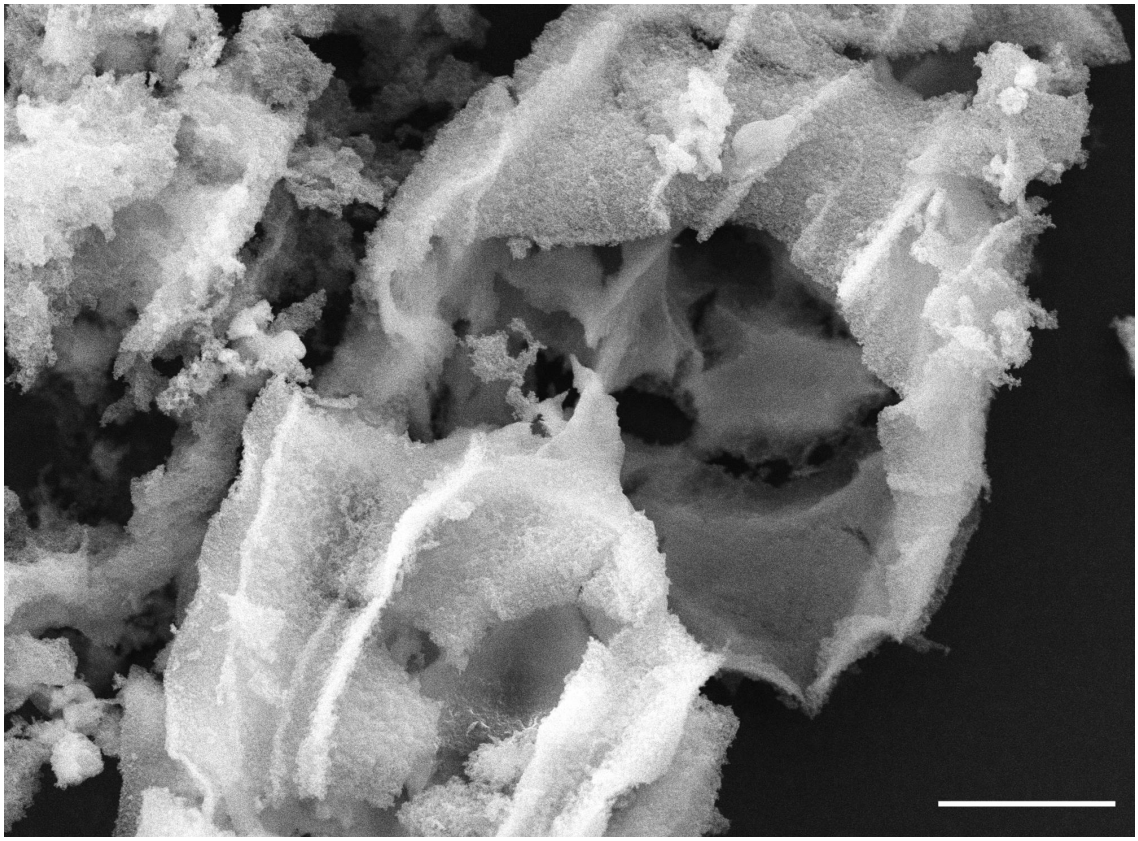

FIGURE A.3. Colloidosomes were formed via handshaking with aqueous phase pH 4. After crosslinking with TMOS and transfer to water, SEM samples were prepared by lyophilisation. Scale bar shows 10 μm.

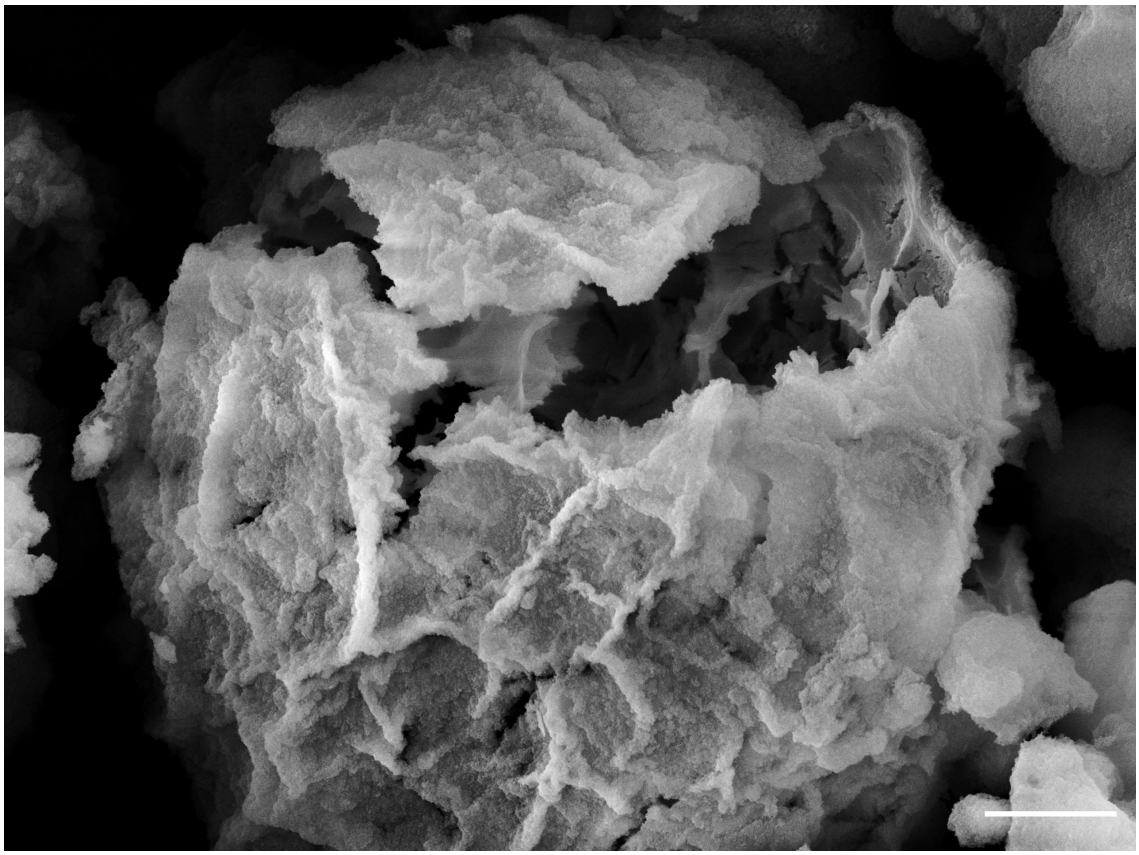

FIGURE A.4. Colloidosomes were formed via handshaking with aqueous phase pH 4. After crosslinking with TMOS and transfer to water, SEM samples were prepared by freeze thawing and subsequent air drying. Scale bar shows 10 μm.

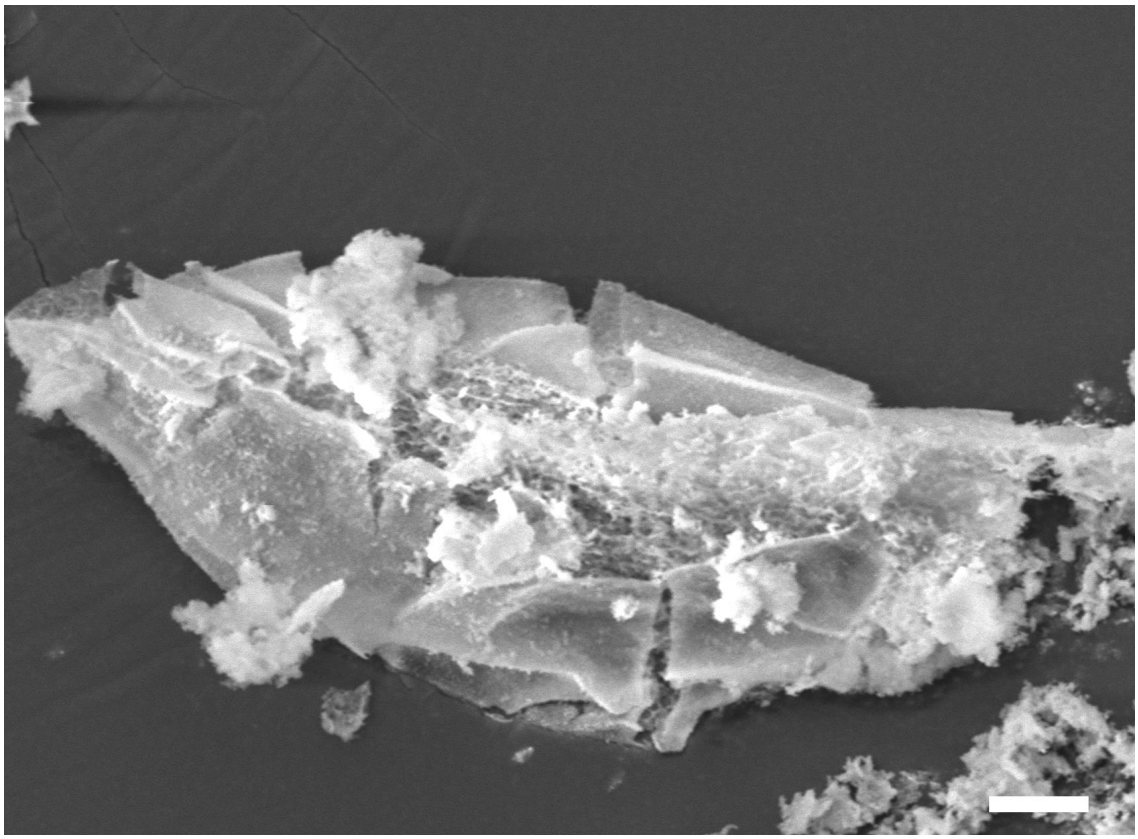

FIGURE A.5. Colloidosomes were formed via handshaking with aqueous phase pH 5. After crosslinking with TMOS and transfer to water, SEM samples were prepared by lyophilisation. Scale bar shows 10 μm.

FIGURE A.6. Colloidosomes were formed via handshaking with aqueous phase pH 7. After crosslinking with TMOS and transfer to water, SEM samples were prepared by lyophilisation. Scale bar shows 10 μm.

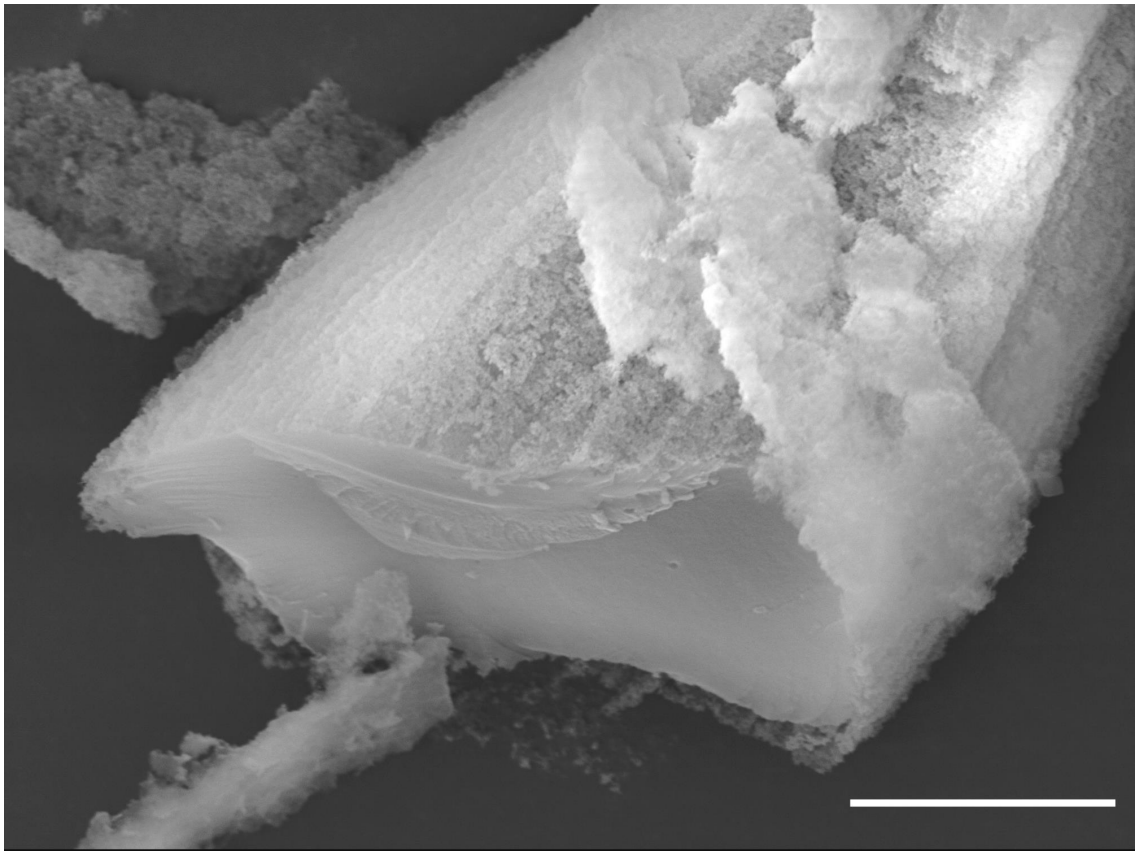

FIGURE A.7. Colloidosomes were formed via handshaking with aqueous phase pH 8. After crosslinking with TMOS and transfer to water, SEM samples were prepared by lyophilisation. Scale bar shows 10 μm.

A.1.3 Colloidosome permeability

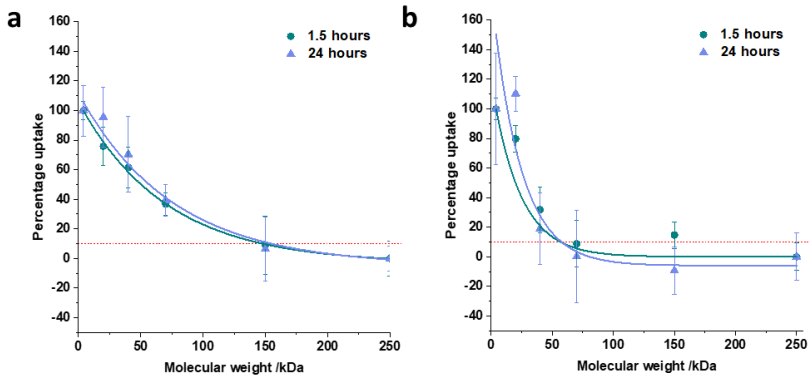

FIGURE A.8. Plots used in the calculation of the MWCO of colloidosomes formed at (a) pH 4 and (b) pH 8. The fluorescence intensity ratio was measured for colloidosomes in FITC-dextran solutions at different molecular weights, after either 1.5 or 24 hours incubation at room temperature. Curves were fitted with a monoexponential decay. To calculate the percentage uptake the uptake of 4 kDa polymer is assumed to be 100% and the uptake of 250 kDa polymer is assumed to be 0%. The molecular weight where only 10% of the polymer diffuses into the capsule is said to be the MWCO.

A.1.4 Protein adsorption by colloidosomes formed at different pHs

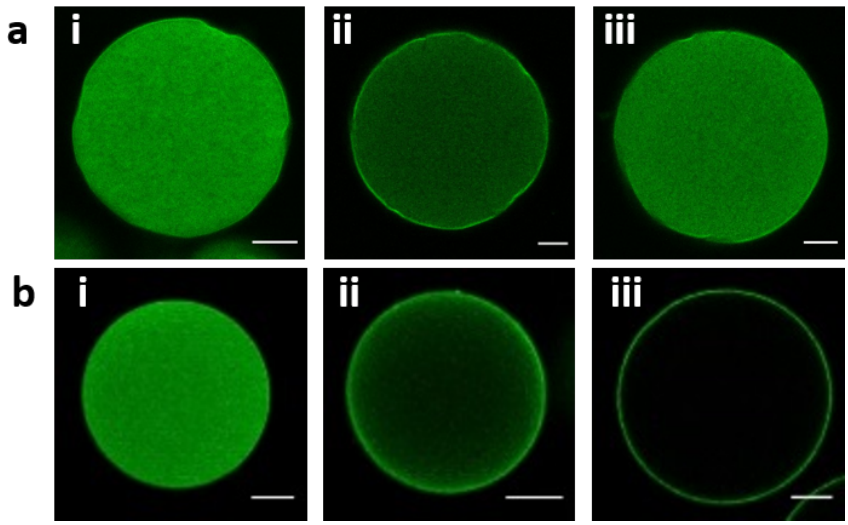

FIGURE A.9. Confocal microscopy images of colloidosomes formed with aqueous phase at (a) pH 7 or (b) pH 8 and incubated with (i) FITC-HRP, (ii) FITC-BSA and (iii) FITC-GOx. Samples were incubated for 24 hours and then washed prior to imaging. All scale bars represent 20 μm.

A.1.5 Enzyme kinetics

Experiments using 450 μM H_2O_2, 500 μM *o*PD and varied colloidosome volumes were run for a total time of 1 hour (by which time all had plateaued) (Figure A.10a). The average values for the final fluorescence intensity are plotted in Figure A.10b. Very low levels of fluorescence are seen when no colloidosomes are added, confirming that HRP colloidosomes are responsible for the reaction. When the colloidosome volume is increased from 10 μL to 50 μL a small increase in final fluorescence intensity is observed. This could indicate that the low colloidosome volume means the reaction is not yet complete, but it may also be within error. Interestingly further increase in colloidosome number to 250 μL or 500 μL leads to a decrease in the final fluorescence intensity, which can be seen in the fluorescence plots as they plateau at a lower level. There are two possible explanations for this: it might be that increased scattering due to high colloidosome density leads to decreased in measured fluorescence, alternatively it may be that due to the adsorptive nature of the silica colloidosomes, some fluorescent product is being retained within the colloidosomes and thus is not in solution to be measured. This effect would obviously be exaggerated with increased colloidosome volumes. Since the fluorescence after one hour was

highest for the samples run with 50 μL colloidosomes, this value was assumed to be equivalent to the fluorescence of 225 μM DAP (maximum concentration based on using 450 μM H_2O_2 and 500 μM *o*PD) and so was used for the conversion of fluorescence intensity to [DAP].

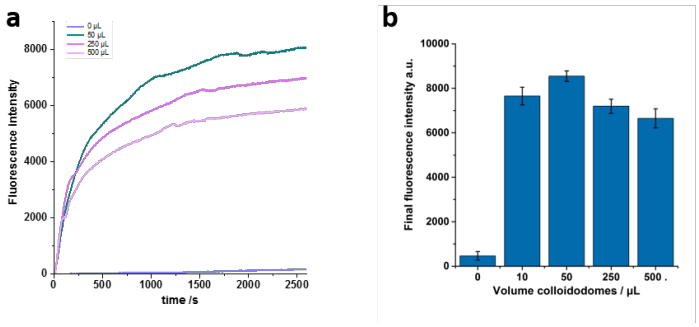

FIGURE A.10. (a) shows plots of fluorescence intensity over time for samples run with different amounts of colloidosome added to the well, all run with 450 μM H_2O_2 and 500 μM *o*PD. The volume of colloidosomes per sample well is indicated in the key. (b) Is a plot of the average fluorenone intensity after 1 hour for samples run with different colloidosome volumes.

A.2 Appendix to Chapter 4

A.2.1 Rheology

Rheological testing is often used to investigate the mechanical properties of hydrogels. Figure A.11 shows SAOS strain sweep experiments carried out on agarose hydrogels with or without colloidosomes. At low strain values agarose hydrogels show a value of the elastic modulus (G‘) which is greater than the viscous modulus (G“) as would be expected for a hydrogel. Due to the low polymer concentration of the gels (1% w/v) the agarose hydrogels showed a linear G‘ only at low strain values and showed relatively high values of G“ (which for many hydrogels are unmeasurable [73]). Agarose hydrogels containing colloidosomes showed linear behaviour up to higher strain values and showed much lower G“ values. The behaviour exhibited still resembled that which would be expected for a hydrogel, and in fact appeared to show an increase in the elastic/ solid nature of the material. This may indicate interactions between the agarose and the silica of the colloidosomes, but more detailed rheological characterisation is needed to understand this. Colloidosome containing hydrogels sometimes tore during the rheological tests, something which was not seen for agarose only hydrogels. This implies that colloidosomes make the hydrogel more brittle.

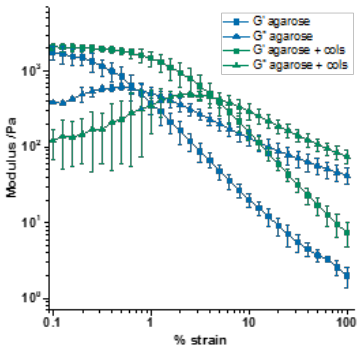

FIGURE A.11. SAOS strain sweeps of agaorse hydrogels with and without imobilised colloidosomes.

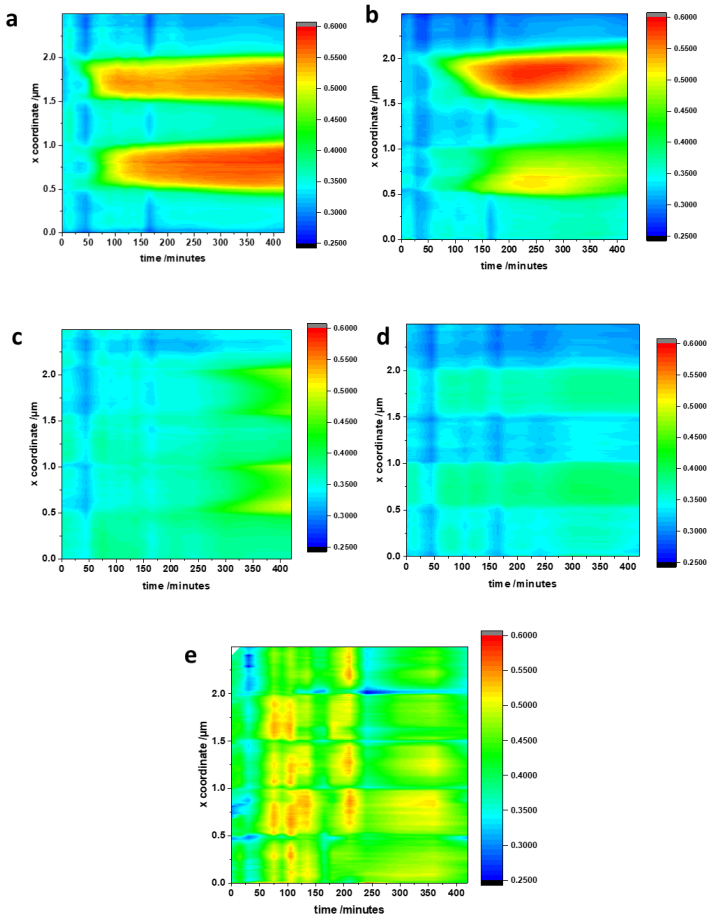

FIGURE A.12. Contour plots of the saturation over time for the composite hydrogels shown in (a) Figure 4.15 (b) Figure 4.16 (c) Figure 4.17 (d) Figure 4.18 (e) Figure 4.20 .

A.3 Appendix to Chapter 5

A.3.1 Refinement of colloidosome formation

Glucose oxidase colloidosomes formed using aqueous phases at various pH's and an enzyme concentration of 2270 U/mL are shown in Figure A.13. The use of acidic pH does not seem to dramatically affect the activity of colloidosomes after transfer to water. GOx colloidosomes formed at pH 4 had non-deformed spherical structures and hence this pH was chosen for formation. The process was repeated for URS colloidosomes with an initial enzyme concentration of 2853 U/mL. The highest activity was achieved with an internal aqueous pH of 8, but colloidosomes were still able to produce a rapid pH change when acidic pH was used. Since Chapter 3 showed that the pH at formation affects the structure of the resulting colloidosomes, a pH of 4.5 was used for URS colloidosome formation for the remainder of this thesis since this gave rapidly acting colloidosomes with spherical structure at a pH similar to that used for GOx colloidosomes.

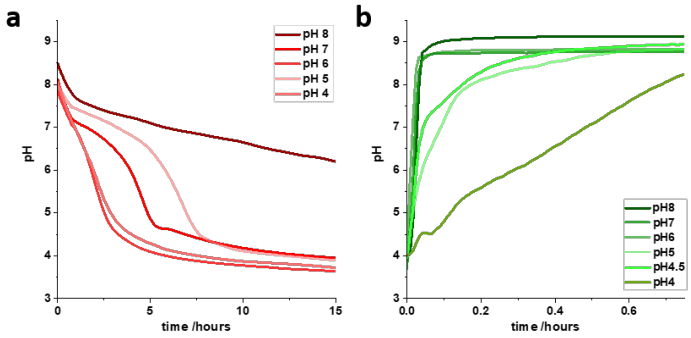

FIGURE A.13. Colloidosomes were formed with varied initial aqueous phase pH and transferred to water. The graphs show the pH changes resulting from addition of (a) 100 mM glucose to GOx colloidosomes or (b) 5 mM urea to URS colloidosomes.

BIBLIOGRAPHY

[1] B. Alberts, A. Johnson, J. Lewis, D. Morgan, M. Raff, K. Roberts, and P. Walter.
Molecular Biology of the Cell.
Garland Science, 6 edition, 2008.

[2] S. Mann.
Systems of creation: The emergence of life from nonliving matter.
Accounts of Chemical Research, 45(12):2131–2141, 2012.

[3] A.J. Dzieciol and S. Mann.
Designs for life: Protocell models in the laboratory.
Chemical Society Reviews, 41(1):79–85, 2012.

[4] M. Li, X. Huang, T-Y.D. Tang, and S. Mann.
Synthetic cellularity based on non-lipid micro-compartments and protocell models.
Current opinion in chemical biology, 22:1–11, 2014.

[5] M. Li, D.C. Green, J.L.R. Anderson, B.P. Binks, and S. Mann.
In vitro gene expression and enzyme catalysis in bio-inorganic protocells.
Chemical Science, 2(9):1739–1745, 2011.

[6] X. Huang, M. Li, D.C. Green, D.S. Williams, A.J. Patil, and S. Mann.
Interfacial assembly of protein-polymer nano-conjugates into stimulus-responsive biomimetic protocells.
Nature communications, 4:2239, 2013.

[7] A.F. Mason and P. Thordarson.
Polymersomes as protocellular constructs.
Journal of Polymer Science, Part A: Polymer Chemistry, 55(23):3817–3825, 2017.

[8] S. Koga, D.S. Williams, A.W. Perriman, and S. Mann.
Peptide-nucleotide microdroplets as a step towards a membrane-free protocell model.
Nature Chemistry, 3(9):720–724, 2011.

[9] J. Fothergill, M. Li, S.A. Davis, J.A. Cunningham, and S. Mann.

Nanoparticle-based membrane assembly and silicification in coacervate microdroplets as a route to complex colloidosomes.
Langmuir, 30(48):14591–14596, 2014.

[10] A.F. Mason, B.C. Buddingh, D.S. Williams, and Jan C.M. Van Hest.
Hierarchical Self-Assembly of a Copolymer-Stabilized Coacervate Protocell.
Journal of the American Chemical Society, 139(48):17309–17312, 2017.

[11] X. Huang, M. Li, and S. Mann.
Membrane-mediated cascade reactions by enzyme-polymer proteinosomes.
Chemical communications (Cambridge, England), 50(47):6278–80, 2014.

[12] M. Nijemeisland, L.K.E.A. Abdelmohsen, W.T.S. Huck, D.A. Wilson, and J.C.M. Van Hest.
A compartmentalized out-of-equilibrium enzymatic reaction network for sustained autonomous movement.
ACS Central Science, 2(11):843–849, 2016.

[13] P. Atkins and J.D. Paula.
Physical Chemistry.
Oxford University Press, 9 edition, 2009.

[14] Y. Chevalier and M.A. Bolzinger.
Emulsions stabilized with solid nanoparticles: Pickering emulsions.
Colloids and Surfaces A: Physicochemical and Engineering Aspects, 439:23–34, 2013.

[15] B.P. Binks.
Particles as surfactants- similarities and differences.
Current Opinion in Colloid & Interface Science, 7(1-2):21–41, 2002.

[16] P.H.R. Keen, N.K.H. Slater, and A.F. Routh.
Encapsulation of amylase in colloidosomes.
Langmuir, 30(8):1939–1948, 2014.

[17] H. Jiang, L. Hong, Y. Li, and T. Ngai.
All-Silica Submicrometer Colloidosomes for Cargo Protection and Tunable Release.
Angewandte Chemie - International Edition, 57(36):11662–11666, 2018.

[18] L. Rodríguez-Arco, M. Li, and S. Mann.
Phagocytosis-inspired behaviour in synthetic protocell communities of compartmentalized colloidal objects.
Nature Materials, 16(8):857–863, 2017.

[19] S. Sun, M. Li, F. Dong, S. Wang, L. Tian, and S. Mann.

Chemical Signalling and Functional Activation in Colloidosome-Based Protocells.
Small, 12(14):1920–1927, 2016.

[20] M. Li, X. Huang, and S. Mann.
Spontaneous Growth and Division in Self-Reproducing Inorganic Colloidosomes.
Small, 10(16):3291–3298, 2014.

[21] M. Li, R. Harbron, J. Weaver, B.P. Binks, and S. Mann.
Electrostatically gated membrane permeability in inorganic protocells.
Nature chemistry, 5:529–536, 2013.

[22] K. Akkarachaneeyakorn, M. Li, S.A. Davis, and S. Mann.
Secretion and Reversible Assembly of Extracellular-like Matrix by Enzyme-Active Colloidosome-Based Protocells.
Langmuir, 32(12):2912–2919, 2016.

[23] Y. Qiao, M. Li, R. Booth, and S. Mann.
Predatory behaviour in synthetic protocell communities.
Nature Chemistry, 9(2):110–119, 2017.

[24] T-Y.D. Tang, D. Cecchi, G. Fracasso, D. Accardi, A. Coutable-Pennarun, S.S. Mansy, A.W. Perriman, J.L.R. Anderson, and S. Mann.
Gene-Mediated Chemical Communication in Synthetic Protocell Communities.
ACS Synthetic Biology, 7(2):339–346, 2018.

[25] S. Hennig, G. Rödel, and K. Ostermann.
Artificial cell-cell communication as an emerging tool in synthetic biology applications.
Journal of biological engineering, 9(1):13, 2015.

[26] R. Lentini, N. Yeh Martín, and S. Mansy.
Communicating artificial cells.
Current Opinion in Chemical Biology, 34:53–61, 2016.

[27] R. Lentini, S.P. Santero, F. Chizzolini, D. Cecchi, J. Fontana, M. Marchioretto, C. Del Bianco, J.L. Terrell, A.C. Spencer, L. Martini, M. Forlin, M. Assfalg, M.D. Serra, W.E. Bentley, and S.S. Mansy.
Integrating artificial with natural cells to translate chemical messages that direct E. coli behaviour.
Nature Communications, 5:1–6, 2014.

[28] P. Carrara, P. Stano, and P.L. Luisi.
Giant Vesicles "Colonies": A Model for Primitive Cell Communities.
ChemBioChem, 13(10):1497–1502, 2012.

[29] P. Gobbo, A.J. Patil, M. Li, R. Harniman, W.H. Briscoe, and S. Mann.
Programmed assembly of synthetic protocells into thermoresponsive prototissues.
Nature Materials, 17(12):1145–1153, 2018.

[30] S. Mantri and K. Tanuj Sapra.
Evolving protocells to prototissues: Rational design of a missing link.
Biochemical Society Transactions, 41(5):1159–1165, 2013.

[31] M.J. Booth, V.R. Schild, A.D. Graham, S. Olof, and H. Bayley.
Light-activated communication in synthetic tissues.
Science Advances, pages 1–12, 2016.

[32] G. Villar, A.D. Graham, and H. Bayley.
A Tissue-Like Printed Material Gabriel.
Science, 46(4):564–574, 2013.

[33] M.J. Booth, V. Restrepo Schild, S.J. Box, and H. Bayley.
Light-patterning of synthetic tissues with single droplet resolution.
Scientific Reports, 7(1):1–10, 2017.

[34] M.J. Booth and H. Bayley.
3D-printed synthetic tissues.
Biochemist, 38(4):16–19, 2016.

[35] B. Escuder and J.F. Miravet, editors.
Functional Molecular Gels.
The Royal Society of Chemistry, 2013.

[36] L.H. Sperling.
Introduction to Physical Polymer Science.
Wiley, 2005.

[37] J. Siepmann, R.A. Siegel, and M.J. Rathbone.
Fundamentals and applications of controlled release drug delivery.
Springer, 2012.

[38] A.Y. Malkin.
Rheology fundamentals.
Chemtec Publishing, 1994.

[39] G. Gerlach and K.F. Arndt.
Hydrogel Sensors and Actuators.
Springer Series on Chemical Sensors and Biosensors, 6:1–15, 2009.

[40] Yohei K. Ravin N. Aoyagi, M.E.
Smart Biomaterials.
Springer, 2014.

[41] H Francis Mark.
Encyclopedia of Polymer Science and Technology, volume 2.
Wiley, 2002.

[42] S.R. Caliari and J.A. Burdick.
A practical guide to hydrogels for cell culture.
Nature methods, 13(5):405–14, 2016.

[43] M.A. Shahbazi, T. Bauleth-Ramos, and H.A. Santos.
DNA Hydrogel Assemblies: Bridging Synthesis Principles to Biomedical Applications.
Advanced Therapeutics, 1(4):1800042, 2018.

[44] J. Clayden, N. Greeves, and S. Warren.
Organic Chemistry.
Oxford University Press, 2012.

[45] M Rinaudo.
Chitin and chitosan: Properties and applications.
Progress in Polymer Science (Oxford), 31(7):603–632, 2006.

[46] C Chang, M He, J Zhou, and L Zhang.
Swelling behaviors of pH- and salt-responsive cellulose-based hydrogels.
Macromolecules, 44(6):1642–1648, 2011.

[47] A. Reeves, R.and Ribeiro, L. Lombardo, R. Boyer, and J.B. Leach.
Synthesis and Characterization of Carboxymethylcellulose- Methacrylate Hydrogel Cell Scaffolds.
Polymers, 23(1):252–264, 2010.

[48] S. Kabir, P.P. Sikdar, B. Haque, M. A. Bhuiyan, A. Ali, and M. N. Islam.
Cellulose-based hydrogel materials: chemistry, properties and their prospective applications.
Progress in Biomaterials, 7(3):153–174, 2018.

[49] N. Fatin-Rouge, A. Milon, J. Buffle, R. Goulet, and A. Tessier.
Diffusion and partitioning of solutes in agarose hydrogels: The relative influence of electrostatic and specific interactions.
Journal of Physical Chemistry B, 107(44):12126–12137, 2003.

[50] B.S. Kim, T.Y. Yeo, Y.H. Yun, B.K. Lee, Y.W. Cho, and S.S. Han.
Facile preparation of biodegradable glycol chitosan hydrogels using divinyladipate as a crosslinker.
Macromolecular Research, 17(10):734–738, 2009.

[51] W.N.E. van Dijk-Wotthuis, O. Franssen, H. Talsma, M. J. van Steenbergen, J. J. Kettenes-van den Bosch, and W. E. Hennink.
Synthesis, Characterization, and Polymerization of Glycidyl Methacrylate Derivatized Dextran.
Macromolecules, 28(18):6317–6322, 1995.

[52] N. Russ, B.I. Zielbauer, K. Koynov, and T.A. Vilgis.
Influence of nongelling hydrocolloids on the gelation of agarose.
Biomacromolecules, 14(11):4116–4124, 2013.

[53] B.G. Amsden, A. Sukarto, D.K. Knight, and S.N. Shapka.
Methacrylated glycol chitosan as a photopolymerizable biomaterial.
Biomacromolecules, 8(12):3758–3766, 2007.

[54] P. Martens and K. S. Anseth.
Characterization of hydrogels formed from acrylate modified poly(vinyl alcohol) macromers.
Polymer, 41(21):7715–7722, 2000.

[55] S. Arnott, A. Fulmer, W. E. Scott, I. C.M. Dea, R. Moorhouse, and D. A. Rees.
The agarose double helix and its function in agarose gel structure.
Journal of Molecular Biology, 90(2):269–284, 1974.

[56] A.S. Hoffman.
Hydrogels for biomedical applications.
Advanced Drug Delivery Reviews, 64:18–23, 2012.

[57] E. Mirzaei B., A. Ramazani, M. Shafiee, and M. Danaei.
Studies on glutaraldehyde crosslinked chitosan hydrogel properties for drug delivery systems.
International Journal of Polymeric Materials and Polymeric Biomaterials, 62(11):605–611, 2013.

[58] J. Duan, X. Liang, Y. Cao, S. Wang, and L. Zhang.
High strength chitosan hydrogels with biocompatibility via new avenue based on constructing nanofibrous architecture.
Macromolecules, 48(8):2706–2714, 2015.

[59] J. Duan, X. Liang, K. Zhu, J. Guo, and L. Zhang.
Bilayer hydrogel actuators with tight interfacial adhesion fully constructed from natural polysaccharides.
Soft Matter, 13(2):345–354, 2017.

[60] V.X. Truong, M.P. Ablett, H.T.J. Gilbert, J Bowen, S.M. Richardson, J.A. Hoyland, and A.P Dove.
In situ-forming robust chitosan-poly(ethylene glycol) hydrogels prepared by copper-free azide-alkyne click reaction for tissue engineering.
Biomaterials Science, 2(2):167–175, 2014.

[61] Y. Gnanou and M. Fontanille.
Organic and Physical Chemistry of Polymers.
Wiley, 2007.

[62] W. N.E. van Dijk-Wotthuis, O. Franssen, H. Talsma, M. J. van Steenbergen, J. J. Kettenes-van den Bosch, and W. E. Hennink.
Synthesis, Characterization, and Polymerization of Glycidyl Methacrylate Derivatized Dextran.
Macromolecules, 28(18):6317–6322, 1995.

[63] S. Kim and C. Chu.
In vitro Release Behaviour of Dextran-Methacrylate Hydrogels Using DOxorubicin and Other Model Compounds.
Journal of Biomaterials Applications, 15:23–46, 2000.

[64] Y.D. Park, N. Tirelli, and J.A. Hubbell.
Photopolymerized hyaluronic acid-based hydrogels and interpenetrating networks.
Biomaterials, 24:893–900, 2003.

[65] D.R. Albrecht, V.L. Tsang, R.L. Sah, and S.N. Bhatia.
Photo- and electropatterning of hydrogel-encapsulated living cell arrays.
Lab on a Chip, 5(1):111–118, 2005.

[66] Y. Yin, X. Lv, H. Tu, S. Xu, and H. Zheng.
Preparation and swelling kinetics of pH-sensitive photocrosslinked hydrogel based on carboxymethyl chitosan.
Journal of Polymer Research, 17(4):471–479, 2010.

[67] G. Hermanson.
Bioconjugate Techniques.
Academic Press, 3 edition, 2013.

[68] D.J. Beebe, J.S. Moore, J.M. Bauer, Q. Yu, R.H. Liu, C Devadoss, and B.H. Jo.
Functional hydrogel structures for autonomous flow control inside microfluidic channels.
Nature, 404(6778):588–590, 2000.

[69] J. Torgersen, X. Qin, Z. Li, A. Ovsianikov, R. Liska, and J. Stampfl.
Hydrogels for two-photon polymerization: A toolbox for mimicking the extracellular matrix.
Advanced Functional Materials, 23(36):4542–4554, 2013.

[70] D. Wang, X. Yang, Q. Liu, L. Yu, and J. Ding.
Enzymatically cross-linked hydrogels based on a linear poly(ethylene glycol) analogue for controlled protein release and 3D cell culture.
Journal of Materials Chemistry B, 6(38):6067–6079, 2018.

[71] A. Vashist, A. Kaushik, A. Ghosal, J. Bala, R. Nikkhah-Moshaie, W. A. Wani, P. Manickam, and M. Nair.
Nanocomposite Hydrogels: Advances in Nanofillers Used for Nanomedicine.
Gels, 4(3):75, 2018.

[72] M. L. Oyen.
Mechanical characterisation of hydrogel materials.
International Materials Reviews, 59(1):44–59, 2014.

[73] J.M. Zuidema, C.J. Rivet, R.J. Gilbert, and F.A. Morrison.
A protocol for rheological characterization of hydrogels for tissue engineering strategies.
Journal of Biomedical Materials Research - Part B Applied Biomaterials, 102(5):1063–1073, 2014.

[74] E.S. Dragan.
Design and applications of interpenetrating polymer network hydrogels. A review.
Chemical Engineering Journal, 243:572–590, 2014.

[75] Y Yang, J.L., L. Zhu, G. Qin, and Q. Chen.
Double Network Hydrogels with Controlled Shape Deformation.
Journal of Polymer Science Part B: Polymer Physics, 56:1351–1362, 2018.

[76] N.S. Kehr, E.A. Prasetyanto, K. Benson, B. Ergün, A. Galstyan, and H. Galla.
Periodic mesoporous organosilica-based nanocomposite hydrogels as three-dimensional scaffolds.
Angewandte Chemie - International Edition, 52(4):1156–1160, 2013.

[77] J.W. Goodwin and R.W. Hughes.
Rheology for Chemists: An Introduction.
RSC Publishing, 2000.

[78] E. Jang, S. Park, S. Park, Y. Lee, D.N. Kim, B. Kim, and W.G. Koh.
Fabrication of poly(ethylene glycol)-based hydrogels entrapping enzyme-immobilized silica nanoparticles.
Polymers for Advanced Technologies, 21(7):476–482, 2010.

[79] S. Rose, A. Marcellan, T. Narita, F. Boué, F. Cousin, and D. Hourdet.
Structure investigation of nanohybrid PDMA/silica hydrogels at rest and under uniaxial deformation.
Soft Matter, 11(29):5905–5917, 2015.

[80] J. Zaragoza, S. Fukuoka, M. Kraus, J. Thomin, and P. Asuri.
Exploring the role of nanoparticles in enhancing mechanical properties of hydrogel nanocomposites.
Nanomaterials, 8(11):1–10, 2018.

[81] S. Schneider and P. Linse.
Monte Carlo simulation of defect-free cross-linked polyelectrolyte gels.
Journal of Physical Chemistry B, 107(32):8030–8040, 2003.

[82] H. Kono.
Characterization and properties of carboxymethyl cellulose hydrogels crosslinked by polyethylene glycol.
Carbohydrate Polymers, 106(1):84–93, 2014.

[83] B. Wang, X.D. Xu, Z. Wang, S. Cheng, X.Z. Zhang, and R.X. Zhuo.
Synthesis and properties of pH and temperature sensitive P(NIPAAm-co-DMAEMA) hydrogels.
Colloids and Surfaces B: Biointerfaces, 64(1):34–41, 2008.

[84] S.Y. Kim and Y.M. Lee.
Drug release behavior of electrical responsive poly(vinyl alcohol)/poly(acrylic acid) IPN hydrogels under an electric stimulus.
Journal of Applied Polymer Science, 74(7):1752–1761, 1999.

[85] A.F. Greene, M.K. Danielson, A.O. Delawder, K.P. Liles, X. Li, A. Natraj, A. Wellen, and J.C. Barnes.
Redox-Responsive Artificial Molecular Muscles: Reversible Radical-Based Self-Assembly for Actuating Hydrogels.
Chemistry of Materials, 29(21):9498–9508, 2017.

[86] Ta Matsumoto, A.I., J. Nishida, H. Matsumoto, K. Kataoka, and Y. Miyahara.
A synthetic approach toward a self-regulated insulin delivery system.
Angewandte Chemie - International Edition, 51(9):2124–2128, 2012.

[87] H. Che, B.C. Buddingh, and J.C.M. van Hest.
Self-Regulated and Temporal Control of a ‚ÄúBreathing‚Äù Microgel Mediated by Enzymatic Reaction.
Angewandte Chemie - International Edition, 56(41):12581–12585, 2017.

[88] J. Ostrowska-Czubenko, M. Gierszewska, and M. Pieróg.
pH-responsive hydrogel membranes based on modified chitosan: water transport and kinetics of swelling.
Journal of Polymer Research, 22(8), 2015.

[89] B. Amsden.
Solute diffusion in hydrogels. An examination of the retardation effect.
Polymer Gels and Networks, 6(1):13–43, 1998.

[90] L. Weng, Y. Lu, L. Shi, X. Zhang, L. Zhang, X. Guo, and J. Xu.
In situ investigation of drug diffusion in hydrogels by the refractive index method.
Analytical Chemistry, 76(10):2807–2812, 2004.

[91] J. Tavakoli and Y. Tang.
Hydrogel based sensors for biomedical applications: An updated review.
Polymers, 9(8):1–25, 2017.

[92] R.A. Sheldon and S. van Pelt.
Enzyme immobilisation in biocatalysis: Why, what and how.
Chemical Society Reviews, 42(15):6223–6235, 2013.

[93] H.P.M. De Hoog, I.W.C.E. Arends, A.E. Rowan, J.L.M. Cornelissen, and R.J.M. Nolte.
A hydrogel-based enzyme-loaded polymersome reactor.
Nanoscale, 2(5):709–716, 2010.

[94] D. Simon, F. Obst, S. Haefner, T. Heroldt, M. Peiter, F. Simon, A. Richter, B. Voit, and D. Appelhans.
Hydrogel/enzyme dots as adaptable tool for non-compartmentalized multi-enzymatic reactions in microfluidic devices.
Reaction Chemistry and Engineering, 4(1):67–77, 2019.

[95] C.A. Deforest and D.A. Tirrell.
A photoreversible protein-patterning approach for guiding stem cell fate in three-dimensional gels.
Nature Materials, 14(5):523–531, 2015.

[96] J. He, Y. Du, J.L. Villa-Uribe, C. Hwang, D. Li, and A. Khademhosseini.

Rapid generation of biologically relevant hydrogels containing long-range chemical gradients.
Advanced Functional Materials, 20(1):131–137, 2010.

[97] S. Sant, M.J. Hancock, J.P. Donnelly, D. Iyer, and A. Khademhosseini.
Biomimetic gradient hydrogels for tissue engineering.
Canadian Journal of Chemical Engineering, 88(6):899–911, 2010.

[98] R. Sunyer, A.J. Jin, R. Nossal, and D.L. Sackett.
Fabrication of Hydrogels with Steep Stiffness Gradients for Studying Cell Mechanical Response.
Plos One, 7(10):1–9, 2012.

[99] S.L. Vega, M.Y. Kwon, K.H. Song, C. Wang, R.L. Mauck, L. Han, and J.A. Burdick.
Combinatorial hydrogels with biochemical gradients for screening 3D cellular microenvironments.
Nature communications, 9(1):614, 2018.

[100] A. Nishiguchi, A. Mourran, H. Zhang, and M. Möller.
In-Gel Direct Laser Writing for 3D-Designed Hydrogel Composites That Undergo Complex Self-Shaping.
Advanced Science, 5(1), 2018.

[101] M. Guvendiren, J. Molde, R.M.D. Soares, and J. Kohn.
Designing Biomaterials for 3D Printing.
ACS Biomaterials Science and Engineering, 2(10):1679–1693, 2016.

[102] M.K. Gupta, F. Meng, B.N. Johnson, Y.L. Kong, L. Tian, Y.W. Yeh, N. Masters, S. Singamaneni, and M.C. McAlpine.
3D Printed Programmable Release Capsules.
Nano Letters, 15(8):5321–5329, 2015.

[103] M.K. Nichols, R.K. Kumar, P.G. Bassindale, L. Tian, A.C. Barnes, B.W. Drinkwater, A.J. Patil, and S. Mann.
Fabrication of Micropatterned Dipeptide Hydrogels by Acoustic Trapping of Stimulus-Responsive Coacervate Droplets.
Small, 14(26), 2018.

[104] M.Y. Chiang, Y.W. Hsu, H.Y. Hsieh, S.Y. Chen, and S.K. Fan.
Constructing 3D heterogeneous hydrogels from electrically manipulated prepolymer droplets and crosslinked microgels.
Science Advances, 2(10):1–9, 2016.

[105] S. Ostrovidov, N. Annabi, A. Seidi, M. Ramalingam, F. Dehghani, H. Kaji, and A. Khademhosseini.
Controlled release of drugs from gradient hydrogels for high-throughput analysis of cell-drug interactions.
Analytical Chemistry, 84(3):1302–1309, 2012.

[106] N.W. Choi, M. Cabodi, B. Held, J.P. Gleghorn, L.J. Bonassar, and A.D. Stroock.
Microfluidic scaffolds for tissue engineering.
Nature Materials, 6(11):908–915, 2007.

[107] B.J. Peret and W.L. Murphy.
Controllable soluble protein concentration gradients in hydrogel networks.
Advanced Functional Materials, 18(21):3410–3417, 2008.

[108] Y. Kim, H. Namgung, and T.S. Lee.
Synthesis of a glucose oxidase-conjugated, polyacrylamide-based, fluorescent hydrogel for a reusable, ratiometric glucose sensor.
Polymer Chemistry, 7(43):6655–6661, 2016.

[109] M. Ikeda, T. Tanida, T. Yoshii, K. Kurotani, S. Onogi, K. Urayama, and I. Hamachi.
Installing logic-gate responses to a variety of biological substances in supramolecular hydrogel-enzyme hybrids.
Nature Chemistry, 6(6):511–518, 2014.

[110] B.A. Firestone and R.A. Siegel.
pH, salt, and buffer dependent swelling in ionizable copolymer gels: Tests of the ideal Donnan equilibrium theory.
Journal of Biomaterials Science, Polymer Edition, 5(5):433–450, 1994.

[111] S.J. Kim, K.J. Lee, I.Y. Kim, D.I. Shin, and S.I. Kim.
Temperature and pH-response swelling behavior of poly(2-ethyl-2-oxazoline)/chitosan interpenetrating polymer network hydrogels.
Journal of Applied Polymer Science, 99(3):1100–1103, 2006.

[112] E. Akar, A. Altinisik, and Y. Seki.
Preparation of pH and ionic strength responsive biodegradable fumaric acid crosslinked carboxymethyl cellulose.
Carbohydrate Polymers, 90(4):1634–1641, 2012.

[113] M. Nakahata, Y. Takashima, A. Hashidzume, and A. Harada.
Redox-generated mechanical motion of a supramolecular polymeric actuator based on host-guest interactions.
Angewandte Chemie - International Edition, 52(22):5731–5735, 2013.

[114] M.A. Hempenius, C. Cirmi, F. Lo Savio, J. Song, and G.J. Vancso.
Poly(ferrocenylsilane) gels and hydrogels with redox-controlled actuation.
Macromolecular Rapid Communications, 31(9-10):772–783, 2010.

[115] I. Tomatsu, K. Peng, and A. Kros.
Photoresponsive hydrogels for biomedical applications.
Advanced Drug Delivery Reviews, 63(14-15):1257–1266, 2011.

[116] M. Nakahata, Y. Takashima, H. Yamaguchi, and A. Harada.
Redox-responsive self-healing materials formed from host-guest polymers.
Nature Communications, 2(1):511–516, 2011.

[117] M. Zelzer, S.J. Todd, A.R. Hirst, T.O. McDonald, and R.V. Ulijn.
Enzyme responsive materials: Design strategies and future developments.
Biomaterials Science, 1(1):11–39, 2013.

[118] X.D. Xu, B.B. Lin, J. Feng, Y. Wang, S.X. Cheng, X.Z. Zhang, and R.X. Zhuo.
Biological glucose metabolism regulated peptide self-assembly as a simple visual biosensor for glucose detection.
Macromolecular Rapid Communications, 33(5):426–431, 2012.

[119] E. Kokufuta, Y.Q. Zhang, and T. Tanaka.
Biochemo-mechanical function of urease-loaded gels.
Journal of Biomaterials Science, Polymer Edition, 6(1):35–40, 1994.

[120] R.W. Jaggers and S.A.F. Bon.
Temporal and spatial programming in soft composite hydrogel objects.
Journal of Materials Chemistry B, 5(36):7491–7495, 2017.

[121] R. Merindol and A. Walther.
Materials learning from life: Concepts for active, adaptive and autonomous molecular systems.
Chemical Society Reviews, 46(18):5588–5619, 2017.

[122] T. Heuser, E. Weyandt, and A. Walther.
Biocatalytic Feedback-Driven Temporal Programming of Self-Regulating Peptide Hydrogels.
Angewandte Chemie - International Edition, 54(45):13258–13262, 2015.

[123] R.W. Jaggers and S.A.F. Bon.
Independent responsive behaviour and communication in hydrogel objects.
Materials Horizons, 4(3):402–407, 2017.

[124] Y.S. Kim, R. Tamate, A.M. Akimoto, and R. Yoshida.
Recent developments in self-oscillating polymeric systems as smart materials: From polymers to bulk hydrogels.
Materials Horizons, 4(1):38–54, 2017.

[125] L. Heinen, T. Heuser, A. Steinschulte, and A. Walther.
Antagonistic enzymes in a biocatalytic ph feedback system program autonomous DNA hydrogel life cycles.
Nano Letters, 17(8):4989–4995, 2017.

[126] T. Heuser, A.K. Steppert, C. Molano Lopez, B. Zhu, and A. Walther.
Generic Concept to Program the Time Domain of Self-Assemblies with a Self-Regulation Mechanism.
Nano Letters, 15(4):2213–2219, 2015.

[127] S.G.J. Postma, I.N. Vialshin, C.Y. Gerritsen, M Bao, and W.T.S. Huck.
Preprogramming Complex Hydrogel Responses using Enzymatic Reaction Networks.
Angewandte Chemie - International Edition, 56(7):1794–1798, 2017.

[128] A. Hanbury.
Constructing cylindrical coordinate colour spaces.
Pattern Recognition Letters, 29(4):494–500, 2008.

[129] M. Horvath.
Hsl-hsv models b, 2010.

[130] W. Rasband.
RGB measure plugin, 2004.

[131] C. Laummonerie and J. Mutterer.
RGB profiler, 2004.

[132] Y.H. Lee, J.J. Chang, W.F. Lai, M.C. Yang, and C.T. Chien.
Layered hydrogel of poly(γ-glutamic acid), sodium alginate, and chitosan: Fluorescence observation of structure and cytocompatibility.
Colloids and Surfaces B: Biointerfaces, 86(2):409–413, 2011.

[133] A. Katchalsky and P. Spitnik.
Potentiometric titrations of polymethacrylic acid.
Journal of Polymer Science, 2(5):487–487, 1947.

[134] V. Bindokas.
White balance macro.

[135] E. Ruiz-Hitzky, K. Ariga, and Y.M. Lvov.
Bio-inorganic Hybrid Nanomaterials: Strategies, Synthesis, Characterization and Applications.
Wiley, 2008.

[136] D.J. Belton, O. Deschaume, and C. C. Perry.
An overview of the fundamentals of the chemistry of silica with relevance to biosilicification and technological advances.
FEBS Journal, 279(10):1710–1720, 2012.

[137] A. Buckley and M. Greenblatt.
The sol-gel preparation of silica gels.
Journal of chemical education, 71:599–602, 1994.

[138] C. J. Brinker.
Hydrolysis and condensation of silicates: effects on structure.
Journal of Non-Crystalline Solids, 100(10):31–50, 1988.

[139] D. Avnir, O. Lev, and J. Livage.
Recent bio-applications of sol-gel materials.
Journal of Materials Chemistry, 16(11):1013–1030, 2006.

[140] U. Hanefeld, L. Gardossi, and E. Magner.
Understanding enzyme immobilisation.
Chemical Society Reviews, 38(2):453–468, 2009.

[141] K. Smith, N.J. Silvernail, K.R. Rodgers, T.E. Elgren, M Castro, and R.M Parker.
Sol-gel encapsulated horseradish peroxidase: A catalytic material for peroxidation.
Journal of the American Chemical Society, 124(16):4247–4252, 2002.

[142] T. Jesionowski, J. Zdarta, and B. Krajewska.
Enzyme immobilization by adsorption: A review.
Adsorption, 20(5-6):801–821, 2014.

[143] J. Meissner, A. Prause, B. Bharti, and G.H. Findenegg.
Characterization of protein adsorption onto silica nanoparticles: influence of pH and ionic strength.
Colloid and Polymer Science, 293(11):3381–3391, 2015.

[144] A.A. Vertegel, R.W. Siegel, and J.S. Dordick.
Silica nanoparticle size influences the structure and enzymatic activity of adsorbed lysozyme.
Langmuir, 20(16):6800–6807, 2004.

[145] M. Lundqvist, I. Sethson, and B.H. Jonsson.
Protein adsorption onto silica nanoparticles: Conformational changes depend on the particles' curvature and the protein stability.
Langmuir, 20(24):10639–10647, 2004.

[146] M. Kramer, J.C. Cruz, P.H. Pfromm, M.E. Rezac, and P. Czermak.
Enantioselective transesterification by Candida antarctica Lipase B immobilized on fumed silica, 2010.

[147] W. Norde and C.E. Giacomelli.
BSA structural changes during homomolecular exchange between the adsorbed and the dissolved states.
Journal of Biotechnology, 79(3):259–268, 2000.

[148] M. Chen, L. Wu, S. Zhou, and B. You.
A method for the fabrication of monodisperse hollow silica spheres.
Advanced Materials, 18(6):801–806, 2006.

[149] C.L. Chang and H.S. Fogler.
Controlled formation of silica particles from tetraethyl orthosilicate in nonionic water-in-oil microemulsions.
Langmuir, 13(13):3295–3307, 1997.

[150] Z. Cao, L. Dong, L. Li, Y. Shang, D. Qi, Q. Lv, G. Shan, U. Ziener, and K. Landfester.
Preparation of mesoporous submicrometer silica capsules via an interfacial sol-gel process in inverse miniemulsion.
Langmuir, 28(17):7023–7032, 2012.

[151] Z. Cao, L. Yang, Q. Ye, Q. Cui, D. Qi, and U. Ziener.
Transition-metal salt-containing silica nanocapsules elaborated via salt-induced interfacial deposition in inverse miniemulsions as precursor to functional hollow silica particles.
Langmuir, 29(22):6509–6518, 2013.

[152] H. Wang, X. Zhu, L. Tsarkova, A. Pich, and M. Möller.
All-silica colloidosomes with a particle-bilayer shell.
ACS Nano, 5(5):3937–3942, 2011.

[153] C. Zhang, C. Hu, Y. Zhao, M. Möller, K. Yan, and X. Zhu.
Encapsulation of laccase in silica colloidosomes for catalysis in organic media.
Langmuir, 29(49):15457–15462, 2013.

[154] J. Van Wijk, T. Heunis, E. Harmzen, L.M.T. Dicks, J. Meuldijk, and B. Klumperman.
Compartmentalization of bacteria in microcapsules.

Chemical Communications, 50(97):15427–15430, 2014.

[155] J.L. Hu, L.B. Luo, X.Z. Yang, R.S. Yao, H.B. Zhang, and H.S. Qian.
Silica-based hybrid microspheres: Synthesis, characterization and wastewater treatment.
RSC Advances, 3(48):25620–25626, 2013.

[156] T. F. Watson.
Fact and artefact in confocal microscopy.
Advances in dental research, 11(4):433–441, 1997.

[157] R.B. Lira, J. Steink$\surd$žhler,*R.L.Knoor*,*andK.A.Dimova*,*R. Riske*.
Posing for a picture: Vesicle immobilization in agarose gel.
Scientific Reports, 6(April):1–12, 2016.

[158] J. Hurler, S. Žakelj, J. Mravljak, S. Pajk, A. Kristl, R. Schubert, and N. Škalko-Basnet.
The effect of lipid composition and liposome size on the release properties of liposomes-in-hydrogel.
International journal of pharmaceutics, 456(1):49–57, 2013.

[159] E. Ruel-Gariépy, G. Leclair, P. Hildgen, A. Gupta, and J. C. Leroux.
Thermosensitive chitosan-based hydrogel containing liposomes for the delivery of hydrophilic molecules.
Journal of Controlled Release, 82(2-3):373–383, 2002.

[160] W. Gao, D. Vecchio, J. Li, J. Zhu, Q. Zhang, V. Fu, J. Li, S. Thamphiwatana, D. Lu, and L. Zhang.
Hydrogel containing nanoparticle-stabilized liposomes for topical antimicrobial delivery.
ACS Nano, 8(3):2900–2907, 2014.

[161] L. Hosta-Rigau, B.E.B. Jensen, K.S. Fjeldsø, A. Postma, G. Li, K.N. Goldie, F. Albericio, A.N. Zelikin, and B. Städler.
Surface-Adhered Composite Poly(Vinyl Alcohol) Physical Hydrogels: Polymersome-Aided Delivery of Therapeutic Small Molecules.
Advanced Healthcare Materials, 1(6):791–795, 2012.

[162] Ravinash Krishna Kumar, Robert L. Harniman, Avinash J. Patil, and Stephen Mann.
Self-transformation and structural reconfiguration in coacervate-based protocells.
Chemical Science, 7(9):5879–5887, 2016.

[163] Mariam Bayoumi, Hagan Bayley, Giovanni Maglia, and K. Tanuj Sapra.
Multi-compartment encapsulation of communicating droplets and droplet networks in hydrogel as a model for artificial cells.
Scientific Reports, 7(April):1–11, 2017.

[164] A. Garcia-Leis, D. Jancura, M. Antalik, J. V. Garcia-Ramos, S. Sanchez-Cortes, and Z. Jurasekova.
Catalytic effects of silver plasmonic nanoparticles on the redox reaction leading to ABTS+ formation studied using UV-visible and Raman spectroscopy.
Physical Chemistry Chemical Physics, 18(38):26562–26571, 2016.

[165] E.N. Kadnikova and N.M. Kostić.
Oxidation of ABTS by hydrogen peroxide catalyzed by horseradish peroxidase encapsulated into sol-gel glass. Effects of glass matrix on reactivity.
Journal of Molecular Catalysis B: Enzymatic, 18(1-3):39–48, 2002.

[166] Y. Zhang, S. Tsitkov, and H. Hess.
Proximity does not contribute to activity enhancement in the glucose oxidase-horseradish peroxidase cascade.
Nature Communications, 7:1–9, 2016.

[167] H. Zeng, Z.Q. Tang, L.W. Liao, J. Kang, and Y.X. Chen.
Electrochemistry of ABTS at glassy carbon electrodes.
Chinese Journal of Chemical Physics, 24(6):653–658, 2011.

[168] K. Oliver, A. Seddon, and R.S. Trask.
Morphing in nature and beyond: a review of natural and synthetic shape-changing materials and mechanisms.
Journal of Materials Science, 51(24):10663–10689, 2016.

[169] X. Le, W. Lu, J. Zhang, and T. Chen.
Recent Progress in Biomimetic Anisotropic Hydrogel Actuators.
Advanced Science, 6(5):1–14, 2019.

[170] J. Shang, X. Le, J. Zhang, T. Chen, and P. Theato.
Trends in polymeric shape memory hydrogels and hydrogel actuators.
Polymer Chemistry, 10(9):1036–1055, 2019.

[171] X. He, M. Aizenberg, O. Kuksenok, L.D. Zarzar, A. Shastri, A.C. Balazs, and J.. Aizenberg.
Synthetic homeostatic materials with chemo-mechano-chemical self-regulation.
Nature, 487(7406):214–218, 2012.

[172] Y.S. Kim, M. Liu, Y. Ishida, Y. Ebina, M. Osada, T. Sasaki, T. Hikima, M. Takata, and T. Aida.
Thermoresponsive actuation enabled by permittivity switching in an electrostatically anisotropic hydrogel.
Nature Materials, 14(10):1002–1007, 2015.

[173] C. Ma, T. Li, Q. Zhao, X. Yang, J. Wu, Y. Luo, and T. Xie.
Supramolecular lego assembly towards three-dimensional multi-responsive hydrogels.
Advanced Materials, 26(32):5665–5669, 2014.

[174] X. Li, X. Cai, Y. Gao, and M.J. Serpe.
Reversible bidirectional bending of hydrogel-based bilayer actuators.
Journal of Materials Chemistry B, 5(15):2804–2812, 2017.

[175] E. Lee, D. Kim, H. Kim, and J. Yoon.
Photothermally driven fast responding photo-actuators fabricated with comb-type hydrogels and magnetite nanoparticles.
Scientific Reports, 5(October):1–8, 2015.

[176] D. Morales, E. Palleau, M.D. Dickey, and O.D. Velev.
Electro-actuated hydrogel walkers with dual responsive legs.
Soft Matter, 10(9):1337–1348, 2014.

[177] V. Chan, K. Park, M.B. Collens, T.A Kong, H.S., and R. Bashir.
Development of miniaturized walking biological machines.
Scientific Reports, 2, 2012.

[178] N. Martin, J.P. Douliez, Y. Qiao, R. Booth, M. Li, and S. Mann.
Antagonistic chemical coupling in self-reconfigurable host‚Äìguest protocells.
Nature Communications, 9(1):1–12, 2018.

[179] T-L. Chen and H.S. Weng.
A method for the determinations of the activity and optimal pH of glucose oxidase in an unbuffered solution.
Biotechnology and Bioengineering, 28(1):107–109, 1986.

[180] M. Fidaleo and R. Lavecchia.
Kinetic study of enzymatic urea hydrolysis in the pH range 4-9.
Chemical and Biochemical Engineering Quarterly, 17(4):311–318, 2003.

[181] Q.Z. Wang, X.G. Chen, N. Liu, S.X. Wang, C.S. Liu, X.H. Meng, and C.G. Liu.
Protonation constants of chitosan with different molecular weight and degree of deacetylation.
Carbohydrate Polymers, 65:194–201, 2006.

[182] H. Trivedi, C. Patel, and R. Patel.
Studies on carboxymethylcellulose: Potentiometric titrations, 3.
Die Makromolekulare Chemie, 182(1):243–245, 1981.